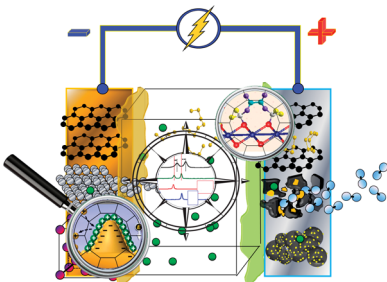


## Electrolytes and Interphases in Li-Ion Batteries and Beyond

Kang Xu\*

Electrochemistry Branch, Energy and Power Division, Sensor and Electronics Directorate, U.S. Army Research Laboratory, 2800 Powder Mill Road, Adelphi, Maryland 20783-1197, United States



### CONTENTS

1. Introduction and Scope	11504
2. Electrolyte Bulk Properties	11505
2.1. Ion Transport	11505
2.2. Li <sup>+</sup> -Solvation	11506
2.3. Li <sup>+</sup> -Solvent Interaction in Electrolyte Solutions	11506
2.4. Li <sup>+</sup> -Solvates in Concentrated Electrolytes	11508
3. Electrolyte Components	11508
3.1. New Solvents	11508
3.1.1. Esters	11509
3.1.2. Sulfones and Sulfoxides	11514
3.1.3. Nitriles	11516
3.1.4. Phosphorus-Based Solvents	11516
3.1.5. Silicon-Based Solvents	11518
3.1.6. Ethers	11519
3.2. Anion Receptors	11520
3.3. New Lithium Salts	11522
3.3.1. Phosphates	11523
3.3.2. Borates and Boron-Based Cluster	11523
3.3.3. Imides	11527
3.3.4. Heterocyclic Anions	11527
3.3.5. Aluminates	11528
3.4. Additives	11528
3.4.1. Additives for Graphitic Anode	11529
3.4.2. Additives and Interphasial Chemistry on Alloy-Type Anodes	11535
3.4.3. Additives for Cathode	11538
3.4.4. Additives for Overcharge Protection	11540
3.4.5. Additive Evaluation with High Precision Coulometry	11542
3.5. Artificial Interphases	11543
3.5.1. Artificial Interphases on Graphitic or Alloy Anodes	11544
3.5.2. Artificial Interphases on Cathodes	11545
3.6. Ionic Liquids	11549
3.6.1. Imidazoliums	11550
3.6.2. Pyrrolidiniums	11551
3.6.3. Other Cyclic and Acyclic Ammoniums and Phosphoniums	11552
3.6.4. A Sober Perspective on Ionic Liquid Electrolytes	11553
3.7. Solid Polymer and Polymer Gel Electrolytes	11554
3.7.1. Solid Polymer Electrolytes	11554
3.7.2. Gel Polymer Electrolytes	11557
3.8. "Quasi-Ionic Liquid" Electrolytes	11558
3.8.1. Carbonate-Li Salt Systems	11558
3.8.2. Ether-Li Salt Systems	11559
3.8.3. Polymer-Li Salt	11559
3.8.4. Other Solvents-Li Salt	11561
4. Degradation and Stabilization of Electrolytes	11561
4.1. Degradation Mechanisms	11561
4.2. Electrolyte Components To Suppress Degradations	11562
4.2.1. Chemical and Thermal Degradations	11562
4.2.2. Degradations with Anode	11563
4.2.3. Degradations with Cathode	11563
4.2.4. Degradations with Aluminum Substrate	11564
5. Understanding Interphases	11564
5.1. Anode/Electrolyte Interphase	11565
5.1.1. Chemistry and Electrochemistry	11565
5.1.2. Properties of Interphasial Components	11571
5.1.3. Formation Mechanism	11572
5.1.4. EC-PC Mystery	11577
5.2. Cathode/Electrolyte Interphase	11577
5.2.1. Spontaneous Reactions	11579
5.2.2. Chemistry and Electrochemistry	11579
5.2.3. Interphase on High Voltage Cathodes	11580
5.2.4. Cathode/Anode Interactions	11581
5.2.5. How Interphases on Cathode and Anode Differ	11582
5.3. Advanced Characterization and Imaging	11583
5.3.1. Ellipsometry and Sum-Frequency Generation Spectra	11583
5.3.2. Electron Microscopes	11584
5.3.3. Acoustics	11585
5.3.4. Neutron-Based Techniques	11585
5.3.5. Fluorescence	11587
5.3.6. Electrochemical Quartz Crystal Microbalance	11588
5.3.7. Scanning Probe Microscopy	11589
6. Electrolytes and Interphases in "Beyond Li-Ion" Chemistries	11592
6.1. Conversion-Reaction Chemistry	11592
6.2. Li/O <sub>2</sub> or Li/Air Chemistry	11592
6.2.1. Carbonates and Ethers	11593

**Special Issue:** 2014 Batteries

**Received:** January 2, 2014

**Published:** October 29, 2014

6.2.2. Other Solvents and Polymer Electrolytes	11594
6.2.3. Additives	11595
6.2.4. Li Salts	11596
6.2.5. Potential Safety Concern of Li/O <sub>2</sub> Chemistry	11596
6.3. Li/S Chemistry	11597
6.4. Protection of Lithium Anode	11598
6.5. Dual-Intercalation Chemistry	11600
6.6. Sodium Ion Chemistry	11602
6.7. Multivalent (Mg <sup>2+</sup> ) Chemistry	11603
7. Concluding Remarks	11605
Author Information	11605
Corresponding Author	11605
Notes	11605
Biography	11605
Acknowledgments	11606
References	11606

## 1. INTRODUCTION AND SCOPE

Ten years ago, a comprehensive review was compiled for a thematic issue of *Chemical Reviews*, covering fundamentals, history, and state-of-the-art for nonaqueous electrolytes, with emphasis placed on the nascent Li-ion chemistry.<sup>1</sup> At the time, this young rechargeable battery already overwhelmed the portable electronics market with its flagship cathode LiCoO<sub>2</sub>, and ternary composition LiNi<sub>1/3</sub>Mn<sub>1/3</sub>Co<sub>1/3</sub>O<sub>2</sub> just emerged as the choice for next generation commercial batteries. Other transition metal oxides or phosphates of layered-, spinel-, or olivine-structures remained laboratory innovations still facing various challenges.<sup>2</sup> The past decade of 2003–2014 witnessed maturation of these materials as well as mushrooming of new cathode chemistries, some of which rapidly evolved into viable choices for the battery industry. The latter include variations of layer-structured mixed metal oxides, such as LiNi<sub>1/3</sub>Mn<sub>1/3</sub>Co<sub>1/3</sub>O<sub>2</sub> and the lithium–manganese-rich modifications (LMR-NMC), the high voltage spinel (LiNi<sub>0.5</sub>Mn<sub>1.5</sub>O<sub>4</sub>), and various olivine phosphates (LiMPO<sub>4</sub>, M = Fe, Mn, Co, or Ni),<sup>3</sup> while other “older” but more aggressive cathode chemistries, such as Li/sulfur<sup>4</sup> and Li/oxygen or Li/air<sup>5</sup> systems, were revisited with new perspectives and approaches. The conversion-reaction concept, based on Li-accommodation in metal oxides and fluorides upon reversible breaking and reforming bonds at nanoscale, has also attracted intense interest.<sup>6</sup> With varying degrees of emphases and successes, all of these materials aimed to increase specific capacity or energy density, to reduce cost, or to improve safety of Li-ion devices. Among them, the success story of lithium ironphosphate (LiFePO<sub>4</sub>) stands out,<sup>7</sup> as this material, once characterized by its low-conductivity, became a cathode of choice for high power Li-ion batteries that is being adopted into the markets of power tools, hybrid electric vehicles, and grid-scale storage media. The anode front has been relatively quieter. While graphitic carbon retained its status of mainstream anode material, significant advances have been made in alloy-type materials (in particular, silicon-based), thanks to the spatial relief provided by rational design and elegant execution of nanostructures.<sup>8,9</sup>

Electrolytes in batteries must cater to the needs of both electrodes; hence, in principle, new battery chemistries would have incurred new electrolyte compositions. Surprisingly, as compared to the active dynamics of cathode research, improvements in electrolytes have been incremental in the past

decade, with the skeleton composition persisting as lithium hexafluorophosphate (LiPF<sub>6</sub>) salt and organic carbonate solvents. This relative stalemate could be attributed to three distinct but interdependent factors: (1) Electrolyte components (especially solvents) are more sensitive to operating potential rather than capacity of electrodes; therefore, as long as the new chemistries operate reasonably within the electrochemical stability window of the carbonate-based electrolytes (as most of the above-mentioned cathode and anode materials do), major changes in the skeleton composition are not mandatory. (2) More effective design and use of electrolyte additives became customary practices, aided by the significant advances in the fundamental knowledge of how “solid electrolyte interphases” (SEI) form on electrode surfaces. These “drop-in” sacrificial components contribute to maintain the electrolyte skeleton compositions more or less static. (3) Perhaps most importantly, confined by cost consideration, the battery industry has been reluctant to change the existing supply chain, unless there is sufficient incentive or benefit. In a sense, the established infrastructures producing LiPF<sub>6</sub> and organic carbonates constitute the biggest hurdle to the adoption of any new electrolyte components. A few exceptions do exist, such as the 5 V class spinel (LiNi<sub>0.5</sub>Mn<sub>1.5</sub>O<sub>4</sub>, 4.6 V) or cobalt phosphate (LiCoPO<sub>4</sub>, 4.8 V) chemistry, whose operating potentials beyond the stability limit of the carbonate-based electrolytes (4.5 V) would require not only additives but also new bulk electrolyte solvents.<sup>10,11</sup> Similar requirements might also arise from “Beyond Li ion” chemistries, in which dynamic phase/structural changes present severe challenge to carbonate-based electrolytes.

This comprehensive Review is constructed on the basis of its 2004 predecessor,<sup>1</sup> omitting fundamentals and histories and focusing on advances made during the past decade. Only nonaqueous liquid, polymer, or polymer gel electrolytes are covered, leaving out glassy/crystalline/ceramic as well as aqueous electrolytes. The scope would reflect the fact that Li-ion battery (LIB) still monopolizes the mobile electronic market as the power source of choice, but proper attention will be given to electrolytes developed for the so-called “beyond lithium ion” chemistries. In addition to covering new electrolyte components, a significant section will be dedicated to the new understandings of interphases on either electrodes, because they have become an integral part of almost any electrolyte work, which includes their chemistry, formation mechanism, continuous growth, as well as Li<sup>+</sup>-transport properties across them.

The references cited will be limited to peer-reviewed literatures published from mid-2003 to early 2014 with a few necessary exceptions. To keep the reference numbers to a minimum, any earlier references already cited in the 2004 review will be referred to ref 1. Although an onerous endeavor was made to ensure comprehensiveness, it is impossible to cover all of the publications available, mainly due to the explosive growth of battery research activities since 2008 driven by worldwide investments in this area. Fortunately, a number of related reviews/monographs/perspective articles were available after 2003, serving as complementary readings to this review.<sup>12–25</sup> Finally, in an attempt to avoid simply chronicling “who did what”, this Review inherits the tradition of its 2004 predecessor; that is, cited literatures were critically examined so that an in-depth analysis or insightful comments could be provided for the benefits of readers.

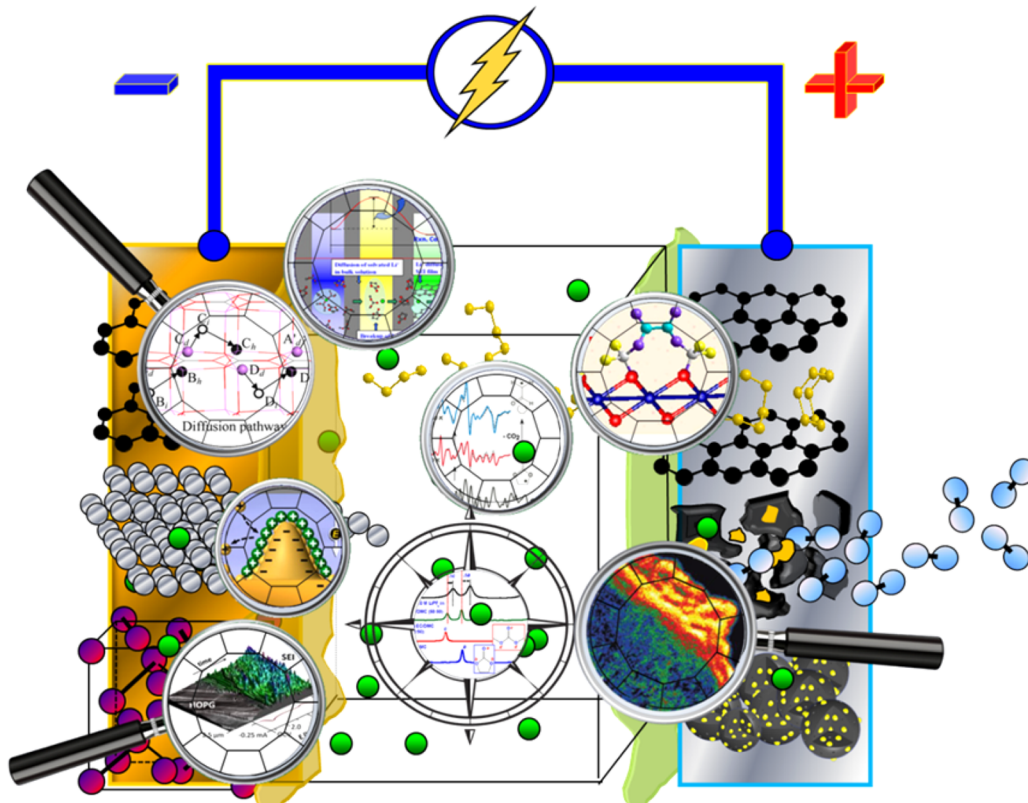


**Figure 1.** During 2003–2014, significant advances have been made in the development of new electrolyte components (lithium salts, solvents, and additives) and fundamental understanding of the related interphasial chemistry in both lithium ion and advanced rechargeable batteries. While stabilization of electrolyte/cathode interfaces at high potentials (>4.5 V) became a topic of high interest with the emergence of 5 V class cathode chemistries, “beyond Li-ion” chemistries present more severe challenges to the electrolytes and interphase with more dynamic changes in their electrode structures during cycling. Protection of the metallic lithium anode was revisited as it may dictate the success of these new battery chemistries with high energy density.

## 2. ELECTROLYTE BULK PROPERTIES

While little has changed in the skeleton composition of electrolytes for LIB during the past decade, major advances were made in understanding how  $\text{Li}^+$  exists and moves in bulk electrolyte, how the interphases are formed and structured at both electrode surfaces, and how  $\text{Li}^+$ -transport occurs across these interphases (Figure 1). In particular,  $\text{Li}^+$ -solvent interaction in bulk electrolyte became a topic of importance, mainly due to the newly revealed effect of  $\text{Li}^+$ -solvation sheath structure on the formation chemistry of interphases and the kinetics of  $\text{Li}^+$ -migration within the formed interphases.

### 2.1. Ion Transport

Ion conductivity is a key electrolyte property, as it quantifies how mobile (and available) the ions are for the ongoing electrochemical reactions, which in part determines the power output of the cell. The ion conductivity of nonaqueous electrolytes formulated for LIB applications is provided by  $\text{LiPF}_6$  salt dissolved in carbonate ester solvents. So far there has been no suitable single solvent available that simultaneously possesses high dielectric permittivity (to dissolve the salt) and low viscosity (to facilitate ion transport), while still meeting requirements of interfacial stability on both anode and cathode. As a compromise, solvents of either high dielectric permittivity or low viscosity must be mixed. The former is ethylene carbonate (EC), now an indispensable ingredient in almost all LIB electrolytes, and the latter consists of a series of acyclic carbonate or carboxylic esters, the most commonly used of

which are dimethyl carbonate (DMC), diethyl carbonate (DEC), and ethylmethyl carbonate (EMC).<sup>1</sup> It was in such mixed solvent systems that ion conductivities of state-of-the-art nonaqueous electrolytes could reach the level of 5–10 mS/cm at ambient temperature, supporting routine cell operations in the range of –30 to +60 °C.

Vast databases of ion conductivity continue to be updated. To better understand how  $\text{Li}^+$  transports, Ding et al. tried to deconvolute the interwoven factors that affect ion conduction in high order mixed solvent systems, including cation and anion species and their interactions, solvents of different dielectric permittivity, solution viscosities, and glass transition temperature,<sup>26,27</sup> arriving at the conclusion that the cation solvated with solvent molecules seemed to play a dominant role in determining its mobility, while anion exerts their influence only through their ability to form ion pairs with cations. This explained why in the same nonaqueous solvents lithium salts would have lower conductivity as compared to their tetraalkyl ammonium counterparts. A similar conclusion was drawn by Aihara et al., who employed a pulse-gradient spin-echo NMR technique to monitor the diffusivity of cation ( $\text{Li}^+$ ), six different anions including  $\text{PF}_6^-$ , tetrafluoroborate ( $\text{BF}_4^-$ ), triflate ( $\text{CF}_3\text{SO}_3^-$ ), bis(trifluoromethanesulfonyl)imide (TFSI), bis(pentafluoroethanesulfonyl)imide (BETI), and bis(oxalato)-borate (BOB), and a single solvent  $\gamma$ -butyrolactone (GBL), and found that GBL moved fastest, followed by anions and then  $\text{Li}^+$  (Figure 2).<sup>28</sup> Apparently,  $\text{Li}^+$  was slowed by its

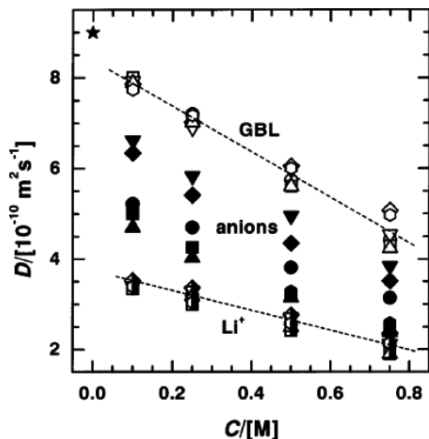


**Figure 2.** Comparison of self-diffusivities for  $\text{Li}^+$ , counter-anions, and solvent molecules and their dependences on salt concentration. The asterisk at 0 M represents  $D_{\text{GBL}}$  of neat GBL. Reprinted with permission from ref 28. Copyright 2004 Electrochemical Society.

association with solvent molecules, while anions remain almost unsolvated.

The use of mixed instead of single solvents raises complications in the effort to optimize ion conductivities. For example, in a ternary solvent mixture (which is not uncommon in commercial electrolyte compositions), thousands of electrolyte compositions might need to be experimentally prepared and measured to generate a complete conductivity contour map, which is a function of temperature, solvent composition, salt species, and concentration in a 5-D space. To circumvent this arduousness, Schweiger et al. developed an algorithm that allows one to rapidly locate conductivity maxima in such complicated environments.<sup>29</sup> On the basis of a simple geometric approach that only needs to depend on a few experimental values to start, “Simplex Algorithm” led to significant reduction of time and sample numbers as compared to the “Interpolation Approach” developed.<sup>30</sup> An initial test of this algorithm was applied to electrolytes consisting of lithium bis(oxalato)borate (LiBOB) in a few ternary and higher order solvent systems, whose isothermal conductivity at  $-25^\circ\text{C}$  is optimized with high efficiency and accuracy. However, caution needs to be exercised because, although “simplex” algorithm can always find a local maximum, it does not guarantee the global maximum be located. Judicious choice of the starting values could significantly lower this risk.

Another transport property, of importance second only to ion conductivity (at least for polymer-based electrolyte systems), is transference number, which quantifies the fraction of ion conductivity that is useful to cell chemistry. In the 2004 review, it was concluded that, differing from ion conductivity, whose measurement is mature and well-defined, transference number results vary with conflicts often arising for the same system investigated.<sup>1</sup> Little has changed since then, although the consensus remains that in those nonaqueous systems  $\text{Li}^+$  is less mobile than its counterions, mainly due to its interaction with solvent molecules or polymer matrix.<sup>31–34</sup> In a systematic study, Zugmann et al. compared four different methods often employed to determine transference numbers,<sup>34</sup> from the most popular Bruce–Vincent approach to the more recently developed pulse-field gradient NMR (pfg-NMR) technique, and concluded that the variations are consequences of different assumptions and constraints applied to establish

those individual methods. In particular, they pointed out that the deviations in pfg-NMR might be more severe for electrolytes at practical salt concentrations (ca. 1.0 M), because the technique cannot distinguish the diffusion of ion pairs and aggregations from that of the free ions, although the former do not contribute to the ionic current under electric field.

From a broader perspective, knowing only ion conductivity and transference number does not suffice to fully characterize an electrolyte and predict its behavior in a Li-ion cell. Valoen et al. believed that salt diffusivity as well as activity matter in dictating the electrochemical performance, especially under high current conditions.<sup>35</sup> They employed a series of classic electrochemical techniques to measure these properties of  $\text{LiPF}_6$  solutions as a function of salt concentration and temperature, and found  $\text{LiPF}_6$  salt activity coefficients to be constantly larger than 1 for most of the applicable salt concentrations, indicating the immobilization of solvent molecules from the bulk of “free” solvent molecules due to  $\text{Li}^+$ -solvation. As a consequence, the electrolyte solutions studied behaved as a concentrated solution even though the actual concentration was only 0.1 M. The availability of these transport parameters allowed analysis of cell performance under different current densities and concentration gradients, and it was concluded that optimization of electrolyte properties must be considered in the context of cell operation. According to Valoen et al., optimized ion conductivity alone does not necessarily predict optimum cell performance; in fact, a conductivity maximum was often deceptive for actual devices. Stewart et al. also evaluated activity coefficients of  $\text{LiPF}_6$  in typical electrolyte solutions by using both concentration cell and melting-point depression approaches, which reaffirmed salt activity coefficients to be 1.1–3.17 at a wide concentration range of 0.0625–1.0 M.<sup>36</sup> Therefore, the high activities of Li salt might be universal in typical nonaqueous electrolytes due to tight coordination of solvent molecules bound by  $\text{Li}^+$ .

## 2.2. $\text{Li}^+$ -Solvation

The interaction of  $\text{Li}^+$  with nonaqueous electrolyte solvents has been explored in more detail since 2003. These efforts can be divided into two distinct categories: (1) conventional solutions, where salt concentration is in the neighborhood of 1.0 M; and (2) highly concentrated systems, where salt exists in comparable molarities with solvent molecules. The former has been mainly spurred by the belief that  $\text{Li}^+$ -solvation sheath structure dictates the initial interphase chemistry on graphitic anodes (to be discussed in section 5.1.3 on interphase formation mechanism), while the latter is remotely related to the efforts employing highly concentrated electrolyte systems as a compromise between neat ionic liquids and conventional electrolyte solutions (to be discussed in section 3.8 on “quasi-ionic liquid” electrolytes).

## 2.3. $\text{Li}^+$ -Solvent Interaction in Electrolyte Solutions

Salt dissolves in nonaqueous media through ion–solvent interaction, and overwhelming evidences indicate that cation–solvent interaction far outweighs that between anion and solvent.<sup>37</sup> For lithium salt solutions, this might be more legitimate as  $\text{Li}^+$  is the second smallest cation, whose binding to nucleophilic sites on solvent molecules is expected to be stronger as compared to any other metal cations. Nevertheless, specific details of these interactions remain to be understood, such as (1) which nucleophilic sites of molecules interact with  $\text{Li}^+$ , (2) how many solvent molecules  $\text{Li}^+$  can accommodate in its solvation sheath, and (3) whether  $\text{Li}^+$  prefers any solvent

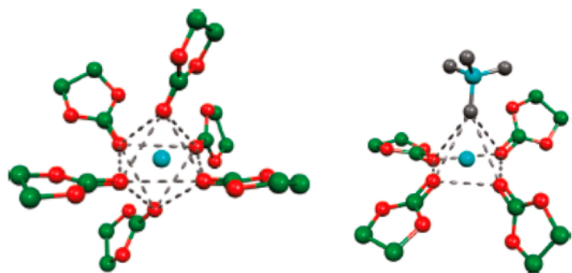


**Figure 3.** Schematic illustrations of the primary solvation sheath of  $\text{Li}^+$  in 0.1 M  $\text{LiBF}_4$  solution in EC-DMC (50:50) with different coordination numbers based on MD simulation of  $\text{LiBF}_4$  in EC/DMC. Reprinted with permission from ref 38. Copyright 2011 American Chemical Society.

molecules in the typical mixture of cyclic and acyclic carbonate solvents.

Spectroscopic and computation seemed to clearly answer the first question by identifying the carbonyl oxygen of carbonates as the binding site for  $\text{Li}^+$  (Figure 3). Both quantum calculations of free energy and molecular dynamics (MD) simulations of various lithium salts in liquid or polymer media painted the picture of a central  $\text{Li}^+$  surrounded by a number of carbonyl groups from carbonate molecules, whose lone-pair electrons should be most effective in neutralizing the Coulombic attraction of the small cation (Figure 3);<sup>38,39</sup> IR, FTIR, and Raman led to the same conclusion as the asymmetric stretching vibration of carbonyl ( $\nu_{\text{C=O}}$ ) at  $\sim 1800 \text{ cm}^{-1}$  was observed to be strongly perturbed by the dissolution of lithium salts.<sup>40–42</sup> As a more site-specific spectroscopy, NMR detected a downfield shift of carbonyls  $^{13}\text{C}$ -nuclei as result of the lithium salts addition, indicating that  $\text{Li}^+$  exerts a deshielding effect on the lone-pair electrons on carbonyl.<sup>43,44</sup> Finally, the most unambiguous answer came from the recent  $^{17}\text{O}$  NMR study, in which the chemical shifts of O-nuclei were monitored as a function of salt concentration, and it was clearly shown that carbonyl O is deshielded while ethereal O is shielded (Figure 4A).<sup>45</sup> That essentially excludes the possibility of ethereal oxygen coordinating with  $\text{Li}^+$ . Because O, instead of C, in a carbonyl

group is the structural unit that directly interacts with  $\text{Li}^+$ , the changes in  $^{17}\text{O}$ -chemical shift (9–20 ppm) were much larger than those of  $^{13}\text{C}$ -nuclei (<1.0 ppm).<sup>43,44</sup> This sensitivity has enabled higher resolution to differentiate the  $\text{Li}^+$ -solvent interaction as a function of salt concentration and solvent molecule ratio in mixtures of carbonates. A distinct change in the chemical shift of  $^{17}\text{O}$ -nuclis in EC rather than DMC was observed to correlate with salt addition (Figure 4A), and quantitative relations were hence established for two-component solvent molecules as a function of salt presence (Figure 4B).<sup>45</sup>

The coordination number of  $\text{Li}^+$  in electrolytes has been believed to be around 4–6, depending on salt concentration, dissociation versus ion-pairing, and dielectric constant of the solvents.<sup>1,37</sup> Recent studies did not change this general picture,<sup>38,40,41,45</sup> although certain departures seemed to exist.<sup>42</sup>

The third question has raised certain controversies. Although most previous literature has been inclined to believe that cyclic carbonate molecules (such as EC and propylene carbonate, or PC) are preferred by  $\text{Li}^+$  due to their higher permittivity and dipole moment,<sup>1,38,44,46–48</sup> some other, based on Raman or computation results, argued that such preferential solvation does not exist.<sup>49,50</sup> In a rare quantitative study using  $^{13}\text{C}$  NMR,<sup>43</sup> Matsubara et al. were able to compare a few solvent pairs and determined that  $\text{Li}^+$  preferential solvation did exist (Figure 5A), and the relative competitiveness of each solvent to enter the primary solvation sheath of  $\text{Li}^+$  seemed to stem from their donicity rather than their dielectric constant. Mysteriously, in their work, the solvent pairs that would be most interesting to battery researchers, that is, cyclic versus acyclic carbonate molecules, were not directly compared. Such direct comparison was eventually made by Xu et al., who used a mass spectrum technique with soft ionization to identify the composition of  $\text{Li}^+$ -solvation species as well as their abundances in the solvation shell.<sup>51</sup> The results from systematic studies undoubtedly confirmed that cyclic carbonate solvents are the preferred members of the  $\text{Li}^+$ -primary solvation sheath (Figure 5B), while neither salt species nor their concentrations have significant impact on this trend.<sup>51,52</sup> Spectral evidence from both  $^{13}\text{C}$  and  $^{17}\text{O}$  NMR has pointed to similar conclusions (Figure 4B),<sup>45,53</sup>

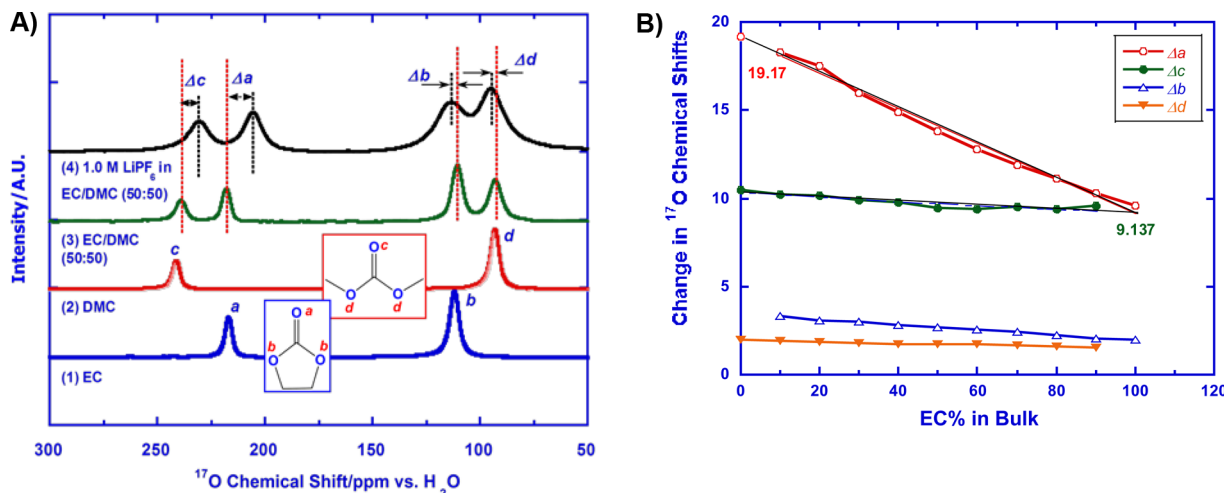


**Figure 4.** Quantitative understanding of interaction between  $\text{Li}^+$  and carbonate molecules: (A) The changes in  $^{17}\text{O}$  NMR chemical shift for cyclic (EC) and acyclic (DMC) carbonates as induced by  $\text{Li}^+$ . Note (a) the deshielding of carbonyl oxygens and shielding of ethereal oxygens and (b) the larger changes in  $^{17}\text{O}$  NMR chemical shifts for cyclic ( $\Delta a$ ) than for acyclic ( $\Delta c$ ) carbonyl oxygens. (B) The dependence of changes in  $^{17}\text{O}$  NMR chemical shifts on bulk electrolyte compositions. Note the steep slope associated with  $\Delta a$  as compared to other oxygens. Reprinted with permission from ref 45. Copyright 2013 American Chemical Society.

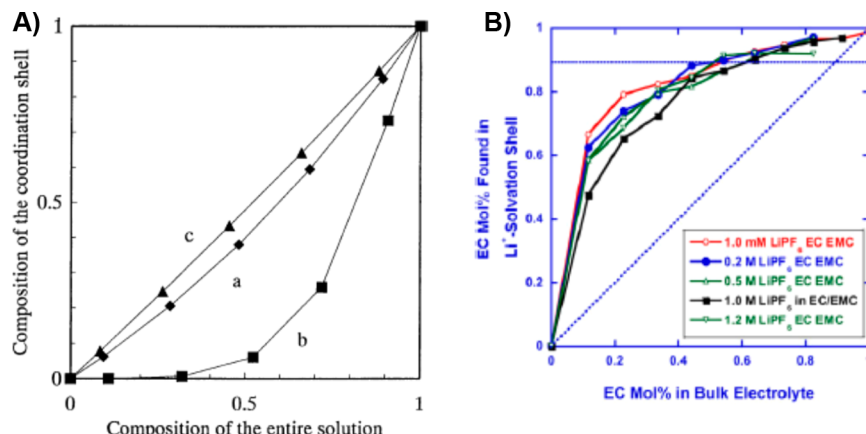


**Figure 5.** Preferential solvation of  $\text{Li}^+$  in nonaqueous electrolytes: (A) Dependence of solvent molecules as found in three solvent pairs by  $^{13}\text{C}$  NMR: (a) methyl propionate (MP)/EMC, (b) *N,N*-dimethylacetamide (DMA)/PC, and (c) MP/ethyl propionate (EP). The y-axis represents the fraction of the weakly coordinated solvent molecules. Reprinted with permission from ref 43. Copyright 1998 Royal Society of Chemistry. (B) Dependence of EC population as found in  $\text{Li}^+$ -solvation sheath with ESI-MS technique on the bulk electrolyte compositions. Reprinted with permission from ref 52. Copyright 2012 Materials Research Society. Note that the deviations from the ideal nonpreferential solvation behavior, as represented by the diagonal straight lines, were detected in both cases by two completely different techniques.

although acyclic carbonate molecules were also found to universally interact with  $\text{Li}^+$ .<sup>45</sup> It was suggested that the acyclic members most likely stay in the secondary solvation sheaths and maintain a weak but persistent interaction with the cation; however, it seemed certain that the primary solvation sheath of  $\text{Li}^+$  is generally occupied by cyclic carbonate molecules. Such a monopoly would be broken when a cosolvent of extremely high donicity was present in the solution system, such as crown ethers or glyme-based solvents.

As will be discussed later, the above asymmetric distribution of cyclic and acyclic carbonate molecules in  $\text{Li}^+$  primary solvation sheath has profound influence over the interphasial chemistry and processes on the graphitic anode within a LIB.

#### 2.4. $\text{Li}^+$ -Solvates in Concentrated Electrolytes

It remains challenging to determine accurate structures of  $\text{Li}^+$ -solvent complexes in the liquid state. As an alternative, researchers turned to study the solid (often crystalline) solvates of lithium salts and solvents, where structural tools such as X-ray single crystal or powder diffraction are widely available. The structures determined in this manner were hoped to offer remote but still reasonable clues to project the actual coordination picture between  $\text{Li}^+$  and solvent molecules in typical electrolytes.

Zavalij et al. used both powder and single crystal diffractions to study the solvates formed by a number of lithium salts, including  $\text{LiPF}_6$  and  $\text{LiBOB}$ , in various solvents.<sup>54</sup> They found that in most of the ethereal- or nitrile-based solvents,  $\text{LiBOB}$  exists in dimeric form, where the ligands act as both chelating and bridging agents, while  $\text{Li}^+$  is coordinated in an octahedral manner (Figure 6a); however, in EC solvent,  $\text{Li}^+$  is solvated tetrahedrally by 4 EC molecules, while  $\text{BOB}^-$  only acts as a counteranion in the solvate. Changing anion from  $\text{BOB}^-$  to  $\text{PF}_6^-$  or  $\text{AsF}_6^-$  results in similar structures. This peculiar configuration of  $\text{Li}(\text{EC})_4$  might reflect the most favored solvation number of  $\text{Li}^+$  in corresponding diluted solutions.

The most systematic investigations on  $\text{Li}^+$ -solvent complexes in concentrated systems were conducted by Henderson and his co-workers,<sup>55–59</sup> who applied combined tools including thermal analyses, spectroscopies, as well as MD simulations to a series of solvates formed by highly associated or highly dis-

sociated lithium salts with nitrile, ethereal, ester, and carbonate solvents, respectively. They noticed that in highly concentrated systems, the populations of solvent molecules, as compared to those of ions, were so sparse that the effect of anion on a number of thermal physical and transport properties can no longer be neglected as in diluted (i.e., ~1.0 M) electrolytes. There was a direct relation between the ion association degree versus the solvation number, as highly associated salts require fewer solvent molecules to stabilize the ions. In particular, with acetonitrile as solvent, both  $\text{LiPF}_6$  and  $\text{LiTFSI}$  form crystalline solvates with stoichiometry of  $\text{Li}(\text{AN})_6$ .<sup>57</sup> Salt concentration expectedly exerts a significant impact on the ionic species present in the solution systems. For example, by deconvoluting peaks in Raman spectra, Seo et al. established the species distribution plots for  $\text{LiTFSI}$  in AN, in which the population of uncoordinated anion  $\text{TFSI}^-$  consistently decreases with salt concentration, but remains even at very high concentrations (Figure 6b).<sup>57</sup> The transport properties, that is, viscosities and ion conductivities, of various lithium salts in AN were also investigated and correlated with the ion–solvent and ion–association properties collected by X-ray diffraction and Raman spectra.<sup>58</sup> Interestingly, the authors suggested that in these highly concentrated systems, the highest ion conductivity might correspond to the highest viscosity, as the conduction mechanism is not merely decided by the solvate species distribution, but also by the dynamics of the solvent molecules and anions in the primary solvation sheath of  $\text{Li}^+$ .

### 3. ELECTROLYTE COMPONENTS

#### 3.1. New Solvents

Electrolyte solvents must be polar enough to dissociate a salt while remaining electrochemically inert in a wide potential range (0–5.0 V vs Li). These two requirements essentially limit the choice of solvents to only a few families of aprotic organic compounds. In commercial LIBs, the electrolyte solvents were still mainly selected from the organic esters of carbonic acid, among which EC became indispensable for a number of properties; however, efforts are still being made to replace, at least partially, these carbonate-based components to achieve certain improvements over the state-of-the-art.

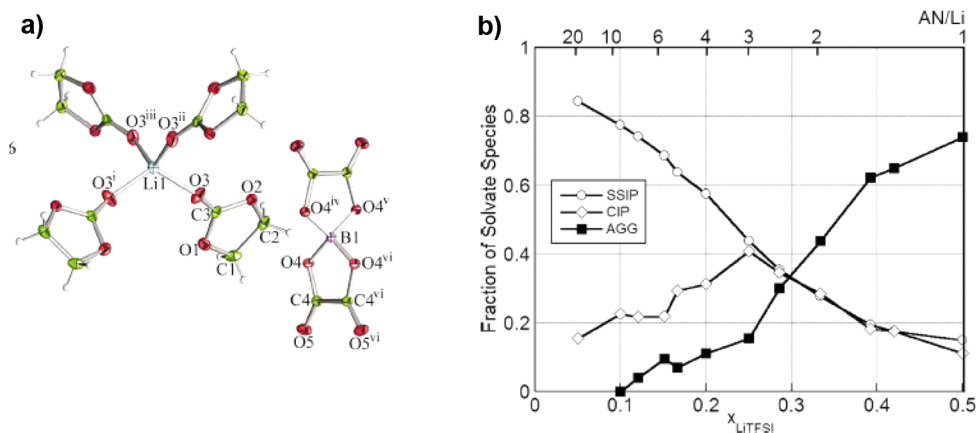


**Figure 6.** Li<sup>+</sup> solvates: (a) Crystal structure of LiBOB solvate formed in EC. Reprinted with permission from ref 54. Copyright 2004 The International Society of Crystallographer (<http://journals.iucr.org/>). (b) Distribution of Li<sup>+</sup>-solvated species in acetonitrile (AN). SSIP, CIP, and AGG stand for “solvent separated ion pair”, “close ion pair”, and “aggregation”, respectively. Reprinted with permission from ref 57. Copyright 2012 Electrochemical Society.

**Table 1. New Solvents: Acyclic Carbonates**

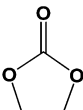
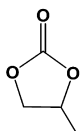
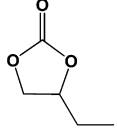
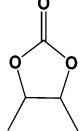
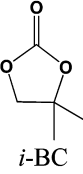
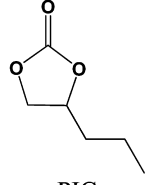
	<b>Ion Conductivity of 1:1 Mixture with EC at RT (mS/cm)</b>	<b>Reversible Capacity for the 1<sup>st</sup> cycle 1:2 in mixtures with EC (mAh/g)</b>	<b>Capacity Retention at 50<sup>th</sup> cycle (mAh/g)</b>
DMC (reference)	11.7	340	88%
n-BMC	5.9	355	93%
i-BMC	5.4	352	95%
s-BMC	6.5	358	94%

**3.1.1. Esters.** Esters were used as electrolyte solvents mainly due to their resistance to anodic decomposition (oxidation) at cathode surfaces, although their higher cathodic decomposition (reduction) potential often makes them unsuitable for anode materials operating at low potentials. Most carbonates can circumvent the latter issue kinetically by forming a SEI to prevent sustained reductions, and with stability toward surfaces of both the oxidizing cathode and the reductive anode. Improvements were made on the carbonate skeleton in an attempt to maximize these interphasial benefits, with the primary goal being suppression of irreversible capacity loss during the first cycle on graphitic anodes.

Continuing their earlier work investigating the effect of acyclic carbonate structures on cell performance,<sup>60</sup> Vetter et al. synthesized a series of new acyclic carbonates with varying degrees of chain branching, as summarized in Table 1.<sup>61</sup> Although compromises in ion conductivity occurred due to their higher viscosities, incremental improvements were obtained in both reversible capacity and cycling life when tested in graphitic anode half cells, and the effect was stronger with the branching site closer to the carbonyl. However, these benefits did not translate into full lithium ion cells with LiCoO<sub>2</sub> cathode chemistry. The rationale behind these phenomena remains to be explored.

New cyclic carbonates were synthesized by Chiba et al. as solvents of higher anodic stability limits.<sup>62</sup> Although developed

Table 2. New Solvents: Cyclic Carbonates

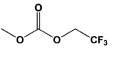
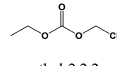
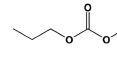
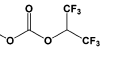
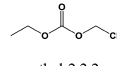
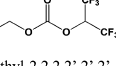
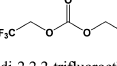
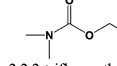
	mp/bp (°C)	$\epsilon$ (25 °C)	$\eta$ (mPa, 25 °C)	HOMO/LUMO (eV)	E <sub>ox</sub> on GC (vs. Ag <sup>+</sup> /Ag, V)
	36/238	90 (at 40 °C)	1.9 (at 40 °C)	-8.02/1.07	2.4
EC					
	-49/242	69	2.5	-7.9/1.01	2.6
PC					
	-53/241	58	3.1	-7.89/1.03	2.8
BC					
	34/243	57	2.8	-7.9/1.06	2.5
2,3-BC					
	25/234	38 (at 35 °C)	2.7 (at 35 °C)	-7.86/1.20	2.2
i-BC					
	<-45/282	46	3.5	-7.88/1.03	2.5
PIC					

for electrochemical double-layer capacitors, the results would likely apply to batteries as well. Table 2 lists these new members of the carbonate family along with their physicochemical and electrochemical properties as compared to those of EC and PC. The oxidation stability limits reported on glassy carbon (GC) vs Ag<sup>+</sup>/Ag would translate into potentials around 5.5–6.0 V vs Li, although experience told us that there is no simple and linear translation between the two.<sup>1</sup> Testing in actual electrochemical capacitors using high surface area

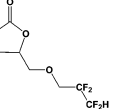
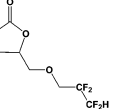
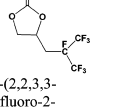
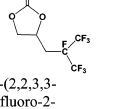
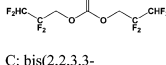
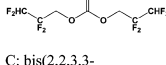
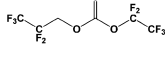
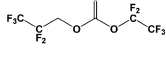
activated carbon as electrodes validated most of the results and identified 2,3-butenylene carbonate as the most anodically stable solvent, being able to withstand 3.5 V cycling. Chiba et al. concluded that any substitution by alkyl groups on the ring of cyclic carbonates would increase the oxidation stability of the solvent. The same philosophy is yet to be proved in batteries.

Fluorination is a commonly used practice to modify electrolyte solvent structures. Generally speaking, introduction of F into an ester results in the drop of energy levels for both

**Table 3. New Solvents: (A) Partially Fluorinated Acyclic Carbonates and Carbamates; (B) Partially Fluorinated Cyclic and Acyclic Carbonates; and (C) Partially Fluorinated Cyclic and Acyclic Carbonates**

A)				
methyl-2,2,2-trifluoroethyl carbonate (MTFEC)		ethyl-2,2,2-trifluoroethyl carbonate (ETFEC)	propyl-2,2,2-trifluoroethyl carbonate (PTFEC)	methyl-2,2,2,2'-hexafluoro-i-propyl carbonate (MHFPC)
		di-2,2,2-trifluoroethyl carbonate (DTFEC)		2,2,2-trifluoroethyl-N,N-dimethyl carbamate (TFCMc)
ethyl-2,2,2,2'-hexafluoro-i-propyl carbonate (EHFPC)	di-2,2,2-trifluoroethyl carbonate (DTFEC)		2,2,2-trifluoroethyl-N,N-dimethyl carbamate (TFCMc)	hexafluoro-i-propyl-N,N-dimethyl carbamate (HFPCm)

B)		$\eta$ (cP, 20 °C)	conductivity (mS/cm at 25 °C)	HOMO (eV)	LUMO (eV)
	4.79	5.5			
A: 4-(2,2,3,3-tetrafluoropropoxymethyl)-[1,3]-dioxolan-2-one				-11.85	0.67
B)		$\eta$ (cP, 20 °C)	conductivity (mS/cm at 25 °C)	HOMO (eV)	LUMO (eV)
	4.79	5.5			
B: 4-(2,2,3,3-tetrafluoro-2-trifluoromethyl-propyl)-[1,3]-dioxolan-2-one				-12.27	-0.01
C)		$\eta$ (cP, 20 °C)	conductivity (mS/cm at 25 °C)	HOMO (eV)	LUMO (eV)
	0.80	0.89			
C: bis(2,2,3,3-pentafluoro-propyl) carbonate				-11.93	0.16
D)		$\eta$ (cP, 20 °C)	conductivity (mS/cm at 25 °C)	HOMO (eV)	LUMO (eV)
	0.80	0.89			
D: bis(2,2,3,3-tetrafluoro-propyl) carbonate				-12.40	-0.30

the highest occupied molecular orbital (HOMO) and the lowest unoccupied molecular orbital (LUMO). The former will lead to higher resistance against oxidation, while the latter to poorer resistance against reduction, which might seem to be a disadvantage, but as taught by preceding experiences and knowledge about interphasial chemistry,<sup>1</sup> it could also signify better (denser) SEI film as the formation starts at a higher potential. For this reason, there have been numerous efforts in fluorinating both cyclic and acyclic carbonates.

Extending their work on low temperature electrolytes using various esters, Smart et al. synthesized a series of partially fluorinated acyclic carbonates and carbamates, and formulated ternary and quaternary electrolytes using them.<sup>63</sup> Table 3A summarizes these new solvents. The mixtures of these carbonates with EC, DMC, and DEC all resulted in benefits such as low temperature performance, high temperature resistance, high Li<sup>+</sup>-transport kinetics, as well as improved safety, probably stemming from a better SEI on anode. The carbamates, however, introduced either higher polarization or mediocre improvements over the state-of-the-art. Table 3B lists more partially fluorinated cyclic and acyclic carbonates that

were reported by Achiha et al.,<sup>64</sup> who used them as cosolvents in typical EC-based electrolytes and found that the oxidative reaction at the Pt surface was suppressed by the addition of compounds A, B, or C (Figure 7A and Table 3B). On the other hand, the reduction of these fluorinated compounds indeed occurred at much higher potential (>2.0 V vs Li, Figure 7B). However, reversible capacity of the graphitic anode in the presence of these fluorinated carbonates was not affected as compared to the baseline electrolytes, and Coulombic efficiency in the first cycle was generally improved. Even with high PC concentration, this improvement remained due to the interphasial chemistry brought forth by these fluorinated carbonates, strongly indicating their participation in SEI formation.<sup>64,65</sup>

The oxidation stability of fluorinated solvents were further confirmed with a cathode of higher voltage, LiNi<sub>0.5</sub>Mn<sub>1.5</sub>O<sub>4</sub> (4.6 V).<sup>11</sup> Zhang et al. formulated electrolytes for this 5 V class chemistry using a number of partially fluorinated solvents including cyclic (same as B in Table 3B) or acyclic carbonate (same as MTFEC in Table 3A) with a highly fluorinated ether (F-EPE, Table 9). Their stability withstood a series of rigorous

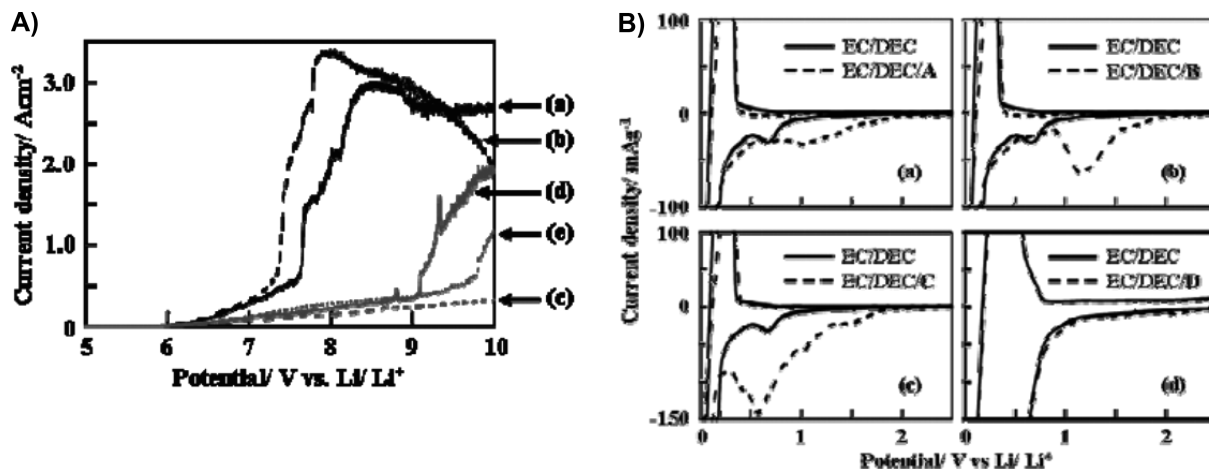


**Figure 7.** Effect of fluorinated carbonates: (A) on oxidative decomposition in electrolyte solutions based on  $\text{LiClO}_4$  in equal-volume mixtures of various solvents, (a) EC/DEC; (b) EC/DEC/PC; (c) EC/DEC/A; (d) EC/DEC/B; (e) EC/DEC/C; and (B) on reductive decomposition at graphitic anodes. Reprinted with permission from ref 64. Copyright 2009 Electrochemical Society.

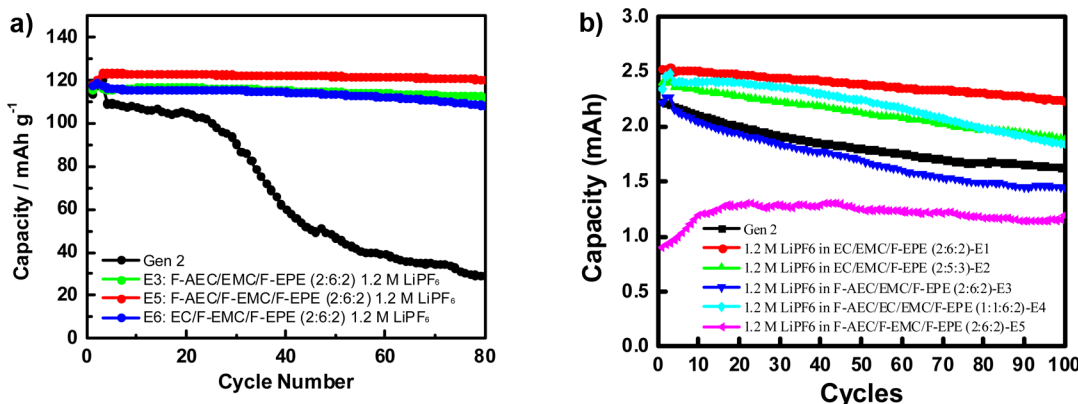


**Figure 8.** Effect of fluorinated carbonates and ethers: The cycling performance of fluorinated electrolytes in full lithium ion cells based on either (a)  $\text{LiNi}_{0.5}\text{Mn}_{1.5}\text{O}_4/\text{Li}_4\text{Ti}_5\text{O}_{12}$  at elevated temperatures ( $55^\circ\text{C}$ ) or (b)  $\text{LiNi}_{0.5}\text{Mn}_{1.5}\text{O}_4$ /graphitic cells at ambient temperature. Reprinted with permission from ref 11. Copyright 2013 Royal Society of Chemistry.

tests on the highly oxidizing surface of  $\text{LiNi}_{0.5}\text{Mn}_{1.5}\text{O}_4$ . Figure 8a and b showed the cycling performance of these electrolytes in full lithium ion cells of either  $\text{LiNi}_{0.5}\text{Mn}_{1.5}\text{O}_4/\text{Li}_4\text{Ti}_5\text{O}_{12}$  or  $\text{LiNi}_{0.5}\text{Mn}_{1.5}\text{O}_4$ /graphite at both ambient and elevated temperatures ( $55^\circ\text{C}$ ). Density function theory (DFT) calculations conducted on the B3LYP/6-311+G(3df, 2p) basis set indicated that the HOMO and LUMO energies were simultaneously lowered as result of fluorination, as Table 3C summarizes.

As compared to carbonates, esters of carboxylic acids generally did not form protective SEI on graphitic anodes; therefore, they were always used at low concentrations together with their carbonate counterparts. Nevertheless, their presence in electrolytes offered certain advantages, such as wider service temperature ranges, better solubility toward certain salts, or faster interfacial kinetics.<sup>1</sup> Lactones serve as such an example: the LiPF<sub>6</sub> solution in GBL induced high irreversibility on graphitic anodes, while LiBF<sub>4</sub> in GBL solution only found a niche market in commercial LIB due to the much lower power density caused by lower conductivity. However, this class of solvents seems to be a perfect match for LiBOB, which does not dissolve to above 0.8 M when cyclic carbonate (EC) was less than 50% of the solvents in a carbonate-only electrolyte, but dissolved readily above 1.0 M as long as lactones were

present above 20%. Figure 9 shows the cell resistance measured for various LiBOB solutions, which indicated the apparent incompatibility between LiBOB and carbonates, while GBL solutions were almost as conductive as the state-of-the-art electrolytes.<sup>66</sup> These electrolytes based on LiBOB and GBL proved to be electrochemically stable, allowing cells to be cycled for over several thousand cycles at ambient temperature with negligible capacity losses, or with less than 12% loss over 800 cycles at  $75^\circ\text{C}$ .<sup>67</sup> The success of LiBOB/GBL combination should be at least partially attributed to the known fact that  $\text{BOB}^-$  is capable of participating in the formation of a rather protective SEI, which complements exactly what GBL/LiPF<sub>6</sub> combination fails to provide in the interphasial chemistry.<sup>1</sup>

Linear carboxylate esters were mainly employed as cosolvents due to their low viscosity and moderate stability against oxidation, which could introduce significant benefits in terms of low temperature ( $<-30^\circ\text{C}$ ) performance, usually the focus of interest for space applications. Yet their less-than-ideal interphasial chemistry on graphitic anodes often required the presence of carbonates or extra additives. Smart and co-workers at Jet Propulsion Lab did perhaps the most exhaustive research on low temperature electrolyte formulations since the late 1990s.<sup>1</sup> The recent work from the group has expanded the lower limit of LIB's service temperature range to  $-60^\circ\text{C}$ , using

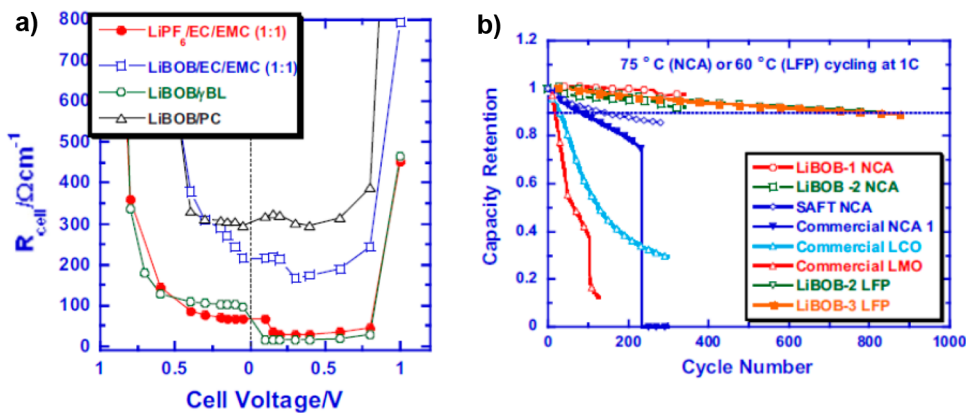


**Figure 9.** LiBOB-based electrolytes: (a) Comparison of overall cell resistance derived from AC impedance for graphitic half-cells operating in various electrolytes during the first lithiation (left) and delithiation (right) cycle. Reprinted with permission from ref 66. Copyright 2008 Electrochemical Society. (b) Improved cycling performance of lithium-ion cells at elevated temperatures (75 °C for  $\text{LiNi}_{0.85}\text{Co}_{0.10}\text{Al}_{0.05}\text{O}_2$  or NCA and 60 °C for  $\text{LiFePO}_4$  or LFP). Also shown for comparison are a few commercial LIB from different manufacturers under the same testing conditions (LCO =  $\text{LiCoO}_2$ , LMO =  $\text{LiMn}_2\text{O}_4$ ). Reprinted with permission from ref 67. Copyright 2008 Electrochemical Society.

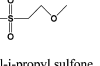
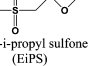
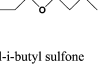
**Table 4. (A) New Solvents: Linear Carboxylates; and (B) Acyclic Carboxylates, Borates, and Aluminates**

A)	mp/bp (°C)	$\eta$ (cP, 25 °C)	$\epsilon$	B)	mp/bp (°C)	$\epsilon$ (25 °C)	T <sub>g</sub> (°C)
	-84/77				-100/33	8.5	
ethyl acetate				methyl formate			
	-87.5/79.8	0.431	6.2		-80/53	7.1	
methyl propionate				ethyl formate			
	-75/99				-84/77	6	
ethyl propionate				ethyl acetate			
	-85.8/102.8	0.541	5.48		/86		
methyl butyrate				methyl difluoroacetate			
	-93/120	0.639	5.18				
ethyl butyrate				B-PEG			
	-95.2/143		4.3				
propyl butyrate				Al-PEG			
	-91.5/164						
butyl butyrate							

a series of carboxylates (Table 4A) along with additives such as vinyl carbonate (VC), monofluoro ethylene carbonate (FEC), and LiBOB.<sup>68,69</sup> The balance between excellent low temperature performance and high temperature resilience seems to

depend on the ratio between EC and those linear carboxylates, with 20% of each in addition to an acyclic carbonate being the best compromise. In cells of  $\text{LiNi}_x\text{Co}_{1-x}\text{O}_2$ /graphite chemistry, such blended formulations delivered >60% of nominal capacity

**Table 5.** (A) New Solvents: Functionalized Sulfones; (B) Linear Sulfones with Branched Alkyl Substituents; and (C) Sulfones with Ether Functional Groups

A)	mp (°C)	$\sigma$ (mS/cm, 25 °C)	$E_{ox}$ (V vs. Li)	B)	mp/bp (°C)	$\epsilon$ (25 °C)	$\eta$ (mPa, 25 °C)	C)	mp/bp (°C)	$\epsilon$ (25 °C)	T <sub>g</sub> (°C)
	-23	-2.0	> 5.0		16/238	55	9.5		-100/33	8.5	
tetramethylene sulfone (sulfolane, or TMS)				methyl-i-propyl sulfone (MiPS)				methyl-i-propyl sulfone (MiPS)			
	33	~2.0	> 5.0		-8/265	55	5.6		-80/53	7.1	
ethylmethyl sulfone (EMS)				ethyl-i-propyl sulfone (EiPS)				ethyl-i-propyl sulfone (EiPS)			
	44	0.35	4.2		-15/261	36	5.5				
butyl sulfone (BS)				ethyl-i-butyl sulfone (EiBS)				ethyl-i-butyl sulfone (EiBS)			
	50	~0.2	~4.5		2/255	42	6.3				
1-fluoro-2-(methylsulfonyl)benzene (FS)				i-propyl-i-butyl sulfone (iPiBS)				i-propyl-i-butyl sulfone (iPiBS)			
	<-40	-3.0	4.2		-20/260	52	6.3				
ethyl vinyl sulfone (EVS)				i-propyl-s-butyl sulfone (iPsBS)				i-propyl-s-butyl sulfone (iPsBS)			
					1/302	26	8.4				
				butyl-i-butyl sulfone (BiBS)				butyl-i-butyl sulfone (BiBS)			

at  $-60^{\circ}\text{C}$  with reasonable rate capability, while maintaining sufficient stability against thermal aging at  $+60^{\circ}\text{C}$ . Yaakov et al. took a similar approach using formates and acetates as cosolvents and VC or LiBOB as additives to assist in forming interphases on graphitic anodes (Table 4B).<sup>70</sup> They set criteria for a successful low temperature electrolyte as (1) ion conductivity  $>1$  mS/cm at  $-40^{\circ}\text{C}$ ; and (2) ability to work in a temperature range of  $-40$  to  $+60^{\circ}\text{C}$ , considering that the introduction of carboxylate esters always constitutes a challenge to the high temperature resilience. The graphitic anode was identified as the “bottleneck” for operations at subzero temperatures rather than cathode, most likely due to the protective interphase there that would become rather resistant because of sluggish Li<sup>+</sup>-transport kinetics.

A rare EC-free electrolyte was reported by Sato et al., who formulated a thermally safe electrolyte using a partially fluorinated ester, methyl difluoroacetate (MFA, Table 4B), as single solvent and VC as additive.<sup>71</sup> The presence of VC was required because MFA failed to form a protective SEI on graphitic anodes. This electrolyte enabled natural graphite to deliver  $\sim 350$  mAh/g reversible capacity and remain thermally stable up to  $450^{\circ}\text{C}$ , ca.  $200^{\circ}\text{C}$  above the thermal decomposition of typical carbonate electrolytes. However, the stability of this electrolyte with cathode chemistries was not described.

Esters of inorganic acid were also considered as possible candidates as new electrolyte solvents. Kaneko et al. synthesized a few polyethylene glycol esters with borate (B-PEG) and aluminate (Al-PEG) (Table 4B), in the hope that they would bring nonflammability to LIB.<sup>72</sup> Yet electrolytes based on both classes showed poor ion conduction as well as electrochemical instability on cathode surfaces such as LiCoO<sub>2</sub> and LiFePO<sub>4</sub>. Strangely, dispersion of ceramic powder AlPO<sub>4</sub> in

such electrolytes significantly improved the cycling performance of the cathode half cells. The authors attributed this to the possible involvement of AlPO<sub>4</sub> in interphasial chemistry. However, even the improved performance remained noncompetitive against typical state-of-the-art electrolytes. Furthermore, the stability of these B-PEG- and Al-PEG-based electrolytes with graphitic anodes has not been described.

**3.1.2. Sulfones and Sulfoxides.** Alkyl sulfones were known for their high dielectric permittivity, low flammability, and excellent anodic stability on various cathode surfaces, but their application in actual LIB was mainly constrained by (1) their inability to form a protective interphase on graphitic anodes, and (2) the poor ion conductivity and wettability toward electrodes and separators, both of which were caused entirely or partially by their high viscosities.<sup>1</sup> Nevertheless, as cathode chemistries of higher voltages were explored, sulfones continued to attract attention as possible electrolyte solvents.

As the pioneer who brought sulfones into solvent repertoire for room temperature electrolytes, Angell and co-workers extended their exploration of this class of highly polar and highly viscous molecules.<sup>73–77</sup> To resolve the issue with high viscosity, they investigated a series of binary systems, including both all-sulfones and sulfone/carbonate mixtures, and reported that ion conductivity of these systems could become comparable to carbonate-based electrolytes at temperatures above  $55^{\circ}\text{C}$ , but ionic movement is severely hindered at ambient or lower temperatures. By applying the classical Walden rule analysis, they came to the conclusion that the loss of potential ion conductivity at these temperatures mainly originated from higher ion association.<sup>73</sup>

The electrochemical stability of sulfones at high voltages outweighs its disadvantage in ion conduction. Abouimrane et al. compared the anodic stability of five cyclic and linear sulfones

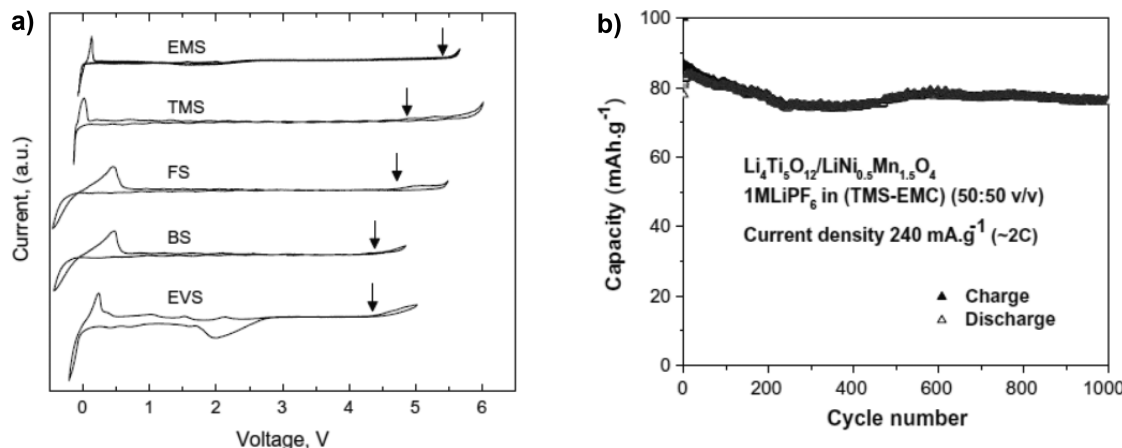


**Figure 10.** Sulfone-based electrolytes: (a) Cyclic voltammograms of 1.0 M LiTFSI in various neat sulfones on Pt working electrode; and (b) cycling performance of a full lithium ion cell based on  $\text{LiNi}_{0.5}\text{Mn}_{1.5}\text{O}_4/\text{Li}_4\text{Ti}_5\text{O}_{12}$  in 1.0 M  $\text{LiPF}_6$ /tetramethylene sulfone/DMC. Reprinted with permission from ref 78. Copyright 2009 Elsevier.

(Table 5A) on Pt working electrodes and concluded that high anodic stability arises from all of them (Figure 10a), with ethylmethyl sulfone (EMS) and tetramethylene sulfone (TMS) being the most resistant to oxidation.<sup>78</sup> When full cells consisting of  $\text{LiMn}_2\text{O}_4/\text{Li}_4\text{Ti}_5\text{O}_{12}$  were tested in electrolytes based on these sulfones as single solvents, stable performances were obtained for hundreds of cycles at high current densities without detectable capacity fade. These results, while confirming the previously reported high anodic stability of sulfones, should be also attributed to the  $\text{Li}_4\text{Ti}_5\text{O}_{12}$  anode used, which operates at 1.5 V vs Li and therefore does not require the formation of an interphase, an ability that almost all sulfones lack.<sup>1</sup> To improve the wettability of sulfone toward electrodes and separator, TMS was mixed with a low viscosity carbonate EMC and tested on a high voltage cathode  $\text{LiNi}_{0.5}\text{Mn}_{1.5}\text{O}_4$ . The extraordinary cell longevity proved that the presence of acyclic carbonates, known for low anodic stability,<sup>79</sup> did not affect the overall stability of the mixture, indicating that the cathode interphase chemistry might be dominated by sulfone instead of its carbonate cosolvent (Figure 10b).

Chiba et al. also described eight linear sulfones with varying branching alkyl side groups (Table 5B).<sup>80</sup> Similar to their carbonate work, these new solvents were originally developed for electrochemical double layer capacitors; however, they would be LIB electrolytes candidates of high interest as well, so is the insight gained regarding the decomposition mechanism. Among these sulfones, ethyl-iso-propyl sulfone (EiPS) and ethyl-iso-butyl sulfone (EiBS) were identified as promising, with properties balanced among anodic stability on activated carbon, liquid range, solubility toward tetraalkyl ammonium salts, as well as ion conductivity. As compared to PC, EiPS could provide extra potential stability of 1.0 V on activated carbon surface, which is significant because the energy output is proportional to the square of operating voltage in this case. Detailed characterizations, including surface and gaseous product analyses, were conducted in an attempt to identify the fundamental reason why sulfones are more stable than carbonates, and the superior anodic stability of EiPS was attributed to its inertness toward water generated by the electrodes upon charging, which would react with carbonates via a hydrolysis procedure and trigger a series of degradation reactions. Xue et al. evaluated a number of all-sulfone and sulfone/carbonate mixtures on both graphitic anode and high

voltage cathode.<sup>74</sup> While the presence of fluorinated sulfone did help with SEI formation at graphitic anode, the anodic stability at  $\text{LiMn}_{1.5}\text{Ni}_{0.5}\text{O}_4$  surface was compromised as evidenced by the fading capacity; on the other hand, a sulfone/carbonate (EMS/DMC) mixture was found to be a more proper system in supporting the high voltage cathode.

Attempts were also made to derivatize sulfones so that their high viscosity and melting point could be managed and interphasial chemistry improved. Sun et al. synthetically attached oligoether linkages of varying lengths to sulfone (Table 5C).<sup>75–77,81</sup> Varying degrees of success were described in half or full lithium test cells despite the concerns of low oxidation stability of ether linkages. Computations on different levels were carried out to identify the functionalities responsible for the oxidative decomposition at high potentials, and experimentally measured oxidation limits were reproduced.<sup>81</sup> Apparently, the stronger electron-withdrawing sulfonyl group (as compared to carbonyl in carbonate molecules) serves to lower the energy level of the HOMO, contributing to higher stability of electrolyte/cathode interface.

Beside the new members added to sulfone family, the commercially available tetramethylene sulfone (TMS or sulfolane, Table 5A) was also more thoroughly explored. Li et al. used a TMS/DEC solvent mixture tailored for LiBOB.<sup>82</sup> This clever combination circumvented two issues that had been troubling LiBOB and TMS respectively, that is, (1) the less-than-ideal solubility of the former in carbonate-based solvents and (2) the inability of the latter to form protective SEI on graphite anodes. The two components complemented each other and formed an electrolyte that supports full lithium ion cells consisting of graphite and  $\text{LiFePO}_4$  with superior reversibility. A 5.3 V oxidation stability of LiBOB/TMS/DEC was obtained via cyclic voltammetry (CV) on a nonporous working electrode, although this high stability limit needs to be further confirmed on a true cathode surface of high operating potential (>4.5 V).

Using MD simulations, Xing et al. attempted to decipher why the anodic stability of sulfone/acyclic carbonate mixture is usually characterized by sulfone instead of carbonate.<sup>83</sup> They found that, for mixtures such as  $\text{LiPF}_6$  in TMS/DMC, the interfacial layer solvent composition might deviate from bulk composition due to preferential adsorption by one of the solvent molecules. TMS happens to preferentially adsorb on the positive electrode surface due to its electron-rich oxygens;

hence, the anodic chemistry would be dominated by its decomposition. Meanwhile, DMC (or other acyclic carbonates) would stay further away from the cathode by ca. 0.8 Å; therefore, its electrochemical oxidation becomes less likely than in EC/DMC mixtures.

As compared to sulfones, sulfoxides are intrinsically susceptible to oxidation due to their insufficient oxidation state (IV vs VI for sulfone). Nevertheless, their possible role as solvents for batteries was also investigated. Sirenko et al. formulated a series of electrolytes using various lithium salts dissolved in dimethyl sulfoxide (DMSO), and found their ion conductivity ranged between 3.2 mS/cm for lithium benzosulfonate ( $\text{LiSO}_3\text{C}_6\text{H}_5$ ) and 11 mS/cm for lithium perchlorate ( $\text{LiClO}_4$ ).<sup>84</sup> The testing of them on cathode materials  $\text{LiMnO}_2$  and  $\text{V}_2\text{O}_5$ , though, confirmed that DMSO did experience oxidation. On the other hand, DMSO has been known to cointercalate with  $\text{Li}^+$  into graphite at ca. 1.0 V vs Li, forming stable ternary graphite-intercalation compounds. This characteristic would disqualify its candidacy as an electrolyte solvent for a number of reasons.<sup>1</sup> However, the recent studies of Yamada et al. shed new insight into the possibility of suppressing this cointercalation.<sup>85</sup> They reported that the intercalation behavior of DMSO-based electrolytes were drastically altered when lithium salt is sufficiently concentrated (~3.2 M), where cointercalation no longer occurred; instead, intercalation of bare  $\text{Li}^+$  was enabled at <0.5 V vs Li. Raman spectra seemed to suggest that the solvation number of  $\text{Li}^+$  by DMSO molecule is the key. This might open new avenues for sulfoxides to be considered as a possible solvent for lithium ion and other rechargeable battery chemistries given that their anodic stability could be resolved.

**3.1.3. Nitriles.** Acetonitrile has been used as electrolyte solvent with popularity only second to esters, thanks to the rare combination of a decent dielectric permittivity and a low viscosity (Table 6), the consequence of which is superior ion conductivities (>30 mS/cm at 25 °C) of acetonitrile-based electrolytes as compared to their carbonate counterparts (<10 mS/cm). Its narrow electrochemical stability window, however, often limits its applications within electrochemical double layer capacitors.

Since 2003, a large number of nitriles were explored for their potential as electrolyte solvents (Table 6),<sup>86–93</sup> among which alkoxy-substituted nitriles were developed to enable high rate capabilities of  $\text{Li}_4\text{Ti}_5\text{O}_{12}$ -based cells, while dinitriles were also developed to increase oxidation stability limits against high voltage cathode chemistries or resistance against thermal degradations.

Wang et al. formulated a series of electrolytes using alkoxy-nitriles (3-methoxypropionitrile or MPN, 3-ethoxypropionitrile or EPN, and (2,2,2-trifluoro)ethoxypropionitrile or FEPN), with or without partial fluorination, and tested their performances in full lithium ion cells based on  $\text{LiCoO}_2/\text{Li}_4\text{Ti}_5\text{O}_{12}$  chemistries.<sup>86,87</sup> These cells were reported to deliver 75% of the nominal capacity under 10–20 C rates. Apparently, the higher operating potential of  $\text{Li}_4\text{Ti}_5\text{O}_{12}$  (~1.5 V vs Li) helps as no interphase is expected to be formed under these conditions. Surprisingly, the ion conductivities of these electrolytes (1.0 M LiTFSI solutions) are not particularly high (3–6 mS/cm at ambient temperature as compared to 8–10 mS/cm of their carbonate-counterparts), indicating a decoupling of electrochemical performances from the bulk ion conductivity. On the other hand, Gmitter et al. tested MPN-based electrolytes on

graphitic anodes, and found that an effective SEI can only be formed in the presence of VC or FEC additives.<sup>88</sup>

Davidson, Abu-Lebdeh, and co-workers explored dinitriles rather exhaustively.<sup>89–92</sup> LiTFSI in adiponitrile (ADN) and glutaronitrile (GLN) was reported to show an oxidation stability limit of 6.0 V vs Li on Pt electrode, but failed to form an interphase to support lithiation chemistry at graphitic anodes.<sup>90,91</sup> Varying degrees of success were obtained in the presence of cosolvents, such as EC, or additives, such as LiBOB. On high voltage cathode  $\text{LiNi}_{0.5}\text{Mn}_{1.5}\text{O}_4$ , it was found that the dinitriles with longer aliphatic chains ( $n > 4$ ) tended to decompose more easily, while dinitriles of shorter aliphatic chains withstood oxidation at the cathode better. However, a contradictory conclusion was withdrawn by Nagahama et al. using a similar approach. They screened a series of dinitriles by cyclic voltammetry and identified sebaconitrile (SEN) as the most anodically stable solvent, yielding an 6 V window on GC electrode or up to 5.0 V on  $\text{LiCoPO}_4$  (Figure 11A).<sup>93</sup> To further confirm the anodic stability of SEN-based electrolytes, they even successfully delithiated  $\text{Li}_2\text{NiPO}_4$  at 5.3 V in the electrolyte of 1.0 M  $\text{LiBF}_4/\text{EC}/\text{DMC}/\text{SEN}$  (Figure 11B). While this electrochemical process might occur at the highest potential ever reported, its sustainability remains a challenge.

In summary, similar to sulfones, nitriles did exhibit peculiar anodic behavior on various cathode surfaces; however, fundamentals of the interfacial chemistry remain to be understood, and overall cycling stability still needs major improvement for this class of solvents to become a feasible electrolyte component.

**3.1.4. Phosphorus-Based Solvents.** Phosphorus-based organic solvents were often used as nonflammable cosolvents to retard possible fire hazard for possible LIB abuse, governed by the radical propagation mechanism usually associated with phosphorus-containing species. The pioneering efforts using various phosphates have been summarized in the 2004 review.<sup>1</sup> More recently, new classes of phosphonates, phosphazenes, and phosphates were added to the family of phosphorus-based solvents (Table 7), with the aims ranging from reducing flammability to enhancing anodic stability against high voltage cathode materials.<sup>94–97</sup>

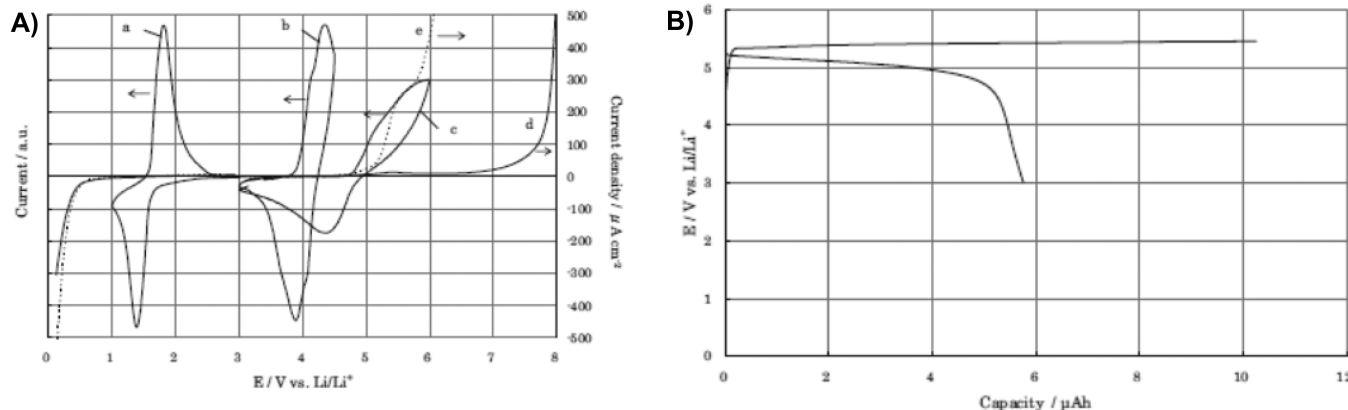
Lucht and co-workers reported dimethyl methylphosphonate (DMMP) first as a flame-retardant cosolvent, then as a high voltage additive. In the first instance, 15–20% of DMMP was used in EC/EMC baseline electrolytes with or without LiBOB additive. Differing from phosphates, no impact by phosphonates on ion conductivity was observed.<sup>94</sup> Significant reduction in self-extinguishing time (SET) was achieved at both concentrations (1.8 s for 15% and 0.8 s for 20%), rendering the electrolytes essentially nonflammable. Tests in anode (graphitic carbon) and cathode ( $\text{LiNi}_{0.8}\text{Co}_{0.2}\text{O}_2$ ) half cells as well as full lithium ion cells indicated that the presence of LiBOB was necessary for stable performance, and there was still a trade-off between capacity and safety. In the second instance, 0.5–1.0% DMMP was used as an additive in baseline electrolyte and tested on  $\text{LiNi}_{0.5}\text{Mn}_{1.5}\text{O}_4$  high voltage cathode up to 4.9 V vs Li.<sup>95</sup> Improvement in capacity retention was described, and postcycling surface analyses via X-ray photoelectron spectroscopy (XPS), scanning electron microscopy (SEM), and surface infrared (IR) spectra suggested that the presence of DMMP was responsible for the inhibition of electrolyte oxidative decomposition at the cathode. At elevated temperatures (85 °C), DMMP also assisted in preventing Mn-dissolution from  $\text{LiNi}_{0.5}\text{Mn}_{1.5}\text{O}_4$  cathode.

Table 6. New Solvents: Alkoxy-nitriles and Dinitriles

	mp/bp (°C)	$\epsilon$ (25 °C)	$\eta$ (cP, 25 °C)
$\text{H}_3\text{C}-\text{C}\equiv\text{N}$ acetonitrile (AN)	-43.8/81.6	36.6	0.37
$\text{H}_3\text{C}-\overset{\text{H}_2}{\underset{\text{O}}{ }}-\overset{\text{H}_2}{\underset{\text{C}}{ }}-\overset{\text{H}_2}{\underset{\text{C}}{ }}-\text{C}\equiv\text{N}$ 3-methoxypropionitrile (MPN)	-57/165	36	1.1
$\text{H}_3\text{C}-\overset{\text{H}_2}{\underset{\text{C}}{ }}-\overset{\text{H}_2}{\underset{\text{O}}{ }}-\overset{\text{H}_2}{\underset{\text{C}}{ }}-\overset{\text{H}_2}{\underset{\text{C}}{ }}-\text{C}\equiv\text{N}$ 3-ethoxypropionitrile (EPN)			
$\text{F}_3\text{C}-\overset{\text{H}_2}{\underset{\text{C}}{ }}-\overset{\text{H}_2}{\underset{\text{O}}{ }}-\overset{\text{H}_2}{\underset{\text{C}}{ }}-\overset{\text{H}_2}{\underset{\text{C}}{ }}-\text{C}\equiv\text{N}$ (2,2,2-trifluoro)ethoxypropionitrile (FEPN)	/172		
$\text{N}\equiv\text{C}-\overset{\text{H}_2}{\underset{\text{C}}{ }}-\text{C}\equiv\text{N}$ malononitrile (MAN)	31/220	48 (30 °C)	
$\text{N}\equiv\text{C}-\overset{\text{H}_2}{\underset{\text{C}}{ }}-\overset{\text{H}_2}{\underset{\text{C}}{ }}-\text{C}\equiv\text{N}$ succinonitrile (SCN)	54/266	55 (55 °C)	2.7 (60 °C)
$\text{N}\equiv\text{C}-\left(\overset{\text{H}_2}{\underset{\text{C}}{ }}\right)_3-\text{C}\equiv\text{N}$ glutaronitrile (GLN)	-29/287	37	5.3
$\text{N}\equiv\text{C}-\left(\overset{\text{H}_2}{\underset{\text{C}}{ }}-\overset{\text{H}_2}{\underset{\text{C}}{ }}\right)_2-\text{C}\equiv\text{N}$ adiponitrile (ADN)	1/295	30	6.1
$\text{N}\equiv\text{C}-\left(\overset{\text{H}_2}{\underset{\text{C}}{ }}\right)_5-\text{C}\equiv\text{N}$ pimelonitrile (PMN)	-31/175 (14 mmHg)	28	7.6
$\text{N}\equiv\text{C}-\left(\overset{\text{H}_2}{\underset{\text{C}}{ }}\right)_6-\text{C}\equiv\text{N}$ suberonitrile (SUN)	-4/325	25	8.2
$\text{N}\equiv\text{C}-\left(\overset{\text{H}_2}{\underset{\text{C}}{ }}\right)_7-\text{C}\equiv\text{N}$ azelanitrile (AZN)	-18/209 (33 mmHg)	23	8.7
$\text{N}\equiv\text{C}-\left(\overset{\text{H}_2}{\underset{\text{C}}{ }}-\overset{\text{H}_2}{\underset{\text{C}}{ }}\right)_8-\text{C}\equiv\text{N}$ sebaconitrile (SEN)	8/220	22	10.7

Jin et al. reported two new phosphates that contain ether-linkages as cosolvents for nonflammable electrolytes. At 30% concentration, nonflammability was achieved, at the expense of negligible compromises in ion conductivity and electrochemical performance in LiFePO<sub>4</sub> half cells.<sup>96</sup> Sazhin et al. resorted to phosphazene compounds for the same purpose, and synthesized two new compounds of the family.<sup>97</sup> Like sulfones and nitriles, one of the challenges that these phosphorus-based solvents must face is their inability to form a protective SEI on

graphitic anodes; hence, electrolytes containing them would always require an additive such as VC or LiBOB to work in a full lithium ion cell. The recent work of Takeuchi et al. shed some light on the cathodic behavior of phosphates.<sup>98</sup> Using trimethylphosphate (TMP), which has been known for its poor interphasial chemistry, they added calcium bis(trifluoromethanesulfonyl)imide (Ca(TFSI)<sub>2</sub>) to the electrolyte mixture and found the dramatic transition in interphasial property as Ca(TFSI)<sub>2</sub> concentration reaches 0.2 M and above, from the typical cointercalation and exfoliation



**Figure 11.** Nitrile-based electrolytes: (A) Cyclic voltammogram of (a) Li<sub>4</sub>Ti<sub>5</sub>O<sub>12</sub>, (b) LiMn<sub>2</sub>O<sub>4</sub>, (c) LiCoPO<sub>4</sub>; (d) glassy carbon with 1.0 M LiBF<sub>4</sub>/EC/DMC/sebaconitrile (25:25:50) and (e) glassy carbon with 1.0 M LiBF<sub>4</sub>/EC/DMC (50:50); and (B) charge–discharge profile of Li<sub>2</sub>Ni<sub>0.98</sub>Co<sub>0.02</sub>PO<sub>4</sub>F in 1.0 M LiBF<sub>4</sub>/EC/DMC/sebaconitrile (25:25:50). Reprinted with permission from ref 93. Copyright 2010 Electrochemical Society.

**Table 7. New Solvents: Phosphorus-Based Solvents<sup>a</sup>**

	%	σ/mS/cm (20 oC)	Self-extinguishing time (SET)/s
	0	8.0	33.4
dimethyl methylphosphonate (DMMP)	15	8.5	1.8
	20	8.3	0.8
	0	7.4	200*
dimethyl(2-methoxyethoxy)methylphosphonate (DMMEMP)	30	4.7	15*
	0	7.4	200*
diethyl(2-methoxyethoxy)methylphosphonate (DEMEMP)	30	6.4	10*
	R <sub>1</sub> –R <sub>6</sub> = CH <sub>3</sub> O-, C <sub>2</sub> H <sub>5</sub> O-, i-C <sub>3</sub> H <sub>7</sub> O etc		
Substituted phosphazenes			

<sup>a</sup>\*: SET normalized against electrolyte amount (s/g).

of graphene (Figure 12a) to the typical reversible intercalation of Li<sup>+</sup> (Figure 12b). They attributed this to the changes in Li<sup>+</sup>-solvation structure incurred by the presence of Ca<sup>2+</sup>, which is a stronger Lewis acid than Li<sup>+</sup> and would dominate the competition with Li<sup>+</sup> in the coordination with solvents. On the other hand, TMP has higher donicity (23.0) than most carbonate molecules (16.4 for EC and 15.1 for DMC); hence, Ca<sup>2+</sup> would be preferentially solvated by TMP and consequently reduce the presence of TMP in Li<sup>+</sup>-solvation sheath. This solvation-sheath control technique, in addition to the

anode film-forming additives, would help make nonflammable electrolyte formulations based on these noncarbonate molecules electrochemically feasible.

**3.1.5. Silicon-Based Solvents.** Siloxanes and silanes are known for their low dielectric constants (hence limited solvation toward Li<sup>+</sup>). To make them viable electrolyte solvents, functional moieties capable of dissociating lithium salts must be attached to them. Amine and Zhang et al. synthesized various oligosiloxanes and silanes with oligoether-linkages of varying lengths, reaching ion conductivities of 0.1–1.0 mS/cm

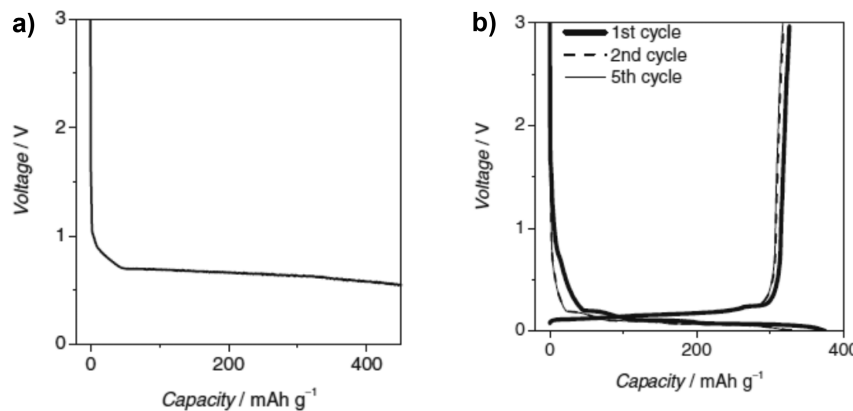


**Figure 12.** Phosphate-based electrolytes: (a) Voltage versus capacity profile for graphitic anode in 1.0 M LiTFSI/EC/DEC/TMP (30:30:40); (b) voltage versus capacity profile for the same graphitic anode in 1.0 M LiTFSI + 0.4 mM Ca(TFSI)<sub>2</sub>/EC/DEC/TMP (30:30:40). Reprinted with permission from ref 98. Copyright 2012 Electrochemical Society.

**Table 8. New Solvents: Siloxane and Silanes**

		$\sigma$ (mS/cm, 25 °C)	Tg (°C)	$\eta$ (cP, 25 °C)	$\epsilon$ (25 °C)
	EO/Li=15 EO/Li=20 EO/Li=24 EO/Li=28 EO/Li=64	0.08 0.13 0.10 0.08 0.05	-59.9 -66.7 -68.6 -71.9 -79.9		
	n=1 n=2 n=3 n=4 n=5 n=7	0.5 (1.0 M LiTFSI) 1.2 (1.0 M LiTFSI) 1.0 (1.0 M LiTFSI) 1.2 (0.7 M LiBOB) 1.0 (0.7 M LiBOB)	-148 -129 -116 -110 -106 -100	0.50 0.9 1.4 3.75 5.4 8.6	3.87 4.68 5.13 5.6 5.93 6.25

depending on the salt species and molecular weight of the oligomers.<sup>99–104</sup> Table 8 lists some of these Si-based solvents and their basic physicochemical properties. Of particular interest is that LiBOB seemed to be favored by these Si-based solvents, beating LiTFSI and LiPF<sub>6</sub> in ion conductivity.<sup>100,102</sup>

The most successful examples among this class of solvents are derivatives of trimethylsilanes, whose LiBOB solutions can support cell chemistry consisting of graphitic anode and cathode of either lithiated nickel–cobalt–aluminum oxide ( $\text{LiNi}_{0.8}\text{Co}_{0.15}\text{Al}_{0.05}\text{O}_2$ )<sup>102</sup> or lithiated spinel oxide ( $\text{LiMn}_2\text{O}_4$ ),<sup>104</sup> both operating up to 4.2 V vs Li (Figure 13). Considering that oligoether linkages ( $\text{CH}_2\text{—CH}_2\text{—O}$ )<sub>n</sub> were known to be intrinsically unstable against oxidative decomposition above 4.0 V, it raises the question about the role of siloxane or silanes on cathode surfaces. On the anode side, it seems that these solvents failed to form the needed interphase; thus the presence of LiBOB contributed the majority of the SEI components, as evidenced by XPS, XRD, and scanning electron microscope (SEM) analyses.<sup>104</sup>

**3.1.6. Ethers.** Compounds from the organic ether family were seldom considered as solvents for LIB because their instability on 4 V class cathode surfaces was well known.<sup>105</sup> However, in the search for flame-retarding cosolvents, Arai et al.

found that fluorinated ethers actually could support  $\text{LiCoO}_2$  cathode chemistry without obvious performance compromises.<sup>106</sup> Following this approach, Naoi et al. explored ethers with varying degrees of fluorination and reported their applications in cells consisting of graphite anode and  $\text{LiCoO}_2$  or  $\text{LiMn}_2\text{O}_4$  cathode chemistries.<sup>107,108</sup> They found that the branched ether 2-trifluoromethyl-3-methoxyperfluoropentane (TMMP) can effectively suppress ignition of electrolyte when its concentration was at 50%, where the anodic stability of the electrolyte solution was sufficient to support lithiation chemistry of graphitic anodes. Electrochemical testing showed that higher rate capability could be obtained with TMMP present.<sup>107</sup> Its linear counterpart, 2-(trifluoro-2-fluoro-3-difluoroproxy)-3-difluoro-4-fluoro-5-trifluoropentane (TPTP), showed similar but slightly better rate capabilities, retaining 80% of the nominal capacity at 12 C rate, while the baseline electrolyte, without those ethers, could only maintain 40% of the capacity.<sup>108</sup> Both ethers seemed to be able to support the fully charged  $\text{LiCoO}_2$  or  $\text{LiMn}_2\text{O}_4$  cathodes at ~4.2 V without apparent breakdown (Figure 14A), and the calculation via molecular orbital package (MOPAC) placed the HOMO of

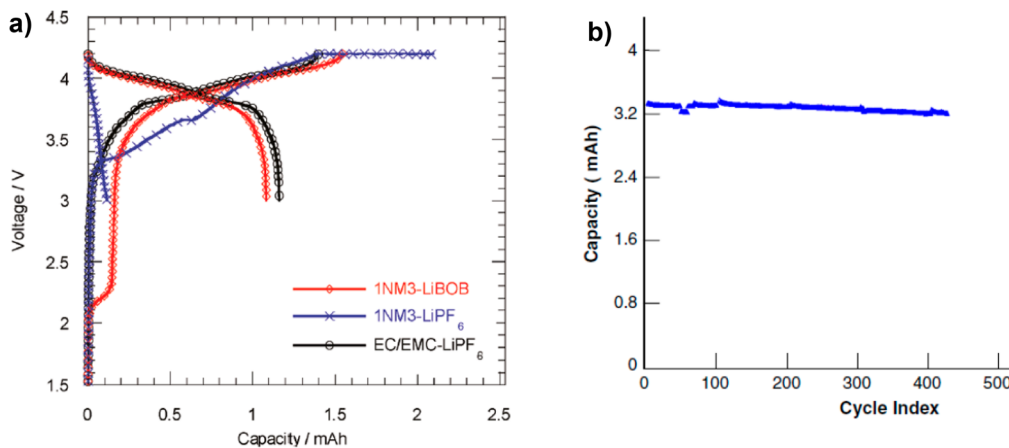


**Figure 13.** Siloxane-based electrolytes: (a) The first charge–discharge profile of the  $\text{LiMn}_2\text{O}_4/\text{graphite}$  cell using 0.8 M LiBOB (red) and 1.0 M LiPF<sub>6</sub> (blue) in a siloxane-based electrolyte as compared to 1.0 M LiPF<sub>6</sub> in EC/EMC (30:70). Reproduced with permission from ref 104. Copyright 2011 American Chemical Society. (b) Cycling performance of a  $\text{LiNi}_{0.8}\text{Co}_{0.15}\text{Al}_{0.05}\text{O}_2/\text{graphite}$  cell in 0.8 M LiBOB/silane-1 electrolyte. Reprinted with permission from ref 102. Copyright 2006 Elsevier.

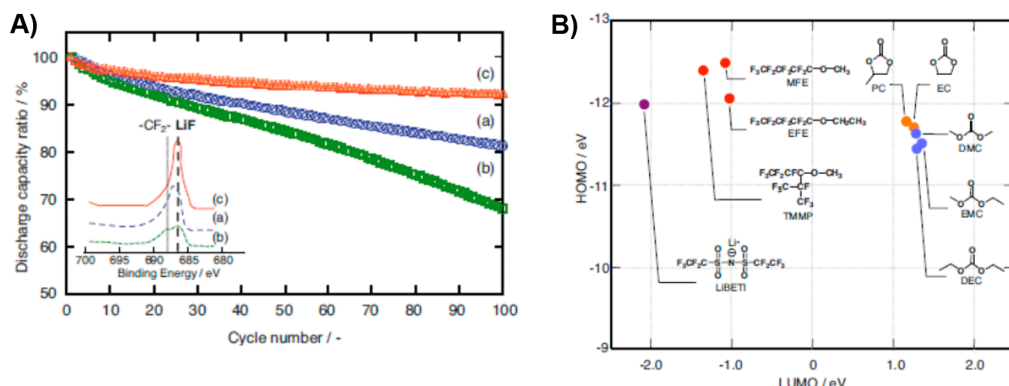


**Figure 14.** Electrolytes based on fluorinated ethers: (A) Cycling performance of a lithium ion cell based on  $\text{LiCoO}_2$  and graphite in 1.0 M LiBetI in (a) EC/DEC (50:50); (b) EC/DEC (5:95); and (c) EC/DEC/TMMP (5:45:50); and (B) HOMO/LUMO energy levels calculated via Molecular Orbital Package (MOPAC) for fluorinated ethers and typical carbonates. Reprinted with permission from ref 107. Copyright 2009 Electrochemical Society.

TMMP at a lower level than those of the typical carbonate solvents (Table 9).

Zhang et al. went further to exploit this benefit of anodic stability brought by fluorination of ethers.<sup>11</sup> Combining fluorinated carbonate with a fluorinated ether, 1,1-difluoro-2,2-difluoroethyl-2',2'-difluoro-3',3'-difluoropropyl ether (F-EPE), they formulated a series of high voltage electrolytes for the 4.6 V cathode chemistry  $\text{LiNi}_{0.5}\text{Mn}_{1.5}\text{O}_4$ , and achieved cycling stability in  $\text{Li}_4\text{Ti}_5\text{O}_{12}/\text{LiNi}_{0.5}\text{Mn}_{1.5}\text{O}_4$  full cells at elevated temperature and graphite/LiMn<sub>1.5</sub>Ni<sub>0.5</sub>O<sub>4</sub> full cells at ambient temperature (Figure 8). The exact chemistry of these fluorinated ethers on either cathode or anode surface remains to be investigated. Table 9 summarized these ether-based compounds.

### 3.2. Anion Receptors

Different from conventional solvents, which employ their nucleophilic sites to coordinate with  $\text{Li}^+$  so that lithium salts can dissolve from their crystal lattices, anion receptors are electrophilic and hence assist lithium salts to dissolve by interacting with their anions. In this sense, they can be viewed as a special class of solvents.

The early anion receptors were constructed on the basis of electron-deficient centers such as aza-ethers, borates, boronates, or boranes, which are enhanced by various electron-withdrawing groups, with fluorinated phenyls being preferred. The most successful example among these seemed to

be tris(pentafluorophenyl)borane (TPFPB), which can dissociate LiF in ether-based electrolytes such as dimethoxy ethylene glycol (DME) and tetrahydrofuran (THF),<sup>1</sup> or  $\text{Li}_2\text{O}$  and  $\text{Li}_2\text{O}_2$  in carbonate solutions.<sup>109</sup> Having identified that LiF is a rather “insulating” component in SEI to both  $\text{Li}^+$  and electron transport, Chen et al. applied TPFPB at small concentrations in electrolyte (<3%) to remove LiF from interphases. As a result, both power capabilities and cycle life of the LIB were improved;<sup>110</sup> however, excess presence of TPFPB has a negative impact on the stability of the electrolyte, because as a strong Lewis acid it will compete with PF<sub>5</sub><sup>-</sup> for F<sup>-</sup>:

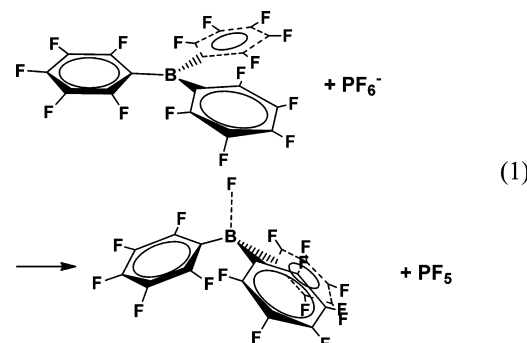
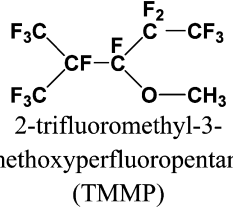
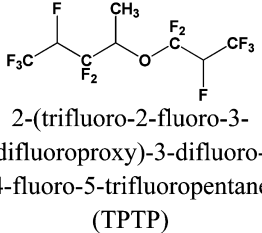
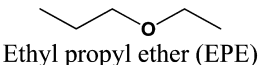
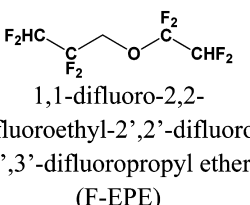


Table 9. New Solvents: Ethers

	mp/bp (°C)	$\eta$	$\epsilon$	$E_{ox}$ (calculated)	HOMO/LUMO (eV)
	-38/96	1.2	6.14		-12.4
	-98/131	1.7	6.35		
	-127/64		5.511		-7.12/0.16 *
		7.24			-9.64/-0.10 **

\*: Converted from atomic units ( $-0.26153/0.00596$ ) used in the original literature. \*\*: Converted from atomic units ( $-0.35426/-0.00356$ ) used in the original literature.

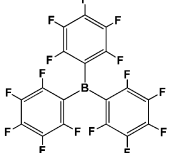
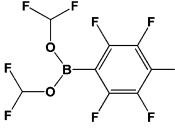
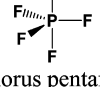
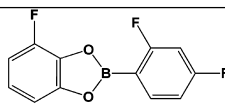
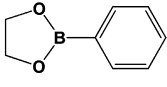
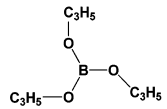
The generated  $\text{PF}_5$  was known to induce accelerated degradation of electrolyte solvents.<sup>1</sup> This negative impact was believed to happen when TPFPB concentration was above 5%. A similar effect of TPFPB was also reported by Lee et al., who found that the improved battery power capability not only came from LiF dissolution, but also from increased  $\text{Li}^+$ -transference number due to the complexation of TPFPB with  $\text{PF}_6^-$  anion.<sup>111</sup> Using ab initio calculations Amine and co-workers systematically studied the structure–property relationships for a series of anion receptors based on borates, boroles, boranes, and boronates (Table 10), and concluded that there was an obvious correlation between the LUMO localization and electrochemical performance.<sup>112,113</sup> It is obvious from the table that the general ability for anion receptors to compete with  $\text{PF}_5$  in coordinating  $\text{F}^-$  increases with number of F on the delocalized substituents and decreases with the oxygens connected to boron center.

An unexpected class of anion receptors is the so-called “inorganic dopants”. It has been well-known that ion conductivities of solid polymer electrolytes could be improved with addition of various silica, zirconia, titania, or alumina;<sup>114,115</sup> the underlying reason, however, was thought to be caused by the

suppression of oligoether-crystallinity because of these inorganic fillers. More recently, the concept was applied to liquid electrolyte, and the authors attributed the increased ion conductivity to preferential adsorption of anions on the acidic surfaces of the silica particles; hence, the dissociation of  $\text{Li}^+$  from ion pairs is promoted.<sup>116–118</sup> The composite electrolyte consisting of inorganic particles soaked with liquid electrolyte was named “soggy sand electrolytes” by the authors, and possess dual characteristics between “liquid” and “solid”, offering both mechanical/dimensional stability and electrochemical activity. The feasibility in actual Li-ion cells was also demonstrated.

A unique class of anion receptor based on supermolecular structure of macrocyclic compounds was reported by Blazejczyk et al.,<sup>119</sup> who tailored calixarenes to make the cavity suitable for anion-trapping. The two Srame[4]arene derivatives are shown in Figure 15a and b. Using the Bruce–Vincent approach, the authors confirmed that when ratios of calixarenes/ $\text{Li}^+$  in polymer electrolyte were above 0.25, the iodide anions were essentially immobilized, yielding a  $\text{Li}^+$ -transference number between 0.77–1.0. To make the cavity bigger so that more types of anions, especially those of special interest to LIB industry

**Table 10. Anion Receptors and Their Fluoride Affinities As Compared to  $\text{PF}_5^-$**

	mp	Fluoride Affinity
	140	406
tris(pentafluorophenyl) borate (TPFPB)		
	411.8	
pentafluorophenyl- bis(hexafluoro-isopropanol) borane		
	369.6	
phosphorus pentafluoride ( $\text{PF}_5$ )		
	297.9	
[2-(2,4-difluorophenyl)-4-fluoro-] 1,3,2-benzodioxaborole		
	195.2	
phenyl-(1,2-ethylene glycol) borane		
	>350 (decomposition)	-22.5
triethyl borate		

( $\text{PF}_6^-$ ,  $\text{BF}_4^-$ ,  $\text{ClO}_4^-$ , or  $\text{TFSI}^-$ ), could fit a modified calixarene with pyrrole moieties, C(6)P, was reported by Kalita et al.,<sup>120</sup> Ciosek et al.,<sup>121</sup> and Golodnitsky et al.,<sup>122</sup> respectively, which employed the heterocyclic planes to interact with those complicated anions. Scheers et al. used both Raman spectroscopy and ab initio calculations to quantify the ability of C(6)P in trapping various anions, and found in general all anions could form complexes with C(6)P, following the preference order:<sup>123</sup>

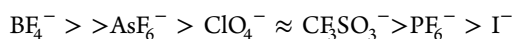
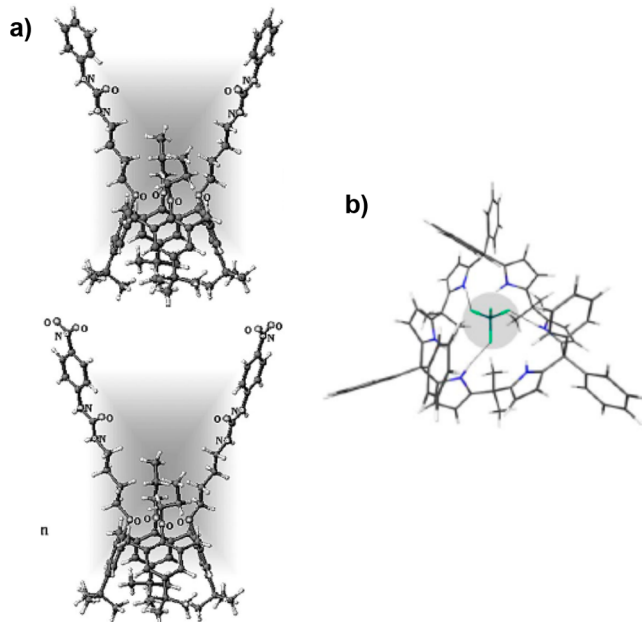


Figure 15b depicts the optimized structure of the C(6)P– $\text{BF}_4^-$  complex. This prediction was confirmed by  $\text{Li}^+$ -transference number measurement. However, none of these calixarene-based



**Figure 15.** Additives with supermolecular structures: (a) Structural conformation of calixarene additives tested. Reprinted with permission from ref 119. Copyright 2004 Electrochemical Society. (b) Optimized structure of a  $\text{BF}_4^-$ -anion captured by anion receptors with a tridentate coordination. Reprinted with permission from ref 123. Copyright 2009 Electrochemical Society.

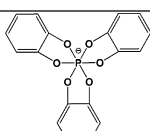
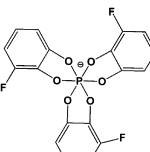
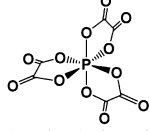
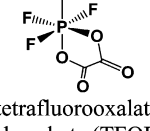
anion receptors were tested in liquid electrolytes, and their practicality in electrochemical cells remains to be confirmed.

### 3.3. New Lithium Salts

$\text{LiPF}_6$  remains the salt used in the majority of commercial LIB manufactured today, and this dominance is unlikely to change in the foreseeable future. The advantage of  $\text{LiPF}_6$  was ensured by its well-balanced properties when evaluated against a collection of requirements that battery environment places on electrolyte components.<sup>1,19</sup> Nevertheless,  $\text{LiPF}_6$  was far from being perfect, with its chemical and thermal instability being the most conspicuous issues, and hence have been held responsible for various compromises in electrochemical performance. Most efforts made to develop new lithium salts have aimed at improving those two shortcomings of  $\text{LiPF}_6$ , driven by the envisioned new markets for LIB, that is, electrification of automotive power systems and large-scale grid storage. In both applications, stability at elevated temperatures (>60 °C) on an extremely long time scale (10–20 years) is required, while electrochemical stability against cathode chemistries of higher voltages (>4.5 V) is expected to bring additional benefits. However, the reality is that the newly developed lithium salts often achieve one of the above goals at the expense of others. The most representative example is perhaps LiBOB, which can offer stable performance in LIB at elevated temperatures, but could not support cathode chemistries above 4.2 V.<sup>1,66,67</sup>

Johansson might be the first researcher who made an explicit link between anions of lithium salts and anodic stability of the electrolytes, despite the common belief that solvents were mainly responsible for the oxidation stability limits.<sup>124</sup> The computational approaches he developed, with empirical corrections, allowed facile calculation of intrinsic oxidation stability of anions, which could be helpful for efforts designing and synthesizing new potential anions for useful lithium salts.

Table 11. New Anions: Chelated Phosphates

	$E_{\text{ox}}$ (V vs. Li)	$E_{\text{red}}$ (V vs. Li)
	3.6~4.1	
tris[1,2-benzenediolato(2-)O,O'] phosphate (TBP)		
	3.6~4.1	
tris[3-fluoro-1,2-benzenediolato(2-)O,O'] phosphate (3-FTBP)		
	6.2 (calc) 5.5	2.07
tris(oxalato)phosphate (TOP)		
		1.7~1.9
tetrafluorooxalato phosphate (TFOP)		

**3.3.1. Phosphates.** Because of the success of  $\text{LiPF}_6$ , it was logical for chemists to modify the chemical structure of the  $\text{PF}_6^-$  anion, with the aim of mitigating its chemical/thermal instability while maintaining its merits. Various attempts have been made to replace the labile P–F bond with more stable linkages such as alkyls, aryls, or oxa-chelate substituents. The latter was obviously inspired by the partial success of LiBOB, whose chelating oxalato-groups imparted certain benefits such as unique interphasial chemistry on graphitic anodes and higher thermal stability during electrochemical cycling.

On the basis of ab initio calculations conducted on a series of chelated anions, Markusson et al. also suggested a new anion structure that is the phosphorus analogue of BOB, tris(oxalato)phosphate (TOP, Table 11).<sup>125</sup> They believed that the lithium salt based on this anion would combine the benefits of both  $\text{PF}_6^-$  and  $\text{BOB}^-$  anions, that is, readily dissociating and conductive in typical carbonate solvents while remaining chemically/thermally stable at elevated temperatures. Interestingly, as the suggestion was being made, this anion and its lithium salt (LTOP) were already synthesized and reported.<sup>126</sup> Wietelmann et al. described LTOP as a crystalline salt that decomposes between 150–190 °C without melting. Preliminary electrochemical tests showed that on graphitic anodes, LTOP was characterized by a reduction process at 2.10 V vs Li, which corresponds to the 1.7 V process of LiBOB, but the irreversible capacity associated with this process was much higher, perhaps due to higher presence of oxalato-bonds in the anion. The anodic stability of LTOP in carbonate solvents was

estimated to be ~5.5 V, but its cycling in actual LIB has not been reported.

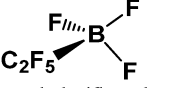
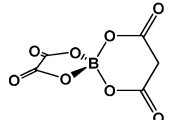
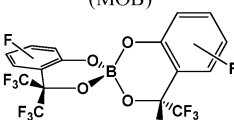
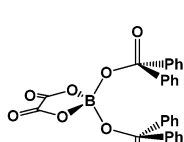
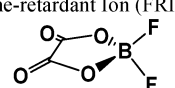
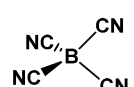
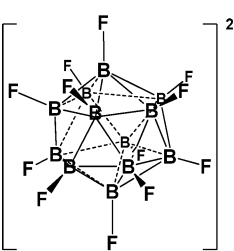
Continuing the work on chelated phosphates, Nanbu et al. reported two borate salts with or without fluorine-substitution, that is, tris[1,2-benzenediolato(2-)O,O'] phosphate (TBP) and tris[3-fluoro-1,2-benzenediolato(2-)O,O'] phosphate (3-FTBP) (Table 11).<sup>127</sup> Because of the high basicity of the diolato-chelating group, the solubility of these salts in typical carbonate electrolyte solvents is limited, while ethereal solvents, such as THF, are preferred. This would severely restrict their applications in LIB with cathode potentials higher than 4.0 V. The presence of fluorine in 3-FTBP resulted in higher ion dissociation, but both salts yielded conductivities lower than that of  $\text{LiPF}_6$  in the same solvent systems (2–5 vs ~10 mS/cm).

Instead of complete fluorine substitution as in TOP, Lucht and co-workers developed the phosphate anion where labile fluorines were only partially replaced by oxalato-chelates, that is, tetrafluorooxalatophosphate (TFOP, Table 11).<sup>128–131</sup> In carbonate solvents, this salt demonstrated ion conductivity similar to that of  $\text{LiPF}_6$  (~8 mS/cm at ambient temperature), which is higher than  $\text{LiBF}_4$  or LiBOB. The electrolytes based on it can support reversible  $\text{Li}^+$ -intercalation chemistries on both graphitic anode and  $\text{LiNi}_{0.8}\text{Co}_{0.2}\text{O}_2$  cathode, indicating necessary interphases were formed on both electrodes. Although there was little difference between the thermal stabilities of  $\text{LiPF}_6$  and LiTFOP in the solid state as measured by thermogravimetric analysis (TGA), the cell storage data at high temperature (65 °C) indicated that TFOP<sup>−</sup>-based electrolyte was more thermally resilient than its  $\text{PF}_6^-$  counterparts.<sup>130</sup> More importantly, the anion showed an obvious reduction process at 1.7 V vs Li,<sup>128,129</sup> which is the characteristic of SEI preformation by oxalate-moieties. Thanks to the more robust (but also more resistant) interphases originating from oxalate, better capacity retentions were reported. Ex situ surface analyses via XPS confirmed the overwhelming presence of oxalate SEI components and much smaller presence of LiF as compared to the  $\text{PF}_6^-$ -originated SEI.

The effect of LiTFOP on thermal stability was further consolidated by Qin et al., who used this salt as additive instead of as the main electrolyte solute in graphite/LiNi<sub>0.33</sub>Mn<sub>0.33</sub>Co<sub>0.33</sub>O<sub>2</sub> cells.<sup>132</sup> They observed obvious improvements in capacity retentions for both cycling and storage at high temperature (55 °C) when 1–3 wt % of LiTFOP was used. Interestingly, the addition of LiTFOP actually increased cell impedance during initial cycles, which agrees well with the knowledge of robust-but-resistant SEI grown by BOB; however, it significantly slowed the impedance rise rate as usually observed for  $\text{LiPF}_6$ -based electrolytes when placed at elevated temperatures. The benefits of this capacity retention were proved to be from the graphitic anode side. Furthermore, thermal safety of LiTFOP in a lithium ion chemistry environment was demonstrated via differential scanning calorimetry (DSC) performed on the electrolyte and lithiated graphitic anode.

**3.3.2. Borates and Boron-Based Cluster.** Similar to phosphates, the most successful salt among borates,  $\text{LiBF}_4$ , serves as a template for the efforts of developing new borates. As compared to  $\text{LiPF}_6$ ,  $\text{LiBF}_4$  offers lower solubility in carbonate solutions due to its higher viscosity (hence lower ion conductivity) as well as less ideal interphasial chemistry on graphitic anodes.<sup>1</sup> Zhou et al. replaced fluorines on  $\text{BF}_4^-$  with a fluoroalkyl,  $\text{C}_2\text{F}_5$ , in the hope that those two issues would be alleviated.<sup>133</sup> The lithium salt obtained, lithium pentafluorethyltrifluoroborate (LiFAB, Table 12), proved to be more

Table 12. New Anions: Borates and Borane Clusters

	$E_{ox}$ (V vs. Li)	$E_{red}$ (V vs. Li)
	> 4.0	
perfluoroethyl trifluoroborate (FAB)		
	> 4.5	< -0.5
(malonatooxalato)borate (MOB)		
		
bis(polyfluorodiolato)borate		
		
Flame-retardant Ion (FRION)		
	~4.2	~1.5
difluoro(oxalato) borate (DFOB)		
	5.65 (calc)	
tetracyanoborate		
	2-	4.65      4.58
dilithium dodecafluoro dodecaborate (Li <sub>2</sub> DFB)		

conductive than LiBF<sub>4</sub> in carbonate solutions due to the better delocalized charge, which renders the anion less associated with Li<sup>+</sup>. As compared to LiPF<sub>6</sub>, however, LiFAB was less conductive at ambient or higher temperatures but more conductive at subzero temperatures (<-10 °C). The electrolytes based on LiFAB can support reversible lithium ion chemistries in graphitic anode as well as a nickel-based 4.2 V cathode, indicating both protective SEI on the former and sufficient anodic stability on the latter. Overall, it provided an electrochemical performance comparable to that of LiPF<sub>6</sub> (Figure 16).

LiBOB has been initially proposed as a possible lithium salt alternative for high temperature operations of LIB; however, its intrinsic disadvantages, such as limited solubilities in carbonates and anodic stability on cathode chemistries above 4.2 V, severely restricted its versatility.<sup>1</sup> Nevertheless, its compatibility with LiFePO<sub>4</sub> (operating potential 3.5 V), lactone solvents,<sup>66,67</sup> and polymers<sup>100,102,134</sup> earned it a certain application niche, in

addition to the “greenness” of its fluorine-free structure. Xu and Angell continued the efforts of developing new orthoborate anions with asymmetric chelating groups, which has been an effective measure in lowering the melting point.<sup>135</sup> However, the lithium salt based on (malonatooxalato)borate (LiMOB, Table 12) was found to be less soluble than LiBOB, probably due to the less electron-withdrawing chelating malonato-moity. On the other hand, Nolan and Strauss synthesized a collection of borates based on chelating dioxo groups with varying degrees of fluorination on the aromatic ring.<sup>136</sup> The general structure representing this class of bis(polyfluorodiolato)-borate is shown in Table 12. While the best members of the class can offer ion conductivities around 5 mS/cm at room temperature and decent electrochemical stability window, the ability of them to stabilize aluminum substrate in these electrolytes strongly depended on the fluorination of the phenyl rings. No test data in actual LIB were available. Shaffer et al., on the other hand, tried to hybridize the substructures of BOB and phosphate into a single anion.<sup>137</sup> Named FRION (flame-retardant ion), the new lithium salt was hoped to possess higher fire safety due to its phosphate-ligands and excellent electrochemical, especially interphasial, properties in LIB. Preliminary data have shown that the salt can support basic lithium ion intercalation chemistries, although further rigorous tests remain to be conducted.

Perhaps the most promising lithium borate salt since LiBOB is its hybridized form with LiBF<sub>4</sub>.<sup>138</sup> The new salt, lithium difluorooxalatoborate (LiDFOB, Table 12), was found to offer the combined advantages of its parent salts: higher solubility than LiBOB in carbonates, rendering the solutions less viscous/more conductive, and hence better subzero-temperature performance, and froming better SEI on graphitic anodes than LiBF<sub>4</sub>, providing much improved performance at high temperatures. The reduction process at 1.7 V indicated that the oxalato-half of the anion indeed participated in SEI formation on graphitic anode, which contributed negligible irreversible capacity to the full cell (Figure 17a). The cycling performance of LiDFOB-based electrolyte in a full cell consisting of graphite anode and LiNi<sub>0.8</sub>Co<sub>0.15</sub>Al<sub>0.05</sub>O<sub>2</sub> cathode remained stable even at 60 °C (Figure 17b). Independently, the same salt was reported by Chen et al. almost immediately after Zhang,<sup>139</sup> confirming the ability of LiDFOB to support stable operation on the different cathode chemistry LiNi<sub>0.33</sub>Mn<sub>0.33</sub>Co<sub>0.33</sub>O<sub>2</sub>. In particular, it was pointed out that, unlike LiBOB, LiDFOB engendered lower cell impedances that are comparable to LiPF<sub>6</sub>-based electrolytes, which enables the cell power densities required by automotive batteries (Figure 18). This interphasial benefit brought by LiDFOB has been confirmed by meticulous electrochemical impedance analyses carried out by Abraham et al., while diagnostic studies by XPS and FTIR revealed that SEI formed by LiDFOB on graphitic anode consisted of a higher concentration of alkylcarbonate species with more complete coverage.<sup>140,141</sup> More recently, fundamental understanding of LiDFOB solvation in various solvents was also achieved via single-crystal structure investigations, which will assist the ongoing studies into how the anion dictates the interphasial chemistry and processes on graphitic anodes,<sup>59</sup> and detailed investigations were also carried out to identify the role of this anion on cathode interphasial chemistry.<sup>142</sup>

A rather exotic borate anion is tetracyanoborate (LiB(CN)<sub>4</sub>, Table 12), in which the central B core is stabilized by four nitrile groups that are strong electron-withdrawing groups. Unlike BOB, DFOB, FAB, and FRION anions, which were

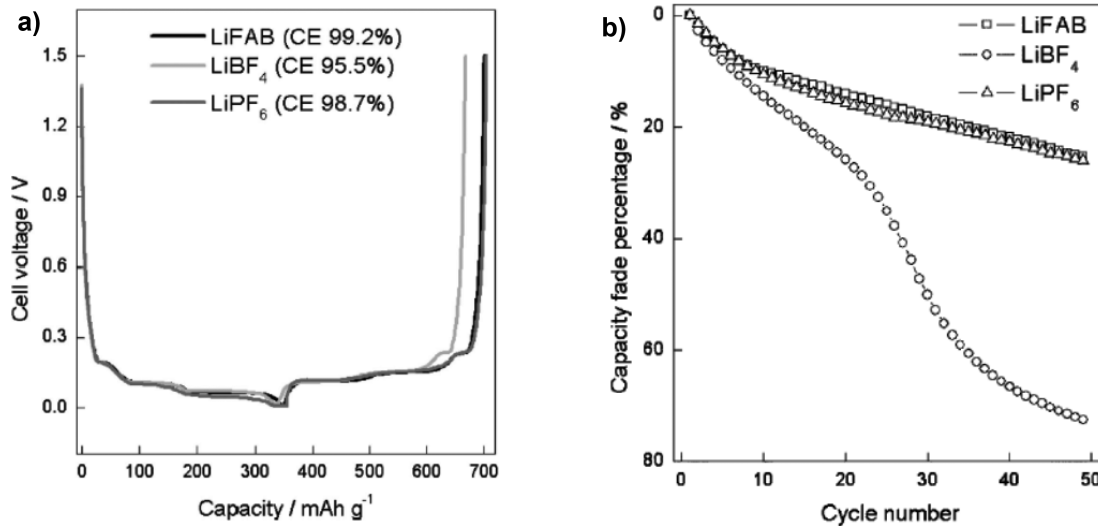


**Figure 16.** New lithium salt LiFAB: (a) Voltage profiles of graphitic anodes in 1.0 M LiFAB, LiBF<sub>4</sub>, and LiPF<sub>6</sub> in EC/EMC (30:70), respectively; and (b) comparison in capacity fading of lithium ion cells in electrolytes based on 1.0 M LiFAB, LiBF<sub>4</sub>, and LiPF<sub>6</sub> in EC/EMC (30:70), respectively. Reprinted with permission from ref 133. Copyright 2005 Electrochemical Society.

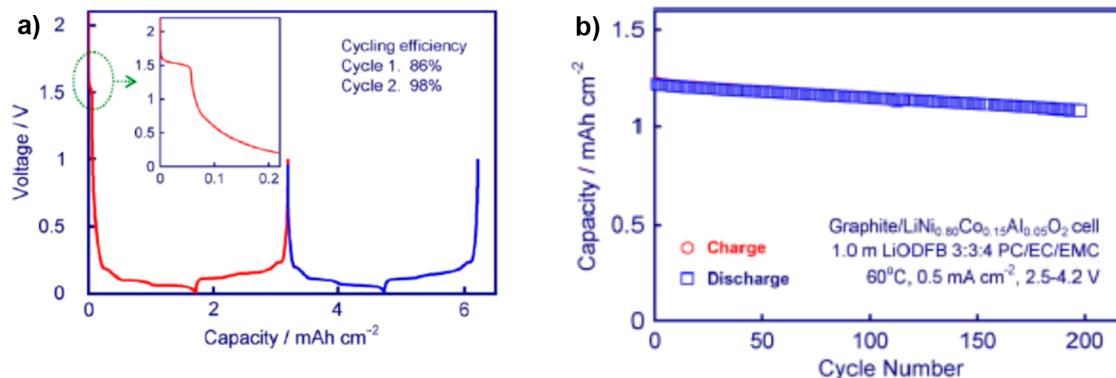


**Figure 17.** New lithium salt LiDFOB: (a) Voltage profile of the first two forming cycles for a graphitic anode in 1.0 m LiDFOB in PC/EC/EMC (30:30:40); and (b) high temperature (60 °C) cycling performance of a full lithium ion cell in the same electrolyte. Reprinted with permission from ref 138. Copyright 2006 Elsevier.

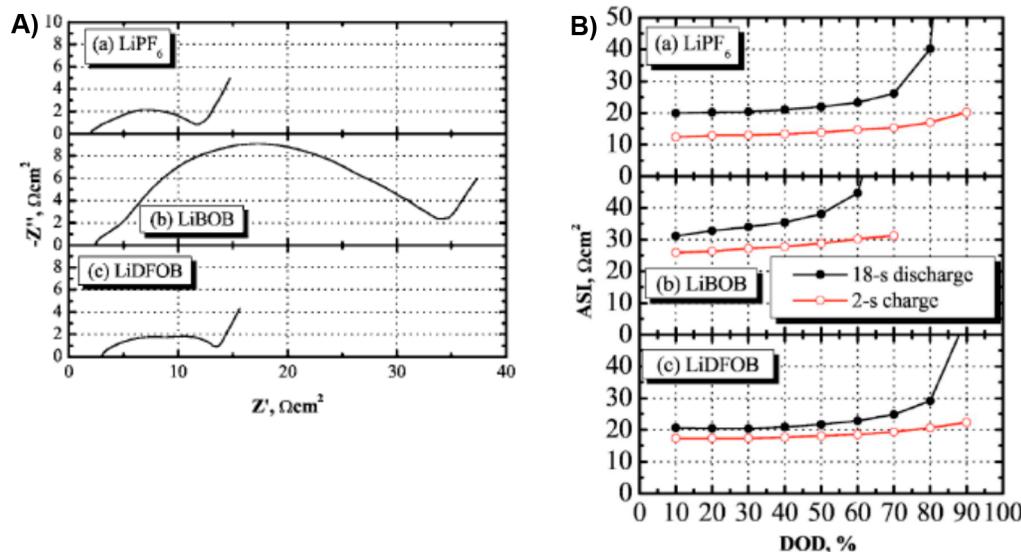


**Figure 18.** New lithium salt LiDFOB: (A) AC impedance of a full lithium ion cell based on a graphitic anode and LiNi<sub>0.33</sub>Mn<sub>0.33</sub>Co<sub>0.33</sub>O<sub>2</sub> in various electrolytes based on three lithium salts; and (B) dependence of area specific impedance on depth-of-discharge (DOD) for the same cells. Reprinted with permission from ref 139. Copyright 2007 Electrochemical Society.

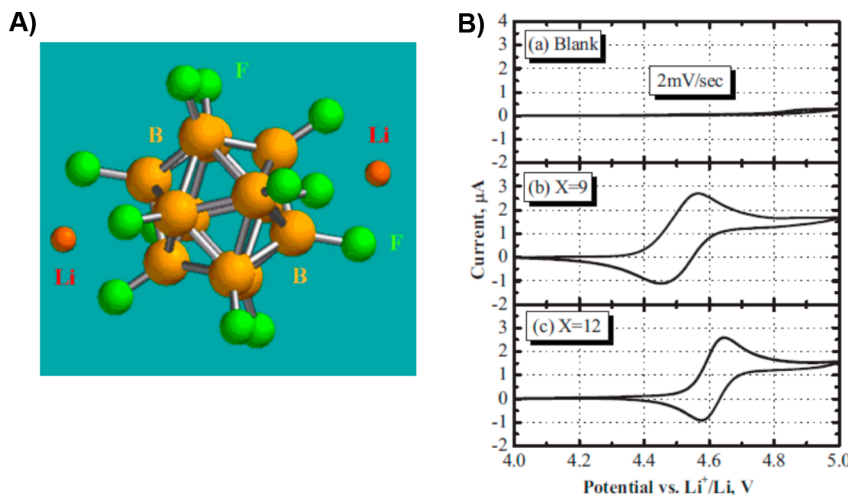


**Figure 19.** New lithium salts based on cluster borate anions: (A) Molecular structure of a lithium salt based on closo-cluster borate anion, dilithium dodecafluorododecaborate ( $\text{Li}_2\text{B}_{12}\text{F}_{12}$ ). Reprinted with permission from ref 150. Copyright 2009 Electrochemical Society. (B) Cyclic voltammetry of (a) 1.0  $\text{LiPF}_6/\text{EC}/\text{EMC}$  (30:70), (b) 1.0  $\text{LiPF}_6/\text{EC}/\text{EMC}$  (30:70) with 0.01 M  $\text{Li}_2\text{B}_{12}\text{H}_3\text{F}_9$ , and (c) 1.0  $\text{LiPF}_6/\text{EC}/\text{EMC}$  (30:70) with 0.01 M  $\text{Li}_2\text{B}_{12}\text{F}_{12}$ , where a three-electrode system was used with Pt and Li as working and reference/counter electrodes, respectively. Reprinted with permission from ref 152. Copyright 2010 Electrochemical Society.

designed and intended for lithium-based battery applications,  $\text{B}(\text{CN})_4^-$ -anion and its salts were synthesized in early 2000 as precursors to ceramics or ionic liquids, independently by two different groups.<sup>143,144</sup> The fact that all four carbons in the anion are identical in  $^{13}\text{C}$  NMR spectra indicated a symmetric structure with its formal charge well delocalized. The lithium salt was noted to have slight solubility in polar aprotic solvents such as acetonitrile (AN), and that it is thermally stable up to  $>500$  °C. The potential of  $\text{LiB}(\text{CN})_4$  as an electrolyte component was evaluated by Scheers et al. through computation,<sup>145</sup> who concluded that it offers a F-free alternative to  $\text{LiPF}_6$ , with comparable dissociation in nonaqueous solvents and equally high stability against oxidation (5.65 V). Scheers et al. investigated the ionic liquids based on this anion and imidazolium cation but only found that the solubility of the corresponding lithium salt in it was rather poor.<sup>146</sup> On the other hand, oligoethers such as polyethylene glycol dimethyl ether (PEGDME) can dissolve  $\text{LiB}(\text{CN})_4$  and offer performance comparable to  $\text{LiBF}_4$  on  $\text{LiFePO}_4$ . Similar electrolytes were applied in  $\text{Li}/\text{O}_2$  cells but did not solve the challenges that face this problematic rechargeable chemistry.<sup>147</sup> More recently, Sheers et al. evaluated  $\text{LiB}(\text{CN})_4$  in PC and glyme-based electrolytes.<sup>148</sup> They found that the ion conductivities of these “fluorine-free” electrolytes were lower than state-of-the-art electrolytes by an order of magnitude, and only at elevated temperatures did these electrolytes become conductive enough ( $\sim 3$  mS/cm) for practical cell operation. In addition to poor ion conduction, multiple issues also arose, such as anodic stability lower than 4.0 V and corrosion against aluminum substrate. Electrochemical performance in the presence of  $\text{LiFePO}_4$  was described,<sup>148</sup> showing that this salt could support the mild battery chemistry, but its advantage as a fluorine-free lithium salt is still yet to be proven.

Another class of boron-based anions that have shown promise in LIB applications are boron cluster dianions with cage-like structures, the perfluorinated version of which, dilithium dodecafluorododecaborate ( $\text{Li}_2\text{B}_{12}\text{F}_{12}$ , or  $\text{Li}_2\text{DFB}$ ), is shown in Figure 19A. Molecular orbital calculations of the dissociation energies indicated that the first  $\text{Li}^+$  can be dissociated as readily as the  $\text{Li}^+$  in  $\text{LiPF}_6$ , but the second  $\text{Li}^+$  is

tightly bound to the anion, making it essentially a mono salt in nonaqueous electrolytes.<sup>149,150</sup> As compared to  $\text{LiPF}_6$ ,  $\text{Li}_2\text{DFB}$  has the advantage of chemical stability against moisture and thermal stability up to 400 °C, which enabled stable operation of LIB at elevated temperatures; however, due to the large anion, the ion conductivities of  $\text{Li}_2\text{DFB}$ -based electrolytes were inferior (<2.5 mS/cm at 25 °C) to those based on  $\text{LiPF}_6$ , resulting in poor rate capabilities, and their solubility in carbonate solvents were usually below 1.0 M. More importantly, it failed to form a protective interphase on graphitic anode even in the presence of EC. Thus, it must be used along with  $\text{LiPF}_6$  as a cosalt, unless the anode is nongraphitic like  $\text{Li}_4\text{Ti}_5\text{O}_{12}$ . The partially fluorinated version of  $\text{Li}_2\text{DFB}$  was also described, which has the nominal formula of  $\text{Li}_2\text{B}_{12}\text{F}_8\text{H}_4$  but actually consists of mixtures of salts with varying degree of fluorination.<sup>151</sup> The results seemed to suggest that the higher degrees of fluorination would be favored in terms of both oxidation stability as well as cell polarization. Perhaps the most unique property of  $\text{Li}_2\text{DFB}$  and its less-fluorinated counterparts is that these boron clusters could serve as overcharge protection by forming redox shuttles for most 4.0 V class cathodes.<sup>152</sup> Chen et al. described this novelty when  $\text{Li}_2\text{B}_{12}\text{F}_9\text{H}_3$  and  $\text{Li}_2\text{DFB}$  were used at additive concentrations in  $\text{LiPF}_6$ -based electrolytes (Figure 19B), in which the former demonstrated a rather reversible oxidation/reduction process between 4.4–4.5 V, while the fully fluorinated anion pushed the redox potential up by  $\sim 0.10$  V, indicating that the redox potential is actually tunable with substitutions on boron. The overcharge protection was confirmed in LIB consisting of  $\text{LiNi}_{0.33}\text{Mn}_{0.33}\text{Co}_{0.33}\text{O}_2$  or  $\text{LiCoO}_2$  cathodes and graphitic anode,<sup>152,153</sup> and electron paramagnetic resonance spectra identified  $\text{B}_{12}\text{F}_{12}^{\cdot-}$  as the radical anion produced by surface oxidation at the cathode.<sup>153</sup>

Combining the fruitions of both LiDFOB and boron-cluster salts, Chen et al. formulated a new class of nonaqueous electrolytes that could support LIB chemistries with both long life and safety.<sup>154</sup> In a cell with  $\text{LiNi}_{0.33}\text{Mn}_{0.33}\text{Co}_{0.33}\text{O}_2$  cathode and graphitic anode, the electrolytes demonstrated tolerances toward both overcharge and thermal abuse, retained 70% of nominal capacity for up to 1200 cycles at 55 °C, and maintained the overcharge protection mechanism active for up to

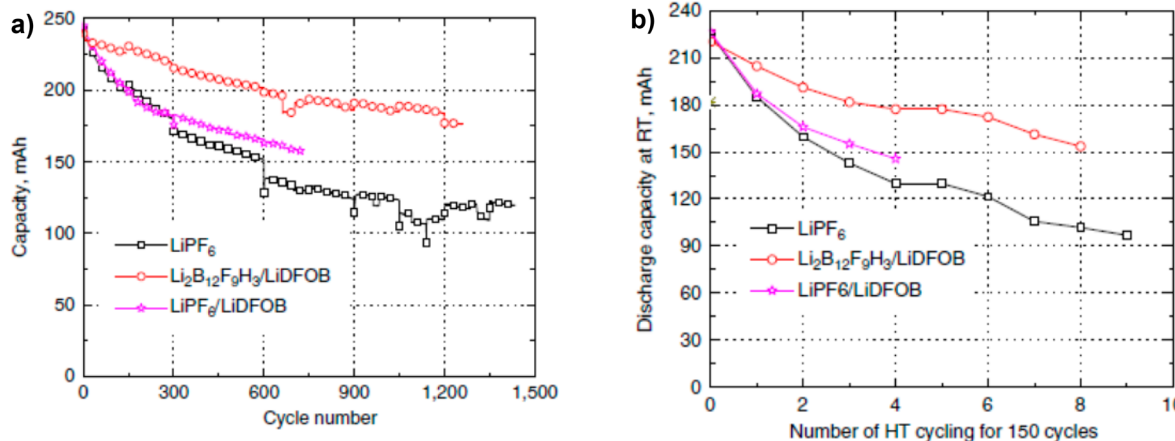


**Figure 20.** Effect of lithium cosalt mixtures: Cycling performance of lithium ion cells based on  $\text{Li}_{1.1}[\text{Ni}_{0.33}\text{Mn}_{0.33}\text{Co}_{0.33}]_{0.9}\text{O}_{1.2}$ /graphite in electrolytes containing various lithium cosalts at (a) high ( $55^\circ\text{C}$ ) and (b) room temperatures. Reprinted with permission from ref 154. Copyright 2013 Macmillan Publishers Limited.

450 abuse cycles (Figure 20a and b). Thanks to the interphasial chemistry brought by LiDFOB, Li<sub>2</sub>DFB could be used as the main salt in the electrolyte, and LiPF<sub>6</sub> was no longer required. Of course, LiPF<sub>6</sub> replacement is only possible when competitive cost could be achieved in those fluorinated boron anions.

**3.3.3. Imides.** As the first imide salt reported and evaluated as electrolyte component for LIB applications, LiTFSI has been well investigated.<sup>1</sup> Subsequent efforts in developing new imide salts naturally focused on how to mitigate the corrosion of this class of anions toward cathode substrate (aluminum).<sup>1</sup>

The nitrogen-based anions rely on the electron-withdrawing ability of the N-substituents to reduce the Lewis basicity, so that the corresponding lithium salts can dissociate readily. For this consideration, there are hardly any other substituents that can more effectively assist in delocalizing the formal charge on N than trifluorosulfonyl groups. Replacing them with non-fluorinated alkyl or nitrile groups only generates salts that are barely soluble in carbonate-based solvents (Table 13),<sup>155</sup> while oligomeric versions of TFSI anion (where  $n = 2-225$ , Table 13) expectedly offer lower ion conductivities than that of the monomeric anion.<sup>156</sup> Using F<sup>-</sup> instead of fluorinated alkyl (LiFSI, Table 13), on the other hand, proved to be more promising, offering higher solubility (up to 5 M, even in acyclic carbonate) and ion conductivity (up to 8 mS/cm) than LiPF<sub>6</sub>-based electrolytes, along with thermal stability up to 180 °C.<sup>157</sup> However, impurities have been constantly plaguing this new salt. LiFSI-based electrolyte can also form protective SEI on graphitic anode; but, its ability to passivate aluminum still fails at potentials above 4.0 V, leaving the electrolytes based on LiFSI only suitable for cathode chemistries such as LiFePO<sub>4</sub>. It should be pointed out that, more often than not, it is hard to determine whether the less-than-ideal electrochemical performance comes from the almost omnipresence of LiF and trace HF or the intrinsic properties of the anion itself, because unlike TFSI, fluorine in FSI anion is labile and readily susceptible to hydrolysis.

An asymmetric version of imide, lithium (fluorosulfonyl)-(nonafluorobutanesulfonyl) imide (LiFNFSI, Table 13), was reported by Han and Zhou et al.<sup>158,159</sup> Besides the usual advantages of imides over LiPF<sub>6</sub>, LiFNFSI can passivate aluminum. Its applications in LIB based on LiCoO<sub>2</sub> and LiMn<sub>2</sub>O<sub>4</sub> cathodes showed that better capacity retentions were achieved at elevated temperatures. For the latter cathode, LiFNFSI was believed to have suppressed the dissolution of Mn<sup>2+</sup>, which has been a major

**Table 13. New Anions: Imides**

	$E_{\text{ox}}$ (V vs. Li)
bis(butanesulfonyl) imide	4.35
cyanamide	
oligomeric fluorosulfonyl imides	
lithium bis(fluorosulfonyl) imide (LiFSI)	> 4.5
lithium (fluorosulfonyl)(nonafluorobutanesulfonyl) imide (LiFNFSI)	

obstacle for this high power, environmentally benign cathode chemistry to be adopted by the LIB industry.

**3.3.4. Heterocyclic Anions.** A few anions based on heterocyclic structures have been reported. In a way, they can be viewed as conjugated and delocalized variations of amides or imides.

Barbarich et al. described the synthesis of an imidazolidine, lithium bis(trifluoroborane) imidazolidine (LiIm(BF<sub>3</sub>)<sub>2</sub>, Table 14), in which two strong Lewis acid units (BF<sub>3</sub>) bind to N and render the corresponding lithium salt readily dissociable.<sup>160</sup> In typical carbonate solvents, this salt can provide ~5 mS/cm of ionic conductivity. On Pt electrode, the electrolyte based on LiIm(BF<sub>3</sub>)<sub>2</sub> showed an oxidation stability of ~4.8 V vs Li, while

Table 14. New Anions: Heterocyclic

	$E_{ox}$ (V vs. Li)
	> 4.5
lithium bis(trifluoroborane) imidazolide ( $\text{LiIm}(\text{BF}_3)_2$ )	
	2.6~3.0 (calc)
lithium 1,2,3-triazole-4,5-dicarbonitrile (LiTADC)	

its performance in cathode and anode half cells using  $\text{LiNi}_{0.2}\text{Co}_{0.8}\text{O}_2$  and graphite, respectively, was similar to  $\text{LiPF}_6$ -based electrolyte, although it takes longer for full capacity utilization to be achieved when  $\text{LiIm}(\text{BF}_3)_2$  was used.

Johansson et al. revisited an anion based on dicarbonitrile that was synthesized previously (lithium 1,2,3-triazole-4,5-dicarbonitrile, or LiTADC, Table 14), via computational approaches, and concluded that it could afford a well-dissociated lithium salt.<sup>161</sup> With ab initio calculation, Armand et al. further evaluated a class of heterocyclic anions based on the general structure of an intraring sulfonyl group as the electron-withdrawing moiety, a representative of which is listed in Table 14.<sup>162</sup> They suggested that, by varying the number of nitrile-substituents on the conjugated ring,  $\text{Li}^+$ -affinity of the anions could be tuned, and a balance between oxidation stability and solubility might be reached to obtain a feasible new lithium salt. More recently, Scheers et al. evaluated LiTADC in both PC and glyme, and found that it behaved similarly to  $\text{LiB}(\text{CN})_4$ ; that is, although electrolytes based on it can support the mild battery chemistry of  $\text{LiFePO}_4$ , its projected anodic stability did not translate into actual stabilities in an electrochemical cell against an aluminum substrate, and its application could be restricted to both elevated temperatures and voltages lower than 4.0 V.<sup>148</sup>

**3.3.5. Aluminates.** As structural analogues to their borate-counterparts, aluminates were also explored. Tokuda et al. reported lithium tetra(1,1,1,3,3-hexafluoro-2-propyl) aluminate ( $\text{LiAl}[\text{OCH}(\text{CF}_3)_2]_4$ , Table 15) as salt for polymer electrolytes.<sup>163</sup> The salt is low melting (mp 120 °C) and can be sublimated, indicating the covalent nature of the Li–Al bond and predicting a tightly bound  $\text{Li}^+$  that would not be available for ion conduction. In lowly polar solvents, such as acyclic carbonates or ethers, however, this salt dissociates well and offers ion conductivities higher than  $\text{LiTFSI}$  and  $\text{LiBF}_4$ . No electrochemical stability, especially with respect to oxidation on cathode, was reported.

Tsuijoka et al., on the other hand, described six lithium aluminates including  $\text{LiAl}[\text{OCH}(\text{CF}_3)_2]_4$  (Table 15). In all of these anions, the central Al was coordinated by ligands with

Table 15. New Anions: Aluminates

	$E_{ox}$ (V vs. Li)
	> 4.0
lithium tetra(1,1,1,3,3-hexafluoro-iso-propyl) aluminate	
lithium tetra(1,1,1,3,3-hexafluoro-2-butyl) aluminate	
	> 4.0
lithium tetra(1,1,1,3,3-hexafluoro-2-propylphenyl) aluminate	
lithium tetra(perfluorobutyl) aluminate	

varying amounts of fluoroalkyl and aryl groups.<sup>164</sup> Besides physicochemical properties and ion conductivities, they evaluated the electrochemical performance of these salts rather thoroughly. The authors showed that most of these lithium salts were thermally more stable than  $\text{LiPF}_6$ , and can effectively passivate aluminum and remain stable up to 4.0 V vs Li, and claimed that the corresponding electrolytes support reversible intercalation chemistry on both graphitic anode and  $\text{LiCoO}_2$  cathode, although no data were presented.

### 3.4. Additives

Each year approximately 15 000–20 000 tons of electrolytes is manufactured globally, delivering decent performance in state-of-the-art LIB of various chemistries.<sup>165</sup> As in any industry, the established infrastructure of electrolyte production makes any drastic change in the status quo difficult, unless there is significant incentive. Therefore, it would be more economical and convenient if certain battery performance improvements can be achieved via incorporating small amounts of components in electrolyte without replacing its skeletal composition. It was for this reason that in the past decade the research activities of various electrolyte additives far outweighed the efforts in developing main electrolyte components themselves.

The additives are often (but not always) sacrificial and intended for the formation of interphases in the initial activation cycles of LIB; consequently, they would be consumed and

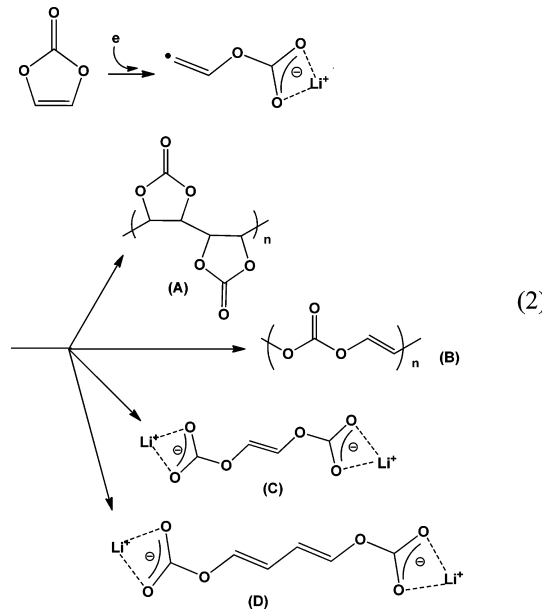
only leave their chemical signatures at the electrolyte/electrode interfaces. Because there is no clear demarcation between an additive and a cosolvent/salt, an arbitrary threshold of 10% is adopted here, below which the new components are considered as additives.

**3.4.1. Additives for Graphitic Anode.** Since the birth of Li-ion chemistry, one of the focuses has been the unique surface chemistries on graphitic anode materials, which provides the key to supporting the reversible intercalation/deintercalation of  $\text{Li}^+$  with graphite that occurs at a potential far well beyond the stability limits of nonaqueous electrolytes, and is hence thermodynamically impossible. The seminal research concerning the chemistry and formation mechanism of the key player in this nonequilibrated chemistry, that is, SEI, has been thoroughly summarized in the 2004 review,<sup>1</sup> while new advances in this area since 2003 will be discussed in detail in section 5. Efforts to tailor this interphase for better protection, less irreversible capacity during formation, and lower resistance have dominated the electrolyte additive developments. As of today, the most successful additive for this purpose remains VC, which is being used in most commercial electrolyte compositions. Given the fact that a protective SEI could not be formed on graphitic materials in electrolytes containing high ratios (>30%) of PC, new additives developed are often evaluated experimentally under these PC-rich “extreme” conditions to “show off” their effectiveness, although it should be kept in mind that these PC-rich electrolytes may never become mainstream compositions for the LIB industry, and that actual usefulness of an additive can only be proven by long-term cycling and storage tests.

On the other hand, many attempts to understand how additives work at fundamental levels were also made via computational approaches, which were increasingly assisted by easy access to more powerful computers nowadays and rapid development of various computing methodologies.<sup>166–171</sup> In one particular instance, high throughput quantum calculation enabled virtual screening of over 7000 structures, which could serve as a “genome library” for additive material design.<sup>168</sup> However, it must be pointed out that, despite the accurate prediction of reduction or oxidation potentials of the target compounds on the basis of their HOMO or LUMO energies, the more important information regarding the reaction products of the target compound and how they would behave as interphasial components were generally not available from computational means. It is the properties of these products, such as adhesion to electrode surfaces, resilience against solvent dissolution/permeation and chemical corrosion, as well as  $\text{Li}^+$ -conduction through them, that dictate the effectiveness of eventual new interphases in devices. Moreover, merely screening of HOMO/LUMO neglects inter- and intramolecular relaxation of the oxidized/reduced clusters of electrolytes that follows vertical electron detachment/attachement. For example, DFT calculations of the solvent dimers and solvent-anion clusters have shown that the H-transfer reactions coupled with the oxidation of the solvent dimers have resulted in the lower oxidation stability of cyclic and linear carbonate, alkyl phosphate, and sulfone components of electrolyte<sup>172</sup>, despite what the HOMO/LUMO calculation would predict.<sup>172</sup>

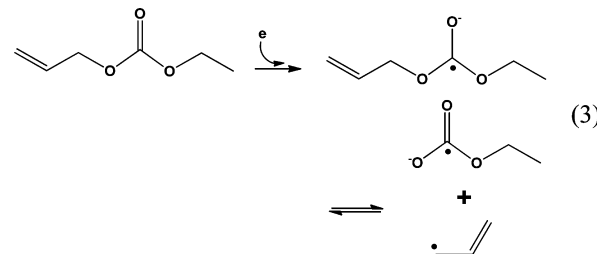
**3.4.1.1. Unsaturated Additives.** Unsaturated compounds have always been favored as potential additive candidates, partially inspired by the success of vinyl carbonate (VC), and partially incurred by the simple vision of a polymeric layer on electrode surface. Apparently unsaturated functionalities (double or triple bonds, cyclic structures, etc.) provide a site for polymerization under reductive (or oxidative) conditions. This hypothesis was confirmed by Quatani et al. in a recent investigation on the mechanism of VC surface reaction in cells,

where they convincingly established, via ab initio calculation and experimental spectroscopy based on the synthesized VC-originated polymers, that the radical polymer product from VC (species A in eq 2) is the main product on both graphitic anode and  $\text{LiCoO}_2$  cathode (Figure 21B):<sup>173</sup>



The radical might be initiated at ~2.5 V vs Li, which was usually observed as a rather small peak in the differential capacity plots (Figure 21A). How the similar polymeric products end up on the cathode surface is still not clear. An oxidation mechanism of VC producing the corresponding radical cation might be possible, so would be a “cathode–anode dialog” mechanism, in which the radical species are sufficiently long-lived to diffuse across the cell and propagate on the opposite electrode surface. According to Dahn and co-workers, the effectiveness of the polymeric interphase generated by VC was actually more pronounced at cathode rather than at anode, as quantified by both Coulombic efficiency as well as irreversible capacity consumed in the first cycle.<sup>174,175</sup> Surprisingly, these authors also found that, using the high precision coulometry technique developed in their lab, the addition of VC induces capacity loss upon storage at both ambient and elevated temperatures.<sup>176</sup>

Lee et al. investigated allylethyl carbonate (AEC, Table 16) as additive for graphitic anodes.<sup>177</sup> This compound showed a conspicuous reduction process at ~1.5 V vs Li, which is higher than the reduction potential of both PC and DEC. The resultant SEI successfully stabilized the graphitic structure in PC-rich electrolytes (PC/DEC 3:2) and enabled a reversible capacity of ~320 mAh/g. The authors suggested an interphasial chemistry that involves the formation of an allylic radical:



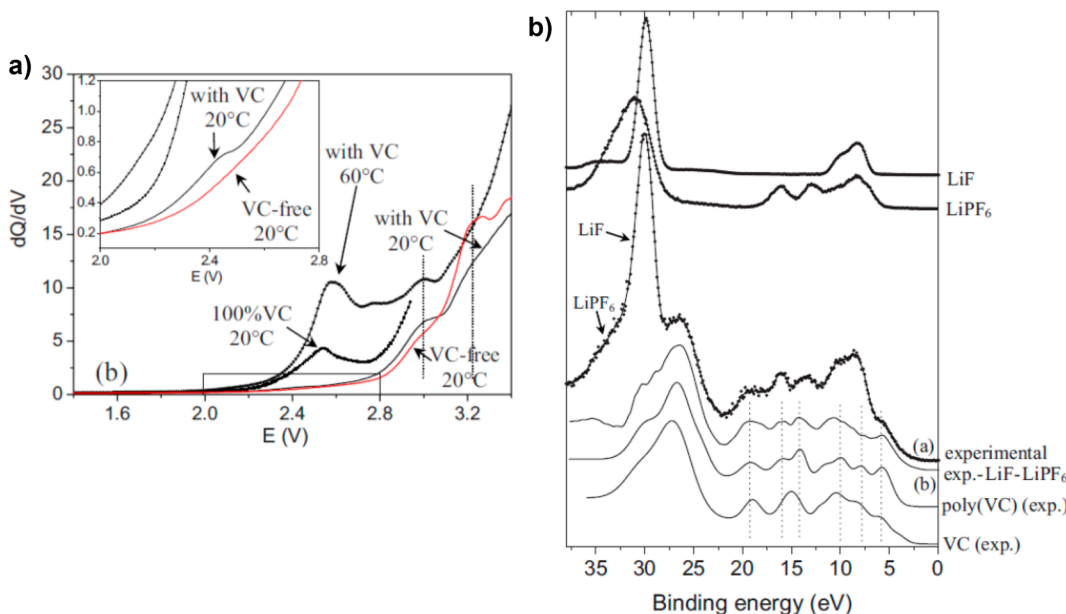


**Figure 21.** Mechanism of VC as electrolyte additive: (a) Differential capacity ( $dQ/dV$ ) plots showing the initiation of VC radical anion on a positive electrode surface; and (b) matching experimental valence spectra of synthesized poly(VC) and graphite surface cycled in neat VC electrolyte. Reprinted with permission from ref 173. Copyright 2009 Electrochemical Society.

**Table 16. Unsaturated Additives for Graphitic Anode**

	$E_{\text{red}}$ (V vs. Li)
allylethyl carbonate (AEC)	~ 1.5
tetrachloroethylene (TCE)	1.3~1.5
propargylmethyl carbonate (PMC)	0.83
propargylmethyl sulfonate (PMS)	1.24
allylmethyl carbonate (AMC)	0.83
allylmethyl sulfonate (AMS)	1.31
2-vinylpyridine (VP)	0.90
4,7,13,16,21,24- hexaoxa-1,10- diazabicyclo[8.8.8]h exacosane (C222)	

Because of the high stability of allylic radical that has been well recognized in organic chemistry, the initial reductive decomposition of AEC would be heavily favored; however, the fate of this stable radical is unclear, as well as how it would impact the effectiveness of SEI. Such a metastable (long-lived) intermediate species may not be desirable in a working LIB because of the possibility of forming a parasitic redox shuttle between anode and cathode, let alone that polymerization becomes unlikely due to difficult radical propagation and chain-growth. No data were reported for AEC's stability/reactivity against cathode surfaces.

Hu et al. described tetrachloroethylene (TCE, Table 16) as an additive, which reductively decomposed at 1.3–1.5 V vs Li and formed an interphase that also can suppress cointercalation of PC and subsequent exfoliation of graphitic structure.<sup>178</sup> With XPS the authors identified the surface of graphite as covered with Li<sub>2</sub>CO<sub>3</sub>, alkylcarbonate, as well as LiCl. Although the anodic stability of the electrolyte containing TCE was demonstrated on LiMn<sub>2</sub>O<sub>4</sub>, they pointed out that the solubility of LiCl in nonaqueous electrolytes could lead to a parasitic shuttling that had been observed with chloroethylene carbonate,<sup>1</sup> the consequence of which is Coulombic efficiency below 99% despite stable cycle life.

To exploit the effect of polymerization, Abe et al. developed a series of unsaturated organic esters and sulfonates, a few representatives of which are shown in Table 16.<sup>179–181</sup> To varying extents, these compounds showed trends of suppressing graphitic exfoliation in PC-rich electrolytes. In particular, interphases formed in the presence of triple bonds (PMC and PMS) were found to be denser and thinner as compared to their double bond counterparts, and XPS and Auger electron spectroscopy identified these interphases as organic-rich. It should be remembered here that, in typical single-electron reduction of EC, about 50% of organic moieties will be retained in the interphase, while the rest would be released as gaseous products during the initial cycles.<sup>1</sup> Apparently the more reactive (and polymerizable) triple bonds helped to preserve the organic moieties in the interphases to a higher degree. Combining these additives with a second additive with double bonds, such as VC, results in thinner SEI (around 2 nm in thickness), lower cell impedance, and better capacity retention (Figure 22),<sup>181</sup> probably thanks to the copolymerization of these different unsaturations.

In most of the cases discussed above, there was a direct correlation between the reduction potential (or LUMO energy level) of the additives and the effectiveness of interphases formed by them, seeming to support the empirical notion that “the more reactive the additives are, the better the SEI they can form”. This relation could be applied to other additive families

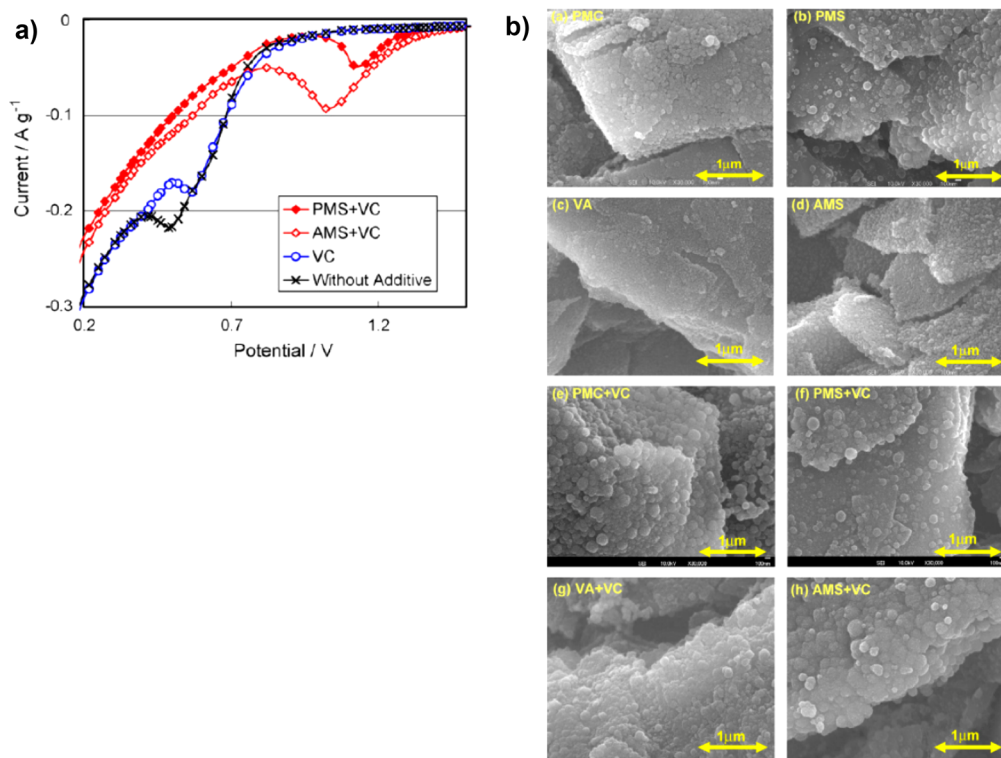


**Figure 22.** Additives with unsaturations: (a) Reduction potentials of various unsaturated additives PMS (propargyl methyl sulfonate), AMS (allyl methyl sulfonate), and VC on graphitic surfaces when used in 1.0 M LiPF<sub>6</sub>/EC/EMC (30:70); and (b) SEM images of graphite electrodes after the 50th cycle in PC-based electrolytes with triple-bond additives. Reprinted with permission from ref 181. Copyright 2008 Elsevier.

with or without unsaturation functionalities in the common sense, such as aromatic esters,<sup>182</sup> oxalato-substituted phosphate,<sup>182</sup> fluorinated,<sup>183</sup> and nonfluorinated cyclic carbonates.<sup>184</sup>

A strange class of anode additives involves the mechanism of “dialog” with the cathode. Spinel LiMn<sub>2</sub>O<sub>4</sub>-based LIB have been known for severe capacity degradation at elevated temperatures (>50 °C), with one of the major reasons being the dissolution of Mn(II) followed by its “deposition” on graphitic anode, either through a reduction process believed to occur at around 1.8 V vs Li that leads to elemental Mn,<sup>185</sup> or simply an “ion-exchange” process that leads to a SEI rich in Mn<sup>2+</sup> and poor in Li<sup>+</sup>-conducting.<sup>186</sup> Attempts were made to suppress the Mn(II) “deposition” on graphite surface, including an electropolymerizable additive 2-vinylpyridine as described by Komaba et al.<sup>187</sup> While the effect of the additive was apparent, no convincing mechanism was given. Interestingly, regarding whether VC blocks Mn “deposition”, there seemed to be controversy,<sup>187,188</sup> indicating that this topic merits further investigation. More recently, Ochida et al. conducted a rather systematic investigation on Mn(II) deposition on the model anode of highly oriented pyrolytic graphite (HOPG) and the effects of various additives on it.<sup>189</sup> They confirmed that, by adding only 100 ppm Mn<sup>2+</sup>, the reduction current corresponding to Li<sup>+</sup>-intercalation at edge-sites of HOPG was significantly reduced; a similar conclusion was drawn by Esbensen et al., who showed that presence of either Mn or Cu on the surface on anode would constitute barrier to Li<sup>+</sup>-migration through the interphase. Both groups proposed that the reduced Mn or Cu deposited on anode surface in the form of a monolayer metallic coating that is impermeable to Li<sup>+</sup>.<sup>189,190</sup> However, this conventional wisdom was recently challenged by Zhan et al.,<sup>186</sup> who convincingly proved that Mn(II) species on the anode surface remained at +2 oxidation state without being reduced

into metallic form Mn(0). What most likely occurred should be a metathesis process, in which Li<sup>+</sup>-embedded in SEI was displaced by Mn<sup>2+</sup>, resulting in an ion-insulating interphase populated by Mn<sup>2+</sup> that constitutes an additional barrier to Li<sup>+</sup>-transport.

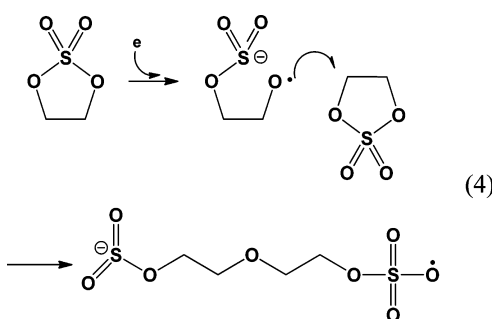
To prevent the emergence of this additional barrier, Ochida et al. used crown-ethers such as 4,7,13,16,21,24-hexaoxa-1,10-diazabicyclo[8.8.8]hexacosane (C222, Table 16), which proved rather effective even at low concentrations (0.084%). The authors suggested that Mn(II) should be tightly trapped by the cage structure of C222 and, therefore, remain in the solution, circumventing its probability of appearing on the anode surface.<sup>189</sup> However, conflicting results seemed to be reported by Ziv et al., who showed that the trapping of Mn(II) by free molecules 18-crown-6 (which provides a cavity size similar to that of C222) actually promoted Mn-dissolution from the cathode and deteriorated cell performance.<sup>191</sup> Only when the structural unit of 18-crown-6 was tethered to polymeric chains can the capacity fading caused by Mn-dissolution be mitigated. The authors attributed the effective Mn-sequestration by the polymeric additive to the rigid backbone of the latter that hinders the reorientation of the chelated complexes. Judged from the new mechanism proposed by Zhan et al., new Mn solvation cages for Mn<sup>2+</sup> might simultaneously encourage the dissolution of Mn<sup>2+</sup> from cathode lattice while mitigating the ability of solvated Mn<sup>2+</sup> in replacing Li<sup>+</sup> in interphase. The net result of the competition between these two reactions determines whether the additive is effective in suppressing the capacity fading caused by Mn<sup>2+</sup>-deposition.

**3.4.1.2. Sulfur-Based Additives.** Table 17 listed a few sulfur-based additives that have been reported for graphitic anode protection. Chen et al. described the family of sulfites, among which butylenes sulfite (BS) at 5% concentration can effectively

Table 17. S-Containing Additives

	$E_{\text{red}}$ (V vs. Li)
butylenesulfite (BS)	~1.8
1,3,2-dioxathiolane-2,2-dioxide (DTD)	~2.2
4-methyl-1,3,2-dioxathiolane-2,2-dioxide (MDTD)	>1.0
4-ethyl-1,3,2-dioxathiolane-2,2-dioxide (MDTD)	>1.0
phenyl cyclic sulfate (PCS)	0.70
1,3-propane sultone (PS)	0.70
butyl sultone (BS)	>1.0
prop-1-ene-1,3-sultone (PES)	

suppress the cointercalation of PC.<sup>192</sup> DFT calculation showed that its lower LUMO (hence higher reactivity at anode) than PC ensured that the resultant interphase consists mainly of lithium-oxy-sulfite ( $\text{Li}_2\text{SO}_3$  and  $\text{ROSO}_2\text{Li}$ ). Electrolytes based on PC/BS (95:5) exhibited oxidation stability up to 4.4 V vs Li on different cathode chemistries. In a rather similar manner, cyclic sulfates also demonstrated higher reduction potentials than carbonates, and enabled protection of graphitic anode in PC-rich electrolytes.<sup>193</sup> Surface analyses on the cycled graphitic anodes by XPS, FT-IR, and pyrolysis GC-MS revealed the absence of alkylcarbonate species, which have been the main component in carbonate-originated interphases; instead, PEO-like polymer embedded with  $\text{Li}_2\text{S}$  was found to cover the surface, and the authors suggested a mechanism producing the following new interphasial chemistry (eq 4):



The PC-rich electrolyte containing one of these cyclic sulfates (1,3,2-dioxathiolane-2,2-dioxide, or DTD) was demonstrated in

a full LIB with 4 V cathode chemistry, in which >80% capacity was retained for >400 cycles.

Another class of sulfur-based compounds described as effective additives for graphitic anode are based on the intramolecular esters of organic sulfonates or sultones (Table 17).<sup>194–197</sup> Li and co-workers reported both saturated and unsaturated members of the family, showing their common merits of forming protective SEI in the presence of high PC-concentration, and claimed that their reduction potential can be tuned by varying the substituents on, as well as unsaturation degrees of, the alkyl ring. The performance of these electrolytes in full LIB was demonstrated.

Before this section ends, it should be noted that some of these sulfur-based compounds, such as organic esters of sulfates, are usually very toxic. The environmental impact of them has to be considered before their large-scale application in the LIB industry.

**3.4.1.3. Boron-Based Additives.** Certain boron-based compounds also have lower LUMO than carbonates, which makes them potential candidates to modify the interphase on anode with varying success. Wang et al. reported the behavior of 3,5-bis(trifluoromethyl)bezeneboronic acid (BA, Table 18)

Table 18. Boron-Based Additives

	$E_{\text{red}}$ (V vs. Li)
3,5-bis(trifluoromethyl)bezeneboronic acid (BA)	1.05~1.6
trimethoxy boroxine (TMOBX)	

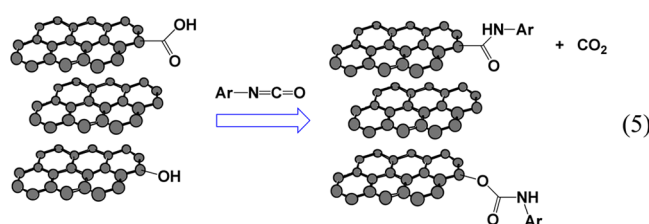
in PC-rich electrolytes, but found that the cointercalation of PC was only partially suppressed.<sup>198</sup> The high background current in corresponding cyclic voltammetry suggested that this acidic species may not be stable against reduction between 1.8–0.8 V vs Li. More recently, Dahn et al. developed a high precision coulometry technique for the investigation of parasitic reactions within an electrochemical cell, which proved to be a rather powerful tool to quantify the effectiveness of additives. Applying the technique, they studied trimethoxyboroxine (TMOBX, Table 18) as an additive in cells based on  $\text{LiCoO}_2$  or  $\text{LiNi}_{0.3}\text{Mn}_{0.3}\text{Co}_{0.3}\text{O}_2$  cathode and graphite anode and found a rather complicated interplay between the additive and the electrolyte composition, electrode chemistries, as well as charging end points.<sup>199,200</sup> In general, the addition of TMOBX at small concentrations (<1%) reduces cell impedance while improving Coulombic efficiency; however, higher concentrations of TMOBX (<1.5%) counter-effect the above. On the other hand, when used in combination with other additives such as VC, the side effects of TMOBX were apparently mitigated.

**3.4.1.4. Isocyanate-Based Additives.** Aromatic isocyanates were first reported by Zhang as electrolyte additives for graphitic anodes. Using phenyl- and 4-fluorophenylisocyanate at 1–5% (Table 19),<sup>201</sup> he noticed that the graphitic anode did not exfoliate in PC-rich electrolytes, indicating that some form

Table 19. Isocyanate-Based Additives

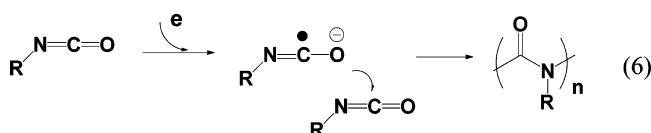
	$E_{\text{red}}$ (V vs. Li)
phenyl isocyanate (PI)	1.62
4-fluorophenyl isocyanate (FPI)	1.25
4-bromobenzyl isocyanate (Br-BIC) benzyl isocyanate (BIC)	1.25
2,4,6-trimethoxy isocyanate (TMPI)	1.25
2,4,6-trifluorophenyl isocyanate (TFPI)	1.45
diethoxyphosphinyl isocyanate (DOPI)	1.47
ethyl isocyanate (EtNCO)	1.10
4-bromoethyl isocyanate (BrEtNCO)	2.00
p-toluene sulfonyl isocyanate (PTSI)	1.5
hexamethylene diisocyanate (HDI)	1.5

of protection was formed, with subsequent benefits, such as lower irreversible capacities and higher Coulombic efficiencies. On the basis of the known chemistry of isocyanate functionalities toward hydroxyl addition, he suggested a mechanism that does not involve electrochemical reduction of the additive (eq 5), in which the N=C double bond experiences addition by the remnant hydroxyls existing on any graphite surface:



His argument seemed to be supported by the following facts: (1) there were no discernible reduction peaks in the cyclic voltammograms that correspond to any reduction process of isocyanates as compared to baseline electrolytes; (2) the substitution at the aromatic ring by fluorine did not induce any changes in terms of Coulombic efficiency and irreversible capacities. However, this mechanism was challenged by Korepp et al., who exhaustively investigated a series of aromatic and aliphatic isocyanates (Table 19) and concluded that an

electrochemical, rather than chemical, process is responsible for the stabilization of graphitic structure in PC-rich electrolytes.<sup>202,203</sup> They proposed an alternative mechanism, in which the unsaturated isocyanates were electrochemically polymerized, leading to a polyamide-like SEI (eq 6).



Their hypothesis was supported by both electrochemical and *in situ/ex situ* surface analyses. Interestingly, what seemed to directly conflict with what Zhang observed was the different onset reduction potential of those isocyanates, obviously varying with the various substituents (Table 19), whose higher reduction potential than 0.8–1.0 V (typical of most carbonates) ensures their qualification as electrolyte additives.

More recently, in a clever approach Wu et al. leveraged the interphasial properties of isocyanates to stabilize graphitic anodes in sulfone-based electrolytes.<sup>204,205</sup> The latter has been known for their high anodic stability on cathodes but, simultaneously, poor ability to form effective SEI on graphitic anodes.<sup>1</sup> The integration of a sulfonyl isocyanate and a diisocyanate (Table 19, *p*-toluenesulfonyl isocyanate or PTSI,

Table 20. Ionic Additives

	$E_{\text{red}}$ (V vs. Li)
lithium salicylatoborate (LiSAB)	
ammonium perfluorocaprylate (APC)	
tetraethylammonium tetrafluoroborate (TEABF <sub>4</sub> )	
silver hexafluorophosphate (AgPF <sub>6</sub> )	
sodium perchlorate (NaClO <sub>4</sub> )	
sodium phosphates	<p style="text-align: center;"><math>n = 0 \sim 2</math></p>

and hexamethylene diisocyanate or HDI) with tetramethylene sulfone (TMS) offered an electrolyte of both SEI-forming ability on graphitic anode and anodic stability up to 5.0 V on various cathodes, such as LiCoO<sub>2</sub> (4.2 V), LiNi<sub>0.33</sub>Mn<sub>0.33</sub>Co<sub>0.33</sub>O<sub>2</sub> (4.5 V), and LiNi<sub>0.5</sub>Mn<sub>1.5</sub>O<sub>4</sub> (4.95 V). Their observation of higher reduction of these isocyanates agreed well with what Korepp et al. have reported.<sup>202,203</sup>

**3.4.1.5. Ionic Additives.** The choice of additives was not limited to molecular compounds only; more often than not ionic compounds (salts) were also found to participate in interphasial formation, with either cation or anion. If the potential of these reductions occurs before the carbonate solvents reduce, there is a possibility that these salts can be used as additives to modify surface chemistries.

Originally proposed as an electrolyte salt, LiBOB was discovered to dominate SEI formation chemistry on graphitic anode surface with its anion-originating chemistry.<sup>1,206</sup> Considering that LiBOB as a main salt brought certain performance compromises, such as higher cell impedances, lower anodic decomposition potential on 4.0 V class cathode materials, and poorer performances at subzero temperatures,<sup>66,67</sup> Xu et al. explored its use as additive at low concentrations to circumvent those “trade-offs”.<sup>207</sup> At concentrations as low as 5%, the interphase on graphitic anode was already overwhelmed by the characteristic of BOB<sup>-</sup>-reduction products, and the cycling of graphite anodes was stabilized by these trace amounts of LiBOB in PC-rich (although not neat PC) electrolytes. When LiBOB was present below 5%, the competition between two extreme interphasial chemistries of “graphite protection” and “graphite exfoliation” could be clearly visualized. The high

reduction potential (~1.7 V vs Li) of BOB<sup>-</sup>-anion makes it a popular choice of additive to modify anode surfaces. The structural hybrid between BOB and BF<sub>4</sub> (i.e., DFOB), on the other hand, seemed to have inherited the merits of both parent anions, characterized by much lower cell impedance but similar reduction potential around ~1.7 V as compared to BOB.<sup>140,142,208</sup> For this reason, LiDFOB has been considered as a more promising additive than LiBOB. In more recent studies, Shkrob et al. used electron paramagnetic resonance spectroscopy to investigate the detailed redox mechanisms of BOB and DFOB anions.<sup>142</sup> They concluded that, upon single-electron reduction on graphitic surface, BOB would lose oxalate and DFOB would lose fluoride, with the concurrent formation of an oxalatoboryl. A boron-containing interphase in both cases is the result of reaction between oxalatoboryl and carbonate molecules. A difference does exist between those two anions though, as the fluoride released by DFOB leads to thinner SEI. When fluorines on boron were replaced by weaker electron-withdrawing chelating substituents, such as salicylato groups (LiSAB, Table 20) as reported by Aubach et al., less ideal effect on performance was found as compared to VC-containing or even baseline electrolytes.<sup>209</sup>

Other ionic additives offer their cations for interphasial chemistry. Wu et al. reported that silver hexafluorophosphate (AgPF<sub>6</sub>, Table 20) at low concentrations can protect graphitic anode in PC-rich electrolytes. They suggested that the reduction of Ag<sup>+</sup> at ~2.15 V formed a porous Ag film over graphite, which prevents PC-cointercalation.<sup>210</sup> It should be cautioned here that, if this Ag film is indeed responsible for the different electrochemical behavior, one should no longer call it “SEI” in a strict sense, because a metallic film, which is electronically conductive, does not possess an electrolyte nature, a prerequisite for the concept of SEI. Two ammonium salts were reported as additives by Huang<sup>211</sup> and Hao,<sup>212</sup> respectively. In both cases, these additives were only tested in anode half cells. Particularly in the former case, 1% of ammonium perfluorocaprylate (APC, Table 20) in electrolyte was found to decompose reductively around 1.9 V and form an interphase enriched with fluoroalkyl moieties, which was more conductive than that formed in the baseline electrolyte despite the fact that the presence of the additive reduced the bulk conductivity. As result of the more conductive interphase, overall cell impedance as well as rate capability benefited from APC presence.

Alkaline salts have also been described as additives. Komaba et al. used NaClO<sub>4</sub> as cosalt with LiClO<sub>4</sub> in EC/DEC and observed some rather interesting interphasial behavior.<sup>213</sup> Although Na<sup>+</sup> was neither reduced at anode nor intercalated, it was by no means just an inert component in the electrolyte; instead, its presence apparently altered the interphasial chemistry, as reflected in the reduced irreversible capacity of graphitic anode as well as kinetics of Li<sup>+</sup>-transfer across the interphase. On the basis of surface analyses by XPS and SEM/transmission electron microscope (TEM), the authors suggested that during the initial SEI formation stages, Na<sup>+</sup> was embedded in the interphase, which somehow allows Li<sup>+</sup> to travel with higher freedom. On the other hand, Sano et al. described a series of sodium phosphate salts as additives for electrolyte based on mixed salt (LiPF<sub>6</sub>/LiTFSI) and EC/DEC, some representatives of which are also listed in Table 20.<sup>214</sup> Positive effects on LiMn<sub>2</sub>O<sub>4</sub>/graphite cells were reported, but no attempts were made to identify how they work or whether they work on the cathode or anode side.

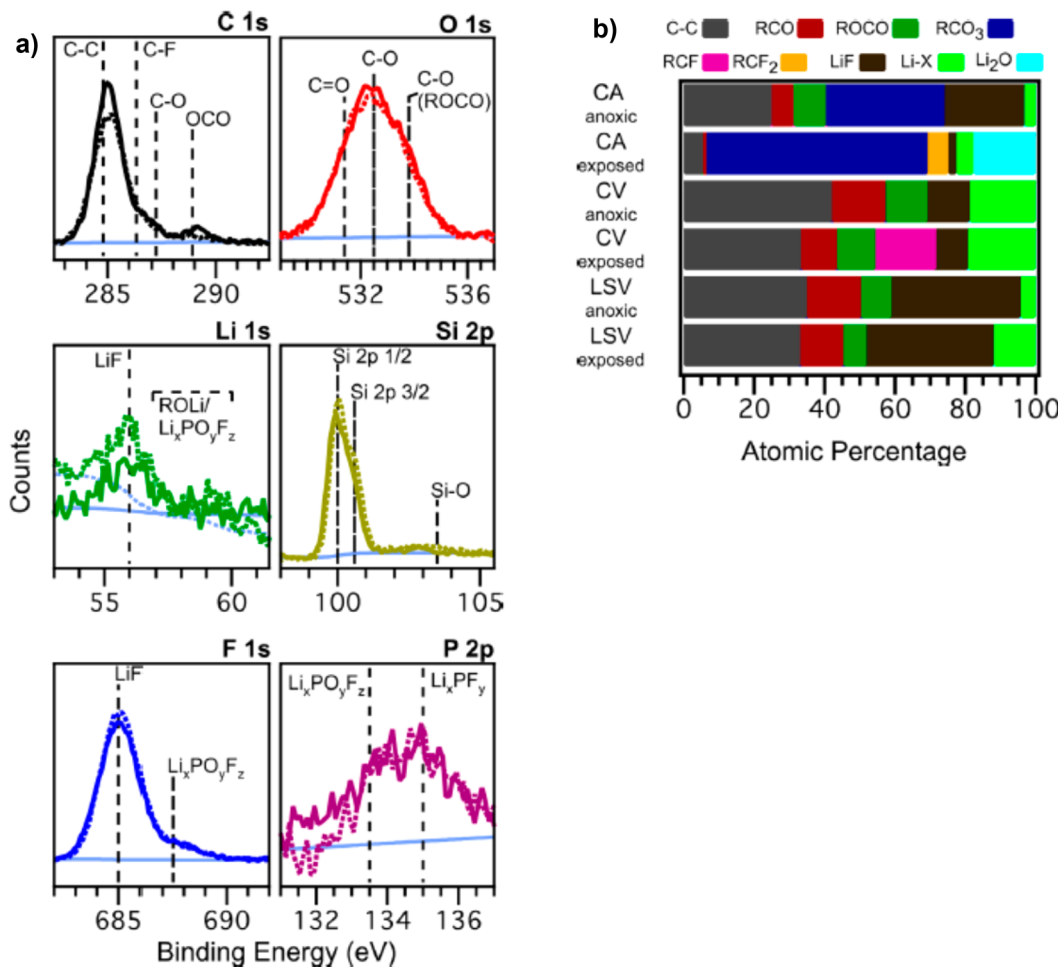


**Figure 23.** SEI compositions on Si anodes: (a) identification of SEI components on Si (001) wafer via XPS, wherein solid lines represent the surface prepared under anoxic conditions, while dashed lines were obtained after 10 min exposure to ambient atmosphere; and (b) quantitative breakdown of SEI components obtained from estimated peak areas after fitting individual contributions from each functionality according to XPS. Reprinted with permission from ref 222. Copyright 2012 American Chemical Society.

Finally, knowing that inorganic lithium salts such as LiF, Li<sub>2</sub>O, LiOH, Li<sub>2</sub>CO<sub>3</sub>, LiOCH<sub>3</sub>, and LiOC<sub>2</sub>H<sub>5</sub> are most likely SEI ingredients, Chrétien et al. directly added these salts into electrolyte and evaluated their effect on the performance of Li-ion cell based on graphitic anode and LiNi<sub>0.33</sub>Mn<sub>0.33</sub>Co<sub>0.33</sub>O<sub>3</sub> cathode.<sup>215</sup> They reported that the cathode was more sensitive to the presence of these additives than graphitic anode, whereas mainly negative results were generated by LiOH and Li<sub>2</sub>O, and positive results by Li<sub>2</sub>CO<sub>3</sub>, LiOCH<sub>3</sub>, and LiOC<sub>2</sub>H<sub>5</sub>. The effect of LiF varied with its concentration. The authors suggested that the cell performance deteriorated due to the aggregation of LiF, which could be inhibited by glyme that effectively chelated to LiF.

**3.4.2. Additives and Interphasial Chemistry on Alloy-Type Anodes.** As a replacement for graphitic anodes with potential improvements in specific capacity up to 10 times, alloy-type anode materials based on Si, Sn, and other metals have been actively explored, despite the knowledge that extreme volume changes (as much as 400%) usually accompany the lithiation/delithiation process and lead to failures stemming from electrochemical, morphological, and mechanical irreversibilities.<sup>8</sup> Recent advances in nanostructure design and synthesis of Si-based materials have rejuvenated the hope of these alloy-type anode materials for commercial LIB,<sup>9,216,217</sup> and numerous activities, from understanding what SEI on Si is

and how it forms<sup>218–223</sup> to searching for proper electrolytes and additives, were accordingly accelerated.

Comparing the formation chemistry and processes of SEI on graphitic and Si anodes, one could find that certain similarities were shared by the two, such as (1) both materials operate around 0.2–0.5 V vs Li, which is outside the thermodynamic stability window of most electrolyte components, and hence reductive decomposition of these components is inevitable and responsible for the interphasial chemistry; and (2) both materials are in the discharged state while pristine, and hence the SEI was formed in a stepwise manner, which provides opportunity for interphase additives to function. However, more uniqueness than similarities rule over the SEI chemistry on Si, as the reductive reactions on its surface are not only mediated by the native film consisting of SiO<sub>2</sub> and silanol functionality (Si—OH) that exist on most Si materials, but also affected by the irreversible morphological conversion during the first lithiation from crystalline to amorphous phases and the large volume changes upon reversible lithiation/delithiation cycles. The latter creates new pristine Si surfaces each time by breaking the already formed SEI and, therefore, induces a new round of the SEI formation process. This continuous growth of SEI, at least in part, accounted for the much faster capacity fade that accompanies Si-based anode materials.

On the basis of spectra and microscopy studies, Lee et al. suggested that, during the continuous growth of SEI, typical electrolyte (EC/DEC) solvents mainly contributed to the formation of SEI on thinfilm Si during charge (lithiation), but anions participated during discharge (delithiation).<sup>218</sup> Therefore, with extended cycling, the SEI composition on Si would become more enriched with LiF rather than organic moieties. Contradicting conclusions seemed to be drawn by Delpuech et al., who used solid-state <sup>7</sup>Li, <sup>19</sup>F, and <sup>13</sup>C NMR with magic angle spinning to monitor the failure mechanism of Si materials in typical carbonate electrolytes.<sup>223</sup> They found that irreversible capacity loss caused in the form of lithium salts was negligible and mainly occurred in the first cycle, while most of the subsequent capacity fading was associated with the continuous production of nonlithiated polymeric moieties. Yen et al. compared the major chemical species found in SEI formed on Si with those on graphite, and concluded that, besides the well-known alkylcarbonates, the presence of LiF and C- and Si-fluorides is much higher on Si. The surprising discovery of C–F species, which are difficult to form under ordinary electrochemical conditions, was attributed to the possible catalysis effect from SiF<sub>x</sub> species.<sup>219</sup> This much conspicuous role of fluorides seemed to be essential for the protection of Si materials, as Profatilova et al. described that reactions between Si and electrolyte components can only be effectively suppressed in the presence of LiPF<sub>6</sub>, and not with LiTFSI.<sup>220</sup> Perhaps the most systematic analyses on Si-SEI were performed by Schroder et al., who meticulously studied the conditions under which a Si electrode surface was prepared, and concluded that not only ambient exposure affects the chemical composition, but the electrochemical techniques employed will also cast significant influence, leading to different SEI components, whose quantitative distribution is summarized in Figure 23.<sup>222</sup> Despite the controversy over SEI chemical composition and whether the presence of LiF is beneficiary, however, it does seem to be apparent that fluorides accounted for a large presence in Si-SEI.<sup>221,223–225</sup> Most efforts to develop additives for Si anode aim to mitigate the issue of continuous SEI growth as well as to reduce LiF presence in the SEI.

**3.4.2.1. VC, LiBOB, and LiFOB.** The success of VC and LiBOB with graphitic anodes would make them natural candidates when one considers improvement of Si electrodes, but the limited literature available implied their limited success with Si.

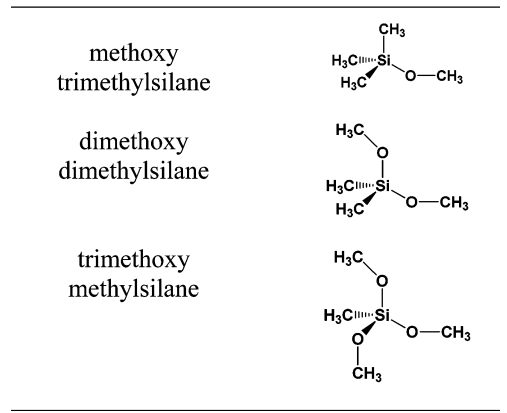
Chen et al. studied the effect of 1% VC as additive in carbonate-based electrolyte on the cycling behavior of thin film Si.<sup>226</sup> Although marked improvements were observed in terms of capacity retention, Coulombic efficiencies, and cell impedances, the presence of VC did not prevent the “cracking” of SEI upon delithiation. XPS analyses revealed that VC did slightly decrease the amount of LiF in the SEI. In a more recent report, Dalavi also described the effect of VC and confirmed its positive effect on cycling performance.<sup>227</sup> The authors attributed the incremental improvements in performance on the polymeric nature of the new SEI imparted by VC, which also reduced LiF presence by preventing salt anion reaction with Si.

Similar positive effects were claimed for LiBOB as well. Choi et al. used 0.7 M LiBOB as additive in typical EC/DEC electrolytes and reported marked improvements.<sup>228</sup> Likewise, the early reduction of BOB<sup>-</sup>-anion helped prevent the participation of other electrolyte components, resulting in a smaller presence of fluorides in the interphase and reducing consumption of

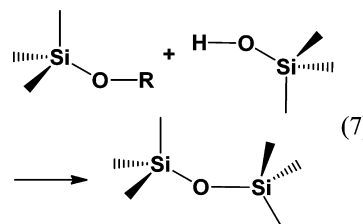
both Li and active Si. Li et al. combined LiBOB with VC at various ratios and studied their effects on a Si/graphite composite electrode.<sup>229</sup> A synergy was described to exist between the two, presenting higher capacity utilization than electrolytes with VC alone, and better capacity retention than electrolytes with LiBOB alone. Surface analyses by XPS and FTIR confirmed the participation of BOB<sup>-</sup>-anion in interphasial chemistry. Dalavi et al. used both LiBOB and LiFOB as additives.<sup>227</sup> Despite the fact that FOB<sup>-</sup>-anion itself is fluorinated, its presence in the electrolyte actually reduced LiF concentration in the SEI as does BOB<sup>-</sup>-anion. Both additives increased the interphasial components originating from the reduction of oxalato-species, but their effect on electrochemical performances was only modest.

**3.4.2.2. Silane.** Ryu reported a series of alkoxy silanes (Table 21) used as additives to passivate Si surfaces,<sup>230</sup> which

Table 21. Silane Additives for Si Electrode



were supposed to react with the interfacial silanol groups and convert to stable siloxane or silicate bonds:



Using the electrochemical quartz crystal microbalance (EQCM) technique, they observed that, in the presence of these silane additives, the accumulation of mass due to the surface reduction of electrolyte components was significantly reduced, which corresponded well with the improvements in electrochemical performance. The number of alkoxy functionalities in the additive, which were responsible for the reaction as illustrated in eq 7, directly correlated with the reduction in mass accumulation, thus confirming the proposed mechanism of how these silane additives work. Song et al. used one of the silane additives reported above and studied how it affected the chemical composition of the interphase.<sup>231</sup> They noted that, with 5% trimethoxymethyl silane, the fluoride content in the SEI was significantly replaced by the components that most likely originated from the solvents, such as lithium salts of alkyl-carbonates. They believed that a SEI dominated by inorganic fluorides in the absence of these organic SEI components was responsible for the poor cycling of Si electrodes, while the

silane additives suppressed the reaction between surface silanol and  $\text{PF}_6^-$ -anion and stabilized the interphase.

**3.4.2.3. FEC.** Perhaps the most reported additive (or cosolvent depending on its presence in the electrolyte) for Si anode is FEC.<sup>224,225,227,232–234</sup> Despite the various Si materials used, the surface analyses of the interphasial chemical composition, and the interpretations or speculations over the possible mechanisms, a general consensus is that FEC-originated interphases tend to be denser and thinner, in contrast to interphases formed in FEC-free electrolytes, which are more porous and permeable by electrolytes.<sup>232,233</sup> The electrochemical performance of Si materials in those FEC-based electrolytes was found to be superior as judged by the capacity retention as well as Coulombic efficiency (Figure 24a).<sup>233,234</sup> However, researchers

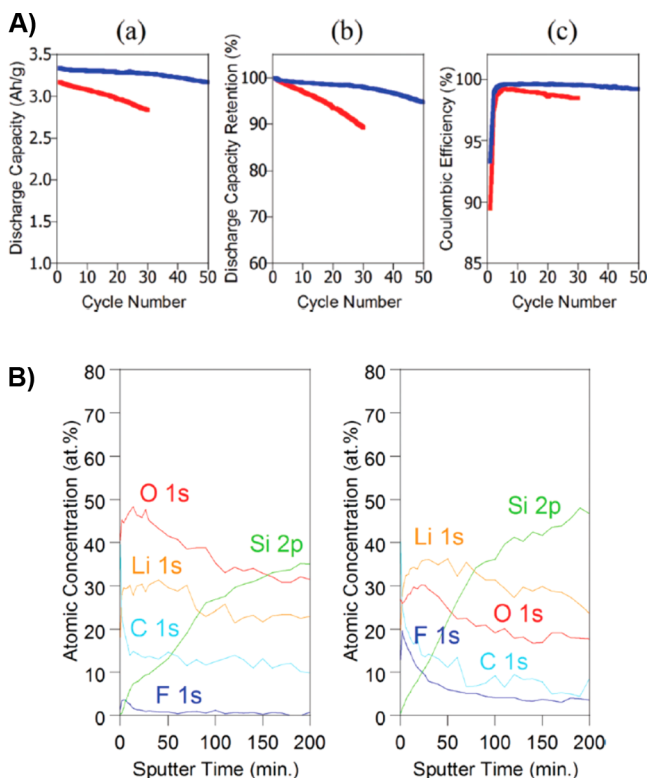
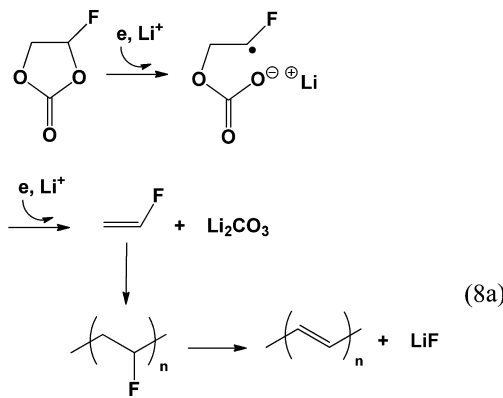


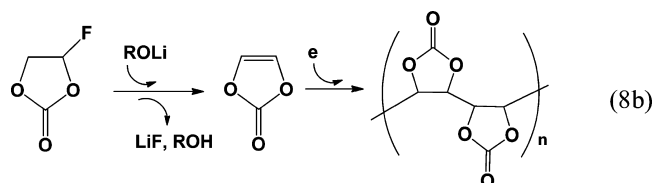
**Figure 24.** Performance of Si-anodes in FEC-based electrolytes: (A) Cycling performance of (a) discharge capacity, (b) discharge capacity retention, and (c) Coulombic efficiency of Si/Li half cells using EC- (red) and FEC-based (blue) electrolytes; and (B) XPS depth-profiles of Si electrodes in (a) EC- and (b) FEC-based electrolytes after 30 cycles. Reprinted with permission from ref 233. Copyright 2011 Electrochemical Society.

are sharply divided over whether LiF was formed in the interphases, and whether the presence of LiF in the interphase was beneficial to electrochemical performances.

Examined with surface analytic tools such as XPS, FTIR, and energy dispersive X-ray spectra (EDX), the chemical composition of FEC-originated interphases was shown to be more enriched with inorganic fluorides, while interphases formed in FEC-free electrolytes have more O-containing species, such as  $\text{Li}_2\text{O}$  and lithium salts of alkylcarbonates, apparently from the reduction of carbonate solvents (Figure 24b).<sup>224,233</sup> Nakai et al. suggested a possible mechanism for FEC to be reduced, eventually leading to an interphase with polymeric species embedded with LiF (eq 8a).<sup>233</sup>



Etacheri et al., on the other hand, proposed an alternative route for the fate of FEC on Si surface,<sup>225</sup> in which FEC also produces LiF but ends up polymerizing into poly(VC) (eq 8b).



It must be emphasized here that the seeming controversy over the role of LiF in SEI formed on Si by either FEC-free or FEC-based electrolytes should not be taken at face value. As one should have learned from the studies of interphases on graphite, it is not merely chemical composition but also how these chemicals are arranged (i.e., morphology) that dictates the properties of the interphase. In other words, LiF produced by one electrolyte composition on a specific Si surface is most likely distributed in a different manner from LiF produced in other cases.

There are other metals or alloys that can serve as hosts for lithiation, but their specific capacities are usually lower than what Si can promise and have received less attention accordingly; nevertheless, they face similar challenges to Si, where volume changes creates new surfaces for SEI to grow at the expense of cell health.<sup>235–238</sup> The SEI on those alloys were reported as distinctively different from their counterparts on graphite, often dominated by inorganic fluorides rather than organic polymer or salts.<sup>235,236</sup> In more than one instance, carboxylate salts of alloy metals were detected,<sup>235,238</sup> indicating that new C–C bonds should have been formed, probably through radical recombination. Making comparison between the “ideal” interphases on graphite and alloy surfaces, Wagner et al. suggested that the former would require a dense film to prevent exfoliation, while the latter a flexible film to accommodate volume change.<sup>236</sup> This concept probably remains true for all alloy-type electrode materials where no topotactic stability is available, and the design of new additives must take intense mechanical stress into consideration.

More recently, a homologous series of FEC were synthesized by Zhu et al. as additives for LIB.<sup>239</sup> Instead of a single fluorine atom, these cyclic carbonates contain a long perfluorinated alkyl tail. The authors suggested that these solvophobic tails, which are electrochemically stable, could enable the additive molecules to self-assemble on electrode (graphitic or transition metal oxide) surfaces and form a dense and membrane-like layer that is impermeable to electrolytes. Although they were yet to be tested on silicon-based electrode surfaces, their

interphasial behaviors on  $\text{LiMn}_{1.5}\text{Ni}_{0.5}\text{O}_4$  and graphite have been generally encouraging, and their interaction with Si would be of high interest.

**3.4.3. Additives for Cathode.** As compared to the efforts spent on anode interphases, the understanding of cathode interphase is rather limited, and very few additives have been developed for the purpose of stabilizing cathode/electrolyte interface until fairly recent. Most of these efforts were initiated after 2008, when the possibility of high voltage (5 V class) cathode materials such as  $\text{LiCoPO}_4$  (4.8 V),  $\text{LiNiPO}_4$  (5.1 V),  $\text{LiCoPO}_4\text{F}$  (4.9 V), and  $\text{LiNi}_{0.5}\text{Mn}_{1.5}\text{O}_4$  (4.6 V) was no longer that remote.<sup>240</sup> Despite reports that conventional carbonate-based electrolytes were sufficiently stable on the highly oxidizing surface,<sup>241</sup> the general consensus remained that carbonates were susceptible to oxidative decomposition beyond 4.5 V,<sup>10,11,65,240</sup> making it imperative that new electrolyte components, especially solvents and additives, be developed to cater to those high voltage chemistries.

**3.4.3.1. Borates and Boroxines.** An unexpected additive for high voltage cathodes is LiBOB. Although already reported as anodically unstable at voltages higher than 4.2 V,<sup>66,67</sup> Täubert et al. reported that using LiBOB at 2% could benefit  $\text{LiNi}_{0.8}\text{Co}_{0.15}\text{Al}_{0.05}\text{O}_2$  cathode as well, besides its known ability to stabilize graphitic anode.<sup>242</sup> The cathode/electrolyte interphase formed in the presence of LiBOB surprisingly led to higher rate capability as compared to its  $\text{LiPF}_6$  counterpart. Dalavi et al. applied LiBOB as additive to high voltage cathode  $\text{LiMn}_{1.5}\text{Ni}_{0.5}\text{O}_4$  and observed significant improvement in both capacity retention and Coulombic efficiency with decreased cell impedance.<sup>243</sup> Ex situ analysis via FTIR and XPS on the cycled electrode surfaces indicated that surface deposition was apparently characterized by the chemical signature of  $\text{BOB}^-$ -anion. They suggested that the new interphasial chemistry could work through two possible mechanisms: (1) the early oxidation of  $\text{BOB}^-$ -anion deactivated certain spots on the cathode surface and prevented further oxidation of the main solvents; and (2) the presence of the  $\text{BOB}^-$ -originated interphase could suppress the dissolution of Mn(II) from the cathode lattice, which is usually catalyzed by acidic species generated by  $\text{PF}_6^-$ -anion. In a similar manner, Aravindan et al. used LiBOB on  $\text{LiCoPO}_4$ ,<sup>244</sup> whose higher voltage (4.8 V) has prevented severe challenges to carbonate-based electrolytes as reflected by fast fading capacity. With 3% LiBOB, the capacity retention was much improved against baseline electrolyte, although fading rate was still too high to be viable.  $\text{LiBF}_4$  was also used for similar purposes by Zuo et al. on  $\text{LiNi}_{0.5}\text{Mn}_{0.3}\text{Co}_{0.2}\text{O}_2$  in an attempt to increase its capacity utilization at 4.5 V charge cutoff.<sup>245</sup> While capacity retention, Coulombic efficiency, and cell impedance were improved, they noted that 1% of the salt resulted in a cathode interphase almost absent of LiF, which has been abundant in SEI generated by control electrolytes.

As the hybridized salt of  $\text{LiBF}_4$  and LiBOB, LiDFOB attracted more attention as a promising additive for various cathode chemistries, including lithium–manganese-rich layer–layer high capacity metal oxides of different compositions as well as high voltage olivine  $\text{LiCoPO}_4$ .<sup>246–249</sup> In general, there was a positive effect on the stabilization of the interaction between electrolytes and the charged cathode surfaces, while Zhu et al. revealed that there were actual synergistic effects from this additive on both cathode and graphitic anode:<sup>249</sup> on the former, LiDFOB functions to minimize dissolution of transition metal elements from the cathode lattice, and on the latter it helps to form a thin and less resistive SEI as described

earlier.<sup>139,140</sup> Shkrob et al. investigated the fundamental oxidation mechanisms of both BOB and DFOB using EPR and DFT calculation.<sup>142</sup> When comparing the behavior of these anions on transition metal oxide surfaces, they found that both experience the loss of  $\text{CO}_2$  upon single-electron oxidation and result in stable acyl radicals, whose recombination at the oxide surface yields dimers that form strong B–O bonds with oxygen hole centers at the surface (Figure 25). Naturally the presence of fluorines in DFOB makes this interaction stronger than those with BOB. The authors believe that this chemisorbed dimeric structure was responsible for the passivation of positive electrode surfaces in electrolyte.

Finally, besides their interphasial properties on graphitic anode,<sup>199,200</sup> boroxine compounds were also explored as cathode additives.<sup>250–252</sup> Horino et al. studied a series of

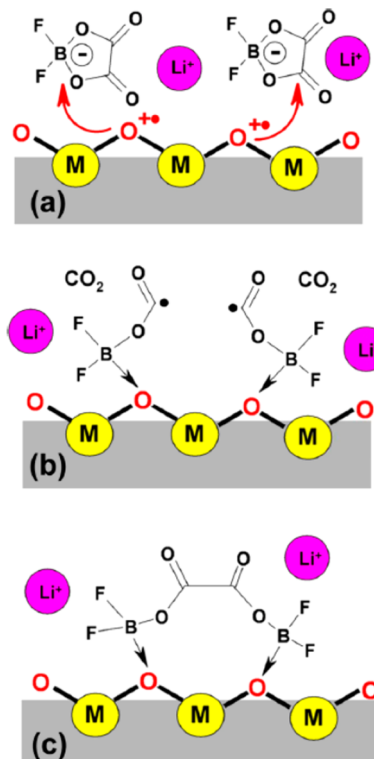


**Figure 25.** Schematic illustration of how the robust interphase is formed on a transition metal oxide surface by LiDFOB additive: (a) adsorbed DFOB anions experience single-electron oxidation; (b) the formed acyl radicals chelate with oxide surface with their Lewis acid center; and (c) recombination of acyl radicals leading to chemisorbed dimeric fluorooxalatoboryl, which constitutes the passivation interphase. Reprinted with permission from ref 142. Copyright 2013 American Chemical Society.

**Table 22. Boroxine Additives for Cathode Surfaces**

alkoxyboroxine R = methyl, ethyl, propyl and iso-propyl	
trimethyl boroxine	

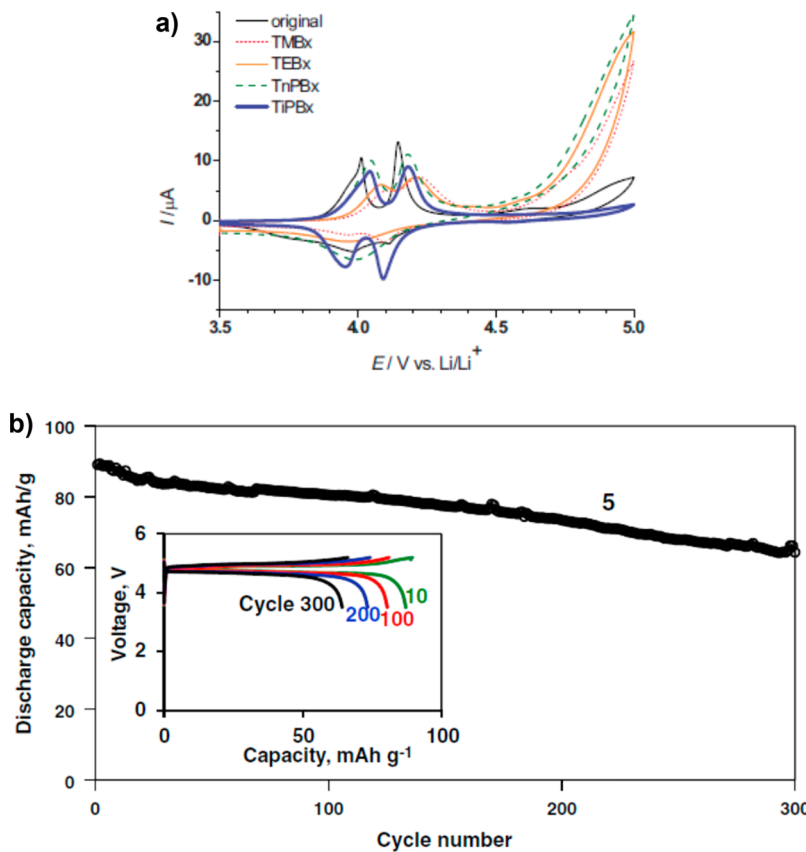
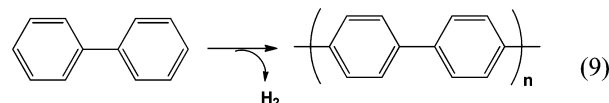


**Figure 26.** Effect of boroxines as cathode additives: (a) Cyclic voltammetry of  $\text{LiMn}_2\text{O}_4$  thin films in baseline electrolyte 1.0 M  $\text{LiCF}_3\text{SO}_3/\text{EC}/\text{EMC}$  (50:50) (solid lines) or electrolytes with TMBX (trimethyl boroxine, thin dash line), TEBX (triethyl boroxine, medium line), TnP BX (tri-n-propyl boroxine, medium broken line) and TiPBX (tri-iso-propyl boroxine, bold line). Reprinted with permission from ref 250. Copyright 2010 Electrochemical Society. (b) Cycling performance of  $\text{LiCoPO}_4/\text{Li}$  half cells in 1.0 M  $\text{LiPF}_6/\text{FEC}/\text{DMC}$  with 0.5% TMBX. Reprinted with permission from ref 252. Copyright 2013 Elsevier.

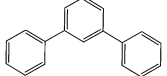
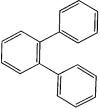
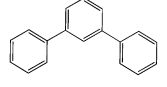
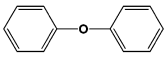
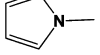
trialkoxy boroxines (Table 22) and found that, when the substituent was iso-propyl, the anodic stability of carbonate electrolytes improved up to 5.0 V on  $\text{Li}_2\text{Mn}_2\text{O}_4$  surface over the baseline electrolyte (Figure 26a).<sup>250</sup> Of course, as a 4.0 V class cathode,  $\text{Li}_2\text{Mn}_2\text{O}_4$  does not have any redox activity in the vicinity of 5.0 V, and it was only used here as a more reliable working electrode than nonporous electrodes such as Pt or glassy carbon. Ping et al. investigated the effect of TMOBX (Tables 18 and 22) on various cathode surfaces such as  $\text{LiNi}_{0.8}\text{Co}_{0.15}\text{Al}_{0.05}\text{O}_2$ ,  $\text{LiNi}_{0.33}\text{Mn}_{0.33}\text{Co}_{0.33}\text{O}_2$ , and  $\text{LiCoO}_2$ ,<sup>251</sup> and concluded that, while there is no obvious oxidation of TMOBX, the cell impedance was decreased when its concentration was below 1%. In a more recent report, Sharabi et al. used trimethylboroxine (Table 22) in FEC-based electrolytes on  $\text{LiCoPO}_4$ , whose cycling seemed to be stabilized as indicated by the extended cycle life (Figure 26b).<sup>252</sup> Of particular interest, they described that the electrolyte/electrode ratio played a critical role in determining the electrochemical performance, which was attributed to the sensitivity of  $\text{LiCoPO}_4$  toward HF contaminants. Despite its apparent effect on electrochemical performance of these high voltage cathodes, the mechanism of the possible interphasial chemistry of boroxines remains to be understood.

**3.4.3.2. Aromatic and Heterocyclic.** Early on, polyphenyl compounds have been applied as overcharge-protection additives in LIB, leveraging its ability to generate gas at voltages above the upper limits of 4 V class cathodes:



The polymeric species piled up on cathode surface increases cell impedance, and gas released activates the pressure-sensitive cap and stops battery operation at  $\sim 4.5$  V.<sup>253</sup> For this purpose, >1% additives were needed for sufficient gas generation. Abe et al. found that, by decreasing the concentration of such polyphenyl compounds to 0.1–0.2%, the formed polymeric film on  $\text{LiCoO}_2$  and spinel  $\text{Li}_{1.09}\text{Mn}_{1.91}\text{O}_4$  cathodes enable higher cycling stability.<sup>254</sup> Extending the concept to a series of aromatic and heterocyclic compounds, representatives of which are listed in Table 23, Abe et al. proposed a mechanism that differs from the protection interphase on anodes.<sup>255</sup> Named electro-conducting membrane (ECM), they claimed that those compounds were selected because of their higher HOMO energy levels (hence lower oxidation potentials) than carbonate solvents, and the passivation film thus formed still allows electron conduction due to the conjugated structure of the polymer species. This newly formed ECM will cover the cathode surface, on which the catalytic and oxidative sites are unevenly distributed, and stabilize the cathode/electrolyte interface. To keep the ECM thickness in the nanometric range, the concentration of those additives has to be much lower than 1%, typically at 0.1%. It must be pointed out here that, despite the improved cycling stability of various cathodes in the presence of those ECM additives, an electronically conductive interphase cannot rationalize why sustained electrolyte decomposition was

**Table 23. Aromatic and Heterocyclic Additives for Cathode Surfaces**

		$E_{ox}$ (V vs. Li)
bi-phenyl (BP)		4.45
<i>o</i> -terphenyl (OT)		4.44
<i>m</i> -terphenyl (MT)		4.25
diphenyl ether (DPE)		4.5
<i>N</i> -methyl pyrrole		3.8
thiophene		4.4
2,5-dihydrofuran		4.6

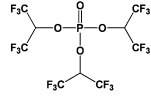
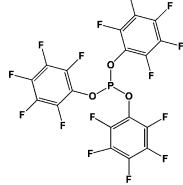
mitigated, which would actually be enabled by electron flow across the interphase.

Among the compounds described by Abe et al., thiophene and its derivatives were perhaps most investigated as indicated by the following reports.<sup>256–260</sup> In particular, they were applied on a few high voltage cathode chemistries such as LiCoPO<sub>4</sub>,<sup>258</sup> Li<sub>3</sub>V<sub>2</sub>(PO<sub>4</sub>)<sub>3</sub>,<sup>259</sup> and LiNi<sub>0.5</sub>Mn<sub>1.5</sub>O<sub>4</sub>.<sup>260</sup> In all cases, cycling stabilities of these challenging materials were improved to varying extents in cathode half cells.

Yang et al. described another heterocyclic compound that might not fit the qualification of ECM, but worked nonetheless. Using 2,5-dihydrofuran (DHF, Table 23) at 0.5–2% on a spinel cathode Li<sub>1.17</sub>Mn<sub>0.58</sub>Ni<sub>0.25</sub>O<sub>2</sub>, they observed marked improvement in capacity retention upon charging to 4.9 V.<sup>261</sup> It should be noted that DHF does not have sufficient unsaturation that would allow it to form an electron conductive film as would other heterocyclic compounds in Table 23.

**3.4.3.3. Phosphorus-Based Additives.** After phosphates were described as flame-retarding cosolvents for LIB electrolytes,<sup>1</sup> Xu et al. discovered that, at additive concentrations (<1%), a highly fluorinated derivative of Srimester of phosphate, tris(hexafluoro-iso-propyl)phosphate (HFiP, Table 24), could stabilize typical carbonate electrolytes with high voltage LiNi<sub>0.5</sub>Mn<sub>1.5</sub>O<sub>4</sub>, minimizing impedance at the cathode surface while extending reversible cycling (Figure 27).<sup>10</sup> It was speculated that phosphorus and fluoroalkyl species decomposed on catalytic spots of LiNi<sub>0.5</sub>Mn<sub>1.5</sub>O<sub>4</sub> and deactivated these spots from further oxidizing main components of electrolytes. Tan et al. applied this additive to high capacity cathode LMR-NMC, which is not “high voltage” itself but whose activation of spinel structure in the first cycle requires a

**Table 24. Phosphorus-Based Additives for Cathode Surfaces**

	$E_{ox}$ (V vs. Li)
tris(hexafluoro-iso-propyl)phosphate (HFiP)	
tris(pentafluorophenyl) phosphite (TPFPP)	

charging process at 4.7 V, and reported that not only was capacity retention improved, the rate capability was also higher, benefiting from the interphase that HFiP formed on LMR-NMC.<sup>262</sup> Of particular interest is that the authors believed that with 1% HFiP in the electrolyte, more Li<sub>2</sub>MnO<sub>3</sub> phase seemed to be activated, resulting in high capacity utilization. The oxidation potential of HFiP was shown to be ~4.2 V.

A similar stabilization effect was observed for LiNi<sub>0.5</sub>Mn<sub>1.5</sub>O<sub>4</sub> with a phosphite (TPFPP, Table 24) as an additive,<sup>263</sup> whose lower oxidation state (III) makes it easy to oxidize, probably at lower potential than HFiP. Post-mortem analyses via XPS and ICP-MS confirmed that the cathode surface after cycling was covered with an interphase that not only prevented sustained oxidation of main electrolyte components but also suppressed dissolution of Mn(II).

**3.4.4. Additives for Overcharge Protection.** A special class of additives that do not modify surface chemistries of either cathode or anode are the so-called “redox shuttle” additives, which interact with both electrodes but do not become part of their interphases. The basic working principle of redox shuttle, for the purpose of overcharge protection, was described in the 2004 review;<sup>1</sup> however, the inherent paradox existing between this class of additives and the working principle of interphases remains to be reasonably rationalized; that is, a successful interphase would insulate any electron tunneling between electrode bulk and electrolyte bulk, while a successful redox shuttle that migrates freely in bulk electrolyte must donate electron to or receive electrons from electrodes with minimum kinetic barrier.<sup>264</sup> Even as one accepts that SEI in real life cannot be an ideal electron-insulator, which causes the continuous growth of interphases that will be discussed in section 4.1, the current that was responsible for redox turnover reactions was obviously higher by orders of magnitude than the parasitic reactions that lead to SEI growth. Moshurshak et al. attributed this selectivity to the larger driving force associated with the redox shuttles, so that electrons can tunnel to or from them through interphases preferably, rather than to or from electrolyte solvent molecules.<sup>265</sup> Alternatively, Tang et al. developed a bilayer model of SEI, which consists of a compact inner layer that allows electron-tunneling and a porous outer layer that is electronically insulating but diffusible toward electrolytes.<sup>264</sup> They believed that it was the difference between the permeabilities of redox shuttle molecules and the electrolyte solvents toward this outer layer that dictates the preference of

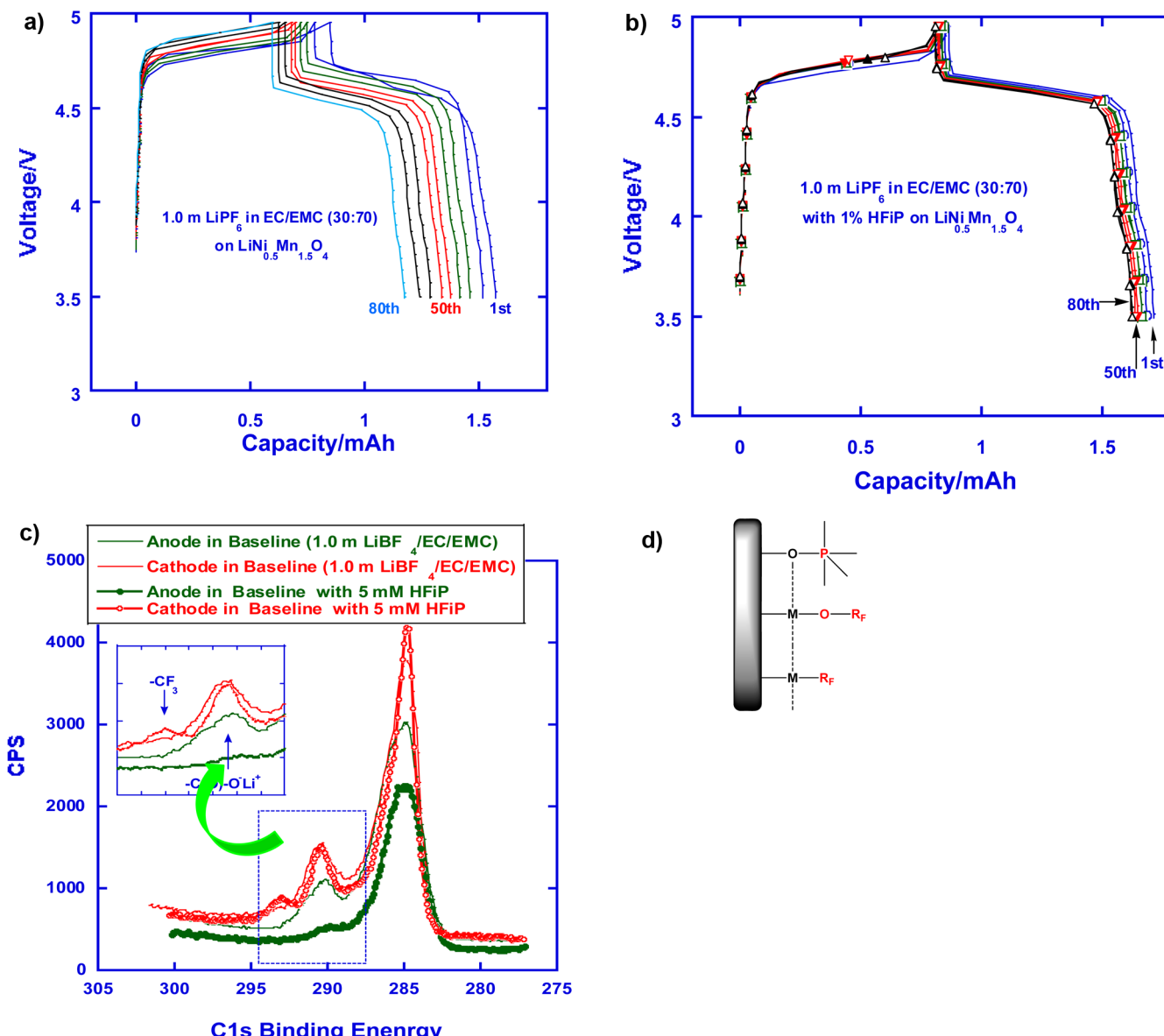


**Figure 27.** High voltage additive HFiP: voltage profiles of  $\text{LiNi}_{0.5}\text{Mn}_{1.5}\text{O}_4$  cathode in (a) baseline electrolyte  $\text{LiPF}_6/\text{EC/EMC}$  (30:70) and (b) the presence of 1% HFiP in baseline electrolyte. Only selected cycles were shown. (c) The fate of HFiP on a cathode surface as revealed by surface analysis via XPS, and (d) the hypothesized mechanism of a cathode surface passivation by fluoro-alkyl in HFiP. Reprinted with permission from ref 10. Copyright 2011 Electrochemical Society.

selectivity. Despite these inspiring concepts, the final resolution of this issue would require further investigations.

The early generation of redox shuttle additives based on ferrocene and heterocyclic compounds normally operated around 3 V. Systematic investigations were conducted by Dahn and co-workers to raise the shuttling potential so that these additives can be applied to LIB cathode chemistries operating between 3.5–5.0 V. On the basis of previous work by Adachi et al.,<sup>1</sup> they found that the reversible redox potentials of alkoxy-substituted aromatic compounds can be readily adjusted through the chemistry, number, as well as location of the ligands.<sup>266–271</sup> In one report, 58 such compounds were screened, and 2,5-di-*tert*-butyl-1,4-dimethoxybenzene was identified as a promising candidate (Table 25), which has a collection of well-balanced properties such as redox potential, solubility, diffusivity, and stability of the corresponding cation radical species. Apparently, the highly steric hindrance assisted

in stabilizing the oxidized form so that it could reach the other side of the cell for reduction before being quenched by other electrolyte components. Its effectiveness was proven in full LIB with a 3.5 V cathode  $\text{LiFePO}_4$ . Similar redox shuttle additives based on aromatic and heterocyclic structures, such as phenothiazines,<sup>270</sup> piperinyl-oxides,<sup>272</sup> and phenyl amines,<sup>273</sup> were also described by the same group.

As compared to olivine-structured  $\text{LiFePO}_4$ , there is more interest in the protection of 4 V class cathodes, whose overcharge could lead to much more severe safety hazards, because of the higher amount of energy stored in the latter as well as its unstable layered structure that tends to release  $\text{O}_2$  at highly delithiated states. Hence, in recent years, efforts were made to seek additives that start their redox shuttling reaction above 4.2 V. Chen et al. employed MO calculations to rationalize the structure–property relationship for aromatic compounds, and found that  $\pi$ – $\pi$  stacking between aromatic substituents played

Table 25. Additives for Overcharge Protection

	$E_{ox}$ (V vs. Li)
2,5-di- <i>tert</i> -butyl-1,4-dimethoxybenzene	3.92
2,2,6,6-tetramethylpiperinyl oxide (TEMPO)	3.45
phenothiazine	3.5
triphenyl amine	3.75
1,3,2-benzodioxaborole (BDB)	4.46
1,4-di- <i>tert</i> -butyl-2,5-bis(2,2,2-trifluoroethoxy)benzene	4.25
<i>N</i> -heterocyclic carbine $\text{PF}_5$ adduct (NHC- $\text{PF}_5$ )	4.75

a critical role in dictating the stability of the cation species.<sup>273</sup> They concluded that, while spatial protection has been found effective, as in the case of 2,5-di-*tert*-butyl-1,4-dimethoxybenzene,<sup>266</sup> full substitution of an aromatic ring would maximize the stability, and electron-withdrawing moieties would raise the redox potential. Following this guideline, they synthesized a fluorinated benzodioxaborole (BDB, Table 25), whose oxidation potential of 4.46 V proved to be suitable for such cathodes as  $\text{LiNi}_{0.8}\text{Co}_{0.15}\text{Al}_{0.05}\text{O}_2$ . Continuing their exploration of aromatic compounds with bulky substituents, Moshurachak et al. also reported that the introduction of fluorine-substitution onto aromatic rings could raise the redox potential to 4.25 V, and the new redox shuttle, 1,4-di-*tert*-butyl-2,5-bis(2,2,2-trifluoroethoxy)benzene (Table 25), could be applied to  $\text{LiNi}_{1/3}\text{Mn}_{1/3}\text{Co}_{1/3}\text{O}_2$  and  $\text{LiCoO}_2$  chemistries.<sup>274</sup>

Theoretical calculations were extensively used to aid the design of redox shuttle additives. As compared to the similar efforts in seeking interphase-forming additives, redox potentials can be more accurately predicted. Besides the successful example of BDB, whose synthesis was guided by molecular orbital calculation,<sup>273</sup> other computational means such as quantum chemistry and density function theory have enabled the screening and evaluation of a large number of chemicals, and many parameters such as ionization potential and binding energy were developed to correlate to their redox potentials as well as radical stabilities.<sup>275,276</sup>

Finally, there is another class of overcharge protection additives that do not form redox shuttle but instead sacrificially decompose, and therefore terminate the cell operation before catastrophic results ensue. These so-called "shutdown overcharge additives" included the pyrocarbonates, cyclohexyl benzene (CHB), and biphenyl (BP).<sup>1</sup> Recently, Lee et al.

reported the higher effectiveness of the combination of CHB and BP,<sup>277</sup> which copolymerized upon overcharging above 4.65 V and insulated the cathode surface. A similar effect was observed for triphenyl phosphite.<sup>278</sup> As an exotic member of the additive family, a complex formed between a stabilized carbene and the strong Lewis acid  $\text{PF}_5$  (Table 25) was described by Dippel et al. The adduct can be oxidized at ~4.75 V and block the cathode electrochemically.<sup>279</sup> All of these compounds were used in electrolytes to provide protection for 4 V class cathodes, such as  $\text{LiCoO}_2$  and  $\text{LiNi}_{1/3}\text{Mn}_{1/3}\text{Co}_{1/3}\text{O}_2$ , and before their activation at >4.6 V, their presence in electrolytes caused none of the effects detrimental to the normal operation of LIB.

### 3.4.5. Additive Evaluation with High Precision Coulometry

Electrolyte additive is one of the most effective and economical ways to improve electrochemical performance of a device; however, due to their trace presence in the bulk electrolyte and sacrificial nature, their characterization and evaluation are usually challenging, in particular for the more successful additives, which would hardly leave any chemical/electrochemical signature for most analytic tools to detect. In this sense, the high precision coulometry technique, originally developed by Dahn et al. to monitor parasitic reactions within LIB cells in long-term (10–50 years) cycling, proved to be a powerful and quantitative tool to evaluate the effectiveness of additives. It revealed a number of new perspectives on how the common additives, such as VC and FEC, interact with graphitic anodes and cathodes of different chemistries individually (in half cells) or altogether (in full cells), both during cycling and upon storage at different temperatures.<sup>174–176,199,200</sup> In combination with EIS, they have suggested three key parameters to fully characterize the impact of an additive to cell performance: (1) Coulombic efficiencies (or Coulombic inefficiencies, CIE = 1 – CE) measured with high precision ( $\pm 0.003\%$ ) that reflects overall capacity fading; (2) "slippage" of charge or discharge capacity point at both electrodes that reflects the rate of parasitic reactions at individual electrodes; and (3) cell impedance that reflects accumulation of insoluble decomposition products on electrode surfaces. This composited approach, emphasizing the combination of desired properties, rather than individual achievement, allowed the initial establishment of what the authors called "the genome of additives", in which 55 additives were screened in LIB either used alone or in combination with others.<sup>280</sup> Cross-examined by those three parameters, the most promising among the 55 additives tested were shown to be, for the electrochemical couple of  $\text{LiCoO}_2$ /graphite, VC and LiBOB used alone or VC, FEC, and LiBOB used altogether (Figure 28 a–c). On the other hand, although TMOBX (Table 18) has been identified as a good impedance reducer, it caused both high CIE and capacity slippage. Only when used in the presence of VC and LiBOB did TMOBX show improvement over control electrolyte (1.0 M  $\text{LiPF}_6$  in EC/EMC 30:70). The reason for the synergy of multiple additives is not understood at this time.

Combining the above composite approach with diversified coin cell configurations, such as symmetric cells and "back-to-back" pseudo full cells, Dahn and co-workers were also able to differentiate the complicated interplay between electrode and additives that would be otherwise camouflaged by conventional half cell or full configurations, for example, the long-suspected electrochemical "dialog" between anode and cathode in a full cell. As a particular illumination to the researchers of

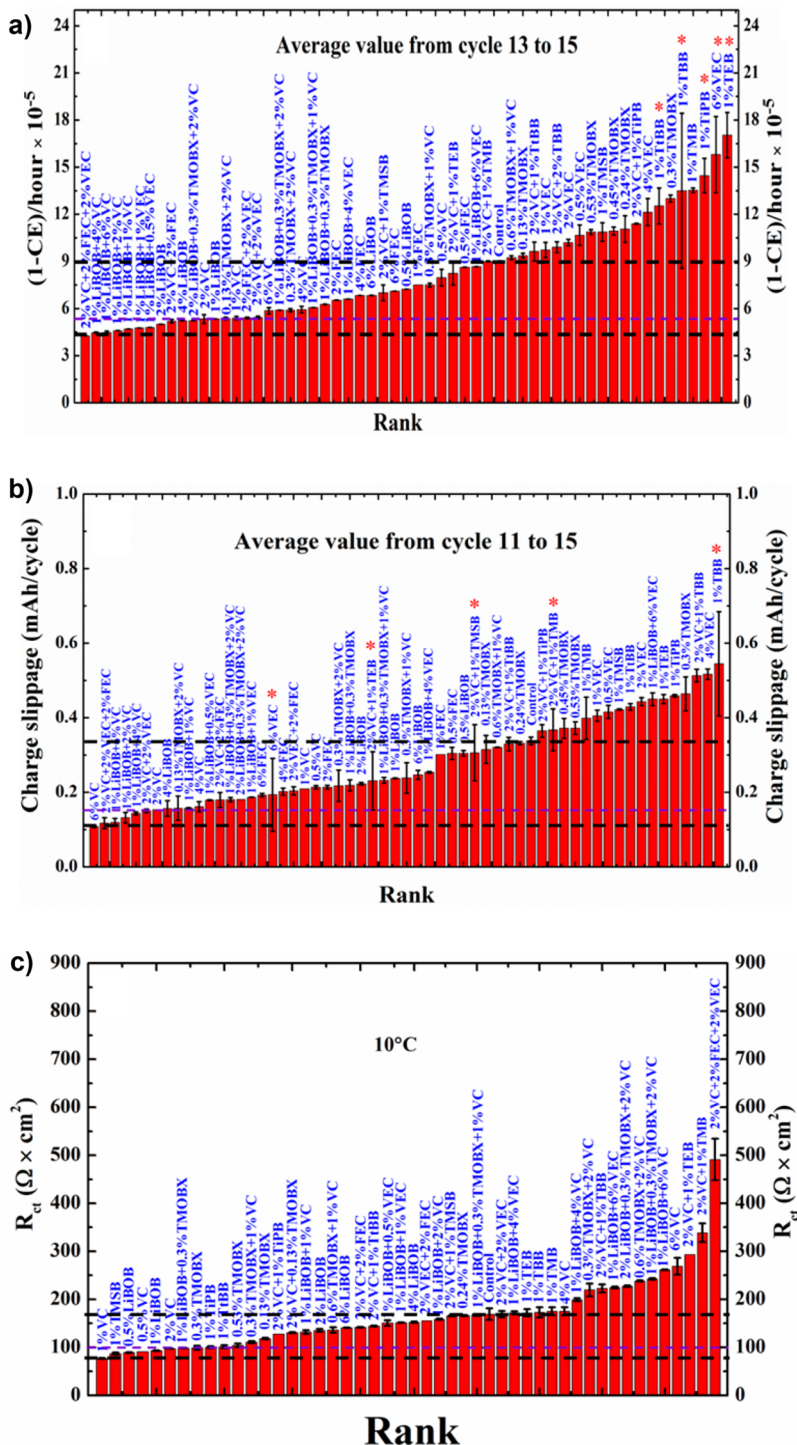


**Figure 28.** “Genome database” for electrolyte additives: (a) Columbic inefficiency (1-CE) per hour (CIE/h), (b) charge end point capacity slippage rates, and (c) charge transfer resistance,  $R_{ct}$ , as evaluated by the combination of electrochemical impedance spectra and high-precision coulometry for LiCoO<sub>2</sub>/graphite pouch cells, where different electrolyte additives were used singly or in combinations. Results were ranked from the “best” (left) to “worst” (right). Reprinted with permission from ref 280. Copyright 2014 Elsevier.

new electrolyte additives, it was revealed that the commonly adopted simple comparison of capacity retention versus cycle number could be deceiving, as certain “improvements” identified this way were actually achieved at the expense of electrolyte- or additive-consumption at matching rates at both electrodes, and therefore could not be sustained.<sup>281</sup> All new additives developed in the future should be subject to this more stringent scrutiny.

### 3.5. Artificial Interphases

Although interphases can be viewed as a battery component that parallels in importance with anodes, cathodes, electrolytes, and separators, it is not an independent material that can be prepared before cell assembly; rather it is formed in the cell, *in situ*, and only when the cell is activated for the very first time, more often than not in an uncontrolled and poorly understood manner. Nevertheless, out of the hope to better tailor

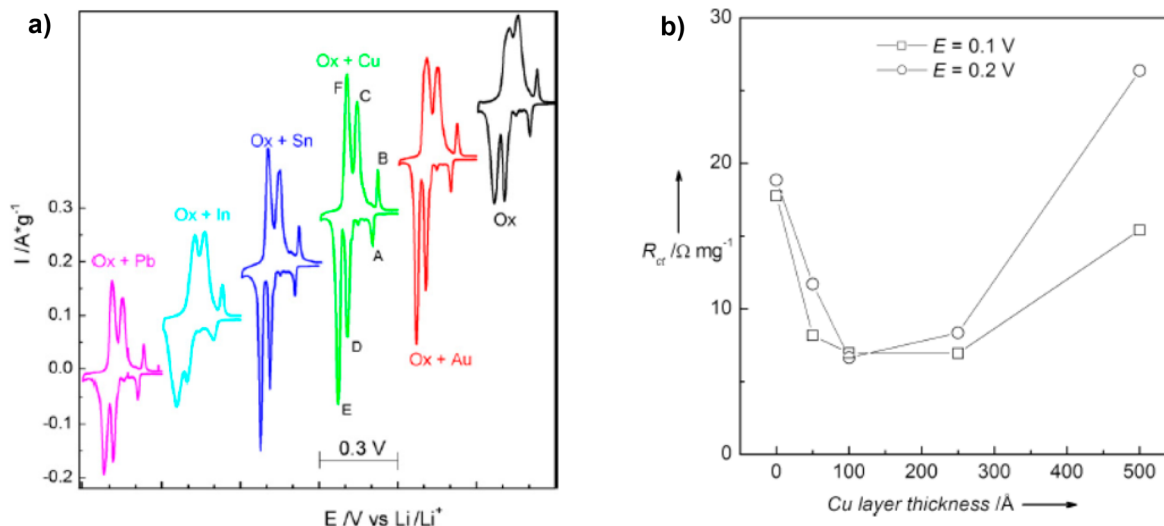


**Figure 29.** Artificial metallic interphases: (a) Cyclic voltammetry of graphitic electrodes coated with various metal layers. Reprinted with permission from ref 284. Copyright 2008 Elsevier. (b) The dependence of fitted “charge-transfer” resistance on the thickness of Cu-layer coated on graphitic anode. Reprinted with permission from ref 286. Copyright 2009 Wiley-VCH Verlag GmbH & Co. KGaA, Weinheim.

properties of the interphases, researchers attempted to engineer artificial interphases via various approaches on electrode surfaces; in some cases, such efforts were made unintentionally when researchers attempted to modify electrode surfaces with coatings. Thus, these coatings could be viewed, in a certain sense, as an electrolyte component that was preassembled on the electrode surfaces. One advantage of this “artificial interphase” approach is that the materials used, with assumed limited solubility in electrolytes, only modify the surface of the electrodes on which they are applied, while additives in an electrolyte might interact with the other electrode in the cell and result in unexpected/undesired consequences.

**3.5.1. Artificial Interphases on Graphitic or Alloy Anodes.** The formation of SEI on graphitic anode prevents the anodes from exfoliation in typical carbonate electrolytes and supports the subsequent  $Li^+$ -intercalation chemistry; however, this process consumes the limited resource of  $Li^+$  from the cathode and introduces higher interfacial resistance.<sup>1</sup> To minimize the latter two undesirable aspects, various attempts were made to prepassivate the graphitic surface. Groult et al. and Komaba et al. applied a thin coating of potassium or sodium salts of either chlorides or carbonates from aqueous solutions on graphite powder, and observed improved electrochemical performance of the processed graphite in typical carbonate electrolytes, such as higher first cycle cycling efficiency, rate capability, reversible capacity utilization, as well as retention.<sup>282,283</sup> Apparently, the presence of larger alkaline cations trapped in the preformed surface coating deactivated parts of the graphite surface, and less electrolytes were sacrificed upon the initial cycle. Marassi and co-workers, on the other hand, coated the surface of partially oxidized graphite with metallic films around 5–50 nm in thickness, and reported remarkable improvements in performance, especially in rate of  $Li^+$ -transport across the interphase (Figure 29a).<sup>284–286</sup> They attributed this faster kinetics to the decrease in  $Li^+$ -desolvation energy, for which the newly formed interphasial chemistry that now contains metallic elements should be somehow responsible. A catalytic effect of the metallic components toward the liberation of  $Li^+$  from its solvation sheath was speculated, but more evidence needs to be presented from further

investigation. There also existed an optimum thickness range, indicating that once the metallic film is thicker than 250 nm, the coating itself constitutes a physical barrier to  $Li^+$ -transport that offsets the benefits from its catalytic effects to desolvate  $Li^+$ .

Ui et al.<sup>287</sup> and Komaba et al.<sup>288</sup> also described the efforts to functionalize graphite surfaces with polymers that have active functionalities, such as carboxylic acids or alcohols. Using poly(acrylic acid) (PAA), polymethacrylic acid (PMA), and poly(vinyl alcohol) (PVA) as binders (Table 26), they

**Table 26. Artificial Interphase Materials on Graphitic Anode**

NaCl, Na <sub>2</sub> CO <sub>3</sub>
Cu, Zn, Ag, Sn
polyacrylic acid (PAA)
polymethacrylic acid (PMA)
polyvinyl alcohol (PVA)

demonstrated that even neat PC-based electrolyte can support reversible  $Li^+$ -intercalation without exfoliating the graphite structure. Sputtering tests in XPS revealed a very thin SEI in the presence of these polymers, and the author believed that the oxygens in them participated in the competitive solvation of  $Li^+$  at the intercalation sites near the graphite surface, thus assisting  $Li^+$  to dissociate from PC or EC. The direct consequence was the stabilization of graphite with PC in the former case, and a thinner SEI in the latter.

Nanosized fume silica was used by Lux et al. to modify the surface of graphite, which interacts with the nanoparticles via weak adhesive forces.<sup>289</sup> Although little effect was observed in the electrochemical behavior during the initial cycles, long-term

stability of graphitic anodes was obtained when 14 nm silica particles were applied to graphite via a dry-coating protocol.

The difficulty of forming a stable interphase on Si surfaces has been mainly caused by the extreme volume changes during the lithiation/delithiation reactions. It is believed that the formed SEI layer would be broken and then reformed repeatedly during this process, inducing incessant irreversible reactions of electrolyte components. Recent report by Wang et al. described the application of a “self-healing” polymer on microsized silicon particles, which, based on interchain hydrogen bonding, was stretchable during the electrochemical reactions and maintained electric contacts between the silicon particles.<sup>290</sup> Although Coulombic efficiency still needed to be improved, the near absence of impedance increase during the 100 cycles tested indicated that the growth of interphase due to volume change was negligible. In this sense, the “self-healing” polymeric film along with the conductive additive formed an artificial layer of interphase that successfully mitigated the parasitic reactions of the electrolyte components.

**3.5.2. Artificial Interphases on Cathodes.** Surface coating was more frequently applied to various cathode materials, with the purpose of releasing more capacity at high voltages, stabilizing electrolyte against oxidation at high voltages, or simply suppressing dissolution of transition metal elements that were sensitive to acidic extraction by electrolytes. Unlike anode surfaces, metallic coatings can not be applied to cathode surfaces considering the usually low oxidation potential of non-noble metals. Exceptions do exist for LiFePO<sub>4</sub>, whose operating potential at 3.5 V falls on the border of most non-noble metal oxidation, and its insulating nature created the need for electronic conductivity improvement.<sup>291–293</sup> Nevertheless, after the seminal work by Chiang and co-workers,<sup>7</sup> LiFePO<sub>4</sub> has become a well-recognized high power density cathode, hence marginalizing the significance of surface coating, while cathode materials of 4 V or higher operating potentials still require surface stabilization. Table 27 summarizes the materials applied to LiFePO<sub>4</sub> surfaces via coating techniques.

Table 27. Artificial Interphase Materials on Cathodes

Ag	
Lauric acid	
Amine-based surfactants	

**3.5.2.1. On LiCoO<sub>2</sub>.** As the first cathode chemistry of LIB, LiCoO<sub>2</sub> (~140 mAh/g) only utilized about 50% of the capacity stored by Li<sup>+</sup> in the lattice (theoretical 273 mAh/g). The attempts to release more capacity have been thwarted in part by

the lattice instability due to overdelithiation, and in part by the oxidation of electrolytes on the delithiated cathode surface when charged beyond 4.2 V. Researchers discovered that, by coating a thin-layer of inorganic “artificial interphase” on LiCoO<sub>2</sub> particles, the material could be charged up to 4.5 V, delivering 170–200 mAh/g. Normally capacity utilization together with retention will be improved due to the coating, while rate capability depended on the thickness as well as the species of coating materials. Various oxides,<sup>294–297</sup> phosphates,<sup>297–300</sup> and fluorides<sup>301–303</sup> have been used with similar effects, with AlF<sub>3</sub> as the most effective artificial interphase that stabilizes the LiCoO<sub>2</sub> structure up to 4.54 V, while minimizing electrolyte oxidation, enabling a capacity of 208 mAh/g.

The mechanism behind the effect of these artificial interphases, however, has been controversial, except the consensus that the coating acts as an interlayer between active LiCoO<sub>2</sub> particles and electrolyte, introducing a new interphasial chemistry. Earlier interpretations were based on the knowledge that the chemical nature of the oxide coatings is basic, which might function as an interfacial scavenger of acidic species such as HF.<sup>295</sup> Surface analysis via XPS revealed that surface Al<sub>2</sub>O<sub>3</sub> suppressed the dissolution of cobalt and slowed the degradation of LiPF<sub>6</sub> salt,<sup>297</sup> and that AlF<sub>3</sub> or NH<sub>4</sub>AlF<sub>4</sub> also seemed to function in a similar manner by delaying the HF leaching of cobalt that would eventually induce undesirable phase transformation.<sup>301</sup> Yet this concept was at least partially challenged by Bai et al., who reported that the coating of YPO<sub>4</sub> actually induces more acidity from the electrolyte.<sup>299</sup>

**3.5.2.2. On Ni–Mn–Co Mixed Oxides.** As compared to LiCoO<sub>2</sub>, spinel- or layered-structured materials based on Ni–Mn–Co mixed oxides must overcome the more severe challenge of transition metal dissolution by acidic electrolytes; therefore, much of surface coating efforts focused on benefits related to this issue in addition to increasing capacity and stabilizing electrolytes.

Sun et al. applied a thin coating of AlF<sub>3</sub> on LiNi<sub>1/3</sub>Mn<sub>1/3</sub>Co<sub>1/3</sub>O<sub>2</sub>, which supported the cycling of the materials up to 4.6 V, with improvements in capacity utilization (~180 mAh/g), cycling stability, as well as rate capability.<sup>304</sup> Transmission electron microscopy (TEM) revealed that the amorphous AlF<sub>3</sub> layer, 5–10 nm in thickness, evenly covered the primary particle of the active material (Figure 30A). They believed that the AlF<sub>3</sub> interphase reduced the reactivity of the cathode surface toward the electrolyte while keeping the cathode structure stable against phase transformations, which are usually triggered by transition metal dissolution from the surface. AlF<sub>3</sub> was also coated on Li[Li<sub>0.2</sub>Mn<sub>0.54</sub>Ni<sub>0.13</sub>Co<sub>0.13</sub>]O<sub>2</sub>, a variation of the LMR-NMC high capacity cathode materials, with the purpose of mitigating the irreversible reaction between cathode and electrolytes during the first cycle activation at high voltage (>4.5 V).<sup>305</sup> While improvements in electrochemical performance were shown (Figure 30B), Zheng et al. also made earnest efforts to decipher how the artificial interphase worked. In situ differential electrochemical mass spectrum (DEMS) was used to monitor the release of gaseous products when Li[Li<sub>0.2</sub>Mn<sub>0.54</sub>Ni<sub>0.13</sub>Co<sub>0.13</sub>]O<sub>2</sub> was delithiated at 4.6 V. Surprisingly, the O<sub>2</sub> (*m/e* 32) detected from AlF<sub>3</sub>-coated cathode was much higher than that from the bare material (Figure 30C), while a reversal was observed for CO<sub>2</sub>-generation (Figure 30D), although the onset potential for the coated cathode was shifted by ~0.35 V. Because O<sub>2</sub> should come from the cathode structure, and CO<sub>2</sub> from the oxidation of electrolyte solvents, the authors thus believed that the role of AlF<sub>3</sub>-coating was actually to form a buffer layer, within which the newly generated atomic oxygen recombined into relatively inactive O<sub>2</sub> molecules. In the

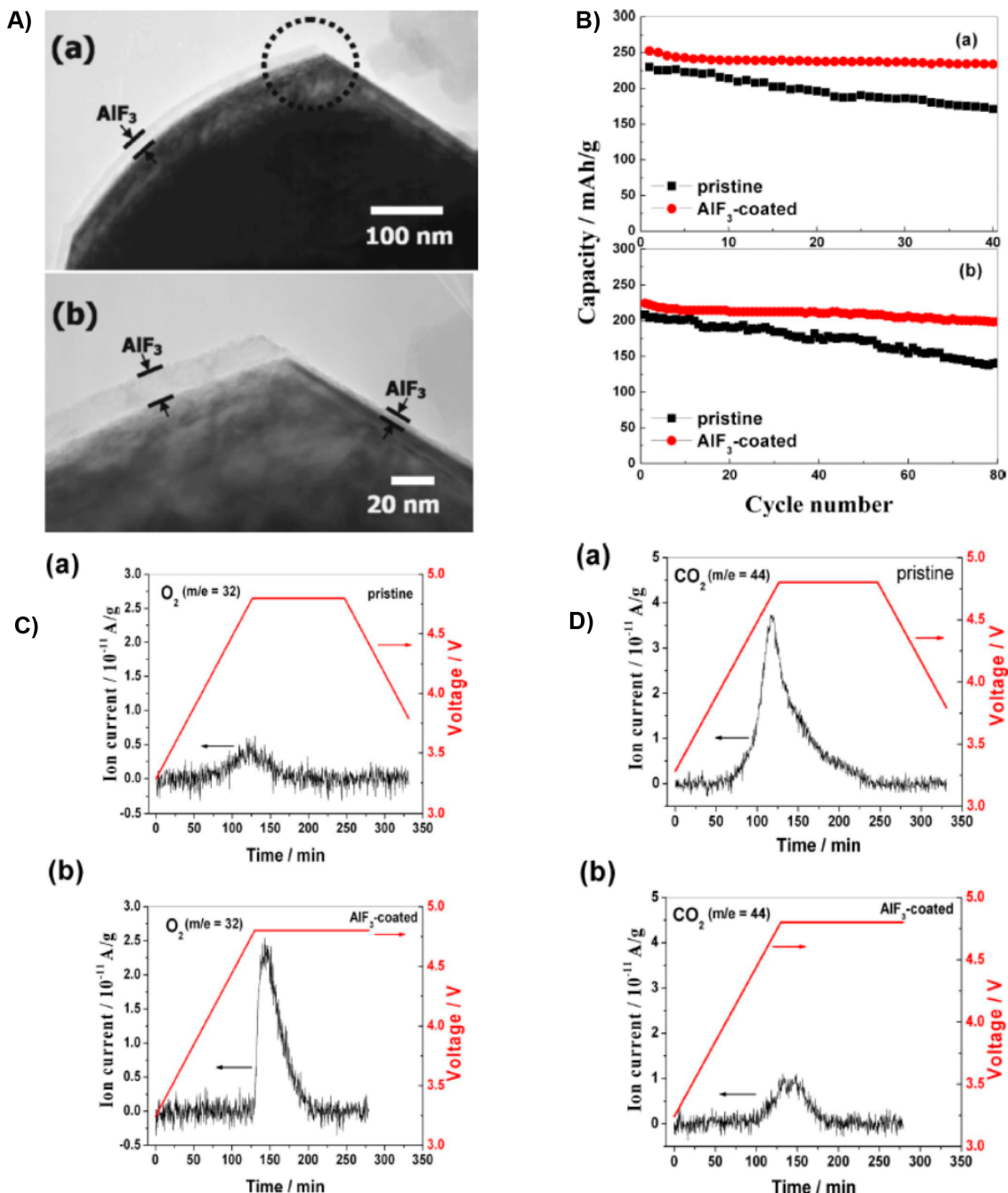


**Figure 30.** Artificial AlF<sub>3</sub> interphase: (A) TEM images of (a) primary particle from a cycled AlF<sub>3</sub>-coated LiNi<sub>0.33</sub>Mn<sub>0.33</sub>Co<sub>0.33</sub>O<sub>2</sub> and (b) magnified image of the selected region in (a). Reprinted with permission from ref 304. Copyright 2007 Electrochemical Society. (B) Cycling performance of uncoated and AlF<sub>3</sub>-coated LiNi<sub>0.33</sub>Mn<sub>0.33</sub>Co<sub>0.33</sub>O<sub>2</sub> electrodes in baseline electrolyte 1.0 M LiPF<sub>6</sub>/EC/DMC (50:50) when charged up to 4.8 V. The measurement of (C) O<sub>2</sub>- and (D) CO<sub>2</sub>-evolutions from (a) uncoated and (b) AlF<sub>3</sub>-coated LiNi<sub>0.33</sub>Mn<sub>0.33</sub>Co<sub>0.33</sub>O<sub>2</sub> cathodes using DEMS technique. Reprinted with permission from ref 305. Copyright 2008 Electrochemical Society.

absence of this buffer layer, the highly reactive atomic oxygen directly oxidized electrolytes, resulting in a resistive interphase and releasing appreciable amount of CO<sub>2</sub>. This mechanism could well accommodate the observation made earlier by Bai et al. that the stabilization effect of artificial interphases seemed to be independent of its capability of scavenging HF in the electrolyte.<sup>299</sup> Similar efforts were made on LiMn<sub>0.5</sub>Ni<sub>0.5</sub>O<sub>2</sub>, where 10 nm thick AlF<sub>3</sub> effectively suppressed the dissolution of transition metals as indicated by secondary ion mass spectrum (SIMS), which detected much lower levels of LiF on the outer surface of AlF<sub>3</sub> as compared to uncoated pristine cathode.<sup>306</sup>

A solid (glassy) electrolyte, lithium phosphorus oxynitride (LiPON), which has found extensive application in thin-film lithium batteries, was also used as an artificial interphase material.<sup>307</sup> Differing from ordinary practices of artificial interphase coating where materials were applied onto all active material particles, Park et al. used radio frequency magnetron sputtering to deposit LiPON onto already-cast composite electrodes. In this way, only the electrode surface exposed to electrolyte would be coated, while interparticle resistance would not be increased due to unnecessary and excessive coating. Improvements in electrochemical performance were reported

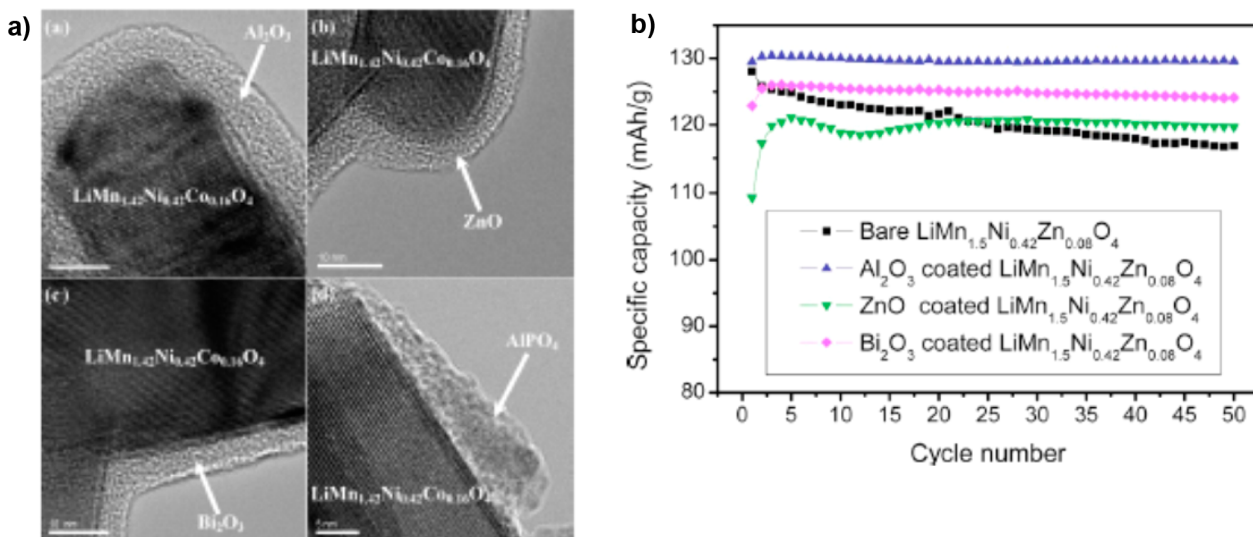


**Figure 31.** Artificial oxide interphases: (a) TEM micrographs of 2% various oxides or phosphate coated on stabilized  $\text{LiMn}_{1.42}\text{Ni}_{0.42}\text{Co}_{0.16}\text{O}_4$ . Reprinted with permission from ref 309. Copyright 2009 American Chemical Society. (b) Effect of  $\text{Al}_2\text{O}_3$ ,  $\text{ZnO}$ , and  $\text{Bi}_2\text{O}_3$  on cycling performance of  $\text{LiMn}_{1.5}\text{Ni}_{0.42}\text{Zn}_{0.08}\text{O}_4$ . Reprinted with permission from ref 310. Copyright 2009 Electrochemical Society.

for  $\text{Li}_{1-x}\text{Mn}_{0.27}\text{Ni}_{0.53}\text{Co}_{0.2}\text{O}_2$  when charged up to 4.5 V; however, the poor thermal stability of LiPON diminished its potential for practical applications.

**3.5.2.3. On High Voltage Spinel.** Cathode materials of high operating voltage, such as  $\text{LiMn}_{0.5}\text{Ni}_{0.5}\text{O}_2$  or  $\text{LiCoPO}_4$ , present severe challenges to the electrochemical stability of electrolytes against oxidation, while their own lattice instability at elevated temperatures also constitutes a hurdle to their application in LIB. These issues have been the targets for efforts. Arrebola et al. described the efforts to coat a gold interlayer on  $\text{LiMn}_{0.5}\text{Ni}_{0.5}\text{O}_2$ , and showed that the results varied a lot depending on both coating method and temperature.<sup>308</sup> In the more successful approach, where Au vapor was deposited on nanometric  $\text{LiMn}_{0.5}\text{Ni}_{0.5}\text{O}_2$ , better electrochemical stability was achieved at low rates, which the authors attributed to the reduced exposure of bare cathode surface to electrolytes and the resultant lessened oxidative decomposition of the latter. This minimized reaction might also act as protection to the cathode itself because the electrolyte decomposition would produce acidic species like HF, which corrodes the Mn-based spinel structure. On the other hand, Au interlayer existed as an extra physical barrier for  $\text{Li}^+$  to migrate across, and its effect became pronounced when the cells were subjected to high rate tests.

Employing the technique of electrostatic self-assembly, Liu et al. deposited a series of nanosized oxides and phosphates of Al, Zn, Bi onto  $\text{LiMn}_{0.5}\text{Ni}_{0.5}\text{O}_2$  or its stabilized variations doped by Co or Zn (Figure 31a).<sup>309–311</sup> These artificial interphases formed effective protection as evidenced by better capacity retention as well as rate capability (Figure 31b). Electrochemical impedance spectra (EIS) and XPS revealed that the thick SEI on pristine  $\text{LiMn}_{0.5}\text{Ni}_{0.5}\text{O}_2$  was the primary origin for the poor electrochemical performance, while those oxide/phosphate coatings, being compact artificial interphases themselves, significantly reduced the amount of electrolyte required to decompose to deactivate the oxidizing surface of those cathode materials, resulting in fast charge-transfer kinetics. Sclar et al. deposited similar oxides on  $\text{LiMn}_{0.5}\text{Ni}_{0.5}\text{O}_2$  using sono-chemical method, which led to overall surface coverage on the active particles.<sup>312</sup> On the basis of Raman, XPS,

and TEM analyses, the authors attributed the superior electrochemical performance of  $\text{ZnO}$  and  $\text{MgO}$  coatings to their ability to suppress dissolution of both Mn and Ni from cathode lattices near the surface.

Aside from inorganic oxides and phosphates, polymers could also be applied as artificial interphase. Kim et al. managed to deposit polyimide on  $\text{LiMn}_{0.5}\text{Ni}_{0.5}\text{O}_2$  via thermal polymerization of polyamic acid.<sup>313</sup> The stability and electrochemical performance of the cathode vastly depended on the concentration of polyamic acid, apparently because excess amounts of the acid would react with electrolytes and produce a host of detrimental substances. The optimum results were obtained at 0.3%, which led to an amorphous, 2 nm thick interphase on  $\text{LiMn}_{0.5}\text{Ni}_{0.5}\text{O}_2$  particles and enabled the cells to deliver stable performance at 55 °C. Similar stabilization against elevated temperatures was also achieved when LiPON of subnanometric thickness was deposited onto  $\text{LiMn}_{0.5}\text{Ni}_{0.5}\text{O}_2$  (Figure 32a), enabling stable cell performance at 60 °C (Figure 32b).<sup>314</sup> The authors attributed these improvements in cycling stability, rate capability, and interphasial impedance to the suppressed metal dissolution as well as mitigated electrolyte oxidation, but they also cautioned that the improved cycling stability was still insufficient for the life of over thousand cycles as required by vehicle electrification. It should also be pointed out here that, while the improved thermal stability brought by artificial interphases to  $\text{LiNi}_{0.5}\text{Mn}_{0.5}\text{O}_2$  indeed advanced the material toward practical application, all of those results were obtained in cathode half cells with Li metal as anode. Experience indicates that, once graphitic anode replaces Li metal, complications could arise due to electrochemical crosstalk between the two electrodes, especially at elevated temperatures.

**3.5.2.4. Artificial Interphases Formed by Atomic Layer Deposition.** Most of the above efforts in forming artificial interphases on anode or cathode were based on wet chemical processes, in which the active electrode powder was exposed to solution-based coating precursors and then heat-treated to form the eventual interphases. The deposition thus obtained might be unevenly distributed, and optimum precursor concentration must be sought after to minimize the detrimental effect caused

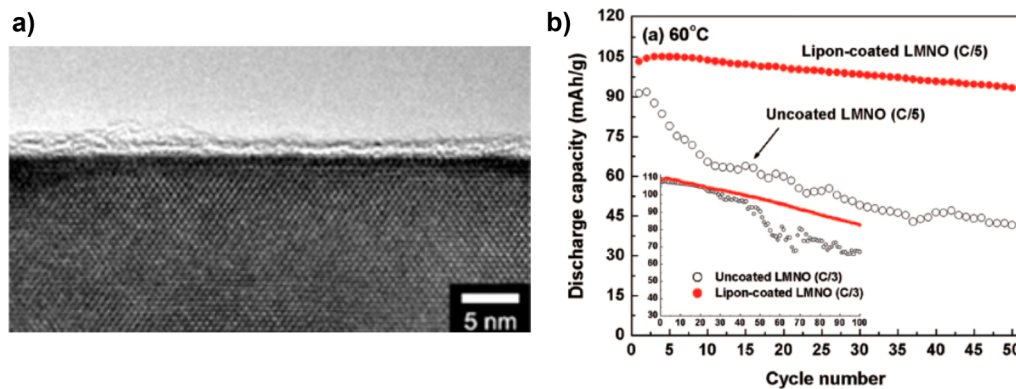


**Figure 32.** Artificial glassy interphases: (a) TEM cross sections of  $\text{LiNi}_{0.5}\text{Mn}_{1.5}\text{O}_4$  coated with subnanometric layer of LiPON; and (b) effect of subnanometric LiPON on the cycling performance of  $\text{LiMn}_{0.5}\text{Ni}_{0.5}\text{O}_2$  at 60 °C. Reprinted with permission from ref 314. Copyright 2013 Electrochemical Society.

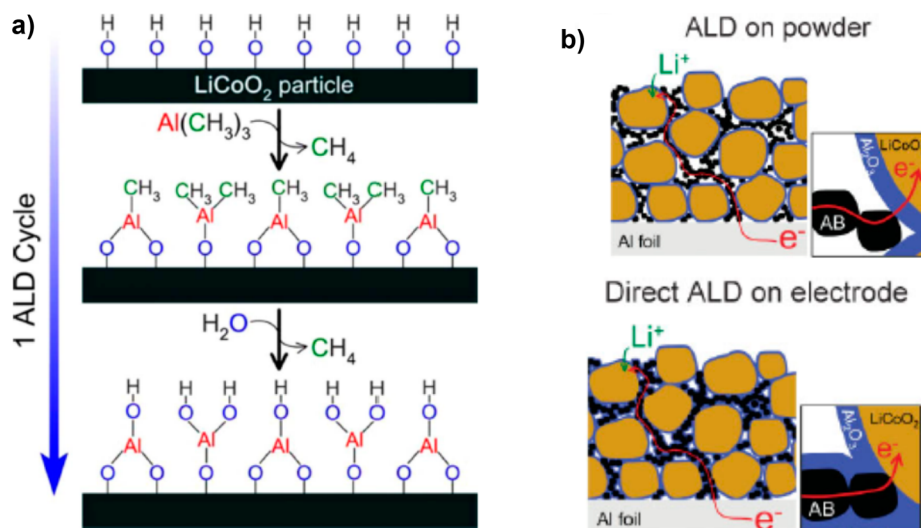


**Figure 33.** Artificial oxide interphases by ALD: (a) Working principle of ALD that places  $\text{Al}_2\text{O}_3$  layers on electrode material particles. Reprinted with permission from ref 316. Copyright 2010 Electrochemical Society. (b) The schematic illustration of the difference of placing an  $\text{Al}_2\text{O}_3$  layer on electrode material particles and directly on composite electrodes. Reprinted with permission from ref 320. Copyright 2010 Wiley-VCH Verlag GmbH & Co. KGaA, Weinheim.

by excessive interphasial materials. To address these issues, atomic layer deposition (ALD) was introduced as a powerful technique to control both distribution and thickness of the artificial interphasial materials.<sup>315,316</sup> The principle of ALD consists of the chemisorption of coating precursors on active material surface, normally leveraging the reaction between the surface hydroxyl functionalities of the electrode and the precursor, followed by sequential reaction and purging. In an ideal scenario, each self-terminating coating cycle would only place one new monolayer over the previous cycles; therefore, the growth of the interphase thickness should be well controlled and evenly distributed (Figure 33A).

Snyder et al. seemed to be the first to apply this technique to  $\text{Li}_4\text{Ti}_5\text{O}_{12}$  surfaces,<sup>315</sup> followed by Jung et al., who deposited subnanometric  $\text{Al}_2\text{O}_3$  layers over  $\text{LiCoO}_2$  powder.<sup>316</sup> In both cases, drastic changes in electrochemical behavior were observed as the result of ALD coatings. In particular, much improved capacity retention was achieved for  $\text{LiCoO}_2$  even when it was charged to 4.5 V. Because the layer was only 0.4–0.5 nm, which is thin enough to allow electron-tunneling,

this improvement in stability would not incur compromises in interphasial kinetics as wet-coating would sometimes.  $\text{Al}_2\text{O}_3$  was also applied by Cheng et al.<sup>317</sup> and Woo et al.<sup>318</sup> to  $\text{LiCoO}_2$ , and by Jung et al.<sup>319</sup> to a variation of LMR-NMC cathode,  $\text{Li}[\text{Li}_{0.20}\text{Mn}_{0.54}\text{Ni}_{0.13}\text{Co}_{0.13}]_{0.2}$ , leading to similar improvements in electrochemical performance with varying degree of success.

In addition to particle coatings, the ALD technique was also used to deposit various oxides on already-fabricated composite electrodes,<sup>317,319,320</sup> where the deposition would only go to the electrode surface to be exposed to electrolyte, without disturbing the contact points between the active particles and the carbon additives or current collector (Figure 33b). The retaining of the interparticle conductive pathway assisted in minimizing the cell resistance and maintaining rate capability.

Despite the apparent advantages of ALD-deposited artificial interphases, the feasibility of scaling-up and cost of this technology have always been a topic of debate, especially because the gaseous precursors not only require capital investment in special equipment but also make it challenging

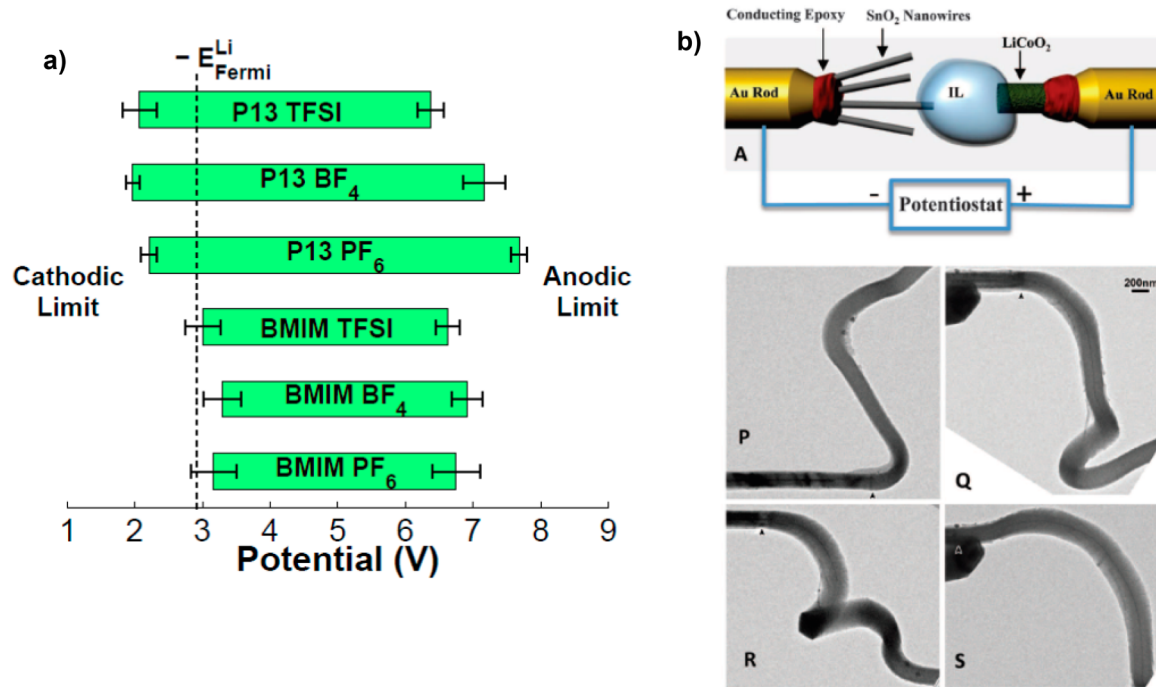


**Figure 34.** Ionic liquids: (a) Electrochemical stability window of RTIL calculated from MD + DFT, where the lithium metal Fermi level was also indicated as a reference. Reprinted with permission from ref 334. Copyright 2011 American Chemical Society. (b) In situ TEM graphs of a SnO<sub>2</sub> nanowire being lithiated in a RTIL electrolyte based on pyrrolidinium. Reprinted with permission from ref 335. Copyright 2010 American Association for the Advancement of Science.

to produce large square-feet of electrodes in a continuous manner. On the other hand, there were also reports that raised suspicion about the stability of oxides such as Al<sub>2</sub>O<sub>3</sub> in LIB. For example, Jung et al. have described the interdiffusion between Al<sub>2</sub>O<sub>3</sub> and active material as result of the heat-treatment, leading to the transformation of Al<sub>2</sub>O<sub>3</sub> into a new phase.<sup>320</sup> Bettge et al. reported a rather interesting electrochemical cross-talk between anode and an artificial interphase on cathode.<sup>321</sup> When Al<sub>2</sub>O<sub>3</sub> was coated on Li<sub>1.2</sub>Ni<sub>0.15</sub>Mn<sub>0.55</sub>Co<sub>0.1</sub>O<sub>2</sub>, another variation of LMR-NMC high capacity cathode material, they found that the dissolution of transition metal was not entirely prevented but instead only inhibited; besides Ni and Mn dissolution, significant accumulation of Al could also be detected on the anode surface. This would cast some doubt on the long-term stability of these ALD-generated artificial interphases against electrolytes in LIB, particularly at elevated temperatures.

### 3.6. Ionic Liquids

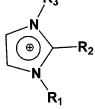
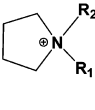
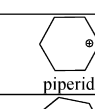
By strict definition, ionic liquids consist of only cations and anions of a salt or salts in molten state, i.e., above melting or glass transition temperatures and in the absolute absence of any molecular species.<sup>37</sup> This standard can be sometimes relaxed when new cations were explored, where an association of a simple ion and a molecular ligand could be considered as a single complex ion instead of an ion–solvent solvate. The demarcation was not always that unambiguous. Because of its small ionic radius, Li<sup>+</sup>-based ionic liquids are usually very high melting,<sup>322</sup> and thus the majority of “room-temperature ionic liquids (RTIL)” were based on nonlithium, larger organic cations. The most popular cations were quaternary ammoniums, usually constructed with a heterocyclic structure with or without conjugation. To make an ionic liquid Li<sup>+</sup>-conductive, lithium

salt has to be dissolved at sufficient concentrations (>0.5 M); thus the current carried by Li<sup>+</sup> was only a fraction of what the ionic conductivity may reflect. Besides cation, the counteranion was also an essential component, which determines not only the melting temperature but also the electrochemical stabilities of the resultant RTIL. These two requirements often conflict, as the most electrochemically stable anions (PF<sub>6</sub><sup>-</sup> and BF<sub>4</sub><sup>-</sup>) always resulted in high melting salts, while the most “plasticizing” anions (halides, aluminohalides, TFSI, and BETI) were usually known for their reactive nature at high voltages, such as corrosion toward aluminum current collector or simply electrochemical oxidation. Fortunately, the corrosion of Al was much mitigated in ionic rather than in nonaqueous media, probably due to the low solubility of Al-TFSI species in the former.<sup>323,324</sup>

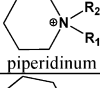
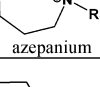
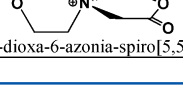
Ionic liquid-based electrolytes were not covered in the 2004 review article,<sup>1</sup> because at the time this class of electrolytes, mainly based on imidazolium cations, was still reluctant to support the intercalation chemistries of Li<sup>+</sup>, due to either their electrochemical instability toward, or inability to form, effective SEI on typical LIB anode materials. The introduction of new chemical structures in ionic liquids, especially cations based on pyrrolidinium and its derivatives,<sup>325,326</sup> has significantly expanded the electrochemical stability, enabling decent results in most LIB chemistries.<sup>327,328</sup> The new anions developed for lithium salts, such as B(CN)<sub>4</sub> (Table 12), FSI (Table 13), and modified phosphates, were also borrowed to formulate new RTIL compositions with imidazolium or pyrrolidinium cations, resulting in improved properties of varying extents.

The past decade has witnessed a dramatic increase of activities in RTIL research, mainly driven by their tempting

Table 28. (A) Representative Imidazolium- and Pyrrolidinium-Based RTILs; and (B) Representative Heterocyclic and Acyclic Ammoniums

A)	Cation	Anion	T <sub>m</sub> (°C)	E <sub>red</sub> (V vs. Li)	E <sub>ox</sub> (V vs. Li)
imidazolium		TFSI	0.8 (R <sub>1</sub> =Me; R <sub>2</sub> =H, R <sub>3</sub> =Et)	1.0 (R <sub>1</sub> =Me; R <sub>2</sub> =H, R <sub>3</sub> =Et)	5.3 (R <sub>1</sub> =Me; R <sub>2</sub> =H, R <sub>3</sub> =Et)
		BF <sub>4</sub> <sup>-</sup>	15 (R <sub>1,3</sub> =Me)		
		PF <sub>6</sub> <sup>-</sup>	58~62 (R <sub>1,3</sub> =Me)		
		TFSI	15 (R <sub>1,2</sub> =Me; R <sub>3</sub> =Pr)	0.64 (R <sub>1</sub> =Me; R <sub>2</sub> =H, R <sub>3</sub> =Hex)	5.73 (R <sub>1</sub> =Me; R <sub>2</sub> =H, R <sub>3</sub> =Hex)
		FSI	-12 (R <sub>1</sub> =Me; R <sub>2</sub> =H, R <sub>3</sub> =Et)	0.7	5.3
pyrrolidinium		FSI	-9 (R <sub>1</sub> =Me; R <sub>2</sub> =Pr)	0.2 (R <sub>1</sub> =Me; R <sub>2</sub> =Pr)	5.6 (R <sub>1</sub> =Me; R <sub>2</sub> =Pr)
		TFSI	-18 (R <sub>1</sub> =Me; R <sub>2</sub> =Bu)		
		TFSI	-7.9 (R <sub>1</sub> =Et; R <sub>2</sub> =Bu)		

B)

 piperidinium	TFSI	2 and 11 (R <sub>1</sub> =Et; R <sub>2</sub> =Bu) <sup>b</sup>	1.8 (R <sub>1</sub> =Et; R <sub>2</sub> =Bu) <sup>c</sup>	4.5 (R <sub>1</sub> =Et; R <sub>2</sub> =Bu) <sup>c</sup>
 azepanium	TFSI	15.5 (R <sub>1</sub> =Me; R <sub>2</sub> =Pr) 23.3 (R <sub>1</sub> =Et; R <sub>2</sub> =Bu)	0.1 (R <sub>1</sub> =Me; R <sub>2</sub> =Pr) 0.4 (R <sub>1</sub> =Et; R <sub>2</sub> =Bu)	4.9 (R <sub>1</sub> =Me; R <sub>2</sub> =Pr) 4.9 (R <sub>1</sub> =Et; R <sub>2</sub> =Bu)
 2-oxo-3,9-dioxa-6-azonia-spiro[5.5]undecane	TFSI	76		

inherent nonflammability and thermal stability.<sup>329</sup> More understanding was achieved at fundamental levels, such as how Li<sup>+</sup> is solvated by counter-anions without solvent molecules,<sup>330,331</sup> how Li<sup>+</sup> migrates under electric field through the ionic media,<sup>332,333</sup> and, most importantly, how cation and anion interact to determine the eventual electrochemical stability windows of the ionic liquids (Figure 34a).<sup>334</sup> The application of RTIL electrolyte in commercial LIB has not been known; however, the availability of RTIL-based electrolyte has enabled the *in situ* TEM observation of how LIB materials reacted electrochemically, under high vacuum, not in a sealed cell, which would be impossible with typical nonaqueous liquid electrolytes.<sup>335</sup>

**3.6.1. Imidazoliums.** RTIL based on aromatic cation imidazolium was perhaps the first of its kind considered for lithium-based battery applications, an archetype of which being ethylmethyl imidazolium bis(trifluoromethanesulfonylimide) (EmImTFSI, Table 28).<sup>336</sup> The main obstacle for this class of RTIL seemed to be the reduction of imidazolium cations on anode materials that operate under 1.0 V vs Li and their inability to form a protective interphase on these materials. On the other side, the anodic stability of RTIL seemed to be mainly determined by the anions,<sup>337</sup> and TFSI-based RTIL were sufficiently stable on most LIB cathode materials, as evidenced by the decent cycling data of EmImTFSI or its variation in LiCoO<sub>2</sub>/Li<sub>4</sub>Ti<sub>5</sub>O<sub>12</sub> cells.<sup>336</sup> In the ionic media,

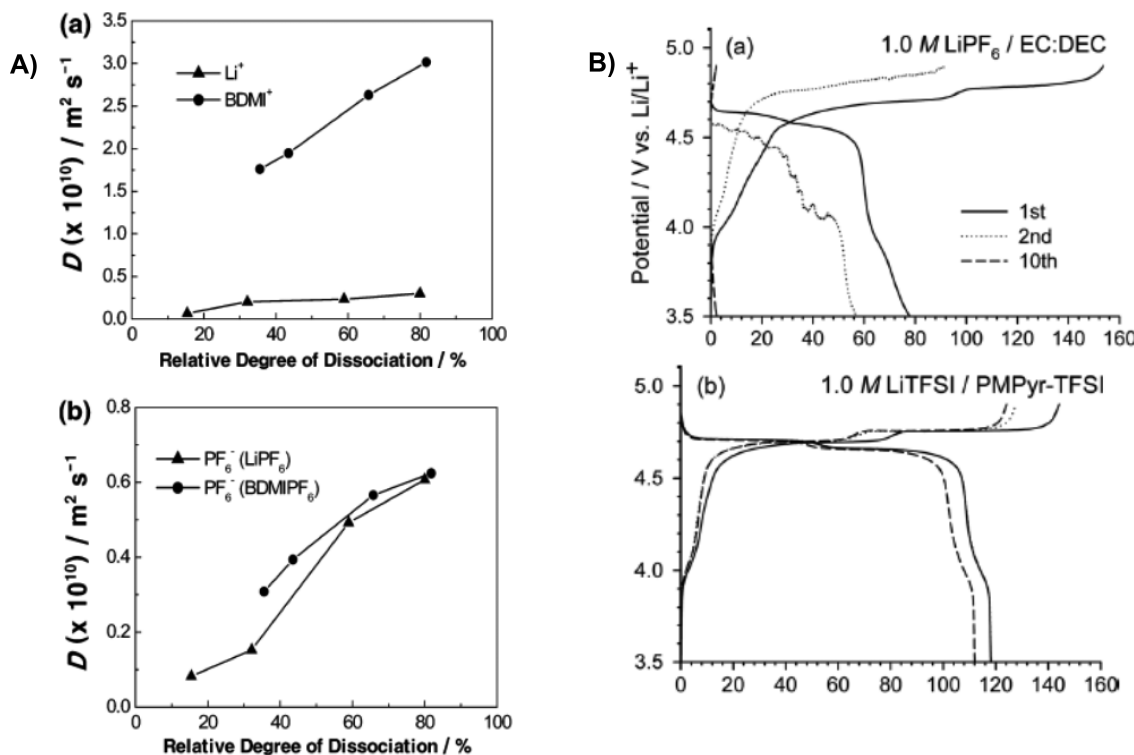


**Figure 35.** Ionic liquids: (A) Comparison of diffusivity of (a) butyl dimethylimidazolium (BDMI) and  $\text{Li}^+$  and (b) their corresponding anion ( $\text{PF}_6^-$ ) as estimated by echo signal attenuation of  $^1\text{H}$ ,  $^{31}\text{P}$ , and  $^7\text{Li}$  NMR spectra, respectively. Reprinted with permission from ref 333. Copyright 2005 American Chemical Society. (B) Comparison of charge–discharge voltage profiles of  $\text{LiNi}_{0.5}\text{Mn}_{1.5}\text{O}_4$  cathode in (a) carbonate-based electrolyte and (b) pyrrolidinium-based RTIL electrolyte. Reprinted with permission from ref 357. Copyright 2011 Electrochemical Society.

$\text{Li}^+$  could be solvated tetrahedrally by two bidentate TFSI anions as revealed by Raman and DFT calculation,<sup>330</sup> or by three TFSI anions according to pulse-gradient echo NMR.<sup>331</sup> The anionic solvation sheath not only slowed the  $\text{Li}^+$  movement, but also might have participated in interphasial reactions. The former was indicated both indirectly by the rather high activation energies (50–70 kJ/mol) associated with the “ion-transfer” process<sup>331</sup> and directly by the measurement of diffusivities of all ionic species (Figure 35A).<sup>333</sup> As expected, the contribution from  $\text{Li}^+$  to overall conductivity was less than that from EmIm cation.

Efforts to stabilize imidazolium cations by removing the active  $\alpha$ -H,<sup>338–340</sup> by coupling them with new anions,<sup>341–343</sup> or by substituting the imidazole ring with longer alkyl chains<sup>344,345</sup> resulted in varying degrees of success, leading to RTIL that can support cells with different cathode chemistries in half cells with Li metal anodes, but the graphitic anode remained an insurmountable hurdle for imidazolium cations, unless a high concentration (5%) of VC was used as SEI-forming additive.<sup>345</sup> Inorganic nanoparticles like silicate were also used to form hybrid electrolytes with RTIL based on imidazolium cations, but limited benefits were found.<sup>346,347</sup> Among all of those efforts, the combination of FSI anion with imidazolium cations represented an interesting case in which the complicated interplay among  $\text{Li}^+$ , imidazolium, and anion eventually resulted in improvements in ion conductivity as well as cathodic stability,<sup>341</sup> with an obvious suppression of lithium dendrite by those FSI-based RTIL. Table 28A summarizes some representative imidazolium-based RTIL with basic physical and electrochemical properties.

**3.6.2. Pyrrolidiniums.** Following the report of MacFarlane et al.,<sup>325,326</sup> it was generally recognized that a nonaromatic cation pyrrolidinium can provide far superior cathodic stability.<sup>334,337,341</sup> Extensive investigations on the thermodynamic<sup>348–350</sup> and transport properties<sup>351</sup> as well as interphasial behavior on metallic lithium surface<sup>352–355</sup> were carried out on this promising class of RTIL. A few representative pyrrolidiniums are summarized in Table 28A. It was reported that rather high conductivity ( $>10^{-3}$  S/cm), high  $\text{Li}^+$ -transference number ( $\sim 0.4$ ), and low viscosity were available from pyrrolidinium-based RTIL as compared to their imidazolium counterparts,<sup>353</sup> and that dendrite lithium, although still inevitable at high rates and during long-term cycling, was effectively suppressed.<sup>354,355</sup> What seemed counterintuitive was the chemical analysis carried out via XPS on the anode surface, which revealed that the main interphasial components consisted of the reduction products of TFSI anion instead of pyrrolidinium cation,<sup>353</sup> although the latter may survive reductive decomposition by lithium and became trapped during the process and embedded in, or become part of, the interphase. Correspondingly, the interphases on cathode materials were revealed to be dominated by oxidative decomposition products from pyrrolidinium cation.<sup>356,357</sup> This paradox against the simple notion that “RTIL anodic and cathodic stability limits be determined by anion and cation, respectively” reflects the complicated interplay between  $\text{Li}^+$ , IL cations, and anions.<sup>334</sup>

The anodic stability of pyrrolidinium-based RTIL was confirmed by cathode half cells built with  $\text{LiFePO}_4$ ,<sup>327,328,355</sup>  $\text{LiCoO}_2$ ,<sup>356</sup> and  $\text{LiNi}_{0.5}\text{Mn}_{1.5}\text{O}_4$ <sup>324,337,357</sup> (Figure 35B), although long-term stability and readiness for practical cell

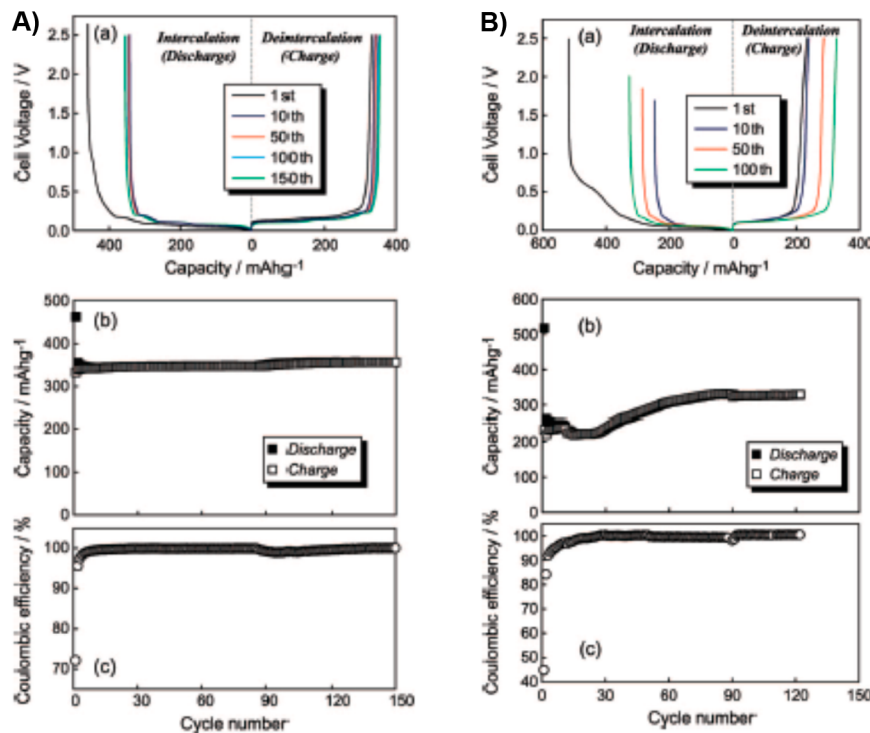


**Figure 36.** Ionic liquids: charge–discharge profiles (a), cycling stability (b), and Coulombic efficiency (c) of graphitic anodes in pyrrolidinium-based RTIL electrolyte with (A) TFSI and (B) FSI anion. Reprinted with permission from ref 361. Copyright 2008 American Chemical Society.

applications remain to be supported by more data. Unsaturated substituent (allyl) on pyrrolidinium assisted in forming a more protective film on LiCoO<sub>2</sub>, suggesting an oxidative polymerization mechanism of pyrrolidinium cation.<sup>356</sup>

The combination of pyrrolidinium with FSI anion yielded RTIL of high ion conductivities and low viscosities, although at the expense of thermal stability due to the labile F in FSI;<sup>341,350,358,359</sup> however, the high ion conductivities and low viscosities failed to translate into higher rate capability when tested in LiCoO<sub>2</sub>-based cells.<sup>360</sup> The introduction of FSI also decreased the cathodic stability toward lithium, raising the suspicion that impurities that came with LiFSI may be responsible for the parasitic reactions on cathode surfaces.<sup>359</sup>

Like imidazolium, pyrrolidinium also encountered the challenge from graphitic anodes. The only reported success of pyrrolidinium-based RTIL with graphitic anode in absence of any anode SEI additives was described by Seki et al., who used 1-methyl-1-propyl pyrrolidinium bis(fluorosulfonyl)imide (Py13-FSI) as ionic media and LiTFSI as solute and achieved reversible Li<sup>+</sup>-intercalation/deintercalation with graphite electrode (340 mAh/g for >100 cycles with Coulombic efficiency of >70% at the initial cycle, Figure 36A).<sup>361</sup> Lower reversibility (300 mAh/g with Coulombic efficiency of 45% at the initial cycle, Figure 36B) was obtained from similar RTIL based on TFSI anion, indicating again the participation of anion in the formation of SEI on negative electrode.

**3.6.3. Other Cyclic and Acyclic Ammoniums and Phosphoniums.** Heterocyclic cations similar to pyrrolidinium were also explored, which included piperidinium,<sup>360,362,363</sup> azepanium,<sup>364</sup> and a quaternary ammonium based on an azo-spiro structure<sup>364</sup> (Table 28B). RTIL based on both 1-methyl-1-propyl piperidinium bis(fluorosulfonyl)imide<sup>360</sup> (PP13-FSI) and 1-ethyl-1-butyl piperidinium bis(trifluoromethanesulfonyl)-imide<sup>362</sup> (PP24-TFSI) showed decent ion conductivity and cycling

stability in LiCoO<sub>2</sub> cathode half cells. The piperidinium cation in 1-methyl-1-propyl piperidinium bis(trifluoromethanesulfonyl)imide (PP13TFSI) even seemed to be able to form an intercalation compound with graphite at ~0.5 V.<sup>362</sup> Although this process did not interfere with the simultaneous Li<sup>+</sup>-intercalation at lower potential, and intercalation of piperidinium in subsequent cycles was prevented by the interphase formed by lithium salt on graphite, it did cast doubt over the actual application of piperidinium-based RTIL in LIB.

A series of azepanium with larger heterocyclic rings were synthesized by Salem et al., who found that asymmetric substituents on N afforded liquids of lower melting points.<sup>364</sup> The electrochemical cycling of corresponding RTIL based on these azepanums was conducted with various anode (graphite and Li<sub>4</sub>Ti<sub>5</sub>O<sub>12</sub>) and cathode (LiFePO<sub>4</sub> and LiCoO<sub>2</sub>) chemistries, and it seemed that the extreme potentials of graphite (0.2 V) and LiCoO<sub>2</sub> (4.2 V) still presented a challenge to the stabilities of these RTIL. Further studies were needed to fully justify their practicality. On the other hand, an azo-spiro ammonium (2-oxo-3,9-dioxa-6-azonia-spiro[5,5]undecane) was designed and synthesized, for the purpose of protecting the carrier of formal charge (i.e., N) from reduction with two rigid ring structures (Table 28B).<sup>365</sup> Its TFSI salt turned out to be a solid with melting point of 76 °C, and its electrochemical stability was measured at 85 °C on Pt electrode, rendering a window of 3.5 V. The addition of LiTFSI expanded the stability window via passivation, and hence lithium deposition/stripping were allowed. It was thus suggested by Lane et al. that the azo-spiro ammonium be used as a high temperature ionic liquid electrolyte, supported by cycling in LiFePO<sub>4</sub> half cells at temperatures as high as 80 °C.

While all cations described above are actually either aromatic or cyclic quaternary ammoniums, the most conventional tetraalkyl ammonium cations were seldom selected to form RTIL,

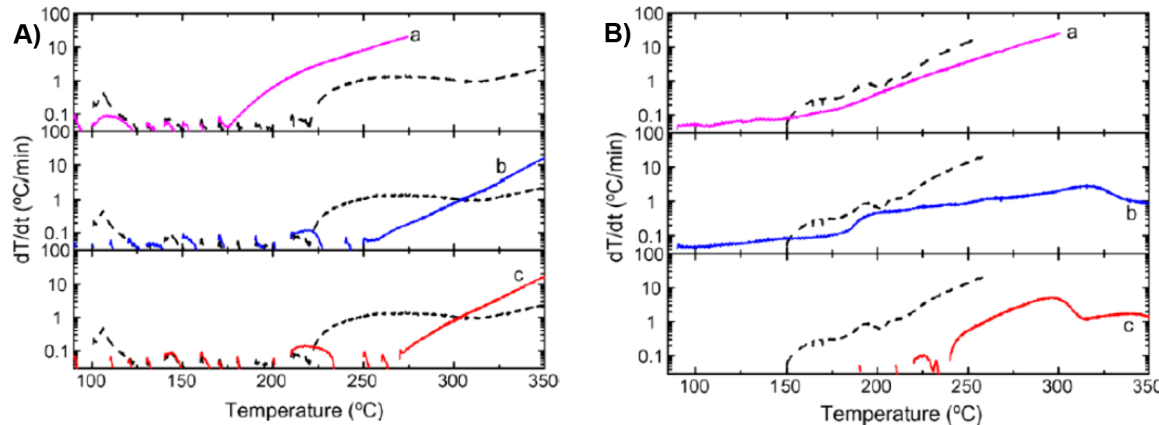


**Figure 37.** Safety of ionic liquids: (A) ARC of imidazolium-based RTIL electrolytes in the presence of lithiated silicon anode ( $\text{Li}_1\text{Si}$ ), (a)  $\text{LiPF}_6/\text{EMI-FSI}$ , (b)  $\text{LiPF}_6/\text{EMI-TFSI}$  and  $\text{LiPF}_6/\text{BMIMI-TFSI}$ ; and (B) ARC of imidazolium-based RTIL electrolytes in the presence of delithiated cobalt oxide ( $\text{Li}_{0.45}\text{CoO}_2$ ), (a)  $\text{LiPF}_6/\text{EMI-FSI}$ , (b)  $\text{LiPF}_6/\text{EMI-TFSI}$ , and (c)  $\text{LiPF}_6/\text{BMIMI-TFSI}$ . Baseline electrolyte  $\text{LiPF}_6/\text{EC/DEC}$  (1:2) was shown as dashed lines in all panels as a reference. Reprinted with permission from ref 379. Copyright 2007 Elsevier.

mainly due to their high melting temperatures. A few exceptions existed, in which the alkyl substituents on N were either functionalized with ether-<sup>362–369</sup> or cyano-<sup>370,371</sup> or rather bulky (longer than four carbon in length) functionalities.<sup>372–374</sup> Most of them were shown to be stable against metallic lithium or lithium/sodium alloy anodes and  $\text{LiFePO}_4$ ,  $\text{LiCoO}_2$ , or  $\text{LiNi}_{0.8}\text{Mn}_{0.1}\text{Co}_{0.1}\text{O}_2$  cathodes with decent cycling efficiencies and life, but none were reported to be compatible with graphitic anode.

RTIL based on phosphonium cations were much less investigated than their ammonium counterparts, mainly due to the higher melting temperatures, higher viscosities, and low conductivities of the former, unless the alkyl substituents were either long enough (>5 carbons in length) or functionalized with alkoxy- or aza-groups.<sup>373,375</sup> Like their ammonium counterparts, the RTIL seemed to be fairly stable against both metallic lithium and various cathode materials,<sup>373–377</sup> and in certain instances impressive cycle life (>500 cycles<sup>378</sup>) was described, but there have been no reports regarding their stability against or ability to form SEI on graphitic anode materials. Serizawa et al. extensively characterized the physical and electrochemical properties of two such phosphonium cations, and correlated the viscosity of the RTIL with the size of alkyl substituents on the cation, which determines the intramolecular mobility.<sup>378</sup>

**3.6.4. A Sober Perspective on Ionic Liquid Electrolytes.** Ionic liquid has been attracting researchers with its mesmerizing beauty of simplicity and ideality, because the absence of molecular solvents would annotate the liberation from a collection of unpleasant complications associated with them, such as their interactions with both  $\text{Li}^+$  and anions, and their parasitic reactions and processes with active materials in electrodes. A neat ionic medium not only provides an extreme fantasy for modeling efforts, but also promises practical advantages such as high ionic populations for intercalation chemistry without depletion concerns, high temperature stability, high tolerance against thermal and electrochemical abuses, and inherent nonflammability.

However, despite these promised advantages and impressive advances made during the past decade, a sober survey of RTIL-based electrolytes reveals that the removal of solvents actually causes more issues than it solves. The cations and anions that form the RTIL must not only maintain the above-mentioned

merits of a pure ionic system, but also need to meet the basic merits that nonaqueous electrolytes already offer, that is, remaining in the liquid state and providing decent ion conductivity in required service temperature ranges, being electrochemically stable with both electrodes, and being compatible with all other cell parts such as current collectors and separators. Among those constraints, electrochemical stability proved to be the most challenging. Without the molecular solvent to serve as sacrificial building blocks for interphases, the mission of forming sufficient protection on both electrodes befalls entirely on the RTIL cations and anions. Because an RTIL based on neat lithium salts only was still not found, most of the “-onium” salts encountered difficulty in shouldering such a collection of tasks, especially on the surfaces of graphitic anodes.

On the other hand, upon examining the electrochemical performance of RTIL, one might come to the conclusion that RTILs are competitive at best with nonaqueous electrolytes, and thus the incentive induced by their safety merits might become marginalized. Even the “inherent safety” of RTIL cannot be entirely taken for granted, because nonflammability does not necessarily translate into higher tolerance against abuse in an electrochemical environment. As revealed by the thermal stability investigation conducted by Wang et al., among the six most popular RTIL electrolytes examined, the majority were either similar to or even worse than nonaqueous electrolytes in terms of safety when they coexist with lithiated anode or delithiated cathode materials<sup>379</sup> (Figure 37), with imidazolium cation and FSI anion being the worst combination. The overall thermal stability seemed to heavily rely on the complicated interplay between lithium salt, RTIL anions, and electrode materials.

Considering the limited benefits, new interphasial challenges and high cost of manufacturing and purification of most RTIL components, the highly fluorinated anions in particular, there is no reason to be optimistic about the large-scale application of RTIL in commercial LIB in the foreseeable future. This picture might change though, with any significant breakthroughs arising from RTIL electrolytes, especially in “beyond Li-ion” chemistries.

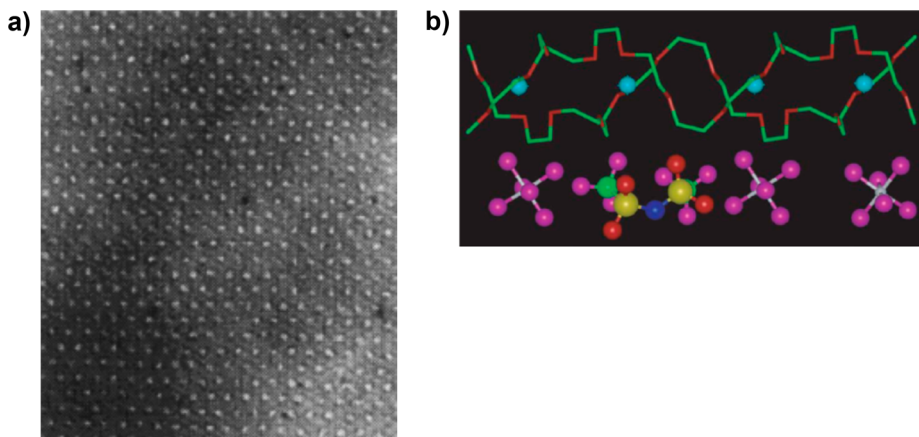


**Figure 38.** Solid polymer electrolytes: (a) Microphase separation of the block copolymer film P(EO-*co*-S), where black regions correspond to PEO phase and white regions to polystyrene phase. Reprinted with permission from ref 391. Copyright 2003 Electrochemical Society. (b) Conduction of  $\text{Li}^+$  (light blue spheres) in the crystalline matrix of  $\text{PEO}_6\text{-LiXF}_6$  with TFSI as additive, where  $\text{Li}^+$  is visualized as mobile within helical structures of the main polymeric backbone. Reprinted with permission from ref 404. Copyright 2005 Nature Publishing Group.

### 3.7. Solid Polymer and Polymer Gel Electrolytes

As the only liquid component in the cell, the electrolyte stands as an obstacle to the efforts to make LIB a solid device so that benefits such as high safety, mechanical strength, and compliability could be harvested. Polymer electrolytes have been actively investigated as a possible solution. Out of practical considerations, the original concept of solvent-free solid polymer electrolytes (SPE) has been extended to gel polymer electrolytes (GPE), which work in a manner more similar to liquid electrolytes in electrochemical mechanisms rather than polymer electrolytes;<sup>1</sup> nevertheless, the pursuit of SPE remained active out of the enthusiasm for a neat polymeric media that allows fast  $\text{Li}^+$  transport while simultaneously providing strong mechanical support. In certain cases, the demarcation between SPE and GPE is no longer that unambiguous, because the “plasticizers” used in the latter are sometimes either polymers themselves or oligomers with molecular weight near the threshold (average  $M$  5000–10 000) of polymers.

#### 3.7.1. Solid Polymer Electrolytes.

As the most well-known polymeric linkage that can effectively dissolve lithium salts, oligoether ( $-\text{CH}_2\text{-CH}_2\text{-O}-$ )<sub>n</sub> constitutes the main structural units of SPE since the discovery of Wright et al.<sup>380</sup> Four decades after Armand’s seminal suggestion, the majority of work performed on SPE still focus on variations of polyether structure, with perhaps the only exceptions being the polycarbonates developed by Tominaga and co-workers,<sup>381–384</sup>

among which the polymeric isomer of EC poly(ethylene carbonate) was shown to possess ion conductivities comparable and  $\text{Li}^+$  transference number superior to their oligoether-counterparts when LiTFSI or LiFSI were used as lithium salts, but their electrochemical compatibility with battery electrode materials still remains to be proven.

The most severe challenges that SPE confronts remained to be the low ion conductivity (or more precisely the trade-off between ion conductivity and mechanical strength), interfacial contacts between electrode and electrolytes, as well as electrochemical stability window. To oligoether-based SPE in particular, the oxidizing cathode often presents an insurmountable barrier as the breaking down potential for ether linkage lies below 4.0 V.<sup>1</sup> Attempts to improve both include using new lithium salts and anion receptors, modifying polymer structure

via copolymerization and grafting, as well as forming composites with inorganic or ceramic fillers/electrolytes.

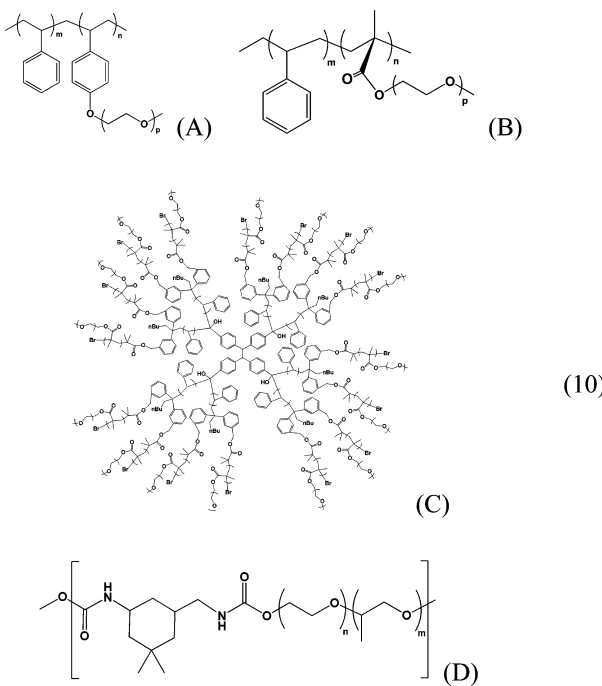
**3.7.1.1. New Salts, Anion Receptors, and RTIL.** The typical ion conductivities of lithium salt complexes with poly(ethylene oxide) (PEO) are below  $10^{-4}$  S/cm at room temperature,<sup>1</sup> partially due to the crystalline phase of oligoether linkages that only melts at  $\sim 60$  °C, and mainly due to the tight coupling of  $\text{Li}^+$ -mobility with the sluggish segmental motion of the PEO backbone. This threshold value could be approached or even broken through when new lithium salts and anion receptors were used, aided by more flexible polymer segments often accompanied by compromises in the mechanical strength. Appetecchi et al. reported the use of LiBOB with PEO via hot pressing.<sup>384</sup> The resultant PEO-based SPE afforded ion conductivity of  $10^{-4}$  S/cm at 40 °C. The crystalline domain of EO-linkages seemed to be effectively suppressed by LiBOB. Niedzicki et al. reported ion conductivity higher than  $10^{-3}$  S/cm at room temperature by using two imidazole-based lithium salts, but that was made possible only by the low molecular weight polymer matrix.<sup>31</sup> Various borate-based anion receptors were used with PEO- or PEG-based electrolytes, either added as additives or bonded covalently to the polymer chains, and the Lewis acidity of the boron center was found to be helpful in promoting both ion conductivity and  $\text{Li}^+$ -transference numbers,<sup>385–387</sup> although neither of these was subject to more rigorous electrochemical characterization, either in half or full LIB cells. On the other hand, RTIL was also incorporated into SPE and has led to improvements in performance, as exemplified by Shin et al., who introduced pyrrolidinium-based RTIL into PEO, and reported successful cycling in  $\text{LiFePO}_4$  or  $\text{V}_2\text{O}_5$  cells,<sup>327,328,388</sup> and more recently by Fischer et al., who developed sulfonium-based RTIL and reported ion conductivities higher than  $10^{-3}$  S/cm at room temperature for a series of anions.<sup>389,390</sup> Both anodic and cathodic stabilities were claimed, but tests of these SPE on active electrode materials have yet to be described.

**3.7.1.2. Copolymers.** The main dilemma for SPE improvement is the unfortunate contradiction between the dual functions expected from its polymer backbone, which acts as both structural unit to provide dimensional stability and functional unit to dissolve lithium salt and conduct  $\text{Li}^+$ . More often than not, improvements in ion conduction were made at the expense of mechanical strength to a degree where the

advantages of a SPE either severely suffered or completely vanished. To promote ion conduction while maintaining mechanical strength at the same time, one needs to decouple Li<sup>+</sup>-movement from the segmental movement of polymer. One strategy to achieve this decoupling is to employ copolymers, in which two or more different structural units would shoulder these two conflicting missions separately. As the almost exclusive functional units in SPE, oligoether linkages are difficult to replace; however, a rich chemical database of structural units is provided by the widely available structural polymer materials such as polystyrene (PS) and polymethacrylates (PMA).

Wang integrated styrene units with ethylene oxide (EO) units, which were attached to PS backbone as pendants<sup>391</sup> (eq 10A). This block copolymer of two completely different chemical domains led to microphase separation as revealed by TEM, in which the EO-rich phase formed a percolating conduction pathway for Li<sup>+</sup> (Figure 38a). The resultant SPE was stable against metallic lithium cycling while being able to support reversible intercalation chemistry of Li<sub>x</sub>MnO<sub>2</sub> up to 3.8 V for extended cycles. Apparently lithium dendrite growth was suppressed due to the high Young's modulus of the copolymer. However, the elegant design and synthesis of polymeric structure still could not resolve the issue of low ion conductivity.

Niitani et al. synthesized a copolymer of similar chemical composition but entirely different supermolecular structure by using a methyl methacrylate (MMA) backbone to carry the EO units (eq 10B). They obtained ion conductivity of  $\sim 2 \times 10^{-4}$  S/cm at



room temperature.<sup>392</sup> Employing the dendrimer strategy, Niitani et al. further manipulated these two structural units and synthesized a “star-shaped polymer” as shown in eq 10C, which consisted of a hard core of PS units and soft outer shell of flexible poly(ethylene glycol-methyl methacrylate)(PEG-MMA) chains.<sup>393</sup> The star-shaped polymer spontaneously formed a well-ordered spherical hierarchy, within which Li<sup>+</sup> transports in the continuous phase of PEGMA. The ion conductivity, however, was still in the range of  $10^{-4}$  S/cm at room temperature

despite the elegant architecture. Both copolymers of ether and styrene units were tested in LiCoO<sub>2</sub> cathode half cells with stable performance.

Balsara and co-workers also developed nanostructured block copolymers of styrene and ether linkages, named SEO, while seeking a fine balance between the mechanical strength and ion conduction.<sup>394–396</sup> Although the room temperature ion conductivity was still short of  $10^{-4}$  S/cm, they found that lithium dendrite growth could be effectively prevented by the rigid polymer film. Earlier, Monroe et al. have predicted via modeling that a shear modulus of 6 GPa was necessary to suppress the germination of dendritic lithium crystals,<sup>397</sup> which was impossible for the soft PEO-based linkages. The rigid styrene units in SEO copolymer, however, seemed to have provided the required resistance, making it possible for this class of SPE to be applied in cells based on metallic lithium anode and LiFePO<sub>4</sub> cathode at elevated temperatures (60 °C). The coupling of SEO polymer electrolyte with these two electrodes proved to create a clever niche because the energy density limit imposed by the cathode was effectively relieved by the anode, and the ion conductivity no longer placed a kinetic hold on cell reaction at 60 °C. Urethane units were also used as the mechanical framework when Jiang et al. copolymerized them with EO and propylene oxide (PO) linkages (eq 10D).<sup>398</sup> The resultant copolymer formed a thin (10–50 μm) membrane directly on electrodes thanks to the dimensional stability brought by urethane linkages, while providing higher ion conductivity ( $\sim 10^{-4}$  S/cm) than its PEO counterparts due to the absence of crystallization by EO-linkages. Tests in cathode half cells with Li<sub>0.33</sub>MnO<sub>2</sub> yielded a capacity of  $\sim 175$  mAh/g at elevated temperature (60 °C), but faded to ca. 50% within 100 cycles.

In the opposite direction, efforts to leverage the more flexible polymer linkages were also made with siloxane units ( $T_g \approx -120$  °C of polydimethylsiloxane vs  $-40$  °C of PEO).<sup>399–401</sup> In certain instances, room temperature ion conductivities higher than  $10^{-4}$  S/cm could be obtained, and cathode half cells using VO<sub>x</sub> yielded stable performance within limited cycles. Naturally, the high ion conductivity was obtained at the expense of mechanical stability, and the SPE in these cases could hardly serve as an independent separator as P(EO-S) copolymer-based SPE do.

**3.7.1.3. Crystalline Polymer.** An alternative strategy to achieve the decoupling of electrochemical function and mechanical property is to seek a different conduction mechanism where Li<sup>+</sup> no longer rely on segmental relaxation to move. Bruce and co-workers were the first to discover that crystalline phases of PEO<sub>6</sub>–LiXF<sub>6</sub> (where X is As, P, and Sb) were not insulators; instead, PEO chains folded to form a helix tunnel for Li<sup>+</sup> to transport via continuous hopping between sites (Figure 38b), although the conductivity remained at low levels ( $\sim 10^{-7}$  S/cm) for a feasible electrolyte.<sup>402,403</sup> Doping the above stoichiometric crystalline compositions with additive levels of TFSI anion did increase ion conductivities by more than an order of magnitude while still maintaining the crystalline nature.<sup>404</sup> Capiglia et al. more closely investigated the crystalline phases that exist in the PEO–LiBeti system, and identified, besides PEO<sub>6</sub>–LiXF<sub>6</sub> solvates, other stoichiometric compositions at varying EO/Li<sup>+</sup> ratios.<sup>405</sup> On the other hand, Golodnitsky et al. reported the anisotropy of Li<sup>+</sup>-conduction in such crystalline phases.<sup>406</sup> By creating preferential alignment of PEO chains, either via mechanical stretching or casting with diamagnetic and ferromagnetic nanofillers under an applied field, they successfully increased the ion conduction in PEO-based

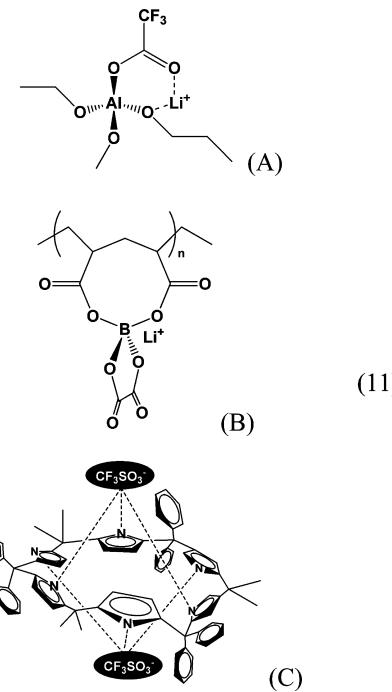
SPE along certain orientations by an order of magnitude ( $\sim 10^{-4}$  S/cm at room temperature), accompanied by a corresponding decrease in SEI resistance. They believed that in those crystalline phases  $\text{Li}^+$  hops within the channels inside the helix of crystallized PEO backbone, with its counteranion moving on its envelope.

If ion conductivities by these new mechanisms could keep improving to a certain level without losing the rigid crystalline nature, they might qualify to act as electrolyte and separator in some electrochemical devices, where the requirement for ion transport flux and rate is not as stringent as in batteries but where thickness and durability would be critical. Such devices include the auxiliary power attachments for flexible displays, conformal solar panels, or smart credit cards.

**3.7.1.4. Single Ion Conducting SPE.** As pointed out in section 2.1, in most electrolytes discussed thus far, the contribution from  $\text{Li}^+$  to the overall cell current is less than 50%, and the “parasitic current” carried by anions often creates concentration polarization at electrode interfaces where they accumulate. In SPE, this polarization is especially difficult to eliminate due to the much higher regional viscosity and would impose additional resistances to the already sluggish cell reaction kinetics. To address this issue, there have been efforts to covalently immobilize anions to the polymer backbone in SPE, as summarized in the comprehensive review by Ratner and Shriver,<sup>407</sup> and as reflected by more recent efforts where the anions of both strong and weak acids have been used, such as fluorinated sulfonates<sup>408</sup> and carboxylates.<sup>33,409,410</sup> In general, these polyelectrolytes are characterized with rather low ion conductivities, much lower than what they should be after the discount of anionic contribution, although their  $\text{Li}^+$ -transference number is unity. This overall loss of ion conduction ability was mainly due to the much more restricted segmental motion of the charged polymer backbone as reflected by the sharp increase in their glass transition temperatures.

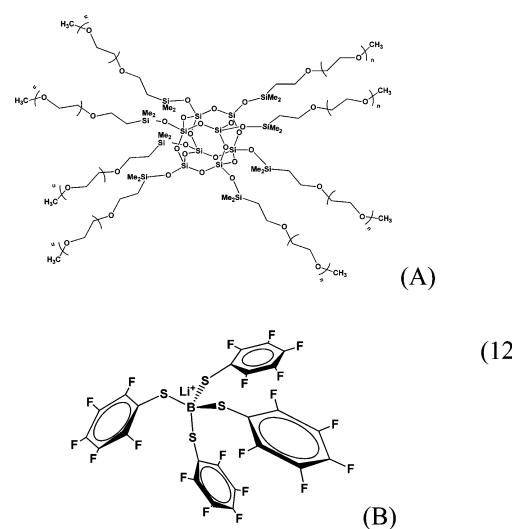
Alternatively, anion-immobilization via “softer” (noncovalent) connections was also attempted, in which the anion mobility was reduced by loosely associating with either polymer backbone or a larger host molecule through ionic or dipole interactions. Aoki reported the formation of aluminate or borate anions on the polymer chain by reacting these Lewis acid centers with lithium alkoxides to form fluorinated dicarboxylate.<sup>411</sup> As illustrated by eq 11A,  $\text{Li}^+$  in such a polymer should be the only mobile species, while the ether linkage (about 12 EO units) acts as relaxation media for  $\text{Li}^+$  to transport. Conductivities of  $10^{-5}$  S/cm were obtained for a borate-based SPE, which was high considering that it entirely consisted of  $\text{Li}^+$  movement. Lithium deposition and stripping were conducted in this polymer.

Zhu et al. transplanted the LiBOB structure into a polymer chain by forming the oxalate-half of the tetrahedrally coordinated B-center after the polymer was prepared (eq 11B).<sup>412</sup> It should be noted that the nature of the chelation bond was more ionic than covalent. However,  $\text{Li}^+$  conductivity of this SPE was only  $\sim 10^{-6}$  S/cm at room temperature even when plasticized by 3% PC, which is barely sufficient to support any electrochemical reaction at a practical rate. Blazejczyk et al.<sup>119</sup> and Golodnitsky et al.,<sup>122</sup> respectively, used macro-molecular anion receptors based on calixarene- or calixpyrrole-structures with the purpose of minimizing the anion motion. In this manner, the anions were immobilized but were not directly associated with the polymer main chain, thus avoiding the devastating effect of anion attachment on the overall chain



flexibility. The cage-like traps did bond anion tight enough to generate a nearly unity  $\text{Li}^+$ -transference number (eq 11C). Nevertheless, besides the novelty of single-ion conduction, modest success was obtained from all of these efforts, because overall ion conduction still suffered from the anion-immobilization, and electrochemical performance thus far remained noncompetitive against their liquid counterparts.

**3.7.1.5. Composite.** Various composites were formed between polymer and an inert material with the intention of suppressing crystallization of EO linkages, so that ion conductivities could be improved. Sometimes, unexpectedly, the transference number of  $\text{Li}^+$  could also benefit. Such examples include organic or inorganic anion receptors that were once described for liquid electrolytes (section 3.2), and more recently the work reported by Wunder and co-workers, who used polyhedral oligosiloxanes with oligoether molecules and found that both ion conductivities and  $\text{Li}^+$  transference number were improved<sup>413,414</sup> (eq 12A). Thanks to the flexible siloxane linkages, the  $T_g$  for the composite ranged between  $-60$  and  $-70$  °C, lower than that of PEO-based SPE, affording



ion conductivities of  $\sim 10^{-4}$  S/cm at room temperature or  $\sim 10^{-6}$  S/cm at  $-20^\circ\text{C}$ .

Wang et al. reported a composite consisting of PEO and a ceramic fiber or mats based on  $\text{La}_{0.55}\text{Li}_{0.35}\text{TiO}_3$ .<sup>415</sup> The high conductivity of the ceramic material itself helped the long-range transport of  $\text{Li}^+$  by forming an additional conduction network besides the EO-phase, resulting in an ion conductivity of 0.5 mS/cm at room temperature accompanied by a  $\text{Li}^+$  transference number of 0.7. This is the highest conductivity ever achieved for SPE; unfortunately, electrochemical performance was not described.

A nanocomposite between PEO and a biopolymer chitin was formed at different ratios by Stephan et al., who reported improvements in both ion conductivity and  $\text{Li}^+$  transference number.<sup>416</sup> In particular, the latter was increased from 0.2 to  $>0.5$  upon addition of chitin. The authors attributed this increase to the formation of a chitin–anion complex due to the presence of surface Lewis acid–base interactions; however, this rationale is not without suspicion, as it is difficult to believe that the glucosamine structural units of chitin could trap anion more than it does  $\text{Li}^+$ . Aoki et al. described a series of ion conducting SPE based on a borate salt, lithium tetrakis(pentafluorobenzenethiolato)borate (eq 12B). By mixing it with either poly(vinylidene fluoride)-based<sup>417</sup> or PEO-based polymers,<sup>418</sup> both ion conductivity and  $\text{Li}^+$ -transference number (0.6–0.7) were improved as compared to the corresponding SPE without the presence of this borate salt. Because the salt was insoluble in either polymeric media, the mixture should be a heterogeneous composite. The absence of an acceptable rationale for the underlying mechanism warrants further investigations.

**3.7.2. Gel Polymer Electrolytes.** Unlike SPE that still remains a laboratory curiosity after nearly four decades, GPE is much more practical, some of which were already in commercial LIBs 10 years ago.<sup>1</sup> In GPE, the polymers were used at additive levels, and the entanglement of their long chain along with miscibility toward carbonate solvents ensured that a semisolid macro-viscosity be maintained despite their small concentrations, while at the microscale  $\text{Li}^+$  only “feels” a liquid environment; hence, its motion is completely independent from the polymeric segmental relaxation. Because of the small polymer presence, the physicochemical and electrochemical properties of GPE bear close resemblance to those of the corresponding nonaqueous liquid electrolytes, characterized by ion conductivities  $>$  mS/cm and electrochemical stability with graphitic anode and most 4.0 V class cathode.

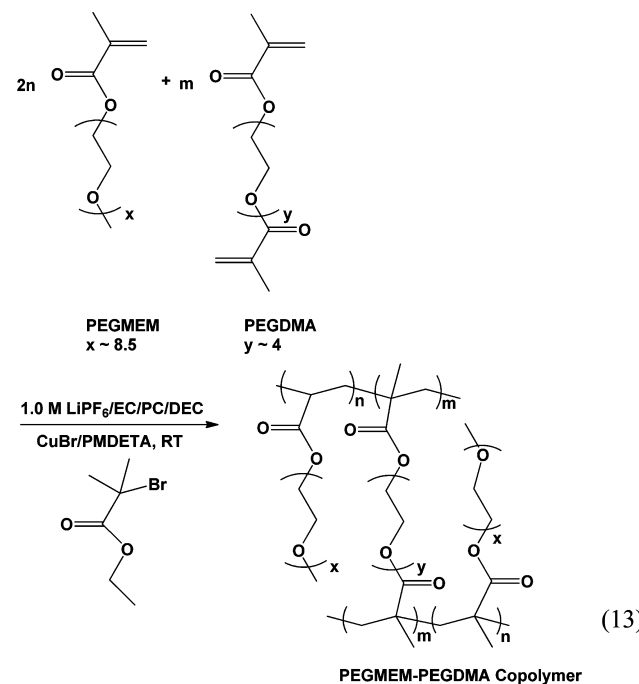
With the exception of the GPE developed by Belcore (now Telcordia),<sup>1</sup> most of the claimed GPE used in today’s “polymer battery” actually do not contain an independent GPE component as one would expect; in most cases, there were just dry polymer coatings applied to either polyolefin separator or electrode surfaces, which were assumed to be gellified after electrolytes were injected. The advantage of GPEs thus formed mainly rests in the increased safety threshold due to lower vapor pressure. This was usually accompanied by a slight compromise in performances such as rate capability and capacity utilization, but special electrolyte compositions formulated for low temperature purposes could compensate such compromises.<sup>419</sup> While most GPE technologies remain proprietary of each battery manufacturer, the Belcore GPE based on copolymer of vinylidene fluoride and hexafluoropropylene (PVDF-HFP) has been thoroughly described and well published.<sup>1,420,421</sup> Hence, these efforts will not be discussed

here; instead, this section will be dedicated to efforts of developing new gellable polymers.

Song et al. used a nonwoven fabric as mechanical support to form a composite electrolyte based on the blend of polymers containing EO, PVDF, and PMMA units.<sup>422</sup> After cross-linking by UV, the composite showed a 1000% electrolyte uptake toward carbonate-based nonaqueous electrolyte and a maximum ion conductivity of 4.5 mS/cm at  $18^\circ\text{C}$ . The authors speculated that the chain entanglement between PEO, PVDF, and PMMA provided a dimensionally stable gel. Preliminary tests in a full LIB based on graphitic anode and  $\text{LiCoO}_2$  yielded satisfactory electrochemical performance. A polymer blend consisting of PEO and PS was prepared by Passerini et al., who apparently planned to combine the ion conduction property of the former and the mechanical strength of the latter via hot-blending.<sup>423</sup> A co-continuous morphology resulted, in which two independent networks existed for these immiscible polymer chains. The blend was gelled by nonaqueous electrolytes successfully, and the resultant GPE was tested in  $\text{LiFePO}_4$  half cells with modest cycling performance.

Polyacrylonitrile (PAN) had been known to form GPE with both ether- and carbonate-based electrolytes. Similar to PMMA, the polar group  $\text{C}\equiv\text{N}$  participates in the solvation of  $\text{Li}^+$  through dipole interactions. Departing from the traditional phase-inversion technique, Choi et al. prepared microporous PVDF and PAN as GPE skeletons using electro-spinning,<sup>424,425</sup> and improvements were reported from both fibrous polymers. In particular, electrospun PAN gelled by EC/DMC electrolytes supported cycling in full LIB based on graphite and  $\text{LiCoO}_2$  for more than 150 cycles with negligible fading.

A few attempts were made to form the gel *in situ* by polymerizing the corresponding monomers of the expected skeleton polymers in the presence of electrolyte. Lee et al. described their efforts to form such a gel at room temperature (eq 13):<sup>426</sup>



The process was initiated via atom transfer radical polymerization (ATRP) to avoid gas formation, and the gel obtained with state-of-the-art electrolyte showed ion conductivity

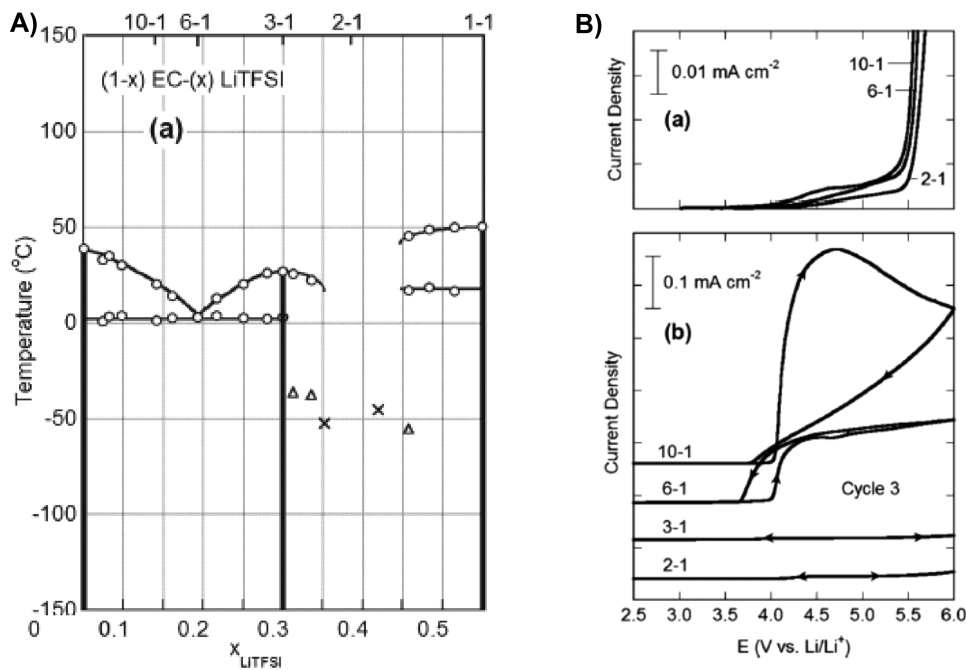


**Figure 39.** “Quasi-ionic liquid” electrolytes based on carbonates: (A) phase diagram of EC–LiTFSI mixtures, in which vertical lines represent solvates  $\text{Li}(\text{EC})_3$  and  $\text{Li}(\text{EC})_1$ , respectively, and “ $\Delta$ ” and “ $\times$ ” represent glass-transition temperatures ( $T_g$ ) for partially crystalline and amorphous states, respectively; and (B) the dependence of anodic stability of EC–LiTFSI solvates at various ratios on Al-electrodes. Reprinted with permission from ref 435. Copyright 2014 Royal Society of Chemistry.

of  $2.1 \times 10^{-3}$  S/cm and  $\text{Li}^+$  transference number of 0.32. However, the initiator that is based on an organic Cu salt would remain in the electrolyte and raised doubt whether it would negatively affect electrochemical performance. Although an electrochemical stability window of  $\sim 5.0$  V was obtained by CV, only anode half cell tests were shown. Similar approaches were explored by El-Enany et al., who directly grew PAN films on electrode surfaces in nonaqueous electrolyte,<sup>427</sup> or Hwang et al., who cationically polymerized a monomer with vinyl functionality.<sup>428</sup> Varying degrees of success were described, but the improvements were incremental as compared to GPE formed through conventional manner.

Single-ion GPE was also reported, in the hope that better ion conductivity might be obtained than its SPE counterparts. Zhu et al. used the hydroxyl groups on the main chain of poly(vinyl alcohol) (PVA) to react with oxalic acid and boric acid, so that a BOB-like anion was formed on the polymer chain (eq 11B).<sup>429</sup> However, even after being gelled by PC, the ion conductivity still remained below  $10^{-5}$  S/cm, reflecting how severe the effect of anion-immobilization was on overall ion conduction. Besides new polymer skeletons, efforts were also made in new electrolyte solutions. Kottekoda et al. used electrolytes based on PC and borate ester to plasticize polymethacrylates grafted with long EO pendants.<sup>430</sup> The Lewis acidity of the borates assisted in increasing  $\text{Li}^+$  transference number to 0.39. Electrochemical tests were conducted with a modified spinel cathode. Morita et al. introduced the flame-retardant trimethyl phosphate (TMP) into conventional carbonate-based electrolyte, and then a GPE based on PVDF-HFP was formed.<sup>431</sup> With 20% TMP, the GPE became essentially nonflammable, while with up to 55% TMP an ion conductivity of  $\sim 3 \times 10^{-3}$  S/cm was obtained with a wide electrochemical stability window (5.0 V on Pt electrode). No cell tests were described.

### 3.8. “Quasi-Ionic Liquid” Electrolytes

Except neat ionic liquids, all electrolyte systems reviewed above are diluted ( $\sim 1.0$  M) solutions of lithium salts, no matter if the solvents are small organic molecules or macromolecules. However, there exists a transition state between the diluted solutions and neat ionic liquids when the salt concentration reaches a certain level. Recently, there have been rather active efforts made on these highly concentrated electrolytes, named “quasi-ionic liquids” by some researchers, for battery applications.

Generally speaking, when salt concentration increases in a diluted electrolyte solution, extensive ion pairing occurs, leading to increased viscosity, decreased ion conductivity, and poor wettability toward pores in electrodes and separators, none of which benefits applications in any electrochemical device. In most cases, crystallization of salt or salt–solvent complexes also occurs, eliminating their usefulness as electrolyte. However, exceptions do exist. In certain systems, the homogeneity of the solutions remains nondisrupted as salt concentration increases, accompanied by drastic changes in physicochemical and electrochemical properties. These systems can be classified into either “highly concentrated electrolytes” or “solvent-in-salt electrolytes”. In the latter case, the salt/solvent molar ratio approaches or even exceeds 1; hence, the limited solvent molecules would be completely bound by overly populated ions, a reversal of the conventional “salt-in-solvent” electrolytes. The “polymer-in-salt” concept proposed earlier can be viewed as the predecessor of such systems.<sup>432</sup>

**3.8.1. Carbonate–Li Salt Systems.** As a natural extension of state-of-the-art electrolytes, the system of highly concentrated lithium salt in carbonate solvents was surprisingly underexplored. Although as early as 2003 Jeong et al. have realized that the intercalation behavior of LiTFSI/PC solution toward graphitic anode drastically changed when the concentration of the former increased from 0.82 to 2.72 M,<sup>433</sup> and more recently

Matsumoto et al. reported that aluminum corrosion by LiTFSI/EC/DEC solutions was essentially eliminated by simply increasing LITFSI concentration from 1.0 to 1.8 M,<sup>434</sup> no efforts were made to extrapolate the concentration of lithium salt into “quasi-ionic liquid” region (equimolar ratio corresponds to 9.8 m LiTFSI), probably due to the difficulty of maintaining homogeneity for these carbonate–salt mixtures. Henderson and co-workers perhaps presented the first carbonate–lithium salt “quasi-ionic liquid” electrolyte in their serial studies of the phase diagrams of highly concentrated electrolytes.<sup>435</sup> They identified that between the two crystalline solvates  $\text{Li}(\text{EC})_1\text{LiTFSI}$  and  $\text{Li}(\text{EC})_3\text{LiTFSI}$  there was an amorphous phase around  $\text{Li}(\text{EC})_2\text{LiTFSI}$ , which supercooled to  $-20^\circ\text{C}$  and melted around  $0^\circ\text{C}$  (Figure 39A). Using Raman spectroscopy, they found that in this solvate composition 95% of EC molecules were coordinated with  $\text{Li}^+$ , and when compared to its diluted counterpart, 1.0 M LiTFSI in EC, marked improvements in thermal and electrochemical stabilities were achieved, as indicated by the resistance toward aluminum corrosion at potentials up to 6.0 V (Figure 39B).

**3.8.2. Ether–Li Salt Systems.** Most “quasi-ionic liquid” systems explored thus far were based on mixtures of various lithium salts with oligoether solvents. Pappenfus et al. described equimolar mixtures of either LiTFSI or LiBeti with tetraglyme (G4), and found that the former could remain noncrystalline in a rather wide temperature range ( $-100$ – $200^\circ\text{C}$ ) thanks to supercooling ( $T_g \approx -61^\circ\text{C}$ ), while the latter melted at  $31^\circ\text{C}$ .<sup>436</sup> The low vapor pressure of G4 in the equimolar mixture indicated the strong interaction between  $\text{Li}^+$  and G4, which otherwise would boil at  $275^\circ\text{C}$  when neat. The authors considered the complexes of  $(\text{Li}–\text{G}4)^+$  a class of new cation, and hence these mixtures could be viewed as new RTIL systems. Ion conductivities of 1.0 mS/cm were obtained, with anodic stability windows higher than 4.5 V as measured on stainless steel electrodes. The same concept was also extended to  $\text{LiPF}_6$ , although with less success, as evidenced by the fact that the  $\text{LiPF}_6$ –G4 equimolar mixture must be incorporated with a third polyelectrolyte component and the accompanying lower ion conductivity.<sup>437</sup> In a similar approach, Shin et al. formed a “quasi-ionic liquid” electrolyte based on LiTFSI, G4, and a pyridinium-based RTIL.<sup>438</sup> Although the presence of LiTFSI in this ternary component system was low (0.2 m), the total ratio of ionic species versus molecular species was nearly equimolar. High ion conductivities were obtained ( $>10$  mS/cm at room temperature), enabling tests in Li/S cells at subambient temperatures.

The most systematic investigations on ether–lithium salt systems were conducted by Watanabe and co-workers, who not only sought new properties from these equimolar or highly concentrated electrolytes by varying lithium salts and ether solvents, but also attempted to rationalize them on a fundamental level.<sup>439</sup>–<sup>444</sup> While LiTFSI formed liquid equimolar mixtures with both triglyme (G3) and G4, either being a true thermodynamic liquid ( $T_m$  23 °C for the former) or aided by supercooling ( $T_g$  –54 °C for the latter, Figure 40A), evidence from both thermal (DSC, TGA)<sup>440,442</sup>–<sup>444</sup> and spectroscopic (NMR)<sup>441</sup> analyses indicated that all glyme molecules are tightly coordinated by  $\text{Li}^+$  (Figure 40A and B). This complete “harnessing” of these oligoether molecules induced dramatic changes in a series of properties that would be otherwise impossible in the corresponding dilute electrolytes, the most significant of which, to battery application, included the thermal stability up to 200 °C,<sup>436</sup> high ion

conductivity ( $\sim\text{mS}/\text{cm}$ ),<sup>440,442</sup> improved  $\text{Li}^+$ -transference numbers (0.5–0.6),<sup>440</sup> and altered electrochemical behavior toward both cathode (stability against  $\text{LiCoO}_2$  when charged to 4.2 V, Figure 40C)<sup>440</sup> and graphitic anode (being able to support reversible  $\text{Li}^+$ -intercalation chemistry, Figure 40D).<sup>443</sup> The improvements in both anodic and cathodic stabilities were particularly surprising, as it was known that diluted solutions of lithium salts in ether-based electrolytes were easily oxidized on cathode below 4.0 V, and would cointercalate with  $\text{Li}^+$  into graphitic structures forming the undesirable ternary graphite-intercalation compounds.<sup>1</sup>

To expand the liquid range as well as improve ion conduction, Watanabe and co-workers also attempted to modify the structures of both glymes and lithium salt anions. In the former approach, an asymmetric structure was introduced into glymes to enable higher degrees of freedom for the equimolar mixtures,<sup>440</sup> while in the latter, nine different anions with varying degree of Lewis basicity were used to correlate the structure–property relationship.<sup>444</sup> The authors found that the thermal, transport, and electrochemical properties of these equimolar glyme–lithium salt mixtures were determined by the competitive solvation of  $\text{Li}^+$  by solvent (glyme) molecules and anions. As a result of this competition, these highly concentrated electrolyte systems could be classified into two distinct categories according to their “ionicity”, a quantity defined as the ratio of molar ion conductivities measured via impedance and NMR techniques, respectively. By this quantification, anions of weak Lewis basicity, such as TFSI and  $\text{ClO}_4^-$ , would form “quasi-ionic liquid” electrolytes, while anions of strong Lewis basicity, such as  $\text{NO}_3^-$  and trifluoroacetate, would favor close ion-pairs with  $\text{Li}^+$ . Intermediate behavior was observed for anions like  $\text{BF}_4^-$ . This rationale would explain why most of the “quasi-ionic liquid” electrolytes investigated thus far were based on large, polarizable anions such as TFSI. Lee et al. studied concentrated solution of LiBOB in G4 (molar ratio 1:4), which showed high ion conductivity ( $>10^{-3}$  S/cm at room temperature) and capability of supporting Sn–C alloy-type anode,<sup>445</sup> although electrolyte of higher concentration was probably prevented by limited solubility of LiBOB in G4 and the high  $T_g$  associated with this salt. The potential of “quasi-ionic liquid” electrolytes for “beyond Li-ion” advanced chemistries was further demonstrated by the mixture of LiTFSI with DME and 1,3-dioxolane at concentrations up to 7 M (salt/solvent molar ratio close to 1.5–2.0), which was shown by Suo et al. that not only high  $\text{Li}^+$ -transference number ( $>0.7$ ) but also the ability to simultaneously suppress Li dendrite growth and polysulfide dissolution<sup>446</sup> resulted from this highly concentrated system. This rare combination makes it a promising candidate for the highly coveted Li/S system to be discussed later.

**3.8.3. Polymer–Li Salt.** Since the work of Angell et al.,<sup>432</sup> the “polymer-in-salt” concept has not been actively pursued due to the difficulty of identifying a lithium salt system that has a melting or eutectic point below or near room temperature while meeting all other transport and electrochemical requirements, especially oxidation stability. Florjańczyk et al. investigated a series of polyacrylates in lithium salts of various anions that included TFSI,  $\text{ClO}_4^-$ ,  $\text{AlCl}_4^-$ , triflate, and  $\text{BF}_4^-$ .<sup>447</sup> Despite increased  $\text{Li}^+$ -transference numbers, moderate conductivities ( $10^{-7}$ – $10^{-4}$  S/cm) were obtained at typical “quasi-ionic liquid” concentrations, with crystalline phases scattered in the system that were most likely stoichiometric solvates between lithium salts and polymer. As in the “polymer-in-salt” concept, the high

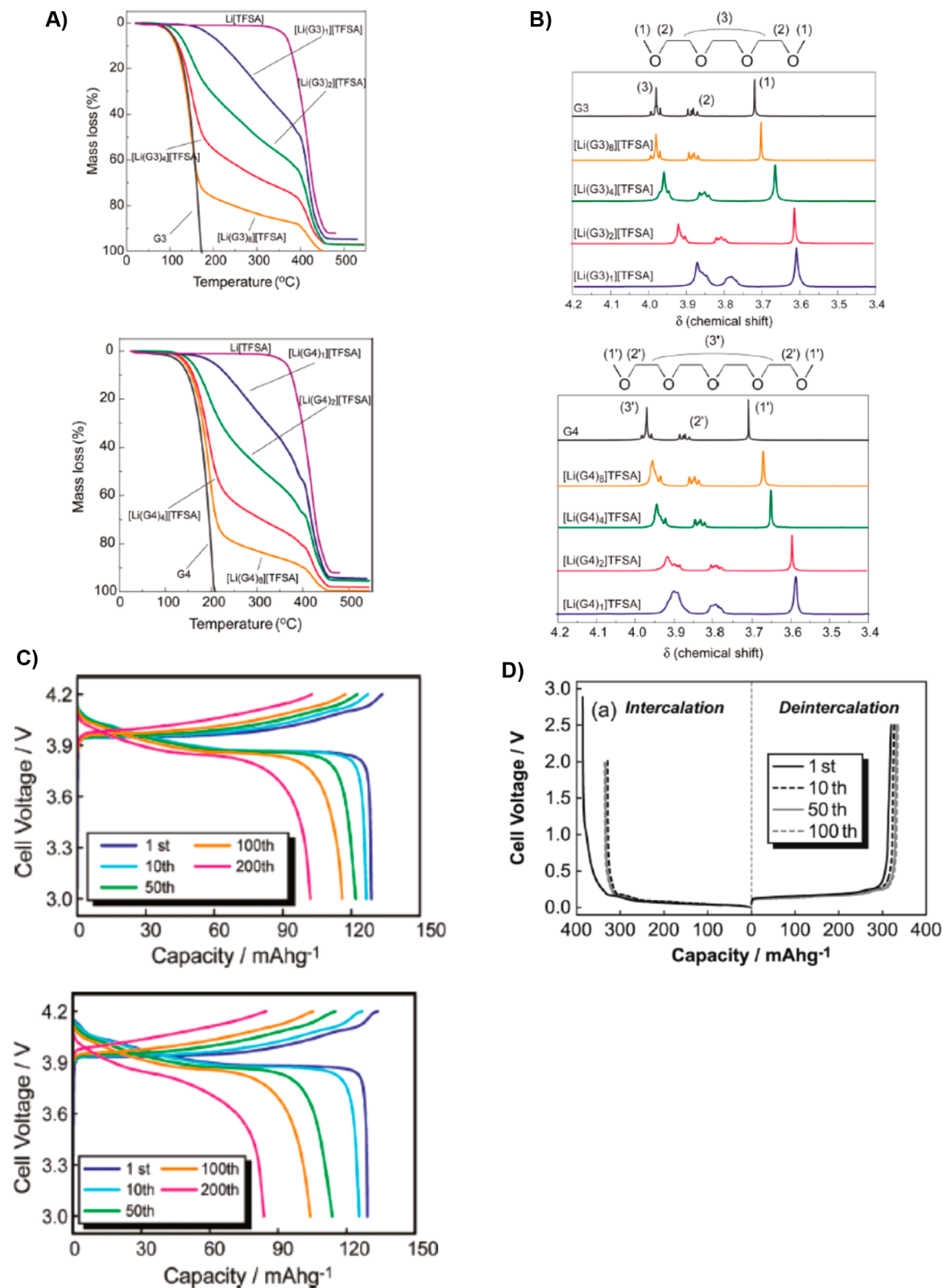


**Figure 40.** “Quasi-ionic liquid” electrolytes based on ethers: (A) Weight loss of glyme–LiTFSI systems at various ratios between LiTFSI and (a) triglyme or (b) tetraglyme molecules as measured by thermogravimetry. Reprinted with permission from ref 442. Copyright 2011 American Chemical Society. (B) NMR glyme–LiTFSI systems showing the gradual disappearance of free glyme molecules as Li<sup>+</sup>-concentration increased. (C) Charge/discharge voltage profiles of LiCoO<sub>2</sub> cathode in highly concentrated glyme–LiTFSI systems (LiTFSI/glyme ratios 1:1). Reprinted with permission from ref 441. Copyright 2011 American Chemical Society. (D) Charge/discharge voltage profiles of graphitic anode in LiTFSI–triglyme at ratio 1:1. Reproduced with permission from ref 443. Copyright 2011 Electrochemical Society.

crystallinity and high melting temperature of lithium salts often constituted the ultimate challenge for the formation of a feasible “quasi-ionic liquid system”.

Considering these difficulties associated with lithium salts, researchers made compromises by introducing a third component beside lithium salt and polymer. The proven RTIL systems based on imidazolium, piperidinium, and particularly pyrrolidinium were often the choices. High ion conductivities ( $>10^{-4}$  S/cm at room temperature) and Li<sup>+</sup>-transference numbers were obtained with both PEO<sup>448,449</sup> and PVDF-HFP<sup>450</sup> in the absence of crystallinity, and preliminary electrochemical tests in cathode half cells were conducted, but more rigorous investigations are still needed to justify their practical applications.

**3.8.4. Other Solvents–Li Salt.** Besides ethers and carbonates, various cyclic and linear amides were also used to form highly concentrated electrolytes with LiTFSI, some of which still bear hydrogen on N.<sup>451–454</sup> The presence of these hydrogen atoms, in addition to the instability of N atoms in amides toward electrochemical oxidation, restricted the electrochemical stability window of the resultant “quasi-ionic liquid” electrolytes in the neighborhood of 3.5 V. For this reason, most of them have not been tested as candidates as battery electrolytes but instead found possible applications in electrochemical double-layer capacitors. The only exception was the recent work conducted by Boisset et al., who used N-methylacetamide with various lithium salts, including LiTFSI, LiPF<sub>6</sub>, and LiNO<sub>3</sub>, to form “quasi-ionic liquids” at room temperature and were able to cycle them in cells constructed with LiFePO<sub>4</sub> cathode and titanate-based anode.<sup>455</sup> Apparently, the active hydrogen was somehow “harnessed” therein as a wide electrochemical stability window (4.7–5.0 V) on Pt was reported. The authors attributed this deactivation to the complexation of H by lithium salt anions, in the easiness order of TFSI<sup>-</sup> > PF<sub>6</sub><sup>-</sup> > NO<sub>3</sub><sup>-</sup>, despite the fact the electrolyte was only tested between the mild electrochemical potentials of LiFePO<sub>4</sub> cathode and titanate-based anode.

Parallel in behavior with its ether- and carbonate-counterparts, acetonitrile, a solvent that was frequently used in electrochemical capacitors and has been considered “unfriendly” toward graphitic anodes, was shown by Yamada et al. to be able to support Li<sup>+</sup>-intercalation chemistry with graphite at a faster rate, as long as the concentration of the lithium salt (LiTFSI) is above 4.0 M.<sup>456</sup> As revealed by surface analyses, the interphase formed on graphite surface would be characteristic of the decomposition products from the anion rather than from the solvent. The authors attributed the above “abnormal” behavior of “superconcentrated” acetonitrile solutions to the altered solvation sheath structure of Li<sup>+</sup>, which will be elaborated in section 5.1.3.

#### 4. DEGRADATION AND STABILIZATION OF ELECTROLYTES

State-of-the-art electrolytes are both chemically and electrochemically metastable, and hence they would be susceptible to irreversible decomposition once exposed to environments that departed from the designed operating conditions of LIB, which are often triggered by elevated temperature, trace moisture, and overcharge or overdischarge outside of safe potential windows. This section will first summarize the varying degradation mechanisms for electrolytes in LIB, and then the efforts in developing new electrolyte components to suppress these undesirable reactions.

#### 4.1. Degradation Mechanisms

According to a collection of seminal studies and reviews published since 2005,<sup>457–465</sup> electrolyte instability plays an essential role in almost all pathways via which an LIB loses its designed performance:

(1) Parasitic (and most likely irreversible) reactions between electrolyte components and charged electrodes. Although kinetic protection is provided by interphases, their formation has not been completed during the initial cycles, as many researchers would believe. As reported by Dahn and co-workers using their high precision coulometry technique,<sup>466–469</sup> these parasitic reactions actually never completely stop, even during the entire life-span of the cell, but rather slow at a rate (dx/dt) that follows the general mathematic relationship in eq 14:

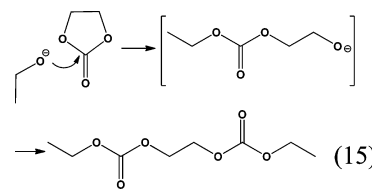
$$\frac{dx}{dt} = \sqrt{\frac{k}{2}} t^{-1/2} \quad (14)$$

where k was a constant given each electrolyte/electrode system and temperature, and x was the hypothetic thickness of an idealized SEI. It must be kept in mind that not all of these reactions contribute to the continuous growth of SEI. The impact of these interphasial reactions was especially conspicuous on lithiated graphite;<sup>458</sup> however, when the cathode potential was above 4.5 V, parasitic reactions on the cathode surface would dominate as indicated by impedance,<sup>463,465</sup> spectroscopic,<sup>465</sup> and high precision coulometry studies.<sup>280</sup>

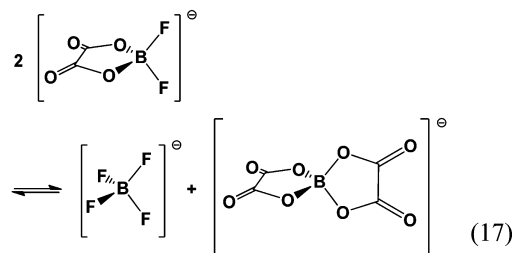
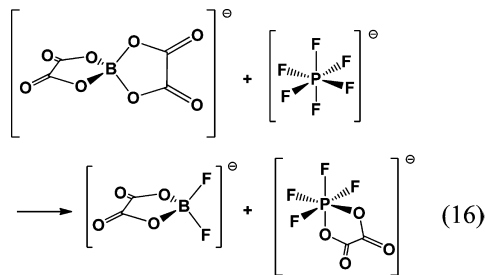
(2) The effect of trace moisture, which is closely intertwined with dissolution of transition metals from cathodes and interaction among electrolyte components. Moisture's affect is more prevalent in more polar systems because the dissociation of LiPF<sub>6</sub> is encouraged therein,<sup>470</sup> and consequently PF<sub>6</sub><sup>-</sup> reacts with moisture to generate undesired HF, an unwanted but ubiquitous impurity in almost all commercial electrolytes, which catalyzes a host of parasitic reactions.

(3) The dissolution of active electrode materials in electrolytes, which is aided by the presence of acidic impurities (HF generated during hydrolysis of PF<sub>6</sub><sup>-</sup> by trace moisture). In particular, transition metals such as Mn and Ni are susceptible to acid leaching, and the higher operating potentials of the 5 V class Ni–Mn spinel further exacerbates the issue.<sup>158,185,249,465</sup>

(4) The inter-reactions of bulk electrolyte components, such as the trans-esterification of carbonates,<sup>1</sup> and similar nucleophilic reactions between cyclic and acyclic carbonates leading to the formation of undesirable alkylidicarbonates (eq 15).<sup>471,472</sup> These reactions again could be initiated by



alkoxide and subsequently catalyzed by acidic impurities. Interactions also exist between salts. For example, Lucht and co-workers described how LiBOB as an additive reacted with LiPF<sub>6</sub> upon thermal storage and generated tetrafluorooxalato-phosphate anion via a disproportionation pathway (eq 16),<sup>128</sup> and how thermally induced ligand exchange of LiDFOB generated LiBF<sub>4</sub> and LiBOB (eq 17).<sup>473</sup> Perhaps the real significance of eqs 15–17 is not the chemistries shown therein, but the alarming reminder about how unreliable the nominal



electrolyte formulation could be. One should always keep in mind that what really exists in an electrolyte system might not be taken at its “face value”.

(5) Dissolution of interphasial components and possible “electrochemical dialogs” between cathode and anode. It has been realized that the key ingredients of SEI, the lithium salts of alkyl carbonates, are soluble in electrolyte solvents.<sup>462,474</sup> Tasaki et al. quantified that, even in acyclic carbonate, these lithium salts could still dissolve at concentrations between  $10^{-5}$  and  $10^{-4}$  mol/L.<sup>475</sup> If these species can be oxidized/reduced at the opposite electrode after diffusing across the cell, such seemingly “low” concentrations can already incur self-discharge current at the level of 0.2–2 mA/(L of electrolyte). Of course, a dynamic equilibrium exists between the dissolution and precipitation of these interphasial species, and hence any form of consumption of these dissolved species at electrode surfaces would encourage more dissolution of interphase, leading to eventual cell impedance buildup.

(6) Corrosion of current collectors by electrolyte components at extreme potentials. These corrosion scenarios include not only the well-known cathode substrate Al-corrosion by salt anions such as TFSI and Beti at high potentials (>4.0 V), but also Cu substrate corrosion at the anode side when the cells are overdischarged. A full LIB at an OCV of 0 V would have brought the potential of the anode to the vicinity of ~3.0 V vs Li, which is dangerously close to the oxidation potential of Cu (~3.3 V vs Li). It must be remembered that, in batteries of large formats where winding configuration of electrodes create complicated tortuosity hierarchies, many electrochemical reactions and processes are actually at nonequilibrium states. Thus, the cell voltage could mislead us from the actual chemical states in local electrode regions, where corosions occur.

(7) Thermal effects, which include both low (subzero) and high (>40 °C) temperatures. In the former scenario, the Li<sup>+</sup>-transport kinetics within the interphase would fall behind those in the bulk solution and graphite interior, leading to regional lithium metal plating and subsequent reaction of lithium with solvents. In the latter scenario, all above degradation processes would be accelerated, as evidenced by the drastic increase in SEI thickness, which increased from 40 to 150–450 nm on graphite as revealed by surface analyses conducted by focused ion beam (FIB), SEM, and XPS,<sup>476</sup> and the increase of rate constant  $k$  in eq 14 with increasing temperature.<sup>466–470</sup> An

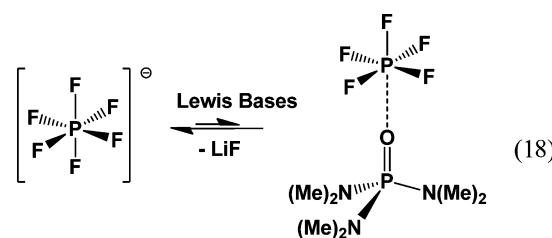
extreme case of high temperature degradation is the so-called “thermal runaway”, which represents the catastrophic chain-reaction that is triggered by thermally induced decomposition of either electrolyte or interphasial components, with heat generation too high to be self-dissipated. The overall outcome is the complete combustion of the entire battery system, in which the cathode serves as the oxidant, while carbonate solvents, polymer binder, and separators serve as the fuels.<sup>477</sup> Various investigations of thermal instability of state-of-the-art electrolytes have placed the blame on the reactivity of PF<sub>6</sub><sup>-</sup>-anion with other electrolyte components<sup>476,478</sup> and electrode materials, especially lithiated graphite,<sup>479–483</sup> while the reactions between delithiated cathode materials with electrolyte components depend on both state-of-charge and the chemistries.<sup>484–486</sup> In general, the reactions of lithiated graphite with electrolytes or interphases occur at lower onset temperatures (80–120 °C),<sup>480,481,483</sup> while reactions between electrolytes and delithiated cathode generate most of the enthalpies responsible for the propagation of thermal runaway.

On the basis of these mechanisms, various models were developed to predict the life of LIB, which were able to reproduce the experimental observations while placing focus on SEI growth on the graphitic anode.<sup>461,464,487</sup> A simple model developed by Burns et al., built upon short-term measurement of parasitic reactions within a LIB at high accuracy, provided a practical tool to select EV batteries without the need to understand the underlying mechanisms.<sup>488</sup>

#### 4.2. Electrolyte Components To Suppress Degradations

To mitigate the effect of electrolyte degradation on cell performance, new electrolyte components were developed in attempts to slow the above-mentioned processes.

**4.2.1. Chemical and Thermal Degradations.** Campion et al. and Li et al. described the use of lithium metal oxides as well as a series of Lewis bases as inhibitors to the thermal decomposition of PF<sub>6</sub><sup>-</sup>-anion.<sup>489,490</sup> They proposed that the autocatalyzed reaction cycle of the unstable salt anion could be interrupted due to the sequestration of PF<sub>5</sub> by those bases (eq 18), which was supported by evidence from multinuclei NMR investigations.



Replacement of LiPF<sub>6</sub> by lithium salts of higher thermal stability was also attempted, where LiFAP, LiBOB, and other borate variations were identified to help mitigate the parasitic reactions at elevated temperatures.<sup>489,491</sup> On the other hand, Sasaki et al. also made efforts to prevent trans-esterification among carbonate molecules.<sup>492</sup> On the basis of the assumption that such inter-reactions occur via nucleophilic attack on the electron-deficient centers of carbonates (eq 15), they believed that the presence of a more electrophilic additive such as VC would effectively suppress the formation of alkyl dicarbonates; better cycle life and rate capabilities seemed to support this belief.

More efforts were made to reduce the inflammability of carbonate-based electrolytes, so that catastrophic chain

reactions, mainly contributed by electrolytes, could be avoided in case of accidental abuses such as overcharging, mechanical shorting, and overheating. Previously, alkyl phosphates have been shown to be effective in suppressing flammability at the expense of certain electrochemical performances.<sup>1</sup> Continued efforts in this line of thought were focused on how to minimize the compromises. Hyung et al. described triphenyl and tributyl phosphates (TPP and TBP) as improved flame-retarding additives that met such requirements.<sup>493</sup> At 5% concentration, these additives were shown to impact the safety of fully charged LIB significantly with negligible performance trade-offs, as evidenced by both standardized flammability tests and accelerating rate calorimetry (ARC) measurements of electrolyte/lithiated graphite couples. The effectiveness of TPP in flame-retarding and its inertness in electrochemistry was confirmed by Nam et al., who used TPP in combination with two other additives vinyl ethylene carbonate (VEC) and biphenyl (BP).<sup>494</sup> A derivative of phenyl phosphate was also reported by Wang et al., who used 4-isopropylphenyl diphenyl phosphate as additive at 5–15%, and found slight compromises in performance in LiCoO<sub>2</sub>-cathode half cells.<sup>495</sup> More recently, Shim et al. reported another derivative of phenyl phosphate, diphenyloctyl phosphate (DPOP).<sup>496</sup> Interestingly, the presence of DPOP (~5%) in electrolyte not only suppressed thermal instability as evidenced by higher onset temperature in DSC measurements but also enhanced cell performance, in terms of better rate capability, capacity retention, higher oxidation stability limit, and interphasial lower impedances. On the other hand, trimethyl phosphate (TMP) was revisited by Wang et al. as a main electrolyte solvent (>70%) instead of additive for a nonflammable system.<sup>497</sup> To address the poor cathodic stability of TMP on graphitic anodes, they employed a combination of SEI additives consisting of VC, VEC, and cyclohexane as well as high concentration (2 M) of LiBeti. The synergistic effects of these components enabled the TMP-based electrolytes to support reversible Li<sup>+</sup>-intercalation chemistry on a graphitic anode that had been coated with an amorphous carbon layer on its surface.

Beside phosphates, other phosphorus-containing compounds were also explored as potential candidates for nonflammable electrolytes. Izquierdo-Gonzales used a phosphamide derivative as a replacement for phosphates and found that it indeed can suppress flammability;<sup>498</sup> however, the electrochemical stability window suffered, probably due to the presence of P–N bonds. Mandal et al. reported a series of phosphate–phosphamides hybrid compounds with phenyl substituents as additives in the carbonate-based electrolytes.<sup>499</sup> When used at 2–5%, their effectiveness in preventing thermal runaway was proved in the presence of metallic lithium with ARC measurements. However, their usefulness still needs to be confirmed in a full LIB environment.

A few phosphorus-free compounds were also investigated for this purpose. Bakenov et al. described a poly(ethylene glycol) borate ester, which is nonflammable, as a polymer host for a SPE,<sup>500</sup> while Zhang et al. described a silane derivative as a flame-retarding additive.<sup>501</sup> In the latter case, when vinyl-tris(methoxydiethoxy)silane (VTMS) was used at 5–15%, the flammability of electrolyte systems was significantly reduced with negligible compromises in cell performance. Surface analyses conducted with XPS found that VTMS participated in forming a passivation layer on LiCoO<sub>2</sub> cathode surface, which might be the key in retarding the thermal reactivity of the delithiated LiCoO<sub>2</sub> toward carbonate solvents.

It must be pointed out here that nonflammability and thermal safety of electrolytes are two completely independent concepts. According to Shigematsu et al., the former concerns the combustion behavior in atmosphere, and the latter the electrochemical reactivity in cell environments.<sup>502</sup> Nonflammability might help enhance thermal safety of device in the event of cell rupture with external ignition sources nearby, while oxidation of electrolyte solvents in an overcharged cell would proceed regardless of their flammability. For this reason, even some excellent flame-retardant solvents did not help with actual cell safety.

**4.2.2. Degradations with Anode.** Various new solvents, additives, or salts were developed, targeting the interphasial stabilities between specific electrolyte/anode couples. It has been well recognized that the reactivity between electrolyte and lithiated anode determines the minimum temperature where chain-like thermal decompositions are irreversibly triggered; hence, the effectiveness of a new component would be measured by its ability to postpone this onset temperature.

Previously, it has been shown that the replacement of LiPF<sub>6</sub> by LiBOB can push the onset temperature higher by ~90 °C; on the other hand, when its partially fluorinated derivative, LiDFOB (Table 12), was used as an additive at <3%, a similar effect would be achieved with onset temperature higher by at least 50 °C.<sup>503</sup> Ratnakumar and co-workers compared the effects of a series of additives on electrolytes' storage stability in the presence of charged graphitic anodes at elevated temperatures.<sup>504,505</sup> They found that not only chemical structure but also concentrations of the additives played the essential role in stabilizing electrode surfaces with electrolytes. Both VC and dimethylacetamide (DMAc) stabilized the interphases effectively at low concentration (1%), while VEC or higher concentration (10%) of DMAc led to worsened electrolyte decomposition as compared to baseline electrolyte. The mechanism of these additives might differ too: DMAc as a Lewis base could neutralize the aggressiveness of PF<sub>6</sub><sup>−</sup>-anion or its reaction products with carbonate solvents; while VC was believed to have formed a polymeric interphase that can offer better protection.

Perhaps the most effective suppression of thermal reaction onset temperature was reported by Ihara et al., who used MFA<sup>71</sup> (Table 4B) as the main solvent for LiPF<sub>6</sub> salt and found with DSC measurements that the partially fluorinated solvent pushed the onset temperature with lithiated graphite up by ~110 °C.<sup>506</sup> Because of higher interphasial resistances, the LIB using MFA-based electrolytes suffers slight compromises in electrochemical performance.

**4.2.3. Degradations with Cathode.** It has also been accepted that the reactivity between electrolyte and delithiated cathode is usually the main source of heat generation leading to catastrophic thermal runaway. Efforts to mitigate this process by developing electrolyte components proved more challenging than the corresponding work on the anode side, because, as pointed out by Shigematsu et al.,<sup>477,502</sup> the electrochemical oxidation of electrolyte solvents or any other organic components (binders, separators) is hardly affected by changes in electrolyte composition or interphasial chemistry. This complication could be best exemplified by the work of Jiang et al., who showed that while LiBOB offered higher thermal stability on lithiated graphite, its reactivity with delithiated 4.0 V class cathode materials such as LiCoO<sub>2</sub> and Li[Ni<sub>x</sub>Co<sub>y</sub>Mn<sub>z</sub>]O<sub>2</sub> was actually deteriorated as compared to baseline electrolytes containing LiPF<sub>6</sub>.<sup>507,508</sup> Cho et al. also showed that the

presence of additives such as FEC or VC in the electrolytes did little to prevent the dissolution of Mn from the delithiated cathode, and VC could only help to minimize the deposition of the dissolved Mn on anode surfaces.<sup>188</sup> However, DMAc, the Lewis base additive developed by Ratnakumar and co-workers and proven to be effective on graphitic anode,<sup>504,505</sup> was observed to be effective in protecting cathode surfaces including LiCoO<sub>2</sub>, LiMn<sub>2</sub>O<sub>4</sub>, and LiNi<sub>0.8</sub>Co<sub>0.2</sub>O<sub>2</sub> from corrosion upon storage, with only 3% present in the electrolyte.<sup>509</sup>

The electrolyte approach was much more effective with cathodes of lower potentials (and lower energy density) as evidenced by the works of Chang et al.<sup>510</sup> and Ping et al.<sup>511</sup> on LiFePO<sub>4</sub>-based cells. In the former, the anion receptor TPFBP (Table 10) was used at concentrations <0.1 M to improve the cycling performance of LiFePO<sub>4</sub> cells at elevated temperatures, and in the latter various salts were tested with charged LiFePO<sub>4</sub> in a calorimeter, showing that the thermal stability of LIB was significantly improved by LiBOB. This conclusion was in good agreement with cathode/electrolyte thermal stability as measured with ARC by Jiang et al.<sup>507,508</sup> However, the low working potentials of LiFePO<sub>4</sub>-based chemistry come with high intrinsic safety and low degradation, thus making the role of electrolyte in stabilization less significant.

**4.2.4. Degradations with Aluminum Substrate.** Another major source of degradation that involves electrolyte components is the corrosion of electrode substrates, particularly the anodic dissolution of cathode substrates at high potentials.<sup>512</sup> While the use of any noble metal is impractical, the thermodynamic stability of most non-noble metals would be lost at potentials >3.5 V.<sup>1,513,514</sup> In state-of-the-art LIB, aluminum has been used as the universal substrate for all cathode chemistries, which is kinetically stabilized via passivation in a manner similar to SEI being formed to stabilize the graphitic structure on the anode side. Limited numbers of systematic investigations on this topic have found that the successful passivation of aluminum relies more on the salt (or salt anion) species rather than solvents,<sup>515</sup> differing from the interphasial chemistry on graphite anodes. PF<sub>6</sub><sup>-</sup> is one of the anions that can passivate aluminum at both high potentials and elevated temperatures,<sup>516</sup> and this ability along with others makes it the salt of choice for LIB industry despite its chemical or thermal meta-stability/instability against moisture and other organic components.<sup>1,19</sup> As pointed out by Krämer et al., perhaps it was these “instabilities” that are responsible for the successful passivation of the substrate, while the apparently more “stable” salt anion TFSI failed.<sup>515</sup> A similar conclusion was once drawn by MacNeil et al. regarding the paradox between the chemical stability and electrochemical instability of various salt anions with cathode surfaces.<sup>1</sup>

The electrolyte degradation on aluminum substrate was thoroughly studied by Winter and co-workers,<sup>515,517</sup> who showed that at least three parasitic reactions compete against each other: (a) the anodic (oxidative) dissolution of aluminum; (b) the oxidation of solvents and salt anions; and (c) the interaction between dissolved aluminum cation with the oxidation products of anions and solvents. The eventual termination of the degradation process depends on the interplay of these processes. Particularly interesting (and surprising) was that a substantial amount of fluoride (F<sup>-</sup>) was detected during the oxidative holding of electrolyte at high potential (5.0 V) in the presence of aluminum. Apparently the strong C–F bond in TFSI was broken in the presence of protons, which was generated by either trace moisture or oxidation of organic

solvents, against the traditional notion that the highly soluble Al(TFSI)<sub>3</sub> be responsible for the main degradation.<sup>1</sup>

While shown in sections 3.6 and 3.8 that corrosion of aluminum by TFSI could be effectively suppressed by using high concentrations of this anion, coupling it with other solvents could also result in successful passivation. One example involves a partially fluorinated ester, methyl difluoroacetate (MFA, Table 4B), in which Kawamura et al. showed that the anodic dissolution of aluminum was inhibited, not by AlF<sub>3</sub> but by an organic passivation layer that might contain [Al(TFSI)<sub>x</sub>]<sup>3-x</sup> complex cations.<sup>516</sup> Other anions were also studied as potential replacements for the thermally unstable PF<sub>6</sub><sup>-</sup>, the promising ones including BOB<sup>514</sup> and variations of TFSI.<sup>517</sup> In the latter effort, Murmann et al. demonstrated a series of dilithium salts based on combined anions of bisimide, imide-methide, and imide-sulfonate, respectively, with the last two approaching the ability of PF<sub>6</sub><sup>-</sup> in passivating aluminum.

Most imide salts would inherit the corrosive nature of LiTFSI toward aluminum, although the severeness would vary with fluoroalkyl substituents on N, either elongated or shortened as in LiBet<sup>1</sup> or LiFSI<sup>518</sup> (Table 13), either cyclic<sup>519</sup> or asymmetric as in LiFNFSI,<sup>158</sup> although Han et al. believed that the corrosion was not necessarily an intrinsic property of these imide salts. At least in one case it came from the impurities that were introduced during synthesis and survived purification processes.<sup>520</sup> The clarification of this issue would rely on the availability of high purity samples manufactured via standardized protocol by material suppliers, which is reminiscent of the early days of LiPF<sub>6</sub>.<sup>1</sup>

Borates, on the other hand, passivate aluminum almost as well as fluorophosphates, with typical examples of LiBF<sub>4</sub> and LiBOB.<sup>1</sup> Among the collection of orthoborates prepared by Nolan et al.,<sup>136</sup> most can be used with aluminum substrates at high potentials as long as solubility and ion conductivity permit, and LiDFOB was reported to be able to stabilize aluminum better than LiBOB did.<sup>521</sup>

## 5. UNDERSTANDING INTERPHASES

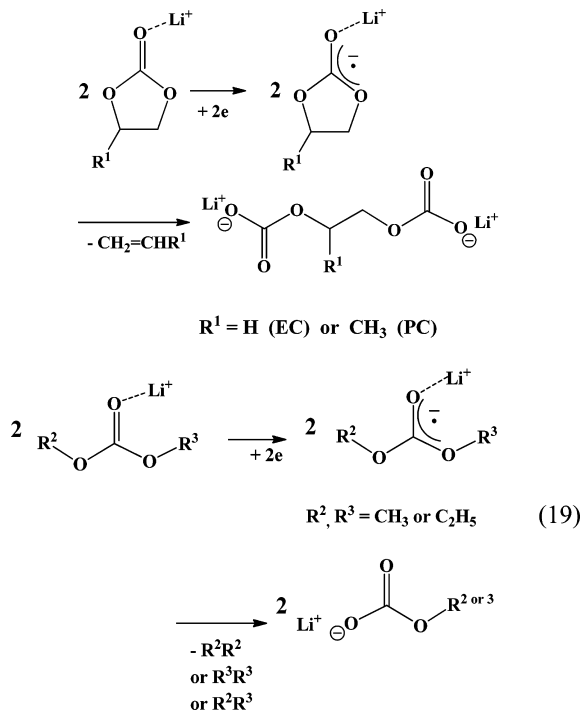
In an electrochemical device, interfaces between electrolyte and electrodes constitute the only “legitimate” sites for electron exchange. In lithium-based cells, because of the extreme potentials where anodes or cathodes operate, these interfaces are no longer the 2D entities frequently encountered in low voltage electrochemical devices (such as aqueous batteries or fuel cells) and well-described in classical electrochemistry textbooks. Instead, they became 3-D independent interphases resulting from the sacrificial decomposition of electrolyte components, named SEI after their electrolyte nature. According to Winter, they are “the most important but least understood component” in LIB.<sup>18</sup> They are important because they are essentially responsible for the reversibility of Li<sup>+</sup>-intercalation chemistries while dictating the kinetics of overall cell reactions; they are difficult to characterize because of their sensitive chemical nature, elusive manner of formation, and the lack of reliable *in situ* characterization tools.<sup>1</sup> As a further complication, the usual selective sensitivity of most spectroscopic tools to certain chemical species and simultaneous blindness to others often reduced our understanding about interphases to a “blindmen-elephant interaction”. It was these challenges that have made SEI one of the most intensively studied topics of LIB, as evidenced by the number of dedicated reviews and books.<sup>18,19,23,52,522,523</sup> Significant advances have been made during the past decade as various new models and tools were

developed,<sup>264,487,524–528</sup> although debate still persists on many issues, even the most basic chemical composition of SEI. In particular, the high precision coulometry technique developed by Dahn and co-workers,<sup>174–176,199,200,280,281,466–469,488,512,529</sup> despite its phenomenological nature, brought about a breakthrough in interphasial characterizations. As a much needed *in situ*, nondestructive, and highly quantitative tool, it allows us to gain insight into these complicated processes occurring at electrolyte/electrode interphases.

### 5.1. Anode/Electrolyte Interphase

Ever since the inception of lithium-based batteries, interphases on anodes have been a topic of interest, with the term “SEI” initially coined to describe the passivation occurring on metallic lithium at the negative potential of  $-3.0\text{ V}$  vs standard hydrogen electrode (SHE). The introduction of graphitic anodes for LIB only intensified the interest, because, in addition to protecting electrolyte from sustained reduction, SEI must also prevent physical disintegration of graphitic anode in view of its “fragile” nature toward solvent cointercalation. During the past decades, efforts on interphases overwhelmingly focused on the anode side, significantly deepening our understanding about this elusive component.

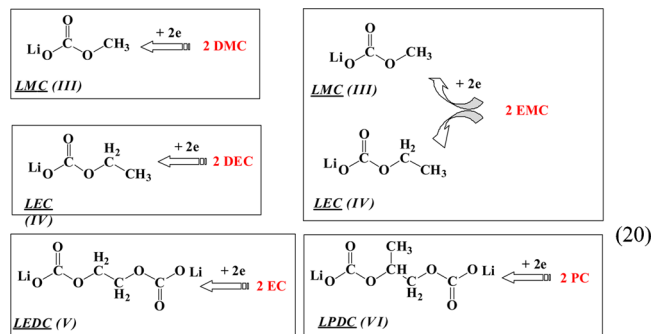
**5.1.1. Chemistry and Electrochemistry.** Thanks to the defining work from Aurbach and co-workers,<sup>1</sup> lithium salts of semicarbonate (also called alkylcarbonate) as reduction products of carbonate solvents via a single-electron pathway were generally recognized with the credit of constructing a protective yet  $\text{Li}^+$ -conducting phase. A possible mechanism was proposed assuming that nucleophilic attacks occur between two radical anions generated by initial electronation of the carbonate molecules, probably assisted by the coordination of  $\text{Li}^+$  with the carbonyl group (eq 19):<sup>530</sup>



In this reduction pathway, one-half of the organic moieties would be maintained in the interphase, while the other one-half would be lost as gaseous products generated in the initial cycling.

While the attribution of semicarbonates remains unshaken and continues to be confirmed by more sophisticated characterization efforts, diversity was also added to interphasial chemistry with a rich collection of species identified in interphases.

**5.1.1.1. Semicarbonates.** Following Aurbach’s initial identification of semicarbonates in SEI on metallic lithium and its subsequent detection on graphitic anodes, researchers around the world focused their attention on this class of organic salts. Among the numerous reports, Dedryvère et al.<sup>531</sup> and Xu et al.<sup>530</sup> perhaps approached the issue in the most fundamental and systematic manner, who independently synthesized the standard semicarbonates that are believed to be single-electron reduction products from all possible carbonate solvent molecules commonly used in LIB (eq 20).



The availability of these compounds in high purity made it possible to establish reliable spectroscopic (XPS, NMR, FTIR) databases for accurate identification of these species in an interphase (Figure 41),<sup>46,532,533</sup> while enabling the investigation on their bulk properties such as conductivity, electrochemical and thermal stability, and chemical reactivity toward ambient and moisture.<sup>530,533,534</sup> Interestingly, while both groups of researchers indeed found these species in actual interphases formed on various electrode surfaces, thus confirming Aurbach’s assignment with high confidence, there was discrepancy in their finding of preferential reduction of carbonate mixtures: Tarascon and co-workers reported that LMC was the main product generated by DMC on CoO or stainless steel surfaces in EC/DMC 1:1 mixture,<sup>531,532</sup> while Zhuang et al. reported the exact opposite on Ni surface, despite the overwhelming majority of DMC in the bulk electrolyte (EC/DMC in 30:70 ratio).<sup>46</sup> The latter preferential reduction of EC was also observed on graphitic surfaces to be discussed later. The presence of semicarbonates on graphitic surfaces has been extensively documented in numerous papers,<sup>533,535–540</sup> while recent studies also found them on silicon<sup>537</sup> or  $\text{Li}_4\text{Ti}_5\text{O}_{12}$ <sup>538</sup> surfaces as long as the latter was polarized below 1.0 V. Most likely semicarbonates are universal species in interphases formed on most electrode surfaces, although their interphasial presence varies with bulk electrolyte composition, electrode surface, and the potential applied. For example, on the basis of XPS C 1s core peak analyses, Dedryvère et al. reported that  $\text{Li}_2\text{CO}_3$  was identified as the main component in the interphase with LiTFSI as salt, while a mixture of  $\text{Li}_2\text{CO}_3$  and semicarbonates was found with LiBeti as salt.<sup>539</sup> The sensitivity of semicarbonates also introduced complications, as its presence in interphases would be decimated by the acidic byproducts of  $\text{LiPF}_6$ .<sup>540</sup>

**5.1.1.2. Other Species and Alternative Reduction Pathways.** Beside semicarbonates, other salt and nonsalt species were also detected as essential interphasial components. Augustsson et al. investigated graphitic anode surfaces cycled

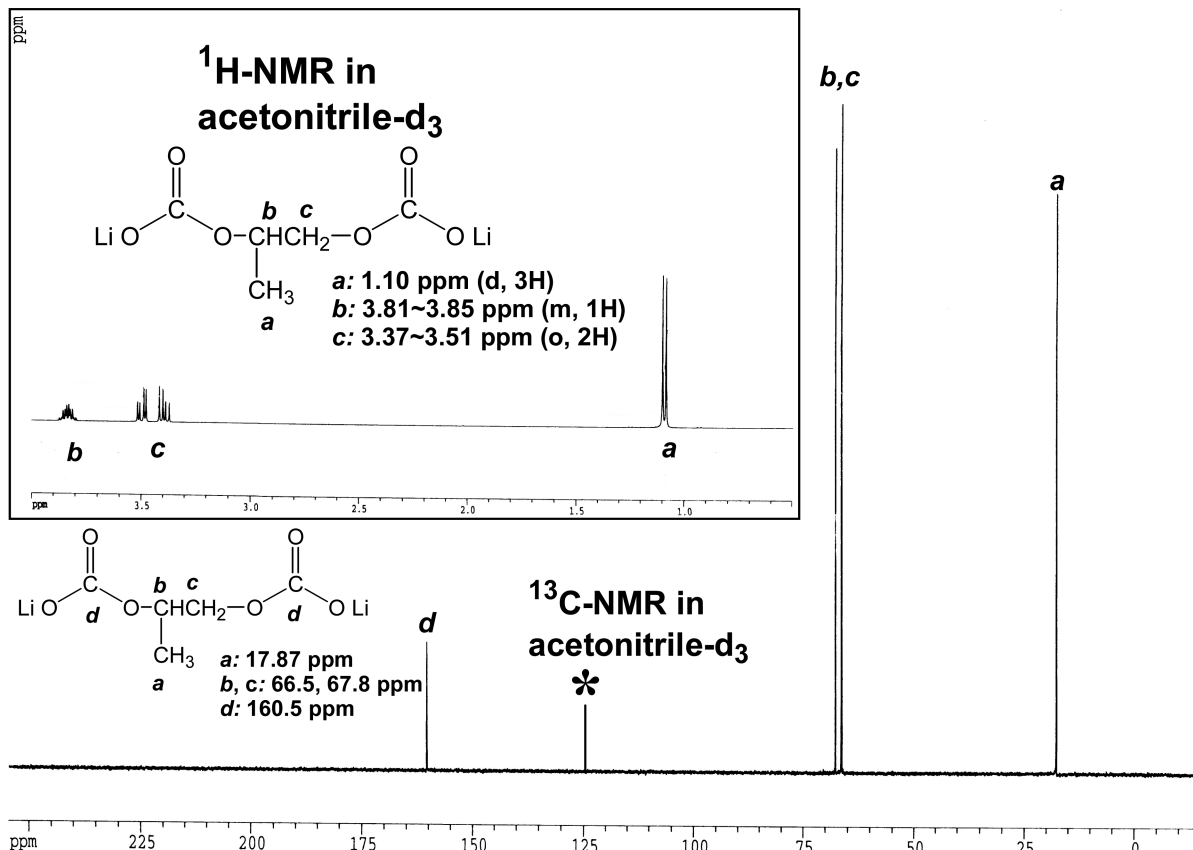
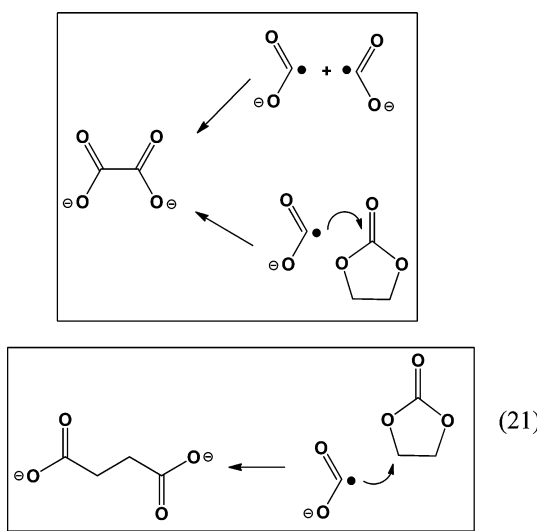


**Figure 41.** Identification of interphasial components: The <sup>1</sup>H and <sup>13</sup>C NMR of the synthesized dilithium 1,2-propylene dicarbonate (LPDC), the proposed reduction product of PC through a single-electron mechanism. The spectra were collected in AN-d<sub>3</sub> with asterisks (\*) marking the solvent signals arising from the proton residuals due to incomplete deuteration. Reprinted with permission from ref 530. Copyright 2006 American Chemical Society.

in EC/PC or EC/DMC electrolytes using selective excitation X-ray emission spectra and found species other than semicarbonates, including oxalate, succinate, and alkoxide.<sup>541</sup> The appearance of these carboxylate species apparently indicated some alternative reduction pathway different from eq 19, because the formation of new C–C bonds must have involved a radical-recombination process following the generation of acyl-radicals. Possible reaction pathways are shown in eq 21, but no detailed mechanism was offered by the authors.



Similar species were found as reduction products of DMC, in addition to the corresponding semicarbonate LMC (eq 20).<sup>533</sup> Zhao et al. also found the existence of oxalate on graphite cycled in typical electrolytes.<sup>542</sup> They believed that these oxalates resulted from further reduction of semicarbonates by the lithiated graphite, which could be accelerated at elevated temperatures.

In addition to direct studies of interphasial components, researchers also turn to the gas products generated during the formation of SEI for possible clues. Among numerous efforts, the online differential electrochemical mass spectra developed by Novák and co-workers proved rather informative, as it could monitor the SEI formation process in real-time.<sup>543–546</sup> While the production of alkenes (eq 19) was detected with high confidence in various electrolytes, La Mantia et al. also reported that they found evidence of a reductive product of CO<sub>2</sub> when the resolution of DEMS was above a level sufficient to detect trace species,<sup>546</sup> which presented a correction to what many studies have stated, that is, CO but not CO<sub>2</sub> was produced at the anode via reductive pathways.<sup>547–550</sup> Onuki et al. once argued that the observation of CO<sub>2</sub> at the anode could be the result of semicarbonate reacting with acidic impurities or moisture,<sup>549</sup> but the existence of oxalate (eq 21) apparently suggested that CO<sub>2</sub> radicals must be formed somewhere, probably as an intermediate, thus explaining the low abundance of CO<sub>2</sub> observed by La Mantia et al.<sup>546</sup>

In a rather elegant approach taken by Onuki et al., they labeled EC and DEC with <sup>13</sup>C-isotope and used gas

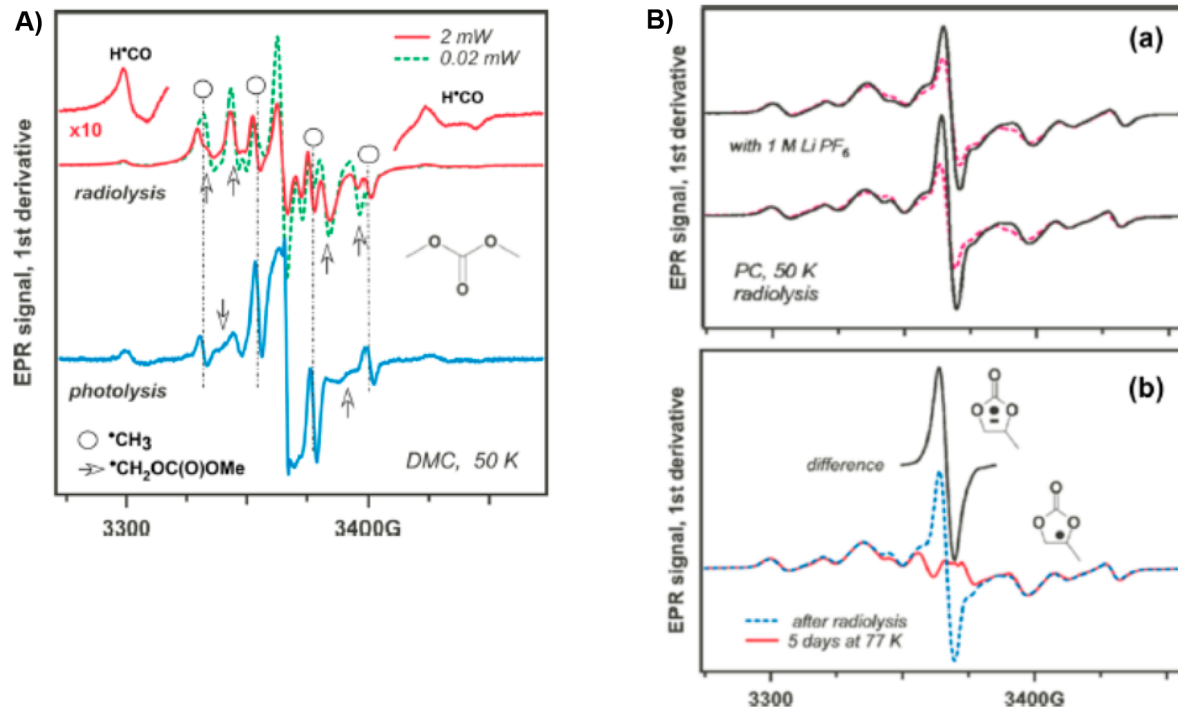
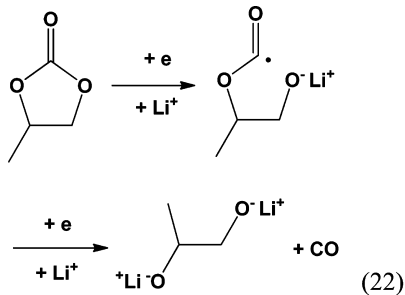


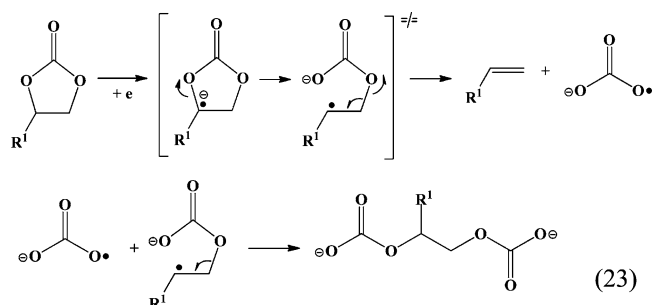
**Figure 42.** Interphasial formation mechanism: (A) first derivative EPR spectra of radical species generated from frozen DMC by 2.5 MeV electrons (top) and 355 nm laser (bottom) at 77 K; and (B) normalized EPR spectra for frozen EC and PC irradiated by 2.5 MeV electrons at 77 K. Reprinted with permission from ref 551. Copyright 2013 American Chemical Society.

chromatography and atomic emission detector (GC-AED) to differentiate the source of gaseous products generated in the initial cycling.<sup>549</sup> In addition to alkane/alkene, they detected CO and traced its origin to EC, thus supporting an alternative EC-reduction pathway in which acyl-oxygen cleavage occurred instead of alkyl-oxygen cleavage as proposed by Aurbach et al. in eq 19:



In fact, Onuki et al. believed that eqs 19 and 22 coexisted in the reaction, as both ethene (from EC) and ethane (from DEC) were detected. These reaction pathways explained the coexistence of alkoxides with semicarbonates and oxalates.

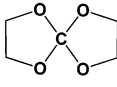
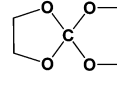
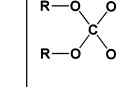
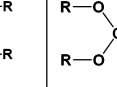
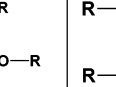
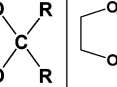
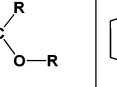
A more recent effort was carried out by Shkrob et al. in an attempt to directly observe the reaction intermediates involved in the formation of SEI and study their fate in the electrolyte media.<sup>551</sup> They employed electron paramagnetic resonance spectra to monitor typical carbonate molecules under irradiation via either radiolysis or photoionization and found that, even under cryogenic conditions (77 K), cyclic radicals were never observed, while ring-opening reactions prevailed (Figure 42). This finding led them to suggest an alternative pathway that might involve carbonate radical anion ( $\text{CO}_3^{2-}\bullet$ , eq 23):



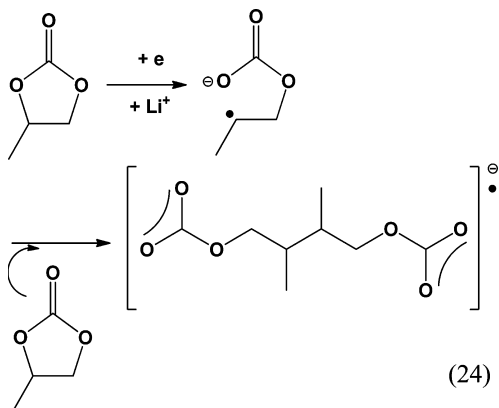
Note that this pathway would generate the same gaseous products with the pathway suggested in eq 19. Because the latter required the recombination of two cyclic radical anions, which should be rather short-lived, especially at ambient temperatures, eq 23 seemed to be more reasonable energetically.

Beside salts, polymeric or oligomeric products from electrolyte reduction were another class of species that have been proposed by many researchers as SEI building blocks.<sup>1,53,538,550,552</sup> Because most frequently used spectroscopic tools (FTIR, XPS, etc.) are not especially sensitive to characterize these macromolecular structures, our understanding about them was limited to possible oligoether compounds resulting from ring-opening polymerization of cyclic carbonates. Indirect inference based on thermogravimetric-mass spectra (TG-MS) of graphite anodes also seemed to suggest polymeric moieties.<sup>480,542</sup> The most explicit identification of polymeric SEI components was achieved by Tavassoli et al., who employed a mass spectrum technique that was tailored to detect macromolecules (matrix-assisted laser deposition ionization, or MALDI), to study SEI formed on Au and Sn electrode surfaces when cycled down to 0.1 V vs Li.<sup>553,554</sup> Long chain oligomers originated with *m/z* ratio as high as 3000 from PC or 1500 from EC/DMC were successfully identified, with repeating units varying with both solvent composition and

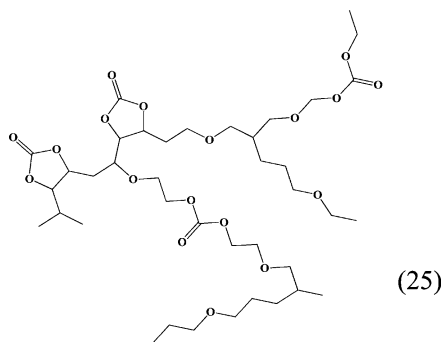
Table 29. Possible SEI Components Based on Solid-State  $^{13}\text{C}$  NMR

						
135 ppm	135 ppm	120 ppm	115 ppm	100 ppm	115~120 ppm	110 ppm

electrode materials. Using DFT calculations, the authors suggested a mechanism that involved radical initiation/propagation, with initiators being generated in the reductive decomposition of the corresponding carbonate solvents (eq 24).



Shkrob et al. strongly proposed that it was polymeric species, not short-chained semicarbonates, that play the key protective role in SEI.<sup>551,555</sup> In their studies on intermediates of carbonate molecule reductions that were generated by either photoionization or radiolysis, they found that these radical species underwent rapid side reactions such as H-abstraction and 1,2-radical migration, which would convert the initially generated 1° radicals into higher order, more stable radicals, such as 2° in case of EC or 3° in case of PC. Thus, anionic polymerization initiated by these higher order radical anions would produce a wide variety of branched 3D networking polymers (eq 25):



Such a 3D network polymer would be additionally cross-linked by the interaction between  $\text{Li}^+$  and ethereal oxygens on the chain. They argued that the unique electrolyte nature of SEI was actually awarded by these densely branched polymers consisting of random ethylene oxide and carbonate units, not by the semicarbonates such as LEDC, which would be too soluble in the solvents.

Finally, a few new species were recently added to the component library of SEI. The solid-state  $^{13}\text{C}$  NMR work performed by Leifer et al. seemed to challenge the above

well-accepted interphasial chemistry based on lithium salts of semicarbonates.<sup>556</sup> Using an approach similar to that of Onuki et al. HYPERLINK “file:///C:/Users/conrad.xu/Desktop/Chem%20Rev%202014%20R2%20Xu.docx” \l “\_ENREF\_544” \o “Onuki, 2008 #1408”<sup>549</sup>, the authors synthesized a series of carbonate solvents labeled by  $^{13}\text{C}$ -isotope, and, via magic angle spinning NMR technique, performed direct analysis on the interphase deposited on graphitic anode by cycling in the corresponding electrolytes. Surprisingly they reported that, while carbonyl groups from the solvent indeed survived the SEI formation and became part of the interphase, the C=O double bond has been disrupted as evidenced by the signals in the range of 100–150 ppm. Leifer et al. assigned them to the  $\text{sp}^3$ -hybridized carbons of orthocarbonate, orthoesters, or acetals (Table 29).<sup>556</sup> While still to be confirmed by other spectroscopic studies, this radical turn of SEI component assignment serves as a good example for the complications encountered in surface analyses, especially within ambient-sensitive systems such as LIB. Schimitz et al., on the other hand, showed that  $\text{Li}_2\text{C}_2$  could be formed on the surface of lithium deposited on a Cu substrate.<sup>557</sup> The existence of this highly sensitive compound was confirmed both by in situ Raman spectroscopy and by mass spectra of the gaseous products when the interphase was hydrolyzed. Note that  $\text{Li}_2\text{C}_2$  was only found on deposited lithium surface, and the authors believed that its formation was only possible under 0 V vs Li; however, its presence in graphitic anode interphases cannot be ruled out in the case of overcharging, where Li deposition occurs locally. Once formed, its fate with other interphasial species, electrolyte solvent molecules, as well as the graphitic anode itself at potentials >0 V vs Li would be of high interest.

**5.1.1.3. A Few Controversial Issues.** The complication of SEI was self-evidenced by the controversies still existing on many fundamental issues, despite intensive efforts in the past decades. Transliterating an ancient Greek proverb, the more we learn about SEI, the more we know how little we understand it. This paradox will remain as we advance our work to understand interphases formed on electrodes of “beyond Li-ion” chemistries, where interphasial chemistry would be more intertwined with the redox reactions occurring in both anode and cathode materials.

**5.1.1.3.1. Over  $\text{Li}_2\text{CO}_3$ .** Perhaps the most debated item in SEI is  $\text{Li}_2\text{CO}_3$ . Beyond any doubt,  $\text{Li}_2\text{CO}_3$  was often detected in SEI on graphitic anodes, and once it was believed to originate from a two-electron reduction pathway of carbonate molecules.<sup>1</sup> It was Aubach and co-workers who established that the actual components of SEI are semicarbonates from a single-electron pathway as shown in eq 19, and that  $\text{Li}_2\text{CO}_3$  was the artifact, probably hydrolysis aftermath of semicarbonate due to poor moisture management. However, that did not terminate the debate: in the following decade, numerous researchers still described  $\text{Li}_2\text{CO}_3$  as an SEI component, while others strongly disagree.<sup>141,522,558–561</sup> Compromising these two opposite opinions are a few studies stating that the presence

of  $\text{Li}_2\text{CO}_3$  might be conditional on both electrolyte composition and cell cycling history. For example, Dedryvère et al. reported that  $\text{Li}_2\text{CO}_3$  was the only major interphasial species identified on graphite after being cycled in LiTFSI-based electrolyte, while a mixture of both semicarbonate and  $\text{Li}_2\text{CO}_3$  would be found with LiBeti electrolyte;<sup>539</sup> alternatively, Zhao et al. suggested that  $\text{Li}_2\text{CO}_3$  was only observed on aged graphite electrodes; no  $\text{Li}_2\text{CO}_3$  can be detected on freshly cycled graphite.<sup>542</sup> More recent surface analyses carried out by Nie et al. seemed to support this observation.<sup>536,537</sup>

Theoretical calculation was employed to clarify the above discrepancy. The DFT calculations conducted by Vollmer et al. seemed to hint that the two electron reductive pathway for EC and PC was hindered by a barrier of 0.5 eV;<sup>166</sup> thus semicarbonate could be the favored species. However, this barrier might not be high enough to make semicarbonates the exclusive interphasial component; thus a reasonable consequence of this would be mixtures of semicarbonates and  $\text{Li}_2\text{CO}_3$ . On the other hand, Leung computationally “revisited” the possibility of two-electron reduction mechanism and concluded that this pathway does not necessarily produce  $\text{Li}_2\text{CO}_3$ ; rather, in the multiple step process following the initial release of CO, the fate of the glycoxide could lead to  $\text{CO}_3^{2-}$ , CO, alkene, alkene dicarbonate (such as LEDC), and even polymeric species.<sup>562</sup>

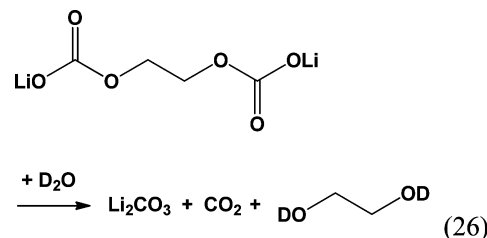
Edström et al. explained this issue from an experimental approach. They noticed that graphite anodes cycled in hermetically sealed vessels and transported in a vacuum sample-suitcase never produce any detectable  $\text{Li}_2\text{CO}_3$  under XPS;  $\text{Li}_2\text{CO}_3$  only formed under exposure to ambient atmosphere. Thus, they suggested that in most previous studies the detected  $\text{Li}_2\text{CO}_3$  was just an artifact created by sloppy control of experiment environment.<sup>559–561</sup> Harilal et al. supported the arguments of Edström et al. and further concluded that  $\text{Li}_2\text{CO}_3$  actually arose from the reaction of  $\text{Li}_2\text{O}$  with  $\text{CO}_2$ .<sup>563</sup>

**5.1.1.3.2. Over LiF.** LiF was another SEI ingredient that raised debates. According to an early model proposed by Peled and Ein-Eli et al., SEI consists of multiple layers, with innermost components being more “inorganic” ( $\text{Li}_2\text{O}$  and LiF) and the outermost being more “organic” (semicarbonates or polymers/oligomers).<sup>1</sup> This “mosaic-like” feature was built on the facts that LiF has been a constantly detected species. Given the labile and moisture-sensitive P–F bonds in  $\text{PF}_6^-$ -anion, it was once believed that  $\text{F}^-$  was produced as an impurity from hydrolysis rather than from electrochemical reduction, and that the presence of LiF in SEI harms cell performance. However, recent studies by Nie et al. revealed new insights.<sup>536,537</sup> Using combined TEM and multinuclei NMR, they showed that SEI composition was actually rather simple, consisting of semicarbonates and LiF, and the ratio of these two components seemed to remain almost constant regardless of the sites of the graphite electrode as well as the cycling evolution. These observations strongly suggested that (1) the accepted layered-structure of SEI may not exist, at least not under those conditions employed; and (2) there was a stable source for LiF formation, more likely from  $\text{PF}_6^-$ -anion via electrochemical reduction than impurity. More importantly, they exhibited that the presence of LiF in SEI component was helpful in protection of Si electrode surfaces.<sup>537</sup> This seeming contradiction to previous findings about interphases on both graphite<sup>128–130</sup> and Si<sup>221,223,537</sup> surfaces leads one to suspect that chemical composition alone might not be sufficient to dictate SEI properties; equally or even more important are their origins,

distribution on electrode surfaces, and local arrangement across the interphase with other species.

**5.1.1.3.3. Over Stability of Semicarbonate LEDC.** Semicarbonate LEDC was perhaps the most important SEI component, not only because it was almost always detected on all electrode surfaces (graphite, Si, Cu, Ni, Pt, etc.) that were cathodically polarized in carbonate-based electrolytes, but also because it was considered the ingredient responsible for effectively supporting the highly reversible Li-ion chemistry. This latter speculation was firmly based on the fact that EC has been the indispensable cosolvent for almost any LIB.

To better understand how chemical properties of LEDC influence the electrochemical behavior, Dedryvère et al.<sup>531</sup> and Xu et al.<sup>46,530</sup> separately synthesized its pure form in vitro, which enabled a series of characterizations that were otherwise impossible in cells. Both groups recognized the extreme moisture sensitivity of LEDC, as evidenced by the visible gas generation (eq 26) when dissolved in  $\text{D}_2\text{O}$ , as well as weight loss in ambient air as measured by a TGA balance.



Thus, Xu et al. believed that the NMR spectra collected in its  $\text{D}_2\text{O}$  solution merely reflected the aftermath of its “deuteroysis”, which coincidentally resembled the spectra of the mother compound.<sup>530</sup> However, Nie et al. recently reported that as long as  $\text{D}_2\text{O}$  extraction was conducted in inert atmosphere (Ar), LEDC could resist “deuteroysis” for appreciable long duration, as evidenced by its characteristic  $^{13}\text{C}$ -carbonyl signal at ~163 ppm; however, the ambient atmosphere accelerated the decomposition and resulted in a rather complicated spectra.<sup>536</sup> The mechanism behind this catalytic effect of “ambient-atmosphere” still remains unclear.

**5.1.1.3.4. Over Preferential Reduction of Carbonates.** Because the majority of electrolytes in LIB are based on mixtures of carbonates, typically one cyclic carbonate (EC) with one or more acyclic carbonates (DMC, EMC, or DEC), a question of vital importance to interphase composition would arise: Is any of these solvents preferentially reduced during the formation stage of SEI? Or does the electrode surface provide equal opportunity of reduction to all solvent molecules?

Zhuang et al. seemed to present the earliest proof that EC was selectively reduced.<sup>46</sup> When comparing the FTIR spectra collected from a Ni surface that was cathodically polarized to 0.50 V in an DMC-dominant electrolyte ( $\text{LiPF}_6$  in EC/DMC 30:70) with the reference compound LEDC synthesized, the authors were surprised to see the “finger-print” matching of the two spectra (Figure 43A), where no LMC, the reduction product from DMC, was found. Xu et al. further investigated this issue by carrying out  $^{13}\text{C}$  NMR on a series of electrolytes with varying ratios between EC and DMC or EMC, and concluded that the interphases formed on graphite anodes were indeed dominated by EC reduction products even when the acyclic carbonate populations were overwhelming (Figure 43B).<sup>48</sup> They attributed this preferential reduction of EC molecules to

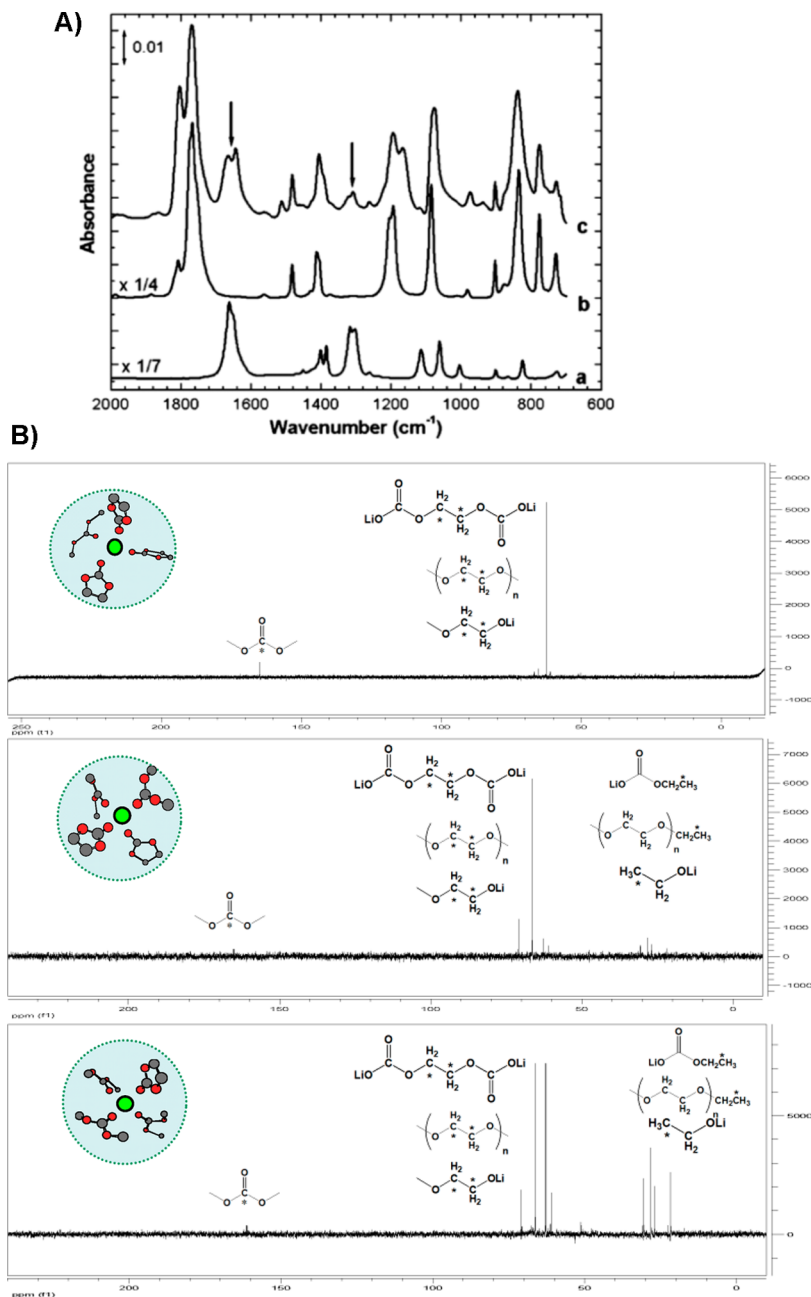


**Figure 43.** (A) Effect of Li<sup>+</sup>-solvation on interphasial components: FTIR spectra of (a) synthesized LEDC as a reference; (b) EC-solvate with LiPF<sub>6</sub>; and (c) the surface of Ni cycled between 0.5–2.5 V vs Li in LiPF<sub>6</sub>/EC/DMC (30:70). Reprinted with permission from ref 46. Copyright 2005 American Chemical Society. (B) Effect of Li<sup>+</sup>-solvation on interphasial components: <sup>13</sup>C NMR of surface species collected from graphitic anodes cycled in LiPF<sub>6</sub>/EC/EMC 30:70 (top), (b) 20:80 (middle), and (c) 10:90 (bottom). Inset drawings: the Li<sup>+</sup> solvation sheath composition and the structure of the original SEI species. The asterisks mark the probable <sup>13</sup>C nuclei that generate the signals. Reprinted with permission from ref 48. Copyright 2007 American Chemical Society.

the consequence of Li<sup>+</sup>-solvation preference in electrolytes and the 3D SEI-formation mechanism driven by initial cointercalation (to be discussed in section 5.1.3). More recent work by Nie et al. seemed to support this conclusion of EC-preference, when the authors reported a LEDC-dominated SEI formed in a EC/DMC 30:70 solution, with only low levels of LMC or LEC.<sup>536</sup> Vatanamu et al. agreed that EC might be preferentially reduced on graphite, but they argued that this preference was not the consequence of preferential solvation of Li<sup>+</sup> by EC in bulk electrolyte as suggested by Xu et al.; instead, it was attributed to the increased fraction of EC

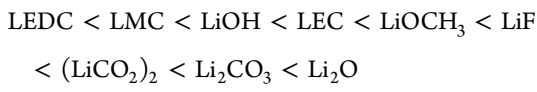
and depletion of DMC from the first Li<sup>+</sup> solvation shell for interfacial Li<sup>+</sup> and the interfacial layer near the graphite vicinity under the effect of electric field.<sup>564</sup> This uneven distribution of solvent molecules was also found at electrolyte/SEI junction. Borodin believed that, when LiPF<sub>6</sub>/EC/DMC electrolyte was in contact with LEDC crystal, an enrichment of EC and PF<sub>6</sub><sup>-</sup> and depletion of DMC occurred at the LEDC surface as compared to bulk electrolyte. As Li<sup>+</sup> desolvated from electrolytes, it tended to first shed DMC as compared to EC. The activation energies for the Li<sup>+</sup> solvation–desolvation reactions were estimated to be on the

order of 0.5 eV for the SEI–electrolyte, which is somewhat lower than the activation energy of 0.64 eV for the Li<sup>+</sup> diffusion in bulk LEDC.<sup>565</sup>

Leifer et al. challenged this conclusion with their NMR studies. They labeled the carbonyl groups in EC and DMC with enriched isotope <sup>13</sup>C, and found from the <sup>13</sup>C NMR spectra collected from the cycled graphite anodes that there was no clear preference with respect to the source of these surface species.<sup>556</sup> While this important issue still needs further investigation, it should be mentioned that the only obvious factor that could have caused the difference between the work of Zhuang et al., Xu et al., and Nie et al. and the work of Leifer et al. is that the SEI on graphite anodes were freshly formed in the former,<sup>46,48,536</sup> but were significantly aged at elevated temperatures in the latter.<sup>556</sup> In other words, the SEI composition might very likely be dynamic, changing with time and temperature.

**5.1.2. Properties of Interphasial Components.** As compared to chemical composition, the more important but less explored topics are the physicochemical properties of the formed interphases. Until today we still know little about how these interphases interact with the electrolytes in a live cell, and how Li<sup>+</sup> moves through them. Most of the time, one can only rely on computational means to speculate on these critical parameters.

Tasaki et al. evaluated the solubilities of a series of lithium salts in both EC and DMC using atomistic simulations.<sup>566</sup> These salts included oxides, alkoxides, carbonates, semicarbonates, fluorides, and oxalates, and represented almost all possible ingredients of an interphase formed on graphite anodes. They found that the heat of dissolution ranged from exothermic for organic salts to endothermic for inorganic salts, in the following order:



This order remains roughly the same in both solvents, but solubilities in EC were generally higher, as expected from the higher polarity of EC. The only exception was LEDC, which dissolves less in EC than in DMC. The authors attributed this deviation to the conformational constraint of LEDC, which allows limited accessibility of oxygens in solvent molecules.

Although it is well-accepted that SEI allows Li<sup>+</sup>-migration under electric field, how Li<sup>+</sup> moves through this heterogenous phase remains little known. Lu and Harris made the very first attempt to understand this process by employing lithium salts containing isotopic <sup>6</sup>Li and <sup>7</sup>Li to form SEI and bulk electrolyte separately, and then monitored the exchange of these two isotopes upon immersion.<sup>567</sup> It was observed that after short exposure (~minutes), <sup>6</sup>Li<sup>+</sup> already immobilized in the interphase can be completely replaced by <sup>7</sup>Li<sup>+</sup> in the bulk electrolyte, suggesting that SEI functions like an “cation-exchanger”, and that Li<sup>+</sup> might move across the interphase via a “Grothuss-like” conducting mechanism as illustrated in Figure 44A. In continuous efforts aided by computational simulation, Shi et al. further revealed possible mechanisms of how a mobile Li<sup>+</sup> is coordinated within the interphase.<sup>568,569</sup> Using crystalline Li<sub>2</sub>CO<sub>3</sub> as a template matrix, they suggested that the transport energy barrier could be significantly reduced if a moving Li<sup>+</sup> sees a series of transition states with penta- or tetra-coordinated O-ligands. This would only happen when this Li<sup>+</sup> replaces

another Li<sup>+</sup> in its original position; otherwise, a longitudinal direct diffusion would encounter much higher energetic barriers (Figure 44B). In an alternative approach, Borodin et al. estimated the Li<sup>+</sup> conductivity within LEDC utilizing MD simulations as a function of temperature, employing the original<sup>570</sup> and revised<sup>534</sup> many-body polarizable force fields for the ordered and disordered structures. They reported that Li<sup>+</sup> was coordinated by approximately four oxygens from different semicarbonates. Because the ion transport within SEI is almost entirely due to Li<sup>+</sup> at temperatures below 393 K, the room temperature conductivity was estimated from MD simulations to be between 10<sup>-10</sup> and 10<sup>-8</sup> S/cm, in good agreement with the experimentally measured value of 10<sup>-9</sup> S/cm. On the basis of its temperature-dependence, activation energy for conductivity was predicted to be 64 kJ/mol for the ordered LEDC. In an alternative approach, Borodin et al. attempted to evaluate the Li<sup>+</sup> conductivity within LEDC using both quantum chemistry-based force field and combination of impedance spectra and molecular dynamics. They reported that while Li<sup>+</sup> is coordinated by averagely 4.6 oxygens from different semicarbonates, the ion transport within SEI is almost entirely due to Li<sup>+</sup>. The conductivities were estimated to be 10<sup>-10</sup> S/cm at -30 °C and 10<sup>-9</sup> S/cm at room temperature.

Using combined analytical tools that included EIS, TOFSIMS, and XPS, Lu et al. further revealed the inhomogeneity of SEI by establishing depth-profiles of the distributions of both F and B.<sup>571</sup> Their findings not only reaffirmed the layered-structure of SEI, but also, more importantly, pointed out that the overemphasis on SEI thickness might be misleading, as the uneven arrangement of interphasial species across the SEI, both chemically and morphologically, renders the interphasial impedance often unproportional to its thickness. The chemical composition as well as morphology might be key factors defining the properties of an SEI.

Because a dense interphase not only insulates toward electron-tunneling, but also prevents solvent molecules from diffusing across it, the desolvation process of Li<sup>+</sup> must occur at the interphase, which could constitute an activation energy barrier for Li<sup>+</sup> to intercalate into an electrode host. Ogumi et al. were the first to realize that Li<sup>+</sup>-desolvation creates additional resistance when a graphitic anode is being charged, thus explaining the unsymmetrical property of Li-ion cells of fast discharging but slow charging.<sup>572–576</sup> They estimated that the energy barrier to a Li<sup>+</sup> migrating into graphite through a formed SEI ranged between 50–100 kJ/mol depending on the solvating molecules, and this resistance was usually represented by the impedance component often ambiguously assigned to “charge-transfer”. By considering systems where no desolvation occurred, such as the intercalation of solvated Li<sup>+</sup> in DME or DMSO solvents, the neat charge-transfer contribution should only be ~25 kJ/mol (Figure 45).

Because desolvation only occurs in the presence of a formed SEI, the 50–100 kJ/mol energy barrier reported by Abe et al. actually reflected the compounded contributions of two separate components: (1) Li<sup>+</sup>-desolvation and (2) migration of desolvated Li<sup>+</sup> across the interphase. Xu et al. went further to differentiate the contribution from these two factors by using a nearly SEI-free electrode, lithiated titanate Li<sub>x</sub>Ti<sub>5</sub>O<sub>12</sub>, where the energy barrier was found to be ~50 kJ/mol.<sup>577</sup> Thus, for a Li<sup>+</sup> attempting to travel from the bulk electrolyte to the interior of a graphite anode, the main contributor to the energy barrier of the entire Li<sup>+</sup>-transfer process should come from the disruption

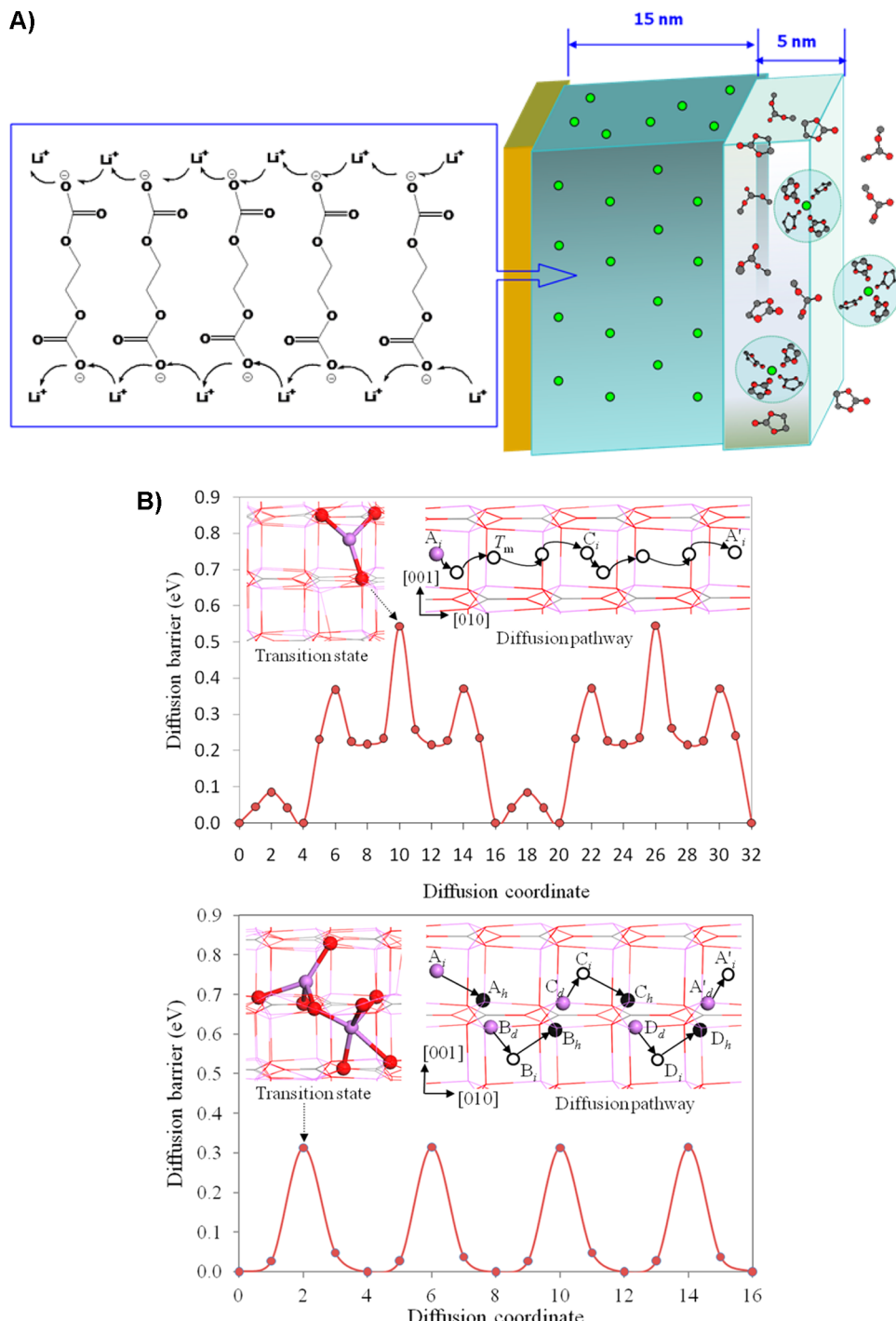


**Figure 44.** (A) Transport through interphase: “Grothuss-like” transportation mechanism of  $\text{Li}^+$  across an interphase. It was proposed that the dense layer of interphase is impenetrable toward solvent molecules, so that solvated  $\text{Li}^+$  has to desolvate and exchange with the  $\text{Li}^+$  already in the interphase. Reprinted with permission from ref 52. Copyright 2012 Materials Research Society. (B)  $\text{Li}^+$ -transport through interphase: Computation simulations depict the corresponding energy barriers of (b) direct longitudinal  $\text{Li}^+$  diffusion through an interphase and (b) “Grothuss-like” mechanism, where  $\text{Li}^+$  is better stabilized. The tetra- or penta-coordinated transition states available only in the latter case effectively reduce the barrier height. Reprinted with permission from ref 568. Copyright 2012 American Chemical Society.

of the  $\text{Li}^+$ -solvation sheath as illustrated in Figure 45. This conclusion applies to graphitic anodes under ideal operating conditions in LIB, and it might change if a more resistive factor is created due to deviations from the ideal conditions, such as additional impedance arising from cycling at elevated temperatures or sustained electrolyte decomposition at high voltages.

**5.1.3. Formation Mechanism.** In the past decade, the 3D formation model of SEI proposed by Besenhard and Winter et al. has been gaining increasing acceptance in the LIB research community.<sup>1,18</sup> The three important signatures of this formation process, that is, solvent cointercalation preceding the formation of SEI, the concomitant expansion of graphite structure, and the preferential reduction of certain solvent

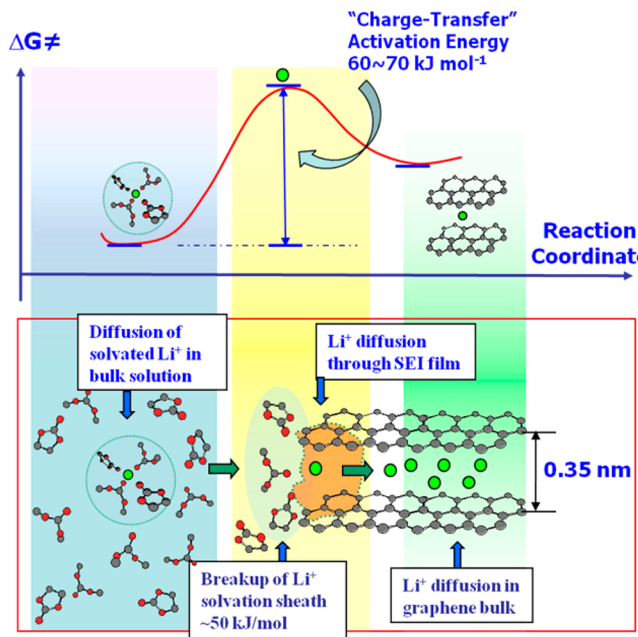


**Figure 45.** Li<sup>+</sup>-transport through interphase: (top) schematic illustration of solvated Li<sup>+</sup> and bare Li<sup>+</sup> intercalation at graphite edges and the corresponding activation energy barriers; (bottom) differentiation of the contributions from Li<sup>+</sup>-desolvation and Li<sup>+</sup>-migration across the interphase. Reprinted with permission from ref 577. Copyright 2010 American Chemical Society.

molecules, have been observed with various in situ and ex situ tools.

It was the dilatometry studies of PC-based electrolytes that led Besenhard and Winter to propose the “3D mechanism”.

Hahn et al. revisited this macroscopic, but nevertheless in situ technique, and applied it to the typical (hence nonexfoliating) electrolytes based on EC/DMC.<sup>578</sup> The linear expansion of most graphitic composite electrodes was observed during the first lithiation cycle above 0.7 V, clearly reflecting the initial cointercalation of solvated Li<sup>+</sup> into graphitic structures and the formation of ternary graphitic intercalation compounds (GIC). The onset of gas generation during this process, according to online electrochemical mass spectrum, also occurred in a similar range (~1.0 V), although this reaction lasted until the potential range where the bare Li<sup>+</sup>-intercalation occurred (<0.3 V).<sup>546,579,580</sup> This may indicate that the solvated Li<sup>+</sup> is actually unstable within the graphite interior because the solvating molecules become more reactive with EC as the potential of graphite drops. Lithiation processes carried out with less graphitized carbon also exhibited the distinct stage of cointercalation by solvated Li<sup>+</sup> at edge planes of the crystalline regions.<sup>581</sup>

Interestingly, Spahr et al. found that, when graphite was heat-treated in inert atmosphere at 1300 °C to reduce its reactivity toward EC, exfoliation could occur even in neat EC-based electrolyte at 0.45 V.<sup>543</sup> Because the heat treatment removes surface functionalities that frequently populate the graphite edge sites, such as hydroxyls, carbonyls, carboxylates, and quionones, this interesting fact hints that (1) the formation of a protective SEI cannot occur when the electrolyte/electrode interface is “too stable”, an analogue to what Dahn et al.<sup>1</sup> and Krämer et al.<sup>515</sup> found regarding the paradox between “chemical instability” and “electrochemical stability”; and (2) the SEI formation probably is mediated by those surface functionalities. In other words, exfoliation of graphene structure, which is the consequence of cointercalation, occurs only because the solvent molecules are “too stable”

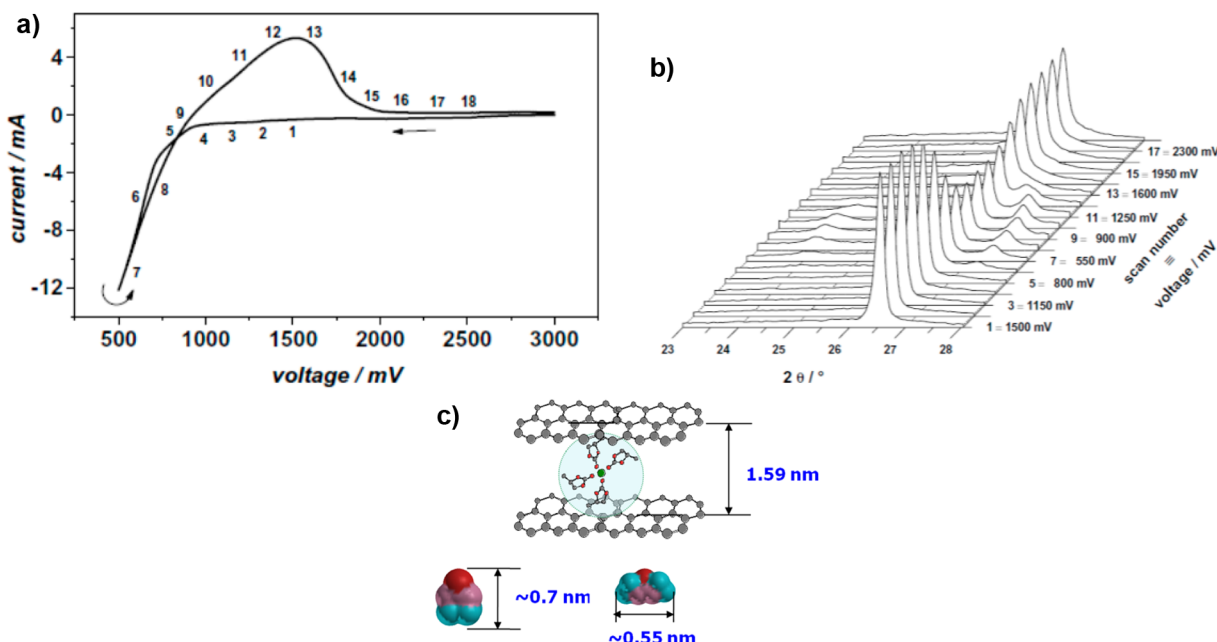


**Figure 46.** Interphase 3D-formation mechanism: (a) intercalation of solvated Li<sup>+</sup> (Li<sup>+</sup>-PC<sub>x</sub>) into the graphitic structure; (b) corresponding in situ XRD collected during the cointercalation process. Reprinted with permission from ref 582. Copyright 2005 Elsevier. (c) Proposed intermediate ternary cointercalation compounds with expanded graphitic interlayer distance. Reprinted with permission from ref 52. Copyright 2012 Materials Research Society.

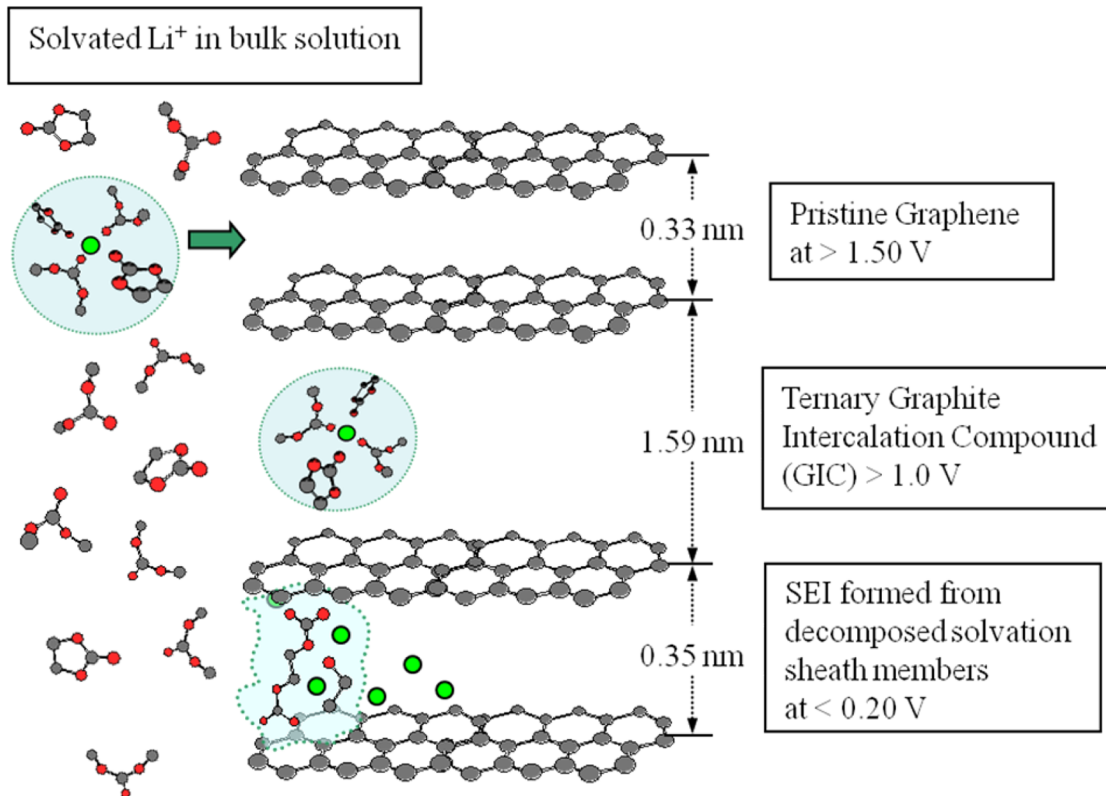


**Figure 47.** Interphase 3D-formation mechanism and the role of  $\text{Li}^+$ -solvation sheath: proposed mechanism that creates the dependence of interphasial chemistry on the solvation sheath structure of  $\text{Li}^+$ . Reprinted with permission from ref 48. Copyright 2007 American Chemical Society.

against electrochemical reactions to develop a passivation chemistry.

The most convincing and direct evidence for “3D mechanism” came from *in situ* XRD performed on a graphite anode in PC-based electrolyte at a fast scan rate down to 0.50 V vs Li (Figure 46a).<sup>582</sup> The new series of diffraction peaks appearing at  $2\theta = 24^\circ$  and  $27.5^\circ$  (Figure 46b) obviously revealed a much larger interlayer distance ( $\sim 1.59 \text{ nm}$ ), which corresponded to the reversible formation of ternary GIC containing solvated  $\text{Li}^+$  with 3–4 solvent molecules in the primary solvation sheath (Figure 46c). Although similar ternary GIC has not been reported for EC-based electrolytes, one can reasonably infer that a similar mechanism must have been followed, while the high reactivity of EC did not allow for the real-time detection.

As Figure 46b showed, a key element hinted at by this “3D mechanism” is the role of the  $\text{Li}^+$ -solvation sheath. Because cointercalation of solvated  $\text{Li}^+$  must precede the formation of SEI, the solvent molecules inside the solvation sheath would become the precursors of SEI when the reduction eventually happens. In other words, the structure and composition of  $\text{Li}^+$ -solvation sheath (a bulk solution property) dictate the SEI chemistry on graphite (an interphasial property). On the basis of this inference, Xu et al. refined the Besenhard–Winter model by adding a solvation sheath element (Figure 47).<sup>23,47,48,577</sup> To establish the chemical connection between  $\text{Li}^+$ -solvation sheath structure and interphasial composition, Xu and co-workers mapped the accurate composition  $\text{Li}^+$ -solvation in various carbonate media with electrospray-ionization mass spectrometry (ESI–MS) on one hand (section 2.3 and

Figure 5B), and determined SEI chemistry on cycled graphite anode with various spectroscopic tool on the other (section 5.1.1.3.4 and Figure 43). The former studies identified EC as the predominant member in the  $\text{Li}^+$ -solvation sheath,<sup>23,51,52</sup> while the latter studies revealed that SEI on graphite indeed bears a heavy chemical signature from EC.<sup>46,48,533</sup> In some cases, LEDC, the exclusive reduction product from EC via the single-electron pathway, overwhelmed SEI composition despite the bulk electrolyte being based on mixtures of carbonate molecules.<sup>46,48,536,537</sup> This apparent link between the chemical compositions of  $\text{Li}^+$ -solvation sheath and interphase serves as strong supporting evidence for the solvation sheath-based 3D model as shown in Figure 47.

More confirmation for this link between  $\text{Li}^+$ -solvation sheath structure and SEI chemistry came from studies on PC-based electrolytes, which were known to cointercalate into graphitic structures and eventually exfoliate the structure without  $\text{Li}^+$ -intercalation. Thus, PC could be used as a convenient SEI-marker as one can effectively manipulate the presence of PC in  $\text{Li}^+$ -solvation sheath while observing the corresponding changes in the interphasial behavior. Jeong et al. observed that when the concentration of LiTFSI in PC was above a certain level ( $> 3 \text{ m}$ ), graphite became stabilized in PC solutions.<sup>433</sup> Later, they expanded this observation to other lithium salts including  $\text{LiClO}_4$  and  $\text{LiPF}_6$ ,<sup>583</sup> realizing that what really matters here is how many PC molecules were averagely recruited by each  $\text{Li}^+$  into its solvation sheath.<sup>583,584</sup> Even at moderate concentration ( $1.0 \text{ m}$ ) that is commonly used in state-of-the-art electrolytes, exfoliation would still not occur as long as the formation stage was carried out at low temperatures ( $15^\circ\text{C}$ ), which Jeong et al.

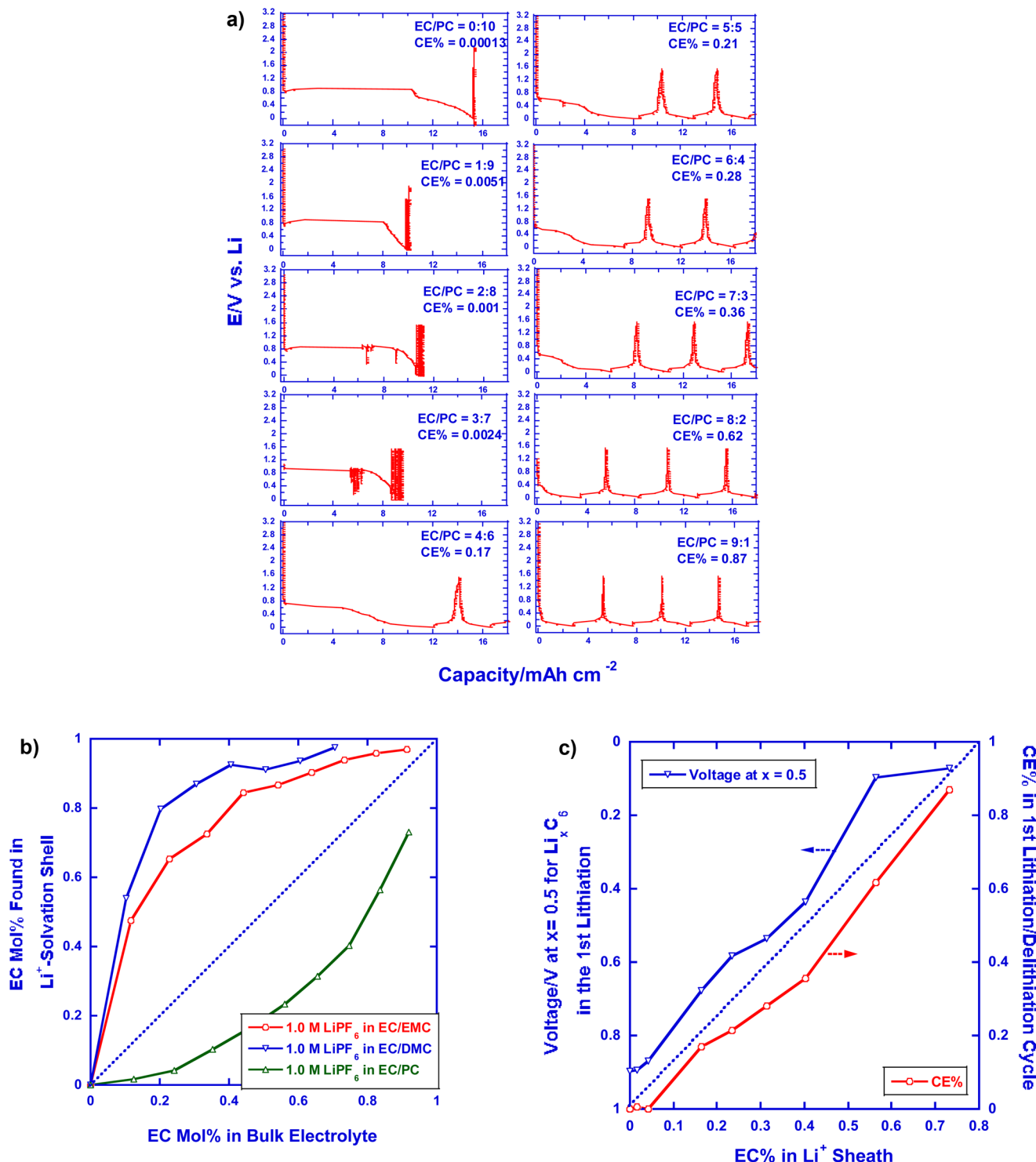


**Figure 48.** Direct correlation between Li<sup>+</sup>-solvation structure and interphasial chemistry: (a) Effect of successive replacement of PC with EC on interphasial chemistry. Note the nonlinear transition from exfoliation at EC% = 0 to stable intercalation at EC% = 80–90. (b) Structure of Li<sup>+</sup>-solvation structure in EC/PC mixture. Note the preferential solvation of Li<sup>+</sup> by PC over EC. (c) Quantitative correlation of Li<sup>+</sup>-solvation structure with interphasial chemistry. The latter was quantified by (1) Coulombic efficiencies in the first lithiation/delithiation cycle and (2) voltage depression at  $x = 0.5$  in the first lithiation process. Note the nearly linear relations of these two quantities when plotted versus EC% as found in the solvation sheath. Reprinted with permission from ref 586. Copyright 2012 American Chemical Society.

attributed to weakened Li<sup>+</sup>–PC interaction.<sup>585</sup> Cresce et al. went further to exploit the use of PC as a quantitative SEI marker.<sup>586</sup> By varying EC/PC ratio, they obtained a series of transition electrochemical behaviors between the two extremes of poor (in neat PC) and ideal SEI (in neat EC), which is the

consequence of two competing interphasial chemistries originated by PC and EC reductions. Upon closer examination, one can easily tell that the above transition was not “linear”; instead, a sudden jump occurred between EC/PC ratios of 70:30 and 80:20 (Figure 48a). On the other hand, through

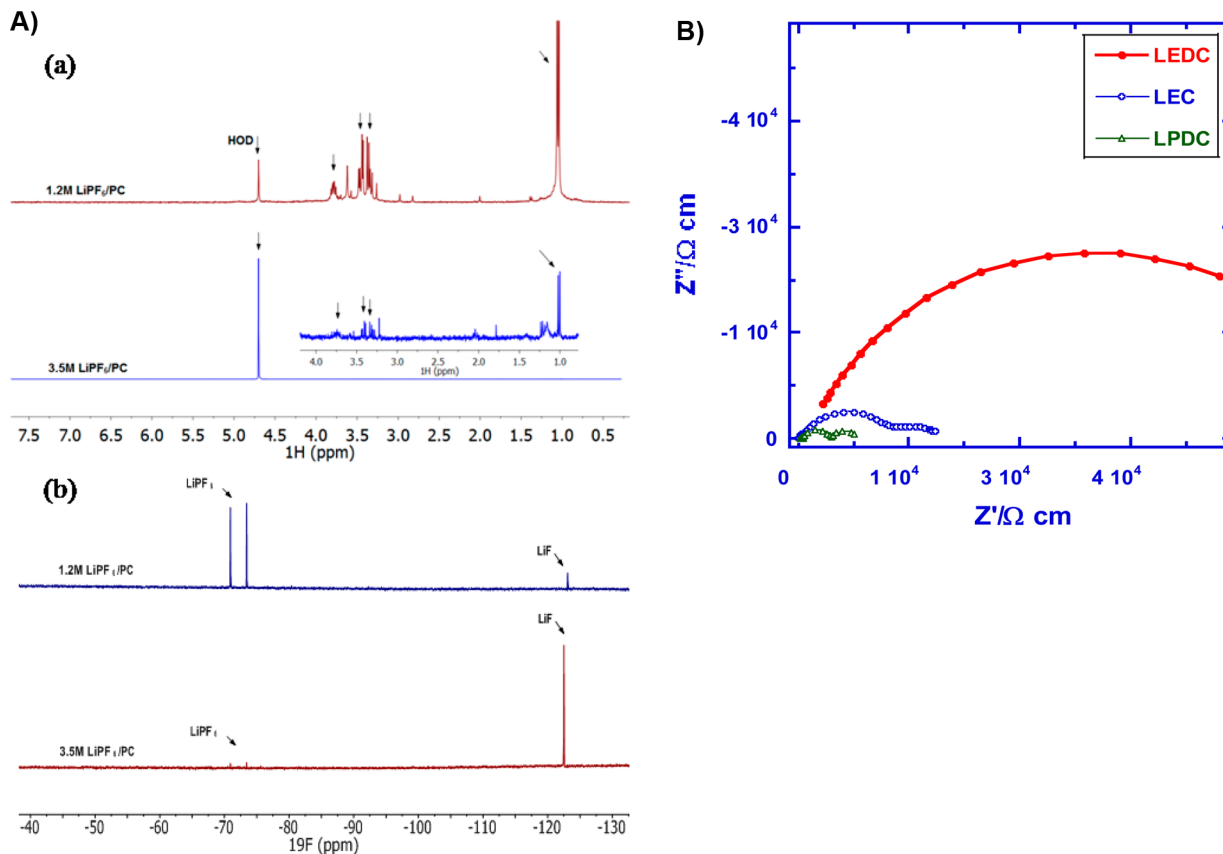
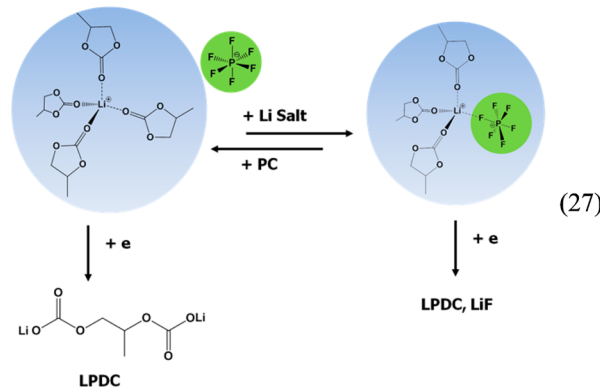


**Figure 49.** Effect of lithium salt concentration on Li<sup>+</sup>-solvation sheath in PC and the consequence on interphase: (A) NMR analyses of (a) <sup>1</sup>H- and (b) <sup>19</sup>F-nuclei on graphitic anodes cycled in 1.2 or 3.5 M LiPF<sub>6</sub>/PC electrolytes. Reprinted with permission from ref 589. Copyright 2013 American Chemical Society. (B) The conductivity (solubility) of synthesized semiconductors LEDC, LPDC, and LEC in nonaqueous solvents. Reprinted with permission from ref 474. Copyright 2009 Electrochemical Society.

application of the ESI-MS, they obtained a statistical distribution of PC molecules within the Li<sup>+</sup>-solvation sheath and its dependence on the bulk electrolyte composition (Figure 48b). Apparently, PC was favored by Li<sup>+</sup> as shown by the negative deviation (which was in sharp contrast to EC-preference in EC-acyclic carbonate mixtures, and the underneath mechanism still remains to be understood with controversy<sup>586–588</sup>), while the “threshold” ratio of EC/PC at 80:20 corresponds to 50% PC in Li<sup>+</sup>-solvation sheath. This observation consolidates quantitatively what Jeong et al.<sup>433,583,585</sup> and Yamada et al.<sup>584</sup> claimed. By plotting the Coulombic efficiencies in the first cycle against the probability of finding PC within the Li<sup>+</sup>-solvation sheath, an excellent linear interdependence with a slope of unity was obtained (Figure 48c), serving as quantitative support for the solvation sheath-based 3D model as shown in Figure 47.

Adding one additional piece to this puzzle were the studies carried out by Nie et al. on the relation between PC-interphasial behavior and lithium salt concentration.<sup>589</sup> Similar to what Jeong et al. observed with LiTFSI/PC solutions,<sup>433,583</sup> they noticed that when LiPF<sub>6</sub> concentration reached a certain level (3.0–3.5 M in this case), the extensive decomposition of PC and exfoliation of graphite would be replaced by reversible Li<sup>+</sup>-intercalation chemistry. Using IR, diffusion ordered NMR, and energy-dispersive X-ray spectroscopy, they convincingly established that the Li<sup>+</sup>-solvation sheath experienced a transition from solvent separated ions to contact ion pairs in the above concentration range (eq 27):



A similar process was observed by Yamada et al. in concentrated LiTFSI/acetonitrile system.<sup>456</sup> In both cases, the depletion of available solvent molecules in the bulk electrolyte makes PF<sub>6</sub><sup>-</sup> or TFSI<sup>-</sup> an inner member of the Li<sup>+</sup>-solvation sheath, which would bring the anion into close contact with graphite upon charging and eventually resulted in an interphase that consists of reduction products not only from solvent (PC or acetonitrile) but also from anion, as shown in Figure 49A. In fact, Nie et al. believed that the enriched LiF population in the interphase, which increased with lithium salt concentration, was responsible for the reversible Li<sup>+</sup>-intercalation that is otherwise impossible in diluted (~1.0 M) LiPF<sub>6</sub>/PC electrolytes. This conclusion further confirmed the above-mentioned correlation

between  $\text{Li}^+$ -solvation sheath structure and interphasial chemistry on graphitic anodes from another angle.

**5.1.4. EC–PC Mystery.** It is impossible to discuss the chemistry and formation of SEI without mentioning a conspicuous phenomenon that has been perplexing the electrochemical community for decades, that is, the disparity between the interphasial behaviors of EC and PC (Figure 48).<sup>474,590</sup> Despite numerous efforts and hypotheses, there is still no consensus over how such a small structural difference (a methyl) could result in two different electrochemical extremes. Considering that the key components of LIB were individually invented in the 1950s (lithiated GIC)<sup>1</sup> and 1970s (layered transition metal oxides),<sup>1,591</sup> and the fact that PC was almost the exclusive aprotic solvent used until the late 1980s,<sup>1</sup> it may not be an exaggeration to state that the different interphasial behavior caused by that small methyl group postponed the emergence of LIB technology for decades.

Although it was well-accepted that PC-based electrolytes could not support the reversible intercalation of bare  $\text{Li}^+$ , debates centered around how it happened. Most of the research community agreed that a certain degree of graphite exfoliation occurred because of the PC-cointercalation; however, there were a few researchers who believed that no graphite exfoliation happened, based either on the fact that the (002) interlayer distance of graphitic anode remained essentially the same after discharge in PC-electrolyte,<sup>590</sup> or on the observation that the same lithiation capacity could be obtained in EC-based electrolyte even after extensive PC-decomposition.<sup>592,593</sup> Instead, they believed that the decomposition of PC occurred in defects or crystalline boundaries, where the gaseous products from the PC reduction created new surfaces by cleaving the bulk graphite crystallites. Examining the evidence presented in each study, one would feel that the above divergence over “exfoliation” actually may relate to the different definitions used by individual researchers. From a microscopic angle, there is no doubt that certain carbonate molecules cointercalate and destroy the local graphitic structure there upon reduction, but whether this would be reflected in a macroscopic and averaging tool like X-ray diffraction depends on the extent of destruction. It is expected that only when medium- to long-range ordering was disrupted would the (002) peak show obvious weakening. In fact, in most of the studies, the (002) peak indeed slightly broadened despite the unchanged peak height and diffraction angle  $2\theta$ . In other words, although the graphitic structure remained intact as a whole, exfoliation did happen at local regions, where sustained solvent cointercalation and reduction occur.

With or without cointercalation/exfoliation, the real question to be answered here remains to be why EC did not behave similarly to PC, but instead formed a protective interphase that suppressed further solvent reductions. There have been very limited efforts trying to understand this difference from a mechanistic approach. Zhuang et al. proposed that EC and PC might undergo different reduction pathways based on *ex situ* FTIR analyses on the reduction products formed on graphite.<sup>594</sup> They found that from PC-based electrolyte  $\text{Li}_2\text{CO}_3$  was the main surface species, while a mixture of organic and inorganic products, such as semicarbonates, oxalate, oligoethers, as well as alkoxide, was obtained from EC-based products. It is possible that PC, while being reduced in the cointercalated (ternary GIC) state, could access more electrons than EC, therefore allowing the two-electron instead of single-electron reductive pathway that leads to exclusively  $\text{Li}_2\text{CO}_3$ . However,

this hypothesis was challenged by the NMR analyses conducted by Xu et al.<sup>48,474</sup> and more recently by Nie et al.,<sup>537</sup> who showed that the surface reduction of PC on graphite also produced the corresponding semicarbonate LPDC as the main product, evidenced by the characteristic 1,2-propyl (Figure 41) moieties that should not have been retained by a two-electron reduction mechanism.

Using the synthesized authentic references of LEDC and LPDC, Xu directly compared the ion conductivities (or solubilities) of these two in typical electrolyte solvents (EC/EMC 30:70).<sup>474</sup> In both blocking and nonblocking cell configurations, LPDC exhibited much higher solubility than both LEDC and LMC (Figure 49b), suggesting that the poor adhesion of PC-reduction products might be the key to its poor protection as an interphase ingredient. This conclusion was consistent with various inferences made in previous reports.<sup>587,589</sup> This argument based on the properties of the decomposition products rather than reduction mechanism path seemed to be echoed by Takenaka et al., who attempted to reveal the atomistic picture of how the compounds originated from EC or PC arrange themselves on a graphite surface through Monte Carlo-Molecular Dynamics simulation.<sup>595</sup> They came to the conclusion that the methyl group in PC prevented the product (LPDC) from efficiently packing into a dense and protective surface layer, in contrast to LEDC, which resulted in a “stable aggregation”.

More recently, Zhao et al. synthesized a homologous series of PC molecules and investigated the correlation between the varying alkyl chain length and the interphasial chemistry observed on graphitic anodes when these molecules were used as cosolvents with PC.<sup>596</sup> Interestingly, they found that exfoliation of graphite no longer took place when the chain length was larger than 4, and an SEI comparable with that formed by EC became available. On the basis of what Zhuang et al. suggested,<sup>594</sup> they attributed this correlation to competitive solvation of  $\text{Li}^+$  by PC and these molecules, whose presence suppressed the cointercalation of PC into the graphitic structure, leading to predominant single-electron reduction of PC and stable SEI.

## 5.2. Cathode/Electrolyte Interphase

While the interphase on graphitic anode is usually more resistive than that on cathode, the latter tends to increase at a quicker pace than the former during long-term cycling, and would eventually take over the role as the more resistant component in the cell at a certain point. Cycling with high voltage cathodes or aging at elevated temperatures accelerates this process.

Unlike its counterpart on anode surfaces, there has been rather limited effort to understand the interphase on cathode surfaces. Few reports were available regarding their chemical composition and formation mechanism, and among them even the existence of such interphases was questioned,<sup>597,598</sup> or at least their role as a protective layer was doubted on the basis that the coverage on cathode surfaces was often found to be incomplete.<sup>599</sup>

There are at least three reasons behind this “anarchy” in cathode interphase studies:

(1) First, as compared to the more pressing necessity associated with anode interphase, there has been lack of motivation to understand cathode interphases. While the fragile graphitic structure held together by weak van de Waals forces is susceptible to solvent cointercalation/decomposition, which

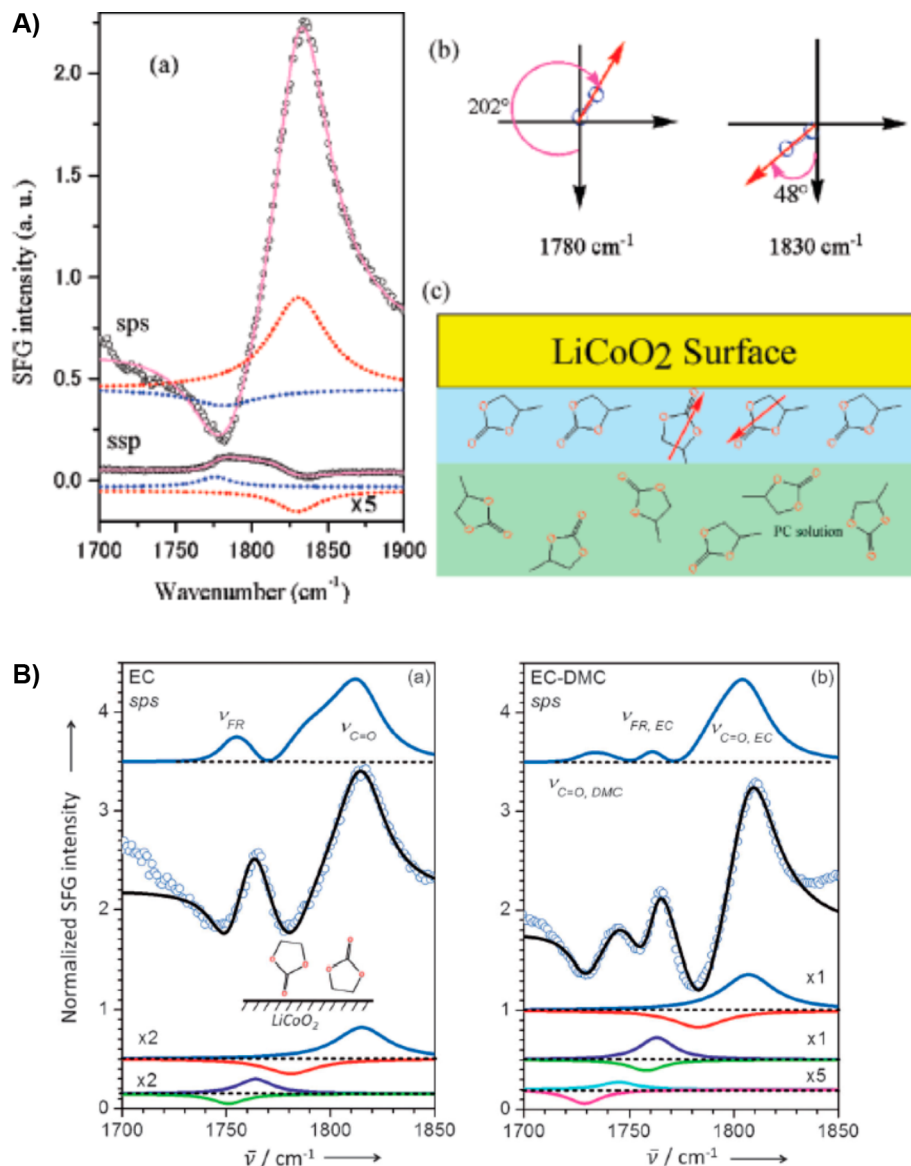


**Figure 50.** Adsorption and orientation of carbonate molecules on cathode surfaces: (A) The sum-frequency generation (SFG) spectra of a LiCoO<sub>2</sub> surface in PC. Two preferential orientations of PC molecules were identified and illustrated. Reprinted with permission from ref 609. Copyright 2009 American Chemical Society. (B) The SFG spectra of a LiCoO<sub>2</sub> surface in neat EC and EC/DMC mixture, where EC seems to adsorb preferentially. Reprinted with permission from ref 610. Copyright 2013 Wiley-VCH Verlag GmbH & Co. KGaA, Weinheim.

often leads to cell failure, the robust cathode structures assembled by Coulombic or covalent bonds are insensitive to solvent cointercalations.

(2) The complicated chemical species on cathode surfaces make it difficult to unambiguously discern the products from electrochemical oxidation of electrolytes; further complications were also introduced by the native surface film on most cathode surfaces (Li<sub>2</sub>CO<sub>3</sub> on transition metal oxides) and its concomitant reactions with acidic electrolyte components.<sup>597–607</sup> Although at least part of these spontaneous reaction products were later inherited by the interphase, both irreversible electrochemical reactions and cathode surface phase transformation occur during the initial charging, making the eventual interphase different in both chemical composition and morphology.

(3) More importantly, the operating potentials of most cathode materials do not depart too much from the oxidation stability limits of the electrolytes; therefore, electrolyte

decomposition might not be mandatory as compared to the situation on graphitic anodes. To illustrate specifically, the operating potentials of fully lithiated graphite (~0.2 V vs Li) and delithiated LiCoO<sub>2</sub> (4.2 V vs Li) could be translated to -3.0 and 1.2 V vs SHE, respectively. While the former (-3.0 V) is well beyond the thermodynamic reduction stability limits for almost any known organic compound, the latter (1.2 V) is reasonably safe for most organic polar compounds such as esters or nitriles. Only with the emergence of “5 V class” cathode materials, such as LiNi<sub>0.5</sub>Mn<sub>1.5</sub>O<sub>4</sub> (4.6 V vs Li, or 1.6 V vs SHE) or LiCoPO<sub>4</sub> (4.8 V vs Li, or 1.8 V vs SHE), would the cathode surface potential become too positive for the thermodynamic stability limits of organic electrolyte components.

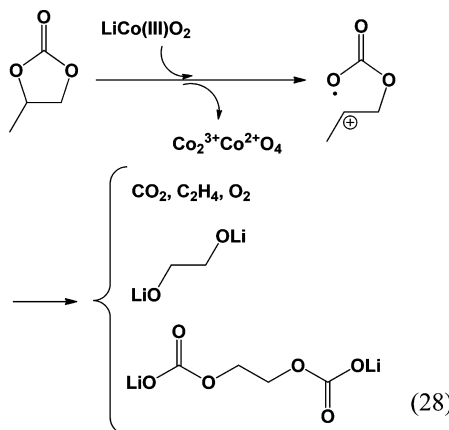
To summarize, the formation of an interphase on a cathode surface went through at least three stages: (1) the formation of native surface film during electrode manufacturing/processing; (2) spontaneous chemical reactions of the native film upon its

exposure to electrolytes; and (3) electrochemical rearrangement of these chemical species formed in stages 1 and 2 during the initial charging.

A seminal review on this subject was compiled by Aurbach et al. in 2007, in which they summarized the previous work on cathode interphases by categorizing against various cathode chemistries involved, including  $\text{LiCoO}_2$ ,  $\text{V}_2\text{O}_5$ ,  $\text{LiMn}_2\text{O}_4$ ,  $\text{LiNi}_{0.5}\text{Mn}_{0.5}\text{O}_2$ , and  $\text{LiFePO}_4$ .<sup>608</sup> This section only intends to cover a few important principles as well as the advances made since that review. More emphasis will be placed on the interphases formed on high voltage (>4.5 V) cathode surfaces, whose interphases have become a subject of vital importance for their practical deployment in LIB.

**5.2.1. Spontaneous Reactions.** Given the basic chemical nature of most cathode materials based on transition metal oxides, a native surface film consisting of  $\text{LiCO}_3$  usually forms during their synthesis, processing, or storage in atmosphere, where  $\text{CO}_2$  reacts with  $\text{Li}_2\text{O}$ . Upon contact with electrolytes, which are acidic in nature thanks to the fluorinated anions used in most commercialized electrolytes ( $\text{PF}_6^-$  or  $\text{BF}_4^-$ ), spontaneous reactions occur producing  $\text{LiF}$  and  $\text{CO}_2$ , and the native surface film would be replaced by a corroded remnant consisting of a mixture of  $\text{LiCO}_3$ ,  $\text{LiF}$ , and  $\text{PO}_x\text{F}_y$  species. Yet spontaneous reactions occur not only between the native surface film and electrolytes; they also involve the intrinsic cathode composition. According to Wang et al.,<sup>600–602</sup> the process was accompanied by the generation of a series of gaseous products that include  $\text{CO}_2$ ,  $\text{O}_2$ , and alkane or alkene that correspond to the carbonate solvents used. Ex situ surface analyses identified not only semicarbonates,  $\text{Li}_2\text{CO}_3$ ,  $\text{LiF}$ , and alkoxide,<sup>601,602,605</sup> but also reduced transition metal species such as  $\text{Co}_3\text{O}_4$  (from  $\text{LiCoO}_2$ ) or  $\lambda\text{-MnO}_2$  (from Mn-based cathode materials such as  $\text{Li}_2\text{Mn}_2\text{O}_4$  or  $\text{LiNi}_{0.5}\text{Mn}_{1.5}\text{O}_4$ ).<sup>608</sup> These results strongly suggested that redox reactions occur even without the electrochemical charging of cathode materials, probably via radical intermediates that were induced by the electron-exchange between transition metal cores and solvent molecules (eq 28):

**5.2.1.1. Adsorption.** Because of the importance of spontaneous reactions between cathode materials and electrolyte in determining the final SEI chemistry, Ye and co-workers carried out *in situ* investigations on how solvent molecules



adsorb on cathode surfaces with sum frequency generation (SFG) vibrational spectroscopy.<sup>609,610</sup> They found that in the absence of  $\text{Li}^+$ , the polar PC molecules mainly adopted two opposite orientations on the surface of  $\text{LiCoO}_2$ , with the

carbonyl group pointing at the surface being the favored conformation (Figure 50A). However, this preferred orientation would be rapidly disrupted as the result of  $\text{Li}^+$ -introduction in the solution, because  $\text{Li}^+$  would assemble carbonate molecules around itself to form a solvation sheath with much stronger Coulombic attractions. On the other hand, when typical carbonate mixtures such as EC/DMC or EC/DEC were used, an obvious preferential adsorption of EC over its acyclic counterparts was detected (Figure 50B), which the authors attributed to the higher dielectric constant of EC, as compared to the acyclic carbonates, and its stronger tendency to solvate  $\text{Li}^+$  in the lithiated  $\text{LiCoO}_2$  that existed at high concentrations (>20 M).<sup>610</sup> The calculated EC-percentages at the  $\text{LiCoO}_2$  surface and in the bulk electrolyte are compared in Table 30.

This preferential accumulation of EC molecules at the cathode surface could cast more profound repercussions on the resultant interphasial chemistry. Upon charging (i.e., removal of  $\text{Li}^+$  from  $\text{LiCoO}_2$ ), it was expected that the EC in the vicinity of

**Table 30. Preferential Accumulation of EC on  $\text{LiCoO}_2$  Surface**

bulk composition	EC in bulk (mol %)	EC at $\text{LiCoO}_2$ surface (mol %)
EC/DMC (1:1)	56	95 ± 1
EC/DEC (1:1)	65	92 ± 1
EC/DMC/DEC (1:1:1)	43	93 ± 1

the cathode surface would capture  $\text{Li}^+$  released by the cathode into the electrolyte; meanwhile, due to the rising potential of the cathode surface, these same EC molecules could also become the preferred “victims” of oxidation and become part of cathode interphase. While this “EC-preference” in cathode interphase was also predicted by MD and DFT simulations,<sup>564,611</sup> it remains to be confirmed by further experimental evidence. One should also note that, as compared to the “EC-preference” in anode interphase that is a direct consequence of preferential solvation, this potential preference at cathode surface would be caused by an entirely different reason.

**5.2.2. Chemistry and Electrochemistry.** The fate of the remnant native film during the electrochemical charging of the cathode remained unclear. While Liu et al. believed that the eventual SEI on  $\text{LiCoO}_2$  surfaces inherited most chemical signatures from the spontaneous reaction products and electrochemical charging merely made the surface film more “uniform”,<sup>605</sup> Ménétrier et al. showed through solid state  $^{7}\text{Li}$  and  $^{1}\text{H}$  NMR studies that changes did occur during the initial charging of a  $\text{LiNiO}_2$  cathode, and an organic-dominant surface film gradually replaced the original inorganic native film.<sup>603</sup> Goonetilleke et al. also believed that an oxidation dissolution of the “left-over” surface film on  $\text{LiMn}_2\text{O}_4$  occurred as a result of the electrochemical charging.<sup>607</sup> They suggested that the dissolution of the surface products formed during a spontaneous reaction stage may involve a regeneration of electrolyte solvents from alkylcarbonate (eq 29), accompanied by the conversion of cathode surface into a mixture of  $\text{LiMn}_2\text{O}_4$  and  $\lambda\text{-MnO}_2$ .

In *in situ* ellipsometry measurements of the interphase thickness on thin-film  $\text{LiMn}_2\text{O}_4$  were conducted by Lei et al., who observed that the rates of thickness increase under electrolyte-exposure and electrochemical cycling differed significantly,<sup>604</sup> indicating that rearrangements of the surface film did occur during electrochemical charging.

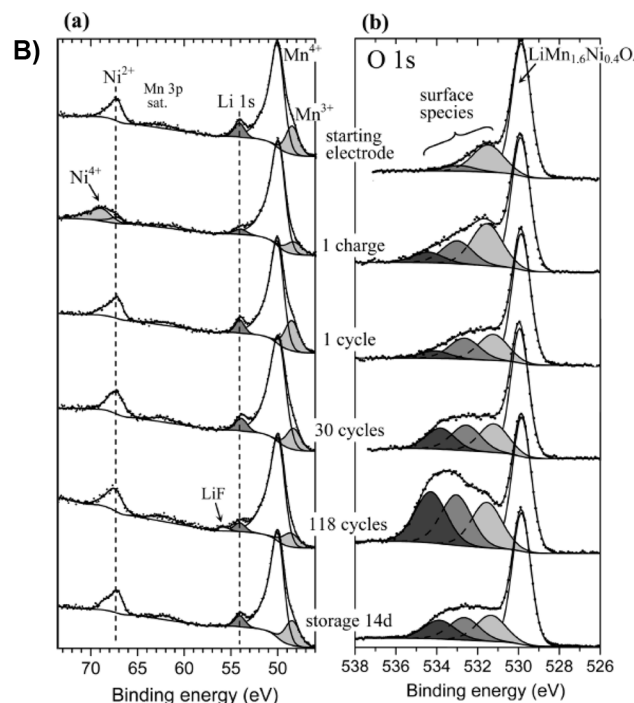
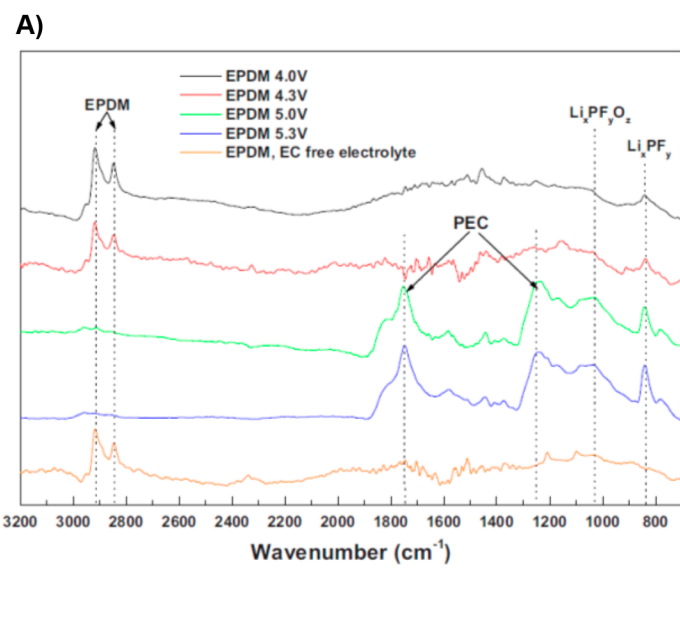
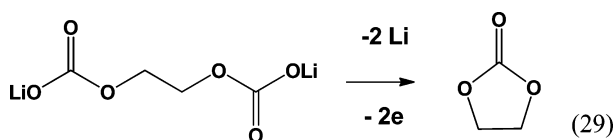
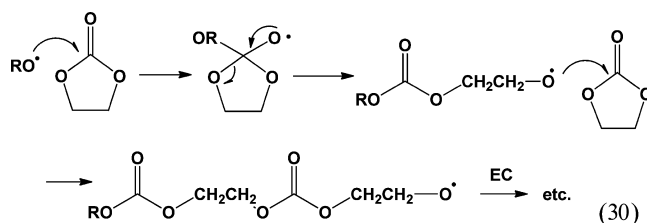


**Figure 51.** Identification of interphasial components on cathodes: (A) FTIR-attenuated total reflectance spectra of  $\text{LiNi}_{0.5}\text{Mn}_{1.5}\text{O}_4$  cycled in EC-based electrolyte. Reprinted with permission from ref 613. Copyright 2010 Electrochemical Society. (B) Ni 3p/Mn 3p/Li 1s (a) and O 1s (b) XPS spectra of  $\text{LiMn}_{1.6}\text{Ni}_{0.4}\text{O}_4$  before and after cyclings as well as after 14 day storage in EC-based electrolyte. Reprinted with permission from ref 617. Copyright 2010 American Chemical Society.



In addition to  $\text{Li}_2\text{CO}_3$  and semicarbonates, LiF was also an ingredient often found in cathode interphases. Wang et al. attributed the appearance of LiF to the oxidation of  $\text{PF}_6^-$ -anion, and believed that fluorides were only produced at high potentials ( $>4.9$  V).<sup>601</sup> This finding seemed to be echoed by Shu, who stated that LiF even appeared on  $\text{Li}_4\text{Ti}_5\text{O}_{12}$  as long as it was polarized to potentials high enough (5.0 V).<sup>538</sup> By using  $^7\text{Li}$  and  $^{19}\text{F}$  double resonance NMR, Murakami et al. not only confirmed the formation of LiF on the  $\text{LiCoO}_2$  surface during the electrochemical charge, but also proved, by examining the effect of  $^7\text{Li}$ – $^7\text{Li}$  spin diffusion between LiF and  $\text{LiCoO}_2$  on the spin-lattice relaxation time, that these LiF aggregated as separate macroscopic domains not directly attached to  $\text{LiCoO}_2$  particles.<sup>612</sup> What lay between LiF and  $\text{LiCoO}_2$  remains to be clarified, but this clearly exhibited the inhomogeneous nature of interphase structures.

Polymerization of cyclic carbonates initiated via oxidative processes was also suggested as a possible route to interphases on cathodes, leading to polycarbonate-like species (eq 30):<sup>608,613</sup>



within the battery community is that the interphase formed in these electrolytes can only stabilize the cathode/electrolyte junction up to  $\sim 4.5$  V, above which sustained electrolyte oxidation would occur.<sup>10,281,613,617–619</sup> The effect of parasitic reactions at high voltage cathodes becomes especially pronounced under high precision coulometry or in a full Li-ion cell configuration where the  $\text{Li}^+$ -source is limited.

Yang et al. showed that ternary electrolytes with composition based on EC/DMC/DEC decomposed substantially when charging  $\text{LiNi}_{0.5}\text{Mn}_{1.5}\text{O}_4$  beyond 4.5 V.<sup>613</sup> FTIR analysis conducted on the cycled cathode surface revealed polymeric species with characteristic absorption peaks of poly(ethylene carbonate) as shown in eq 30 (Figure 51A). A slightly different cathode material ( $\text{LiMn}_{1.6}\text{Ni}_{0.4}\text{O}_4$ ) was analyzed by Dedryvère et al. with both XPS and impedance spectra, who found that both electroadSORption and film formation occurred during the first cycle.<sup>617</sup> Interestingly, on the basis of XPS spectra of the 1s core-shells of Li, O, and C, they concluded that the interphasial species were dominated by organic rather than lithiated (salt) species (Figure 51B), which, in sharp contrast to what was found on graphitic anode surfaces, would be consistent with a polymeric interphase.

A few other researchers differed slightly from the above conclusions. While acknowledging that cyclic carbonates were subject to ring-opening polymerization leading to copolymers consisting of ether-carbonate repeating units, Demeaux et al.<sup>616</sup>

and Duncan et al.<sup>618,619</sup> believed that abundant salt species such as LiF or  $\text{Li}_x\text{P}_y\text{O}_z$  also coexisted in the cathode interphase. A rather unique work was reported by Carroll et al., who compared the surfaces of both composite and thin-film  $\text{LiNi}_{0.5}\text{Mn}_{1.5}\text{O}_4$  in state-of-the-art carbonate electrolytes, and found only minimal decomposition of electrolyte components on the latter.<sup>620</sup> Thus, they concluded that, despite the high operating voltage,  $\text{LiNi}_{0.5}\text{Mn}_{1.5}\text{O}_4$  is intrinsically stable toward carbonate solvents, and the oxidative decomposition of electrolytes was actually induced by the “inactive” ingredients of the composite electrode, such as carbon conductive additives (carbon black) and polymeric binder.

As compared to spinel  $\text{LiNi}_{0.5}\text{Mn}_{1.5}\text{O}_4$ ,  $\text{LiCoPO}_4$  presented a more severe challenge to electrolyte stability due to its higher potential (4.8 V). Markevich et al. have proposed that the instability might involve the cathode chemical composition, as the olivine phosphate moieties in the delithiated state could be susceptible to nucleophilic attack from fluorides (eq 31), which commonly exist in most commercial electrolytes containing  $\text{LiPF}_6$  as salt (Figure 52).<sup>621</sup>

The formed species  $\text{PO}_2\text{F}_2^-$  is soluble in electrolyte, whose leaving the cathode surface leads to a series of progressive damaging steps that include lithium depletion, lattice deg-

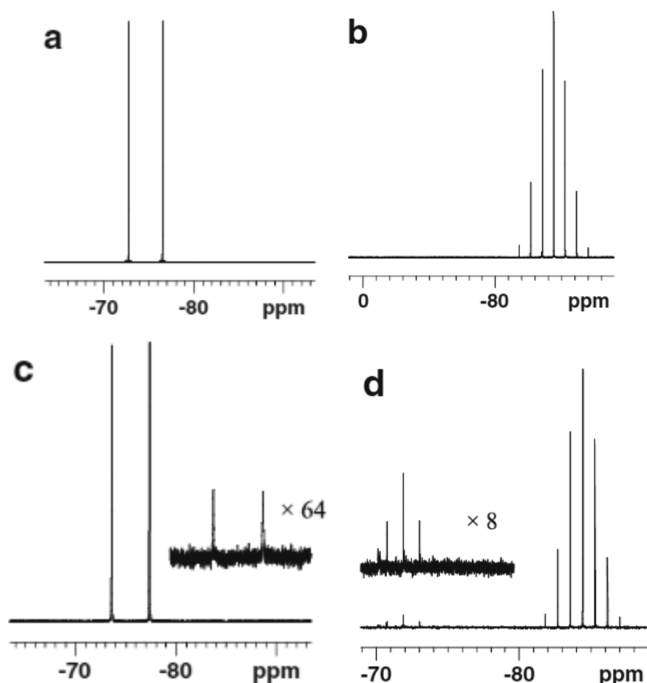
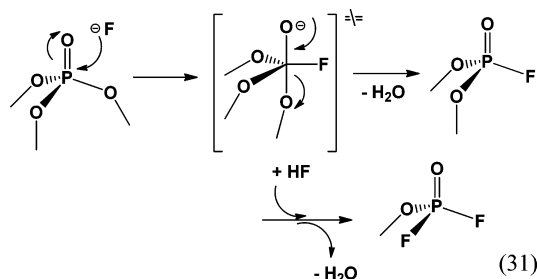


**Figure 52.** Electrolyte decomposition on  $\text{LiCoPO}_4$  cathodes:  $^{19}\text{F}$  (left) and  $^{31}\text{P}$  (bottom) NMR spectra of a fresh electrolyte (a and b) and an electrolyte recovered from a cycled  $\text{LiCoPO}_4$  cathode (c and d) with DMC-rinsing. Reprinted with permission from ref 621. Copyright 2012 Elsevier.

radiation of  $\text{LiCoPO}_4$ , and exfoliation of carbon conductive layer.

A number of efforts were made to stabilize electrolytes against these high voltage cathode materials, using either various additives<sup>10,260,622</sup> or fluorinated solvents.<sup>11,623</sup> The detailed mechanism of how these phosphates- or thiophene-derivatives work remains to be understood.



**5.2.4. Cathode/Anode Interactions.** The interphasial processes occurring at cathode and anode surfaces were once considered as if they were isolated from each other, but ever increasing evidence reveals that certain forms of “conversation” exist between cathode and anode, as interphasial species generated on one electrode often appear on the other with unexpected impacts.

Perhaps the first cathode/anode dialog recognized was the dissolution of Mn(II) from  $\text{LiMn}_2\text{O}_4$  and its subsequent deposition on graphitic anodes, which was described by Komaba et al. as detrimental to the anode intercalation chemistry.<sup>185</sup> According to Delacourt et al., the deposited Mn(0), which were embedded in the middle of the interphase, actually serve as electrochemical mediators to tunnel electrons through the electronically insulating SEI, the result of which is the sustained reduction of electrolyte components.<sup>624</sup> On the other hand, Zhan et al. proved with X-ray absorption near edge spectra that the Mn species deposited on various anode surfaces predominantly remained in the oxidation state of +2, and the capacity fade caused by Mn(II) dissolution from cathode lattice was actually the result of an ion-exchange process between  $\text{Mn}^{2+}$  in bulk electrolyte solution and  $\text{Li}^+$  embedded in anode interphase.<sup>186</sup> Despite the mechanism, a quantitative evaluation of capacity fading contributed by this Mn(0)-catalyzed electrolyte reduction was recently conducted by MahootcheianAsl et al., who inserted a  $\text{Li}^+$ -conducting solid electrolyte to block the migration of Mn(II) toward graphite anodes (Figure 53a), and therefore was able to differentiate the “intrinsic” degradation in cycling performance of high voltage  $\text{LiNi}_{0.5}\text{Mn}_{1.5}\text{O}_4$  in the absence of any Mn(II)-dissolution/deposition (Figure 53b).<sup>625</sup> They found that Mn(II)-dissolution/deposition was actually responsible for most of the capacity loss as observed in conventional LIB configuration. In fact, transition metal cores in almost all layer or spinel structures were susceptible to acid leaching by HF, which is a common impurity in  $\text{LiPF}_6$ -containing electrolytes; therefore, numerous efforts were made to prevent the dissolution or mitigate the deposition, either by cathode surface coating<sup>297,304,312,314,321</sup> or by electrolyte component/additive approaches,<sup>95,159,187,188</sup> which have been covered in preceding sections.

What also interested researchers recently is the possibility of oxidized or reduced electrolyte species that could migrate across the cell and reach the other end. Dedryvère et al. once coupled high voltage  $\text{LiMn}_{1.6}\text{Ni}_{0.4}\text{O}_4$  cathode with  $\text{Li}_4\text{Ti}_5\text{O}_{12}$  anode, whose redox potential at 1.5 V vs Li makes it an “SEI-free” electrode, and observed that organic species accumulated on  $\text{Li}_4\text{Ti}_5\text{O}_{12}$  surface as an obvious result of oxidation processes occurring on the cathode.<sup>617</sup> Obviously, some species that originated from the oxidative process at the cathode were soluble in the bulk electrolyte and migrated across the cell before being intercepted and perhaps reduced by the anode. This suspicion was recently confirmed by Li et al., who used an innovative cell configuration of a

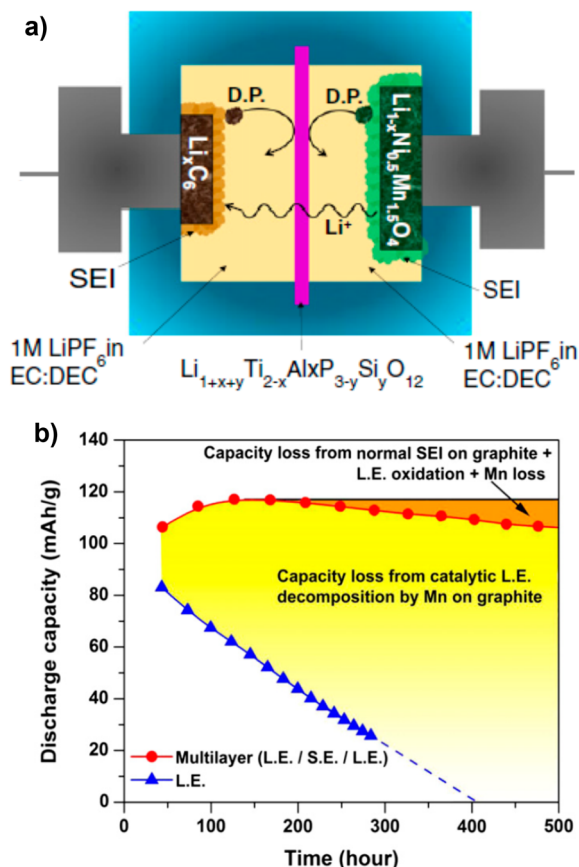


**Figure 53.** Identifying electrolyte decomposition on cathodes: (a) schematic illustration of a multielectrolyte cell with an interlayer that selectively allows Li<sup>+</sup>-transport; (b) differentiating contribution to capacity fading from Mn deposition on an anode surface and electrolyte oxidation. Reprinted with permission from ref 625. Copyright 2013 Elsevier.

"pseudo-full cell", and successfully "interrupted" such cross-cell interaction.<sup>626</sup>

A more visual demonstration of electrolyte/cathode reaction was described by Norberg et al.<sup>627</sup> While it has been known earlier that fluorescence species were generated during the electrochemical oxidation, often as inconveniences to Raman spectra measurements, the authors took advantage of the in situ fluorescent spectra and observed that at least part of the oxidation products formed on the surface of LiNi<sub>0.5</sub>Mn<sub>1.5</sub>O<sub>4</sub> diffuse away into bulk electrolytes. It should be emphasized here that, although the existence of these interphasial species has been confirmed in the above experiments, their identities remain unknown. Needless to say, it would be of paramount importance to identify these shuttling species, to develop better electrolytes, or to design new battery chemistries, or simply to minimize degradations in current LIB.

Beside material exchange between cathode and anode, these two electrodes also influence each other's operation through a more "immortal" manner. Krueger et al. described in detail how the SEI growth on graphitic anodes caused charge imbalance in a full cell where the Li<sup>+</sup> source is limited, which eventually led to overcharge of the cathode and subsequent irreversible processes, such as impedance hike and electrolyte oxidation, etc., as long as a charging protocol with constant cutoff voltage was maintained.<sup>628</sup> Their discovery emphasized that the components within a battery are not

isolated from each other; rather, a holistic system approach should be adopted to address these strongly interrelated processes.

### 5.2.5. How Interphases on Cathode and Anode Differ.

Before concluding this section, I would like to cite an actual device as an example, that is, the concept of semisolid lithium ion flow battery,<sup>629</sup> to demonstrate how interphases on anode and cathode in LIB differ. Adopting the mature flow battery configuration of low voltage, aqueous chemistries, Duduta et al. creatively designed a LIB device in which the active material masses are stored remotely away from the electrochemical reaction sites (current collectors), thus decoupling the energy density of the cell from the cell size that is often subject to space or weight limitations of environment. Such a design could represent a breakthrough in battery applications on mobile platforms such as vehicles.

In this semisolid flow cell, active particles of both cathode and anode materials were suspended in slurries made from nonaqueous liquid electrolytes and circulated with a peristaltic pump, either continuously or intermittently, through the electrochemical chamber. Energy can be extracted from or stored in these moving phases (slurries) with typical reversible Li-ion chemistry characteristics (Figure 54a).

Upon closer examination, however, one would wonder how such a cell works when considering interphases formed on both anode and cathode surfaces (Figure 54b). Because these active

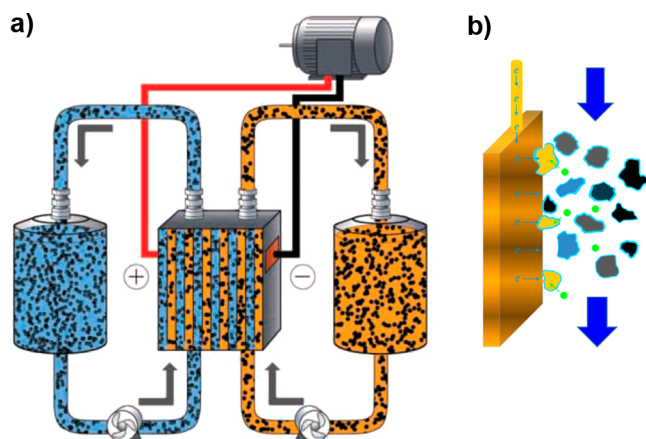


**Figure 54.** A Li-ion battery without SEI? (a) Schematic illustration of semisolid Li-ion flow cell with active electrode materials suspended in slurries consisting of electrolyte. Reprinted with permission from ref 629. Copyright 2011 Wiley-VCH Verlag GmbH & Co. KGaA, Weinheim. (b) The supposed electron and Li<sup>+</sup>-transfer between mobile phases in such Li-ion flow cells. Note that if SEI does form on active particles, the electron has to hop through multiple layers of such interphases.

particles are mobile and detached from their own electrode current collector, the existing picture of electrode/electrolyte interphases separating ionic conductor and electronic conductor no longer applies. For each mobile phase of active materials to be charged or discharged, electrons must travel through multiple electrode/electrolyte interphases before they can arrive at either current collector or active particles in closest vicinity of the current collector, similar to what a redox shuttle additive must experience under the overcharge conditions (Figure 54b). Therefore, this flow cell chemistry would work against what SEI stands for if the SEI as we used to understand

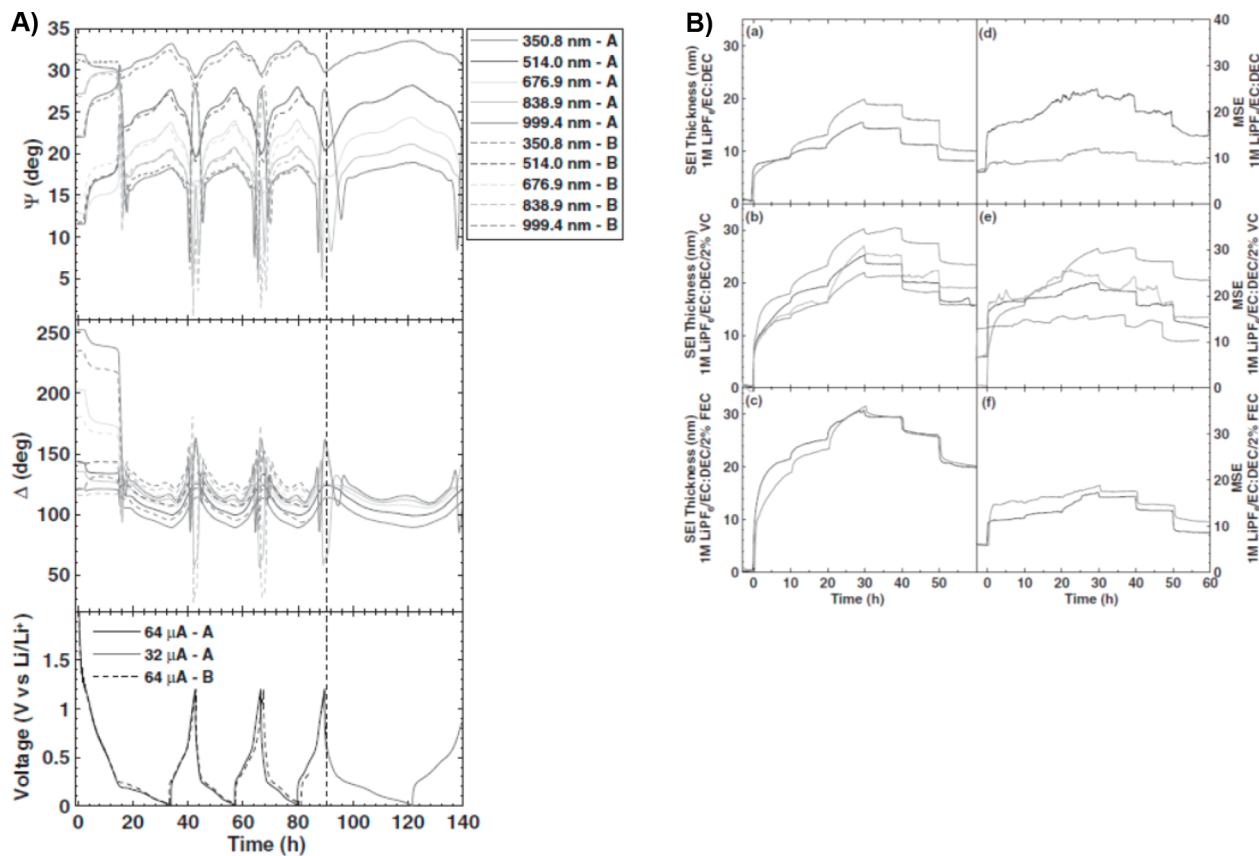


**Figure 55.** In situ investigation of SEI with ellipsometry: (A) time-dependence of ellipsometric parameters (amplitude  $\Phi$  and phase  $\Delta$ ) during the electrochemical cycling of a-Si anode between 0.005 and 1.2 V in 0.1 M LiPF<sub>6</sub>/EC/DEC (1:2); (B) SEI thickness determined by ellipsometry on a TiN electrode surface in baseline electrolytes (1.0 M LiPF<sub>6</sub>/EC/DEC 1:2) with or without additives VC or FEC. Reprinted with permission from ref 636. Copyright 2012 Electrochemical Society.

exists. Interestingly, what really happened in this flow cell was that both LiCoO<sub>2</sub> (4.2 V vs Li or ~1.2 V vs SHE) and LiNi<sub>0.5</sub>Mn<sub>1.5</sub>O<sub>4</sub> (4.6 V vs Li or ~1.6 V vs SHE) indeed worked at the cathode side with characteristic capacity and voltage profiles, while at the anode side only lithiated titantate (1.5 V vs Li or ~−1.5 V vs SHE), known to be “SEI-free”, could work. The graphitic anode, whose lithiation potential (0.2 V vs Li or ~−3.0 V vs SHE) deviates too much from the stability limit of the electrolyte, could not support this flow cell chemistry due to the blocking effect of its SEI.

This novel cell design, besides its practical significance, made us reexamine the relation between electrode operating potentials and the “perfectness” of interphases. Evidently, the interphase present on most cathode surfaces is further from being an electronic insulator than its counterpart on graphitic anodes.

### 5.3. Advanced Characterization and Imaging

The characterization of interphase chemistry and formation has been especially challenging, because of the elusive nature of the interphase, and also because of the usual absence of effective and noninvasive *in situ* techniques until recently. Most traditional surface-analytical tools are *ex situ* in nature, whose sample preparation and handling often introduce significant artifacts by altering or even damaging the fragile chemistry and morphology of interphases. For example, Edström and co-workers have pointed out earlier that the presence of Li<sub>2</sub>CO<sub>3</sub> as detected by XPS in interphases formed on graphitic anode was most likely the result of sample exposure to ambient

CO<sub>2</sub>.<sup>559–561</sup> Recently, this popular surface analysis tool was more critically examined by Niehoff et al., who found that charging effects could shift the binding energy of chemical species by as much as 1 eV, and that ultrahigh vacuum conditions actually led to partial decomposition of PF<sub>6</sub><sup>−</sup> anion.<sup>630</sup> In particular, the interphasial thickness derived from the sputtering technique of XPS should be treated with extra caution, as the bombardment of ions significantly induces chemical reactions of not only the interphasial species but also graphite itself. Thus, more sensitive, reliable, and less invasive surface analytical tools are needed to understand interphases.

Since 2008, driven by instrumentation progress, heightened interest, as well as increased investments of resources, numerous advanced techniques aiming at probing and imaging LIB have emerged, mostly with *in situ* capabilities at the focus of attention. While there are a few recent reviews already in publication,<sup>631,632</sup> this section will cover only those directly related to interphase characterization.

#### 5.3.1. Ellipsometry and Sum-Frequency Generation Spectra.

The thickness of SEI was one of the key interphase parameters under debate, with a wide range from 5 to 500 nm reported by different experimental means. The recent application of UV-visible and vibrational spectroscopy techniques to interphase studies seemed to have “shed the light at a correct angle” on this topic.

As a surface-sensitive optical tool, ellipsometry measures the change in polarization after a beam of linearly polarized light was shed at certain incidence angle on and interacted with/reflected

from a smooth surface (Figure 55A). From amplitude  $\Phi$  and phase  $\Delta$ , information regarding the surface such as surface dielectric, roughness, and density could be derived using a reasonable model. If an *in situ* experiment could be designed, ellipsometry would become an ideal tool to monitor the live growth of the interphase due to the noninterfering nature of light beams, and thickness measurement of high accuracy (ideally of subnanometer scale) would be possible. Unfortunately, the requirement for a highly smooth sample surface heavily restricted its versatility, while developing such a reasonable model for data interpretation remains challenging.

There have been a number of efforts in applying ellipsometry to the study of SEI in LIB,<sup>633–636</sup> among which McArthur et al. reported the most meaningful analysis of interphase growth and thickness observed on thin-film a-Si and TiN surfaces by using an *in situ* setup constructed within a fused quartz tube. As a-Si was lithiated, its optical properties changed from transparent and semiconducting to opaque and metallic, corresponding to the formation of a-Li<sub>x</sub>Si alloy. Because this transformation occurred simultaneously with the formation of SEI, it was not possible to decouple them and hence derive SEI thickness. With inert TiN, however, they successfully derived the thickness of interphases formed in baseline electrolytes (1.0 M LiPF<sub>6</sub>/EC/DEC 1:2) with or without additives such as VC and FEC. Interestingly, they found that the interphase thicknesses increased with the presence of these additives, with 18 nm in baseline electrolyte versus 25 nm for 2% VC and 30 nm for 2% FEC.<sup>636</sup>

Another variation of vibrational spectroscopy that is “interface-sensitive” is sum-frequency generation (SFG). Beside its application to the understanding of how solvent molecules adsorb and oriente on electrode surfaces,<sup>609,610</sup> it was also used to reveal the chemistry of the interphase after reactions occurred between the adsorbed solvents and electrode surface. When the electrode surfaces (Cu and Au) were cathodically polarized down to 0.20 V vs Li, SFG clearly detected the existence of two separate interfaces in addition to the original electrode/electrolyte interface (Figure 56A).<sup>637</sup> Mukherjee et al. assigned it to the appearance of SEI, which creates two interfaces, that is, electrode/SEI interface and SEI/electrolyte interface. FTIR identified both LEDC and ethylene oxide linkages as the main components of SEI. While the thickness of the SEI increased/decreased periodically during cyclic charging/discharging, these chemical compositions remained unchanged.

**5.3.2. Electron Microscopes.** Electron microscopes enabled direct and visual measurement of interphases, but their *ex situ* nature and often invasive procedures of sample preparation could introduce artifacts and misleading results; the electron beams were also known to cause degradation of organic species such as the interphase ingredients. Sometimes the question also arose about how representative the localized observation could be when applied globally and macroscopically. Nevertheless, electron microscopes, especially in transmission mode, became increasingly popular tools adopted by researchers to image interphases.

Under TEM, the amorphous interphases usually appeared in strong contrast against the crystalline electrode on which it grew. Figure 57a–d shows interphases observed on LiCoO<sub>2</sub> cathode, graphitic, or silicon anodes after either soaking or cycling in electrolytes,<sup>536,537,605,638</sup> whose SEI thickness of 10–50 nm agrees with the general estimate from other techniques.<sup>462,567</sup> Of particular interest is the work of Wang et al.,

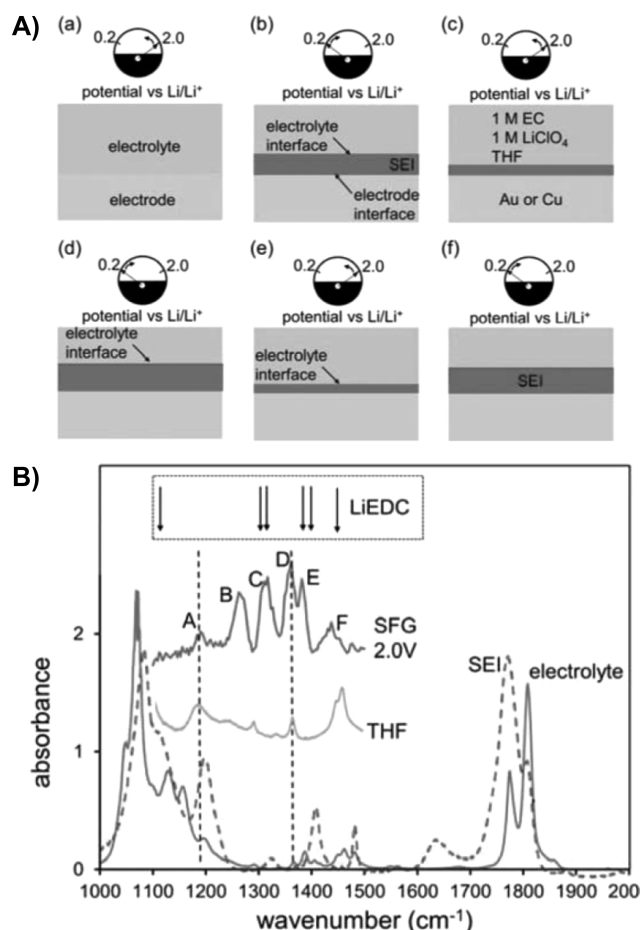


**Figure 56.** In *situ* investigation of SEI with sum-frequency generation (SFG) spectra: (A) schematic illustration of the appearance of an independent interphase and how it grows and shrinks during cycling; (B) the SFG spectra along with FTIR for electrolytes based on EC/THF and THF. The known signatures of LEDC are marked. Reprinted with permission from ref 637. Copyright 2012 Electrochemical Society.

who showed that SEI covered both edge and basal planes and was enriched with lithium that is different from the interior of graphitic structures (Figure 57b).<sup>639</sup> However, only LiF was detected in the experiment, in sharp contrast to the results of Nie et al.<sup>536</sup> By using a low energy electron beam, Lee et al. developed a SEM-based technique with extra-high resolution, where differentiated images of interphases can be obtained due to the secondary electron contrast mechanism.<sup>638</sup> With ion etching at a proper angle, it is possible to not only clearly visualize SEI but also more accurately measure local SEI thickness, thus revealing its multilayered structure (Figure 57d). A compact inner layer was estimated to be 10–15 nm thick and a porous outer layer 20–30 nm thick.

The SEI thickness on cathode, as its existence, has also been a subject of controversy. In general, the interphases were considered much thinner when compared to its counterpart on graphitic anodes. Reports have placed the value in a wide range from a few to 10<sup>2</sup> nm.<sup>599,605,640</sup> However, with continuous cycling and especially high temperature aging, the interphase increases in thickness, while its resistance takes over as the kinetic bottleneck of the overall cell chemistry. Using combined SEM/TEM analysis, Dupre et al.<sup>599</sup> and Dedryvère et al.<sup>617</sup> estimated an average of 2–20 nm thickness for cathode

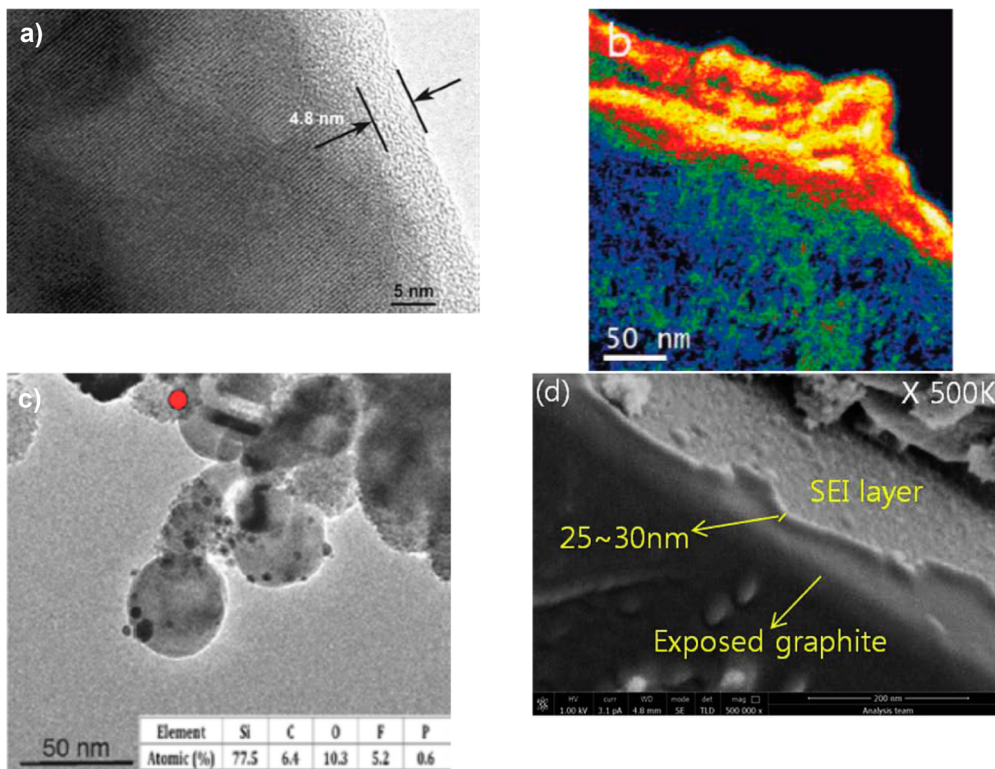


**Figure 57.** Visualizing SEI with electron microscopes: Images of SEI grown on: (a) A nano  $\text{LiCoO}_2$  particle after cycling in 1.0 M  $\text{LiPF}_6/\text{EC}/\text{DMC}$ . Reprinted with permission from ref 605. Copyright 2006 Electrochemical Society. (b) Graphite after lithiation to 10 mV as viewed by Li elemental mapping. Reprinted with permission from ref 639. Copyright 2011 American Chemical Society. (c) A silicon nanoparticle anode after first lithiation in  $\text{LiPF}_6/\text{EC}$ , where red dots indicate locations of EDX analysis with results summarized in the inset table. Reprinted with permission from ref 537. Copyright 2013 American Chemical Society. (d) Extreme high-resolution SEM image of SEI formed on a graphitic anode in  $\text{LiPF}_6/\text{EC}/\text{EMC}/\text{DEC}$  with VC and FEC as additives after  $\text{Ar}^+$ -etching for 5 min. Reprinted with permission from ref 638. Copyright 2014 Elsevier.

interphases after the spontaneous reaction, but because the cathode surface was not covered by a homogeneous layer, they thus argued that this reaction was not a “real passivation”. This argument agrees with prior reports that often conflicted on whether interphases could be detected on cathode surfaces. The complication seemed to arise not only from the different chemical nature and operating voltage, but also from less controllable factor such as preparation route, porosity, and surface morphology of cathode materials.

**5.3.3. Acoustics.** A noninvasive and surprisingly informative technique is acoustic emission measurement, which allows *in situ* monitoring of SEI growth by registering the transient elastic waves generated by the stress built up within electrode materials during the electrochemical reactions. The earliest effort to relate acoustic events with electrochemical processes of LIB material was perhaps made by Ohzuku et al., whose pioneering work using acoustic emission (AE) on electrolytic manganese dioxide proved that acoustic events were closely associated with particle fracturing upon initial lithiation.<sup>641</sup> After a hiatus of a decade, researchers’ interest in this technique was revived due to the advantage of its intrinsic passive nature (hence nondestructive) and high sensitivity.<sup>642–644</sup> The more interesting work was performed on materials of emerging chemistries such as Sn-, Si-, as well as conversion reaction electrodes because of the drastic volume changes (hence conspicuous stress and acoustic response) associated with those materials. For example, Rhodes et al. applied AE to investigate the legendary volume changes in crystalline Si electrodes and performed the first rigorous waveform analysis (Figure 58a),

where the duration, amplitude, counts, and frequency were correlated with corresponding electrochemical information.<sup>642</sup> The initial lithiation of Si was found to be accompanied by the largest number of emissions, mainly caused by surface fracture of Si particles, its transformation from crystalline into amorphous phases of lithiated silicon, as well as the formation of SEI. In the subsequent charging/discharging cycles, the emission events were characterized by distinct bursts, reflecting reversible volume expansion/contraction due to formation or disappearance of various  $\text{Li}_x\text{Si}$  alloy phases. AE was also applied to graphitic anodes to detect the process of SEI-formation. Kircheva et al. revealed that the acoustic hits or the absolute energy released recorded in the first cycle far outnumbered those in the subsequent cycles (Figure 58b).<sup>644</sup> They attributed the source of these acoustic events to the formation of SEI accompanied by the generation of gaseous products as well as fracture of graphite crystallites during  $\text{Li}^+$ -intercalation. Note that the largest accumulated energy occurred during the voltage range 1.5–0.75 V, which was considered to be the potential range where carbonate molecules start to decompose reductively.

**5.3.4. Neutron-Based Techniques.** An underexplored *in situ* tool is neutron techniques, apparently due to its limited availability to most potential users. In fact, the sensitivity of neutron techniques to light atoms such as Li makes it a unique complement to electron-beam (such as TEM) or X-ray techniques, while the low energy (meV) and charge neutrality of cold neutrons makes it an essentially nondestructive probing particle that can monitor, *in operando*, the dynamic distribution

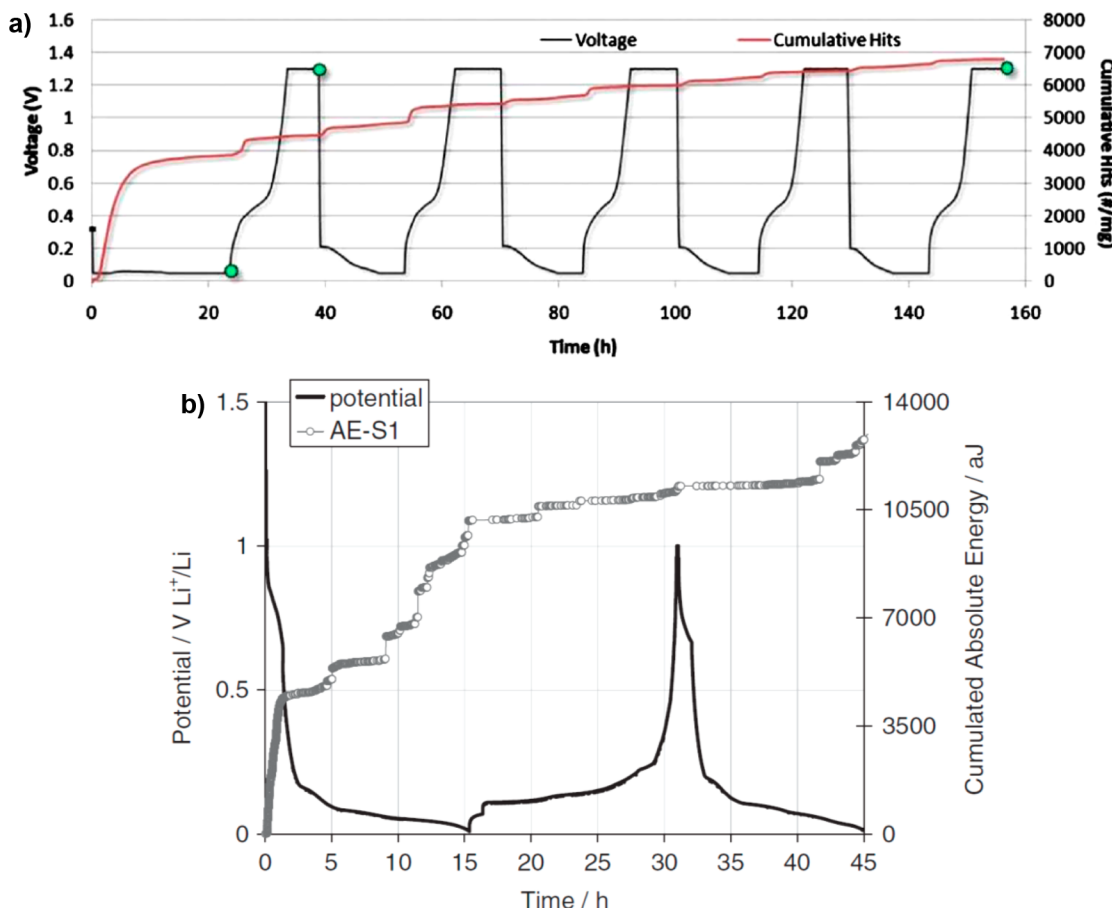


**Figure 58.** In situ investigation of SEI with acoustics: cumulative acoustic response and corresponding voltage profile of (a) Si and (b) graphitic anode during electrochemical cycling. Reprinted with permission from ref 642. Copyright 2010 Electrochemical Society. Reprinted with permission from ref 644. Copyright 2011 Electrochemical Society.

of Li<sup>+</sup> throughout the battery during electrochemical reactions. There are a number of techniques based on neutron diffraction, reflection, scattering, absorption, or charged particle emission, from which tomography and depth profile of Li distribution within an electrode material could be obtained,<sup>645</sup> but only limited efforts were made to adapt them for interphase investigations.

Small-angle neutron scattering was used by Bridges et al. to monitor the formation and evolution of SEI on hard carbon electrodes.<sup>646</sup> Using electrolytes that are partially deuterized for better differentiation, the authors observed that SEI formed in the pores of the carbon framework, while the initial components seemed to be dominated by Li<sub>2</sub>CO<sub>3</sub> or semi-carbonates, followed by increasing concentration of simple inorganic salts such as Li<sub>2</sub>O, LiOH, or LiF (Figure 59a). Additionally, an increase in contrast between carbon framework and pore, in conjunction with an increase in pore–pore separation, occurs for all cells during the initial stage of discharge. These observations are consistent with an increase in the concentration of solvated lithium species near the carbon surface via adsorption/intercalation of lithium species.

As compared to diffraction techniques that would be blind to amorphous species, neutron reflectivity (NR) is apparently more suitable for interphase studies. This high-resolution tool probes structure and composition with subangstrom accuracy when a monochromatic neutron beam is directed onto a target and the intensity of the reflecting beam is recorded as the function of the incident angle. Fitting this reflectivity data can

determine the depth profile of the scattering length density (SLD), which is related to composition. The SLD is the sum of the bound coherent scattering length of each isotope in a material multiplied by that isotope's number density. Therefore, isotope substitution can be used to determine a depth profile of specific element in the target, and isotopic labeling of reactants can be used to determine the relative amounts of each contributing to a deposited layer such as the SEI. NR is particularly sensitive to Li and H, for example, because both have a large isotope effect and a negative scattering length due to their natural abundances, in sharp contrast to most elements. The ease of in operando NR measurements allows the dynamic mapping of various interphasial layers during charge/discharge and provides valuable insight into how interphases thickness and SLD changes with the electrochemical states of the batteries. In a recent neutron reflectometry study by Owejan et al., the progressive growth of SEI thickness was observed to increase from 4.0 nm after 10 CV cycles to 4.5 nm after an additional 10 CV cycles and eventually to 8.9 nm after a series of potentiostatic holds was placed on the target electrode, where the depth profile was measured at several increasing and decreasing potentials equivalent to a charge–discharge cycle (Figure 59b).<sup>647</sup> These depth profiles indicate an increase in SLD for higher potentials and a decrease for lower potentials relative to Li/Li<sup>+</sup>. It should be noted that the subangstrom sensitivity of neutron reflectivity proves to be a “double-edged sword”. On one hand, it provides well-resolved information about the targets investigated; on the other, just like

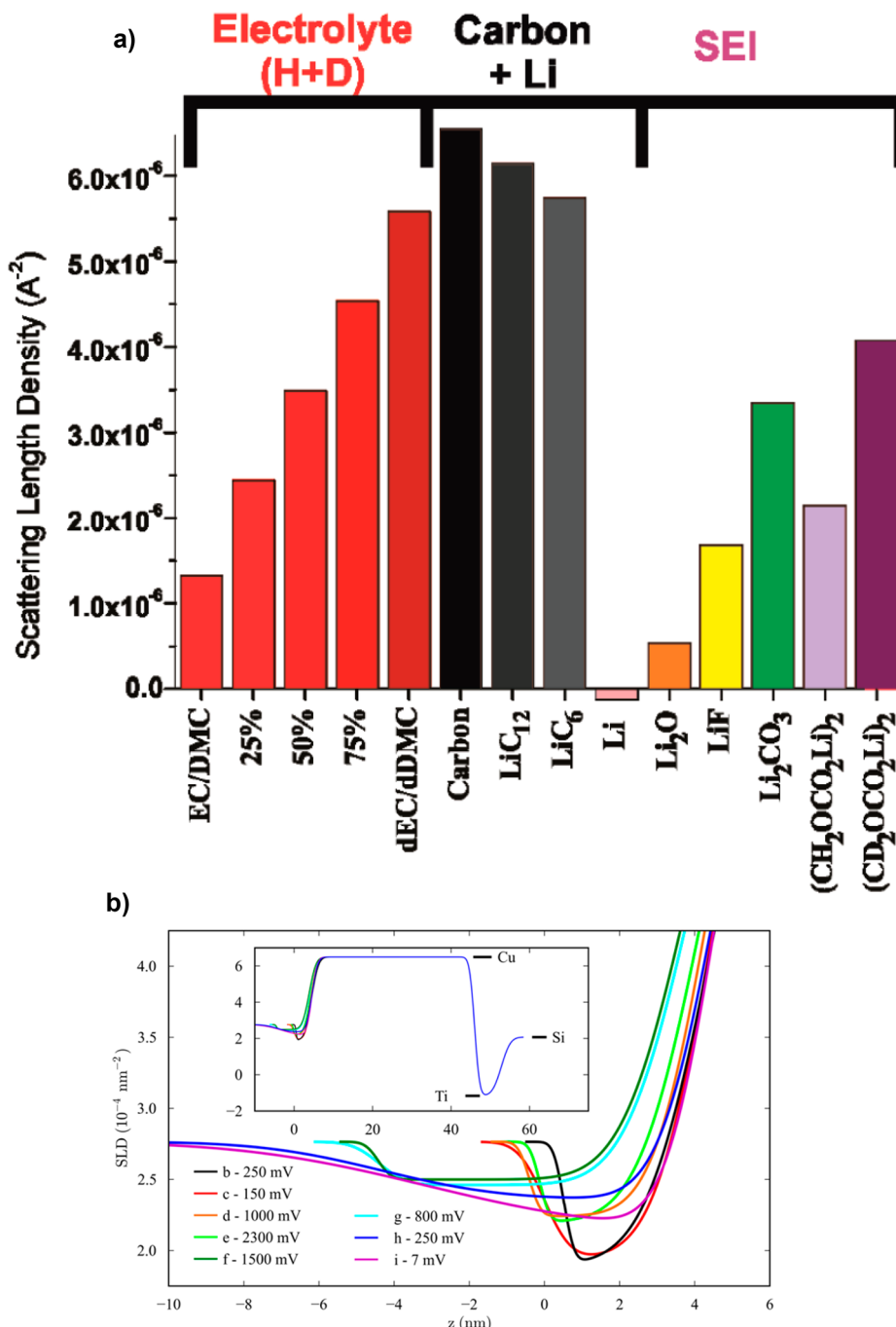


**Figure 59.** In situ investigation of SEI with neutron techniques: (a) distribution of Li salts across SEI formed on mesoporous carbon anode in electrolytes based on deuterated carbonates, as observed with small-angle neutron scattering (SANS); and (b) the fitted SLD profiles as a function of potential as measured by neutron reflectivity technique (NR) and the derived SEI thickness formed on Cu surface. Reprinted with permission from refs 646 and 647. Copyright 2012 American Chemical Society.

ellipsometry technique, it also imposes stringent, sometimes prohibitive, restrictions on the roughness of the target surface, which could be extremely difficult to satisfy. This latter feature severely limits the versatility of this powerful tool for both materials and environments close to real-life devices, and often shifts the focus on the experiments where useful information can be learned from idealized surfaces. Seeking a technique of both high resolution and high intolerance toward surface roughness, or at least finding a balance between, remains a challenge for neutron spectroscopists and battery/material scientists.

**5.3.5. Fluorescence.** It has been known from the Raman investigations of cathode materials that cathode/electrolyte interactions usually generated certain fluorescent species, which contributed to a high background and required nuanced spectra analysis and interpretation (Figure 60a).<sup>648,649</sup> While the identities of these fluorescent species remain unknown, Norberg et al. creatively leveraged this inconvenience and turned it into an unexpected in situ tool that not only visualizes “hot-spots” on cathode surfaces (Figure 60b) but also elegantly correlates the generation of these species with the oxidation of Ni sites on the surface of LiNi<sub>0.5</sub>Mn<sub>1.5</sub>O<sub>4</sub> cathodes

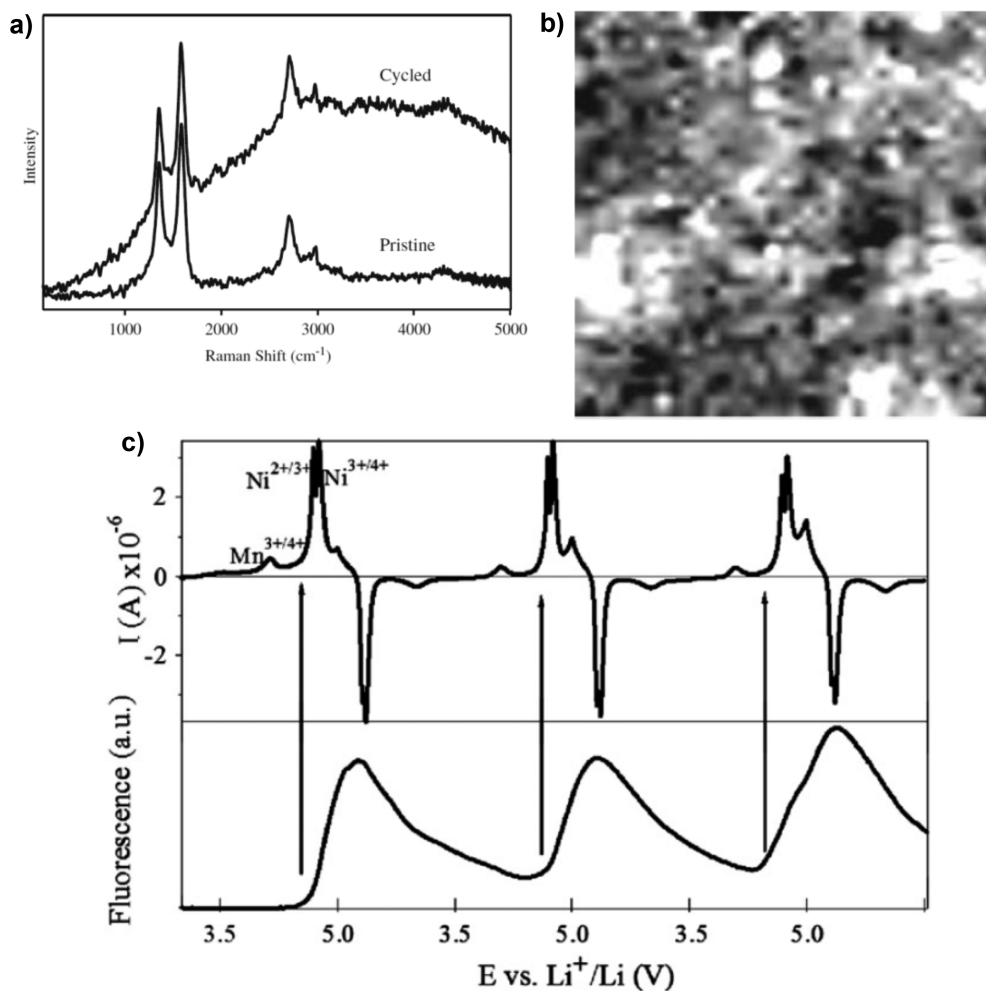


**Figure 60.** In situ investigation of cathode SEI with fluorescence: (a) Raman spectra of a pristine and cycled  $\text{LiNi}_{0.5}\text{Mn}_{1.5}\text{O}_4$  cathode. Note the higher fluorescent background of the cycled electrode due to electrochemical oxidation of electrolytes. (b) The corresponding fluorescent image of the cycled cathode surface. (c) The current and the integrated fluorescent intensity in an in situ cell as the  $\text{LiMn}_{1.5}\text{Ni}_{0.5}\text{O}_4$  cathode was cycled. Note the synchronized response between the two as Ni-sites experienced oxidations. Reprinted with permission from ref 627. Copyright 2013 Elsevier.

(Figure 60c).<sup>627</sup> By cycling a  $\text{LiNi}_{0.5}\text{Mn}_{1.5}\text{O}_4$  single particle in carbonate electrolytes, the rise in fluorescent intensity was found to be well synchronized with the oxidation of Ni(II) to Ni(IV). Because the distribution of fluorescent spots was not uniform on the cathode surface (Figure 60b), one could speculate that only the specific locations, where Ni sites were accessible to electrolytes, catalyzed the cathode/electrolyte reaction.

Although the identity of the fluorescent species has not been determined, the authors suggested that they might consist of transition metal ions complexed by organic species that decomposed oxidatively at these hot spots. Apparently these species, probably only existing as intermediates in the cell, can dissolve in bulk electrolyte and diffuse away, with their eventual fate being at the anode side where transition metal deposits.

**5.3.6. Electrochemical Quartz Crystal Microbalance.** Electrochemical quartz crystal microbalance (EQCM) monitors the mass increase on an electrode mounted on a piezo-crystal and relates it to the electric charge simultaneously passed through the electrode. This “electrogravimetric” analysis provides a rare combination of both quantitative and in situ capabilities, and has been applied extensively to investigations of those electrochemical phenomena that are sensitive to

changes in surfaces, such as corrosion, electroplating, electrolysis, as well as interphasial formation in LIB.<sup>631</sup> In the ideal situation, the increase of mass per charge (MPE) should exactly reflect the electrochemical reduction/oxidation stoichiometry, such as MPE = 6.9 for  $\text{Li}^+$ -intercalation into graphite electrode, or MPE = 80.9 for the formation of LEDC on graphitic surfaces, but such beauty of simplicity was almost never encountered; more often than not, precise assignment was difficult to make with EQCM results because of the complications in the oscillation frequency of piezo-crystals caused by multiple parasitic processes, such as their asymmetric mechanical stress or change in electrolyte viscosity near the vicinity of the electrode surfaces.<sup>633,650</sup>

In most cases, MPE detected during SEI formation was actually smaller than expected. For example, Larush-Asraf et al. compared the first cycle cathodic scan of Ni electrodes in various electrolytes, and determined MPE of 13–24 for  $\text{LiPF}_6$ , 12–25 for  $\text{LiClO}_4$ , and 17–45 for  $\text{LiBOB}$ ,<sup>491</sup> none of which corresponds to any known interphasial species of definite compositions. Li et al. reported similar results that EQCM failed to produce the corresponding MPE, whose values were lower than what was predicted theoretically, even though semicarbonates were identified by in situ microscope Fourier-transform infrared (MFTIR).<sup>651</sup> Only in the potential range

where SEI-formation was nearly completed could MPE start to approach 7, reflecting that the reduction/intercalation of Li<sup>+</sup> dominated the electrochemical process (Figure 61).<sup>650,651</sup>

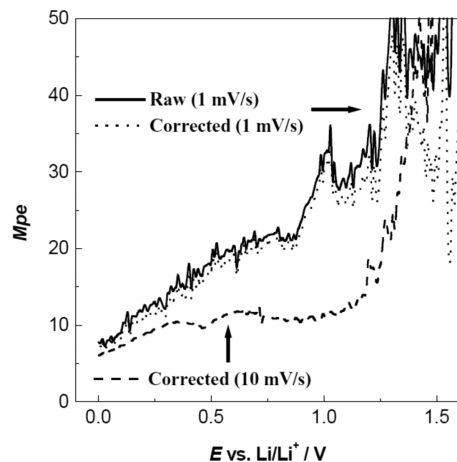


**Figure 61.** In situ investigation of SEI with electrochemical quartz crystal microbalance (EQCM): The dependence of mass accumulation per charge (MPE) on electrode potential during the first cathodic scan of a thin-film carbon electrode mounted on EQCM. Reprinted with permission from ref 650. Copyright 2004 Elsevier.

Nevertheless, rich qualitative information can still be extracted from EQCM experiments, such as the potential range where the main accumulation of mass occurs, the effect of electrolyte components on the possible thickness of interphases, or even how viscosity and ion conductivity changes near the electrode surfaces during charge and discharge.<sup>230,491,553,652</sup> For example, from Larush-Asraf et al.,<sup>491</sup> it is apparent that LiBOB would lead to a thicker SEI on graphite, which is consistent with previous studies' approach with other experimental means; meanwhile, the effect of additives on interphase formation could be evaluated in a more quantitative manner.<sup>230</sup>

**5.3.7. Scanning Probe Microscopy.** Scanning probe microscopy (SPM) covers a range of microscopic techniques where a physical tip is moved by piezoelectric actuators to probe the sample surface in a manner of raster scan, so that surface images of the sample could be generated by monitoring and analyzing the tip–surface interaction. The most conspicuous examples from the SPM family that are closely related to interphasial studies are scanning tunneling microscopy (STM), which measures the electronic current between the surface and the tip, and atomic force microscope (AFM), which measures force and has been shown to be useful in characterizing the surface topography.<sup>631</sup> The latter proved to be more useful, as in most cases one wants to keep the tip as a “neutral observer” instead of an “active participant” of the delicate imaging process. Like most of the high-resolution tools, both STM and AFM imposed stringent requirements on the low roughness of target surfaces, which restricted their application with real composite electrode materials used in LIB. Thus, thin-film electrodes prepared with various sputtering and vacuum deposition approaches were often used, while highly oriented pyrolytic graphite (HOPG), whose freshly cleaved surface often has atomic-flatness, provides a “close-enough” surrogate to graphitic anodes.

Beside other pioneers,<sup>646–655</sup> it was the contributions made by Inaba and Ogumi et al. that helped enable in situ

electrochemical STM and AFM as viable techniques for interphasial studies in liquid electrolytes.<sup>656,657</sup> Figure 62A–C shows topographs of HOPG surfaces during electrochemical lithiation in electrolyte based on EC/DEC as imaged by STM. Because the tip of STM requires the surface to be electronically conductive, only images above 1.1 V were available, which suggests that an electronically insulating layer (SEI or its precursor) should form at potentials below 1.0 V. Prior to the appearance of this interphase, hill-like features were observed near the edge sites with an increase of ~1.0 nm in interlayer spacing,<sup>657</sup> which could correspond to the formation of ternary intercalation compounds by solvated Li<sup>+</sup> as shown in Figures 45–47. Images under 1.0 V were provided by AFM (Figure 62d and e), in which depositions that smeared the originally clear images of HOPG surfaces were found on both basal and edge sites. These surface depositions could be scraped off by the AFM tip, constituting the foundation of SEI-thickness measurement practiced in most AFM work thereafter. Differentiations in interphases formed on basal against edge sites were also made by Domi et al., who used an edge-populated HOPG as a model graphitic anode, and found that, due to the higher reactivity, the formation of SEI was more complete at edge-sites during the first lithiation cycle.<sup>658</sup>

Although rough surfaces of composite electrodes presented severe challenges for obtaining clear images due to the presence of porous carbon conductive additives and polymeric binder, numerous efforts were still made to generate meaningful images.<sup>653,657,659,660</sup> This was generally achieved by selecting a certain graphite particle or flake near the surface of the composite electrode and then tracing its change during electrochemical lithiation (Figure 63a and b). Swelling of the particle edges was observed prior to lithiation at 1.1 V (Figure 63c), followed by thick interphasial deposition (Figure 63d). Jeong et al. further classified the graphitic structural changes in EC-based electrolyte into three types: (1) curling, (2) swelling, and (3) exfoliation, the competition among which determines the eventual passivation of graphitic edge sites against sustained electrolyte solvent cointercalation and reduction.<sup>660</sup> However, in PC-based electrolytes the corresponding cathodic scan was dominated by vigorous exfoliation and disintegration of the graphitic structure, as evidenced by the visible disappearance of certain edge steps at 0.90 V,<sup>660</sup> unless concentrated lithium salts were used to drastically reduce the number of PC molecules in the solvation sheath of Li<sup>+</sup>.<sup>583</sup>

The thermal stability of interphases at elevated temperatures was also evaluated with in situ electrochemical AFM. Edström et al. reported that the formed SEI on HOPG started thermal decomposition at around 50 °C, as evidenced by the growth of “blisters” across the surface.<sup>653</sup> Higher temperatures witnessed the significant decomposition of electrolytes, mainly concentrated at the edge sites (60–70 °C). Inaba further identified two distinct mechanisms of SEI-breakdown at elevated temperatures: (1) in the discharged state, apparent dissolution and agglomeration of interphase could be observed; (2) in the charged state, SEI significantly grew, accompanied by serious self-discharge of the lithiated graphite.<sup>661</sup> The presence of additives such as VC effectively suppressed these thermal degradations of SEI.

Beyond topographic images, AFM techniques were also used to extract more chemical, mechanical, or quantitative information about the interphases. For example, Ochida et al. used edge-dominated HOPG to investigate the effect of

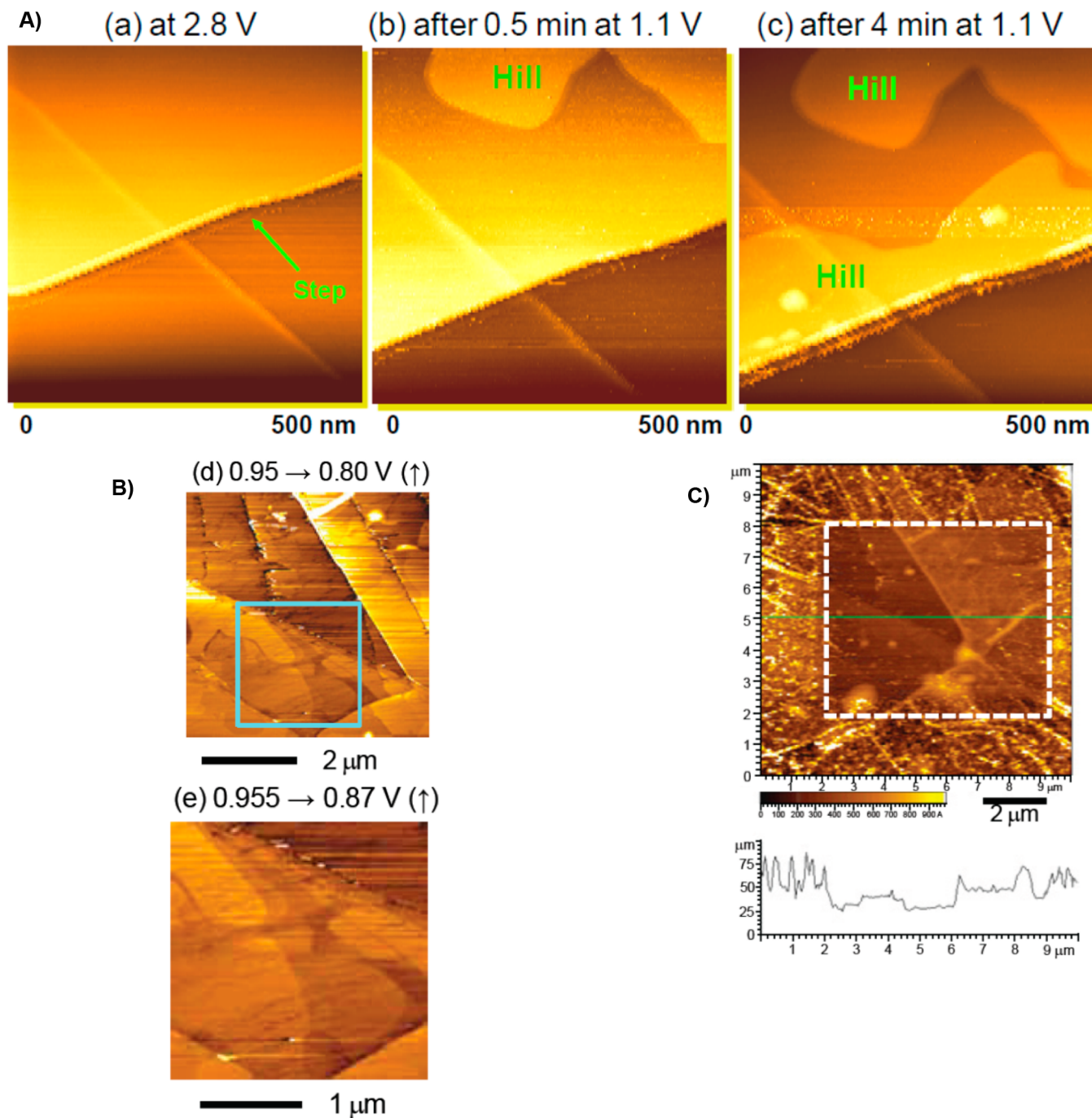


**Figure 62.** In situ investigation of SEI with scanning probe microscopes: (A) STM topographic images of a HOPG electrode at (a) 2.9 V, (b) 0.5 V, and (c) 1.1 V with 4 min holding in  $\text{LiClO}_4/\text{EC}/\text{DEC}$ . (B) Electrochemical AFM topographic images obtained under similar conditions. (C) Height profile of the interphase obtained at 2.9 V after the first cycle. Reprinted with permission from ref 659. Copyright 1997 Elsevier.

Mn-deposition on the SEI-degradation,<sup>662</sup> Zhang et al. measured the Young's modules of SEI formed on MnO anodes,<sup>663</sup> and Balke et al. mapped the dynamic distribution of ionic current across electrode surfaces in local regions at resolutions as high as 100 nm;<sup>664</sup> but among all, the most significant application of AFM technique is the measurement of SEI thickness, which has been based on the removal of interphasial species by the AFM tip in contact mode followed by the height measurement (Figure 62C).<sup>657,664</sup> The thickness thus measured ranged between 5 and  $10^2$  nm, with 20–40 nm as the most accepted values, depending on

graphitic surface, electrolyte composition, and especially additive chemistries.

This thickness measurement approach was increasingly challenged by the recent realization that these “removable” parts might not be the essential component of SEI that provides the protection.<sup>665–668</sup> At least in a few instances, it has been shown that there is no clear correlation between the electrochemical performance of the electrode and the “SEI thickness” as measured by AFM, and a decoupling exists between the “quality” and the “thickness”, as thinner SEI formed by certain additives could be actually harder to scrape

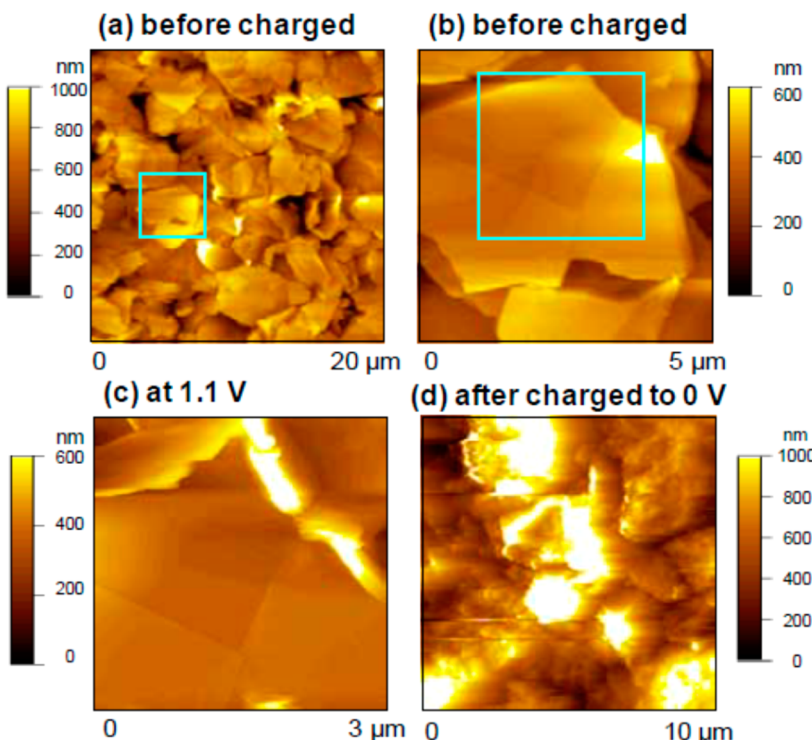


**Figure 63.** In situ investigation of SEI on composite graphitic electrodes with electrochemical AFM: topographic images obtained during and after cycling in LiClO<sub>4</sub>/EC/DEC. The squares in (a) and (b) indicate the areas under investigation in (b) and (c). Reprinted with permission from ref 660. Copyright 2003 Elsevier.

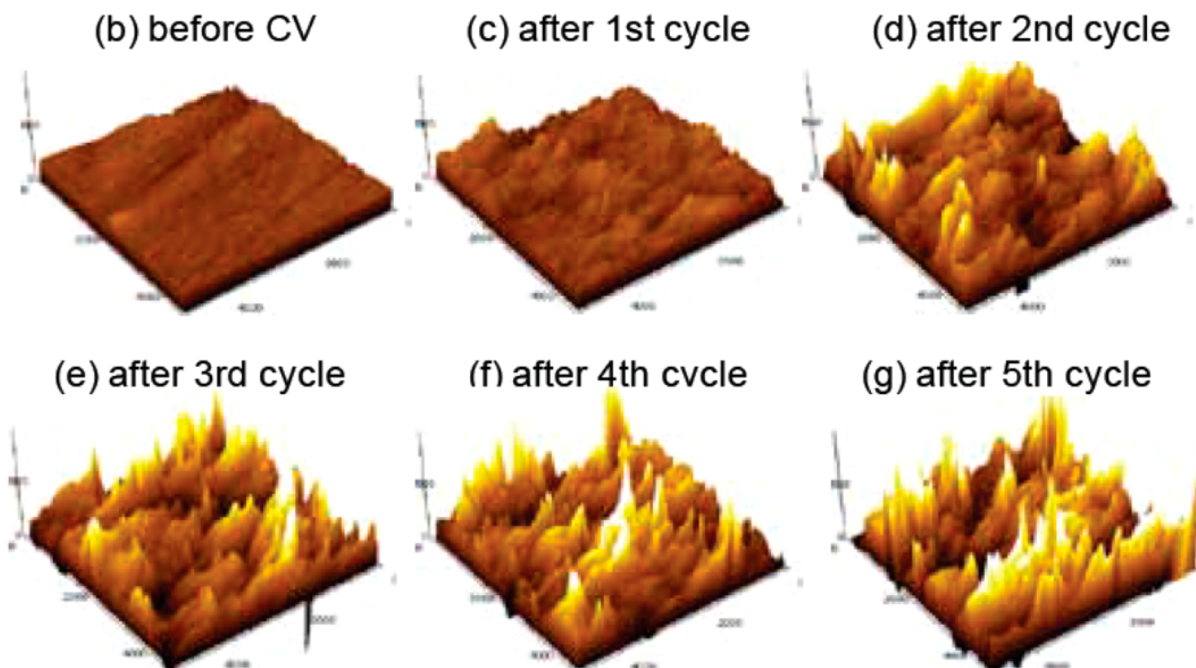


**Figure 64.** In situ investigation of SEI on Sn electrodes with electrochemical AFM: topographic images obtained during the cycling of Sn thin-film in LiClO<sub>4</sub>/PC. Note the dramatic roughening of the Sn surface, which was caused by electrode disintegration as well as SEI breaking and reformation. Reprinted with permission from ref 670. Copyright 2005 Elsevier.

with AFM tip.<sup>667</sup> Additionally, Cresce et al. showed that, even after repeated scanning, the “under-layer” of SEI remaining on the HOPG surface was still distinctly different in chemical composition from the pristine surface according to XPS,<sup>669</sup> while Domi et al.<sup>665,666</sup> and Tsubouchi et al.<sup>667</sup> reported that this “under-layer” actually could still serve as passivating layer.

All of these findings suggested that the SEI-thicknesses previously reported with AFM approaches probably should be reexamined.

The lithiation of alloy-type anodes such as Sn- or Si-based materials was also visualized with in situ AFM, which were typically characterized by a drastic volume change.<sup>665,668,670</sup>

As Figure 64 shows, a significant increase of surface roughness occurred on Sn during the electrochemical cycling, and the accompanied breaking and reformation of interphases along with the mechanical disintegration of the electrode apparently accounted for the loss of capacity.<sup>657</sup> Tokranov recently revisited Si surface with an *in situ* AFM technique of higher resolution, and revealed that, while most reductive processes occur at ~0.60 V vs Li before Si is lithiated, the quality of the interphase depended critically on the rate of its formation; that is, faster lithiation led to thinner and smoother SEI.<sup>671</sup> Even though this initially formed SEI would inevitably subject to physical disruption by the expanding/contracting electrodes upon cycling, some of its legacy would still remain after subsequent cyclings.

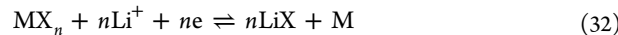
## 6. ELECTROLYTES AND INTERPHASES IN "BEYOND Li-ION" CHEMISTRIES

The intrinsic limit on LIB energy density was imposed by the masses of the "inert" intercalation hosts (cf, Whittingham in this issue). The ratio of this parasitic weight to active ingredient (i.e., Li<sup>+</sup>) is especially high on the cathode side, where typically only one Li<sup>+</sup> could be accommodated per transition metal element in the fully lithiated state. To break through this limit, numerous efforts have been made in recent years to seek cathode chemistries beyond that of Li<sup>+</sup>-intercalation, where inert masses could be kept to a minimum.<sup>14,17,672</sup> Li/sulfur and Li/air systems represent extreme cases of these chemistries in which host weight is essentially zero and the energy densities boast to approach >10 000 Wh/kg. Less ambitious chemistries with storage mechanisms of conversion-reaction or multivalent ion (Mg<sup>2+</sup>) pursue the same goal by leveraging multielectron reactions, promising energy densities up to 500 Wh/kg. Alternatively, other battery chemistries that emphasize low cost or environmental friendliness (instead of high energy density) were also actively sought after, with the projected application mainly concentrated in the areas where the volume or weight of the batteries were no longer of primary concern due to their stationary nature, but their sheer scale (>MWh) sets severe restrictions on the cost-effectiveness, safety, as well as environmental impact. Examples of such applications include energy-storage components for grid-stabilization or renewable energy harvest system for intermittent sources (e.g., solar, wind, and ocean wave), and examples of such chemistries include ambient temperature Na-ion intercalation<sup>672,673</sup> and dual-ion intercalation systems.<sup>674,675</sup> While the majority of these "beyond Li-ion" devices face challenges in the chemistry and synthesis of electrode materials, the surfaces of these new materials often induce new interphasial processes when in contact with electrolyte components, and the carbonate-based electrolyte systems inherited from LIB have to be adjusted. Understanding the interactions between these new materials and electrolytes and the concomitant interphases would play significant roles in determining their future success.

With dedicated chapters on these advanced battery chemistries in this issue (cf, Luntz et al. for Li/O<sub>2</sub> chemistry, Manthiram et al. for Li/S chemistry, Komaba et al. for Na chemistry, and Muldoon et al. for multivalent ion chemistry), this section will only discuss the work concerning electrolyte and interphase in these systems.

### 6.1. Conversion-Reaction Chemistry

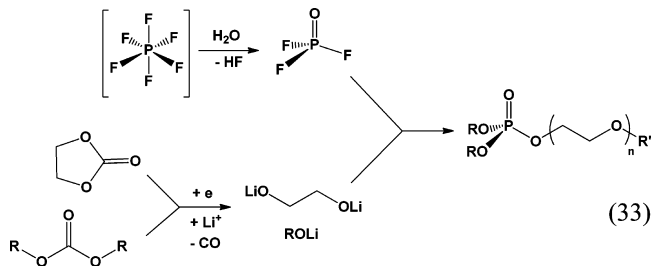
This new rechargeable chemistry consists of a reversible redox process, during which the metal oxides, sulfides, or fluorides were reduced into nanodomains of transition metal clusters and lithium oxide/sulfide/fluoride upon discharging and vice versa upon charging:



where M was a transition metal such as Fe, Cu, or Co, etc.; and X = 1/2S<sup>2-</sup>, 1/2O<sup>2-</sup>, or F<sup>-</sup>, with n = 2 or 3. This chemistry apparently benefited from the ability to accommodate more than one Li<sup>+</sup> per transition metal core in the reaction, and the nanostructured material was considered the key to its rechargeability.

Among the many issues that still plague their commercialization, instability of electrolyte components on these newly formed nanocrystalline transition metal surfaces contributed significantly to the poor cycle life and hysteresis between charge and discharge potentials, in addition to the intrinsic electrochemical irreversibility associated with breaking/reforming of M-X bonds in each cycle. It has been reported that polymeric species were formed in the initial discharge,<sup>676–680</sup> which has been attributed to the reduction of carbonate molecules. Perhaps because of the catalyst effect of these nanotransition metal particles, the reductive decomposition of carbonate molecules occurred at much higher potential (~2.0 vs 0.80 V on graphitic anode).<sup>680</sup> More interestingly, it has been noticed that in some cases the polymeric species on electrode surfaces would disappear upon recharge,<sup>679,681</sup> while exceptions did exist.<sup>672</sup> It is unclear what these polymeric species were.

On the other hand, Laruelle et al. succeeded in identifying a series of phosphate esters of varying lengths in the interphases formed on conversion-reaction CoO<sub>x</sub>, which seemed to be the esterification products between phosphoryl fluorides POF<sub>3</sub> and PEG-like alkoxides,<sup>681</sup> with the former generated from PF<sub>6</sub><sup>-</sup>-anion by moisture and the latter from the radical-induced decarbonylation of cyclic or linear carbonate molecules (eq 33):



Strangely, similar esterification processes were never reported in interphases of LIB, although both POF<sub>3</sub> and alkoxides should be present in the system.

Contrary to the indispensability of EC in LIB, Gmitter et al. reported that linear carbonate performed more stably on nanocrystalline Bi.<sup>679</sup> This observation was echoed by Oh et al.,<sup>680</sup> although the linear carbonates were still not an ideal solution to the performance difficulties of these conversion-reaction chemistries because of the high charging potential (>4.0 V). Gmitter suggested that noncarbonate electrolytes such as ethers, nitriles, or ionic liquids be explored for conversion-reaction systems instead.

### 6.2. Li/O<sub>2</sub> or Li/Air Chemistry

As a member of the broad metal-air battery family, Li/air system has been investigated as a primary cell chemistry since

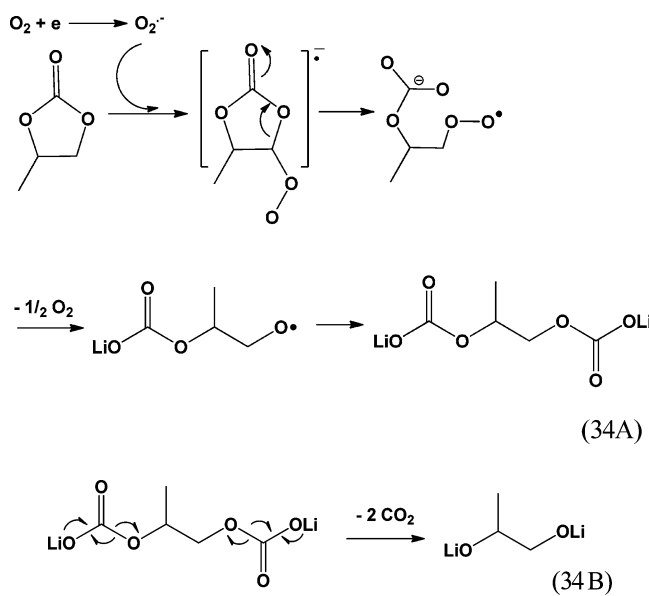
the mid 1990s.<sup>682,683</sup> The recent revival of interest in this chemistry was sparked by the discovery that it could become rechargeable under certain conditions,<sup>5,684</sup> providing the possibility of a “super battery” whose promised theoretical energy density approaches that of gasoline in an internal combustion engine (13 000 Wh/kg).<sup>685</sup> This expectation was enabled by the fortuitous combination of facts that Li anode is the metal with the smallest gravimetric density and the lowest atomic number, and that the active cathode material ( $O_2$ ) is stored in the ambient and often not counted as part of device mass. In reality, however, the above optimistic number is often decimated by practical considerations to exclude the invasive nature of ambient air (moisture,  $CO_2$ , etc.), leading to the most frequently described configuration of Li/ $O_2$  cell. In addition to the numerous materials challenges faced by a Li/air or Li/ $O_2$  cells, such as catalysts on the gas cathode, the protection of Li metal anode, and the stabilization of  $O_2$ -reduction product at the desired stage (i.e.,  $Li_2O_2$  instead of  $Li_2O$ ), electrolytes were generally considered as a key element that affects or even determines the device performance in terms of chemical/electrochemical reversibility, cycle life, rate capability, as well as energy efficiency. An ideal electrolyte for Li/air system is expected to possess, besides what LIB electrolytes must possess, (1) high  $O_2$  solubility and mobility; (2) high chemical stability toward peroxide ( $Li_2O_2$ ), superoxide ( $LiO_2$ ), and other highly reactive intermediates; and (3) tolerance against dendrite growth at the metallic lithium anode. Numerous studies have been carried out to understand the bulk and transport properties of Li/ $O_2$  cell electrolytes, such as viscosity/ion conductivity,  $O_2$  solubility/diffusivity, solvent polarity/contact angle on carbonaceous air cathode, and their relation to the population of triphase sites, in various systems based on polymer-gel,<sup>682,686</sup> carbonates,<sup>683,684,687</sup> ethers,<sup>688</sup> and ionic liquids.<sup>689</sup> The most recent focus has been on the suitability of polar/aprotic compounds serving as nonaqueous electrolyte solvents in Li/air devices due to their chemical reactivity with peroxides and superoxides. While this work from a fundamental perspective provided generally useful guidelines in selecting new electrolyte components for Li/ $O_2$  chemistry,<sup>690–696</sup> actual device testing might deviate and present surprises.

**6.2.1. Carbonates and Ethers.** As state-of-the-art electrolyte components, carbonates were naturally tested as the default solvent for Li/ $O_2$  chemistry, but their chemical stability against the highly reactive intermediates was soon found to be an issue.

Freunberger et al. reported that during the initial discharge of oxygen, the formed superoxide radical  $O_2^{\bullet-}$  would attack carbonate molecules as a strong nucleophile, initiating their reductive breakdown into semicarbonates via a carbonate-peroxide intermediate (eq 34A).<sup>690</sup>

While the above reduction process is somehow similar to what happens on graphitic surface in LIB, it should be noted that semicarbonate in this case is formed on the surface of cathode instead of anode. Therefore, the formed LPDC will oxidatively decompose upon recharging to >4.0 V (eq 34B).

Equations 34A and 34B only showed representative reduction and oxidation products, while the actual chemistries might be more complicated, leading to a mixture of inorganic species such as  $Li_2CO_3$ , carboxylate,  $Li_2O$ , etc., along with  $H_2O$  and  $CO_2$ . Freunberger et al. believed that the above process occurred in every charge/discharge cycle on the air cathode, until all electrolytes were consumed. On the other hand, the formation of alkoxides eventually led to a thick gel coating on



the Li anode surface. These irreversibilities in the chemistry were in part responsible for the significant voltage hysteresis usually observed in the Li/air system, in addition to the kinetic barriers introduced by catalyst inefficiency. Probably what matters in the above irreversible process is not only the compromised reversibility of cell reaction, but its sustainability, because in at least a few cases what was reported as the cell capacity turned out to be contributed from the irreversible decomposition of electrolyte components.

This instability of carbonate solvents was further confirmed by other researchers. McCloskey et al. labeled organic solvents with  $^{18}O$ -isotope and used differential electrochemical mass spectrometry to monitor the gaseous products generated during the cycling.<sup>691</sup> They found that carbonate molecules irreversibly decomposed upon discharge, with negligible signs of peroxide detected, while DME remained stable against peroxides (Figure 6SA and B); upon charge, however, DME would be oxidized by the oxygen released from peroxide, in good agreement with the knowledge about excellent cathodic but poor anodic stabilities of ethereal compounds.<sup>1</sup> Xu et al. further confirmed with synthesized standard reference compounds LEDC and LPDC that these semicarbonates could indeed be electrochemically oxidized upon charge, releasing both  $CO_2$  and  $CO$ ,<sup>692</sup> and concluded that the reversibility of Li/ $O_2$  chemistry previously observed in carbonate-based electrolytes was actually constructed on the unsustainable basis of consuming carbonate solvents. In particular, the high reactivity of superoxide  $O_2^{\bullet-}$  toward organic polar solvents, which often possess electrophilic centers by nature, presented the most severe challenge.<sup>693</sup> Takechi et al. echoed with the observation that the combination of  $Li^+$  and  $O_2^{\bullet-}$  makes an especially reactive species toward most solvents,<sup>694</sup> while peroxide ( $Li_2O_2$ ), according to Chalasani et al., seemed to pose no apparent nucleophilic attack on most carbonate or non-carbonate solvents up to 55 °C.<sup>695</sup>

Although still not ideal in terms of anodic stability, ethers did serve as better solvents than carbonates, and most of the promising cycling data were generated from tetraglyme because it seemed to favor the formation of  $Li_2O_2$  as the main discharged product.<sup>696–700</sup>

On the other hand, numerous studies revealed that the linear ethers such as tetra- or triglymes did react irreversibly during

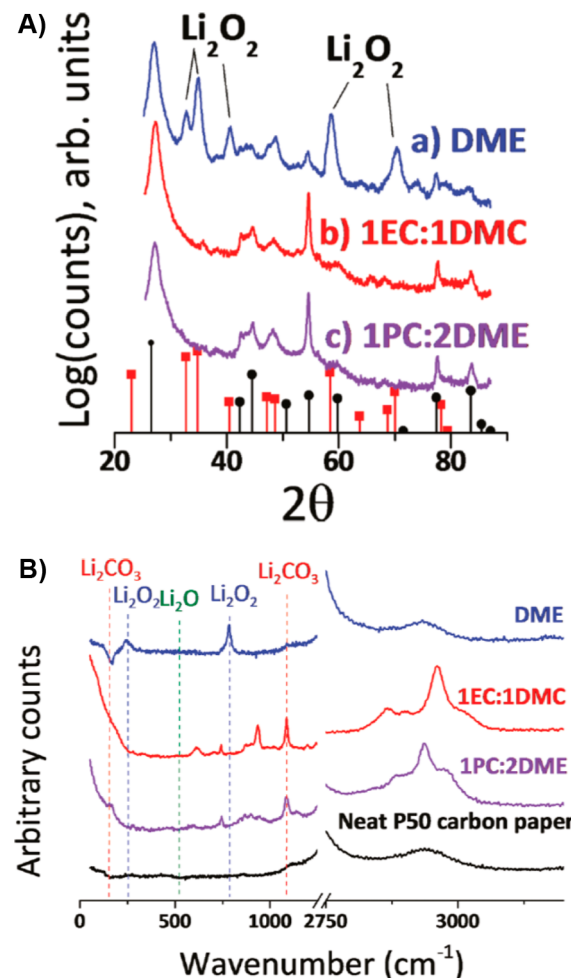
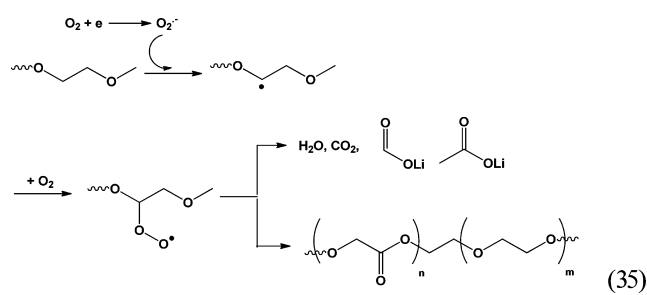


**Figure 65.** Electrolytes in Li/O<sub>2</sub> batteries: (A) XRD patterns of discharged carbon cathodes from cells cycled in electrolytes based on (a) DME, (b) EC/DMC (50:50), and (c) PC/DMC (50:50), respectively; and (B) Raman spectra of the above carbon cathodes. Reprinted with permission from ref 691. Copyright 2011 American Chemical Society.

the discharge. On the basis of FTIR, Freunberger et al. proposed a mechanism, in which ether peroxide was formed as intermediate as result of H-abstraction by superoxide radical, and eventually led to carboxylates, polyether/esters, and CO<sub>2</sub> (eq 35):<sup>696</sup>



Ryan et al. drew similar conclusions on the instability of ether.<sup>701</sup> Sharon et al. used EQCM to monitor the reaction process *in situ*, and confirmed the formation of lithium superoxide (LiO<sub>2</sub>) during the initial discharge between 2.7–2.5 V (MPE ~39.28), and the subsequent formation of peroxide (Li<sub>2</sub>O<sub>2</sub>) between 2.3–2.0 V (MPE ~20.94);<sup>702</sup> however,

further analyses in conjunction with a series of ex situ tools convinced them that polyethers were intrinsically unstable for Li/air batteries during long-term cycling. This conclusion was supported by Barile et al., who found that, regardless of what catalyst is used at the cathode, the amount of oxygen produced upon charge was always substantially less than expected from complete Li<sub>2</sub>O<sub>2</sub> oxidation.<sup>703</sup> Therefore, they also believed that tetraglyme was not a suitable solvent for this cell chemistry. The stark contrast between the conservative assessments and optimistic reports in the same electrolytes<sup>698,700</sup> reflected what a highly dynamic field the Li/O<sub>2</sub> battery is.

### 6.2.2. Other Solvents and Polymer Electrolytes.

Besides carbonates and ethers, McCloskey et al. screened diversified organic polar solvents including nitriles, sulfoxide, lactam, and ionic liquid as well as a wide spectrum of lithium salts using the combination of computational and experimental approaches. They reported that none of these electrolytes was truly “rechargeable”.<sup>704</sup> It seems that the two constraints that an ideal Li/air electrolyte solvent must satisfy simultaneously are often inversely correlated, that is: (1) low electrophilicity to remain stable against the attack from strong nucleophiles such as superoxide O<sub>2</sub><sup>•-</sup> and (2) high ionization to remain stable against oxidation. Ethereal and ester compounds serve as examples at two extremes of these paradoxical criteria, as the former were generally less susceptible to nucleophilic attack from O<sub>2</sub><sup>•-</sup> but vulnerable to oxidation, while the latter were known for better anodic stability against oxidation but reacted readily with O<sub>2</sub><sup>•-</sup>. Other requirements such as solubility and transport properties of salt and oxygen just add to the already stringent requirements.

Among these nonconventional electrolyte solvents, perhaps dimethyl sulfoxide (DMSO) was the most reported.<sup>694,699,705–708</sup> The formation of peroxide Li<sub>2</sub>O<sub>2</sub> seemed to be favored in DMSO as evidenced by cyclic voltammetry using rotating disc electrode (RDE), while the kinetics of its reoxidation was much facilitated. The best results indicated ~95% capacity retention within 100 cycles if a porous gold electrode, a catalyst itself, was used,<sup>706</sup> and the charge-discharge hysteresis was also improved as compared to other nonaqueous electrolyte systems.<sup>708</sup> Trahan et al. attributed the latter benefit as a result of the stabilization of superoxide radical species (O<sub>2</sub><sup>•-</sup>) by solvated Li<sup>+</sup> in DMSO.<sup>708</sup>

Various ionic liquids were also employed as electrolyte solvents for Li/O<sub>2</sub> chemistry,<sup>694,699,709,710</sup> with varying results. De Giorgio et al. reported that the use of pyrrolidinium-based RTIL led to comparable performance with ether-based electrolytes according to cyclic voltammetry,<sup>709</sup> while the stability of RTIL in longer term against superoxide species was more thoroughly investigated by Hayyan et al., who screened a series of RTIL based on piperidinium, pyrrolidinium, and phosphonium.<sup>710</sup> The suitability of these RTIL as electrolyte in actual Li/O<sub>2</sub> devices is yet to be confirmed.

Blended electrolytes using carbonate and RTIL were proposed by Kim et al., who believed that at optimum ratios PC and a pyrrolidinium-based ionic liquid functioned complementarily to each other.<sup>711</sup> While the RTIL has been known to be more stable against the nucleophilic attack from superoxide species, the presence of such RTIL in blended electrolytes apparently suppresses the decomposition reactions of carbonate, as indicated by the reduced presence of Li<sub>2</sub>CO<sub>3</sub> in Figure 66a. On the other hand, more polar but less viscous carbonate solvents would improve the charge (Li<sup>+</sup>) and mass (O<sub>2</sub>) transport properties of the blended system. A synergistic

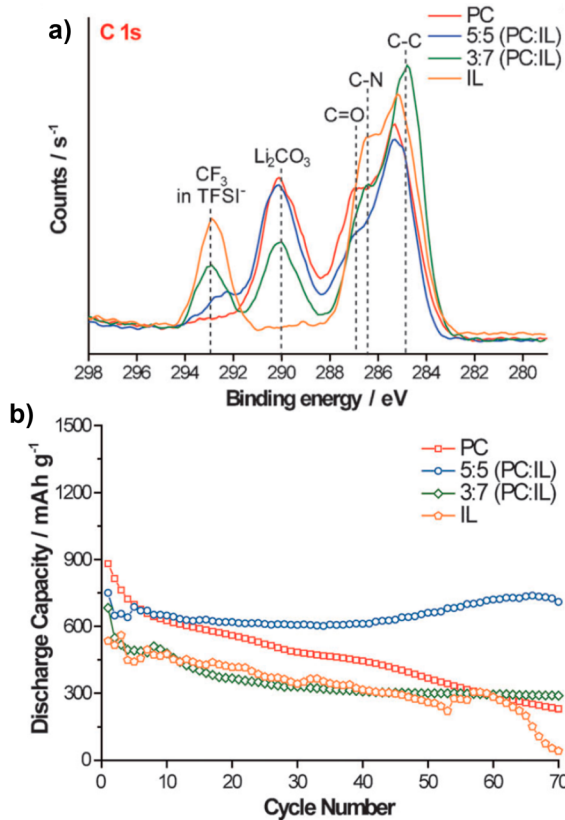


**Figure 66.** Electrolytes in  $\text{Li}/\text{O}_2$  batteries: (a) C 1s XPS of carbon air cathode in the discharged state after being cycled in various electrolytes based on carbonate, RTIL, or a blend of both; and (b) cycling performance of the systems in (a). Reprinted with permission from ref 711. Copyright 2013 Wiley-VCH Verlag GmbH & Co. KGaA, Weinheim.

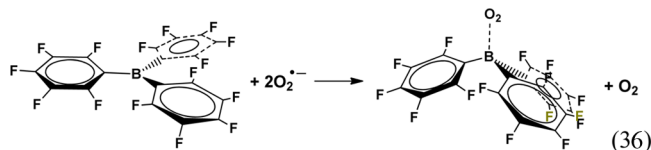
effect was achieved at equi-weight ratio of PC/RTIL, as shown in Figure 66b.

Using DFT, Bryantsev et al. screened a vast family of solvents, and based on the complementary cyclic voltammetry experiments suggested N-containing solvents such as amides, lactams, and nitriles<sup>712,713</sup> as stable supporting electrolytes for the  $\text{Li}/\text{O}_2$  system. Linear amides such as dimethylacetamide (DMA) showed superior stability against superoxide radical species,<sup>714</sup> but this class of compounds was known for their inability to form a protective SEI on the metallic lithium surface. While  $\text{LiNO}_3$  as electrolyte solute helped protect lithium due to the formation of a dense layer of inorganic compounds rich in N–O on anode,<sup>714,715</sup> fluorinated amides were used as additive in amide-based electrolytes, whose reduction to  $\text{LiF}$  prevented sustained reduction of amide solvents.<sup>715</sup> However, despite the encouraging voltammetric data, the suitability of these new solvents is yet to be confirmed in actual  $\text{Li}/\text{O}_2$  cells. Chen et al. described another member of the family, dimethylformamide (DMF), as electrolyte solvent.<sup>716</sup> Although reversible formation/reoxidation of  $\text{Li}_2\text{O}_2$  dominated the initial charge/discharge cycles, irreversible decomposition of DMF increased with cycling while generating lithium formate, carboxylate, and NO on the cathode surface. Considering the intrinsic reactivity of amide compounds toward metallic lithium, the suitability of amide-based electrolyte is still in question. Similar conclusions were drawn for siloxane,<sup>701</sup> acetonitrile,<sup>699</sup> and phosphate,<sup>699</sup> despite their obvious stability against superoxide or peroxide species in

short-term experiments such as voltammetry.<sup>717,718</sup> On the other hand, Zheng et al. demonstrated that under certain conditions potential benefits could be obtained even from acetonitrile, which was well-known for its reactivity with metallic lithium.<sup>719</sup> Upon mixing with carbonate solvent that can effectively passivate Li surface, a blend electrolyte based on acetonitrile results in substantially improved  $\text{O}_2$  solubility and diffusivity.

To circumvent the instability of organic solvents toward superoxides, polymer structures including natural rubber, PVDF-HFP, as well as polyether were introduced as macromolecular electrolyte components, either as the only solvent (as in SPE) or as mechanical skeleton to be gelled by small organic solvents (as in GPE).<sup>720–724</sup> Although some of these polymers did exhibit certain advantages, such as improved stability toward the highly reactive intermediates during cycling, their overall performance in  $\text{Li}/\text{O}_2$  cells did not match their liquid counterparts.

**6.2.3. Additives.** There were only limited reports where additives were used to improve the performance of  $\text{Li}/\text{O}_2$  batteries (Table 31). Xu et al. used crown ethers of varying sizes in electrolytes and found that 12-crown-4 and 15-crown-5 were effective in improving discharge capacity when used at 15%, while 18-crown-6 showed negative impact.<sup>725</sup> They attributed the size effect to their individual ability of solvating  $\text{Li}^+$ , which may have assisted in dissolving the discharge products  $\text{Li}_2\text{O}_2$  and prevented it from clogging the porous structure on the air cathode. Similar results were observed when the anion receptor tris(pentafluorophenyl) borane was used, which served as a strong coordinator to the peroxide anion  $\text{O}_2^{2-}$ .<sup>687,709,726</sup> The corresponding boron–peroxide complex was believed to promote the reoxidation of peroxide with better kinetics (eq 36):<sup>726</sup>



Leveraging the known ability of fluorinated compounds in dissolving  $\text{O}_2$ , a few studies explored partial- or perfluorinated compounds as additive to increase  $\text{O}_2$ -solubility in the nonaqueous electrolytes, which include fluorinated phosphite and phosphate reported by Zhang et al.,<sup>727</sup> and tris-(perfluorobutyl) amine reported by Wang et al.<sup>728</sup> Because the oxygen-reduction process in nonaqueous media is often diffusion-limited, significant increase of oxygen concentration in the electrolyte resulted in substantial improvements in both capacity utilization and rate capability.

Efforts were also made to stabilize the highly reactive superoxide and peroxide species, so that the oxygen reduction process could stop at the desired stage instead of proceeding to the oxide or carbonate species that are either very difficult or impossible to reoxidize. Laoire et al. described that superoxide  $\text{O}_2^{2-}$  could be effectively stabilized by ammonium cation, making this highly reactive species “long-lived”, and led to an oxygen-reduction process dominated by single-electron reduction.<sup>705</sup> When ammonium cation was replaced by  $\text{Li}^+$ , however, stepwise reduction occurred, leading to peroxide or oxide in an irreversible or quasi-reversible process. These authors believed that, according to Pearson’s hard soft acid base (HSAB) model, the “soft–soft” interaction within the ammonium–superoxide

Table 31. Additives for Primary/Rechargeable Li/O<sub>2</sub> Chemistry

Additives	Properties Targeted
12-crown-4 15-crown-5 18-crown-6	Li <sup>+</sup> coordination
tris(pentafluorophenyl) borane	Li <sub>2</sub> O <sub>2</sub> solubility
tris(2,2,2-trifluoroethyl)phosphate tris(2,2,2-trifluoroethyl)phosphite	O <sub>2</sub> solubility and diffusivity
perfluorotributylamine	O <sub>2</sub> solubility and diffusivity
tetrabutyl ammonium hexafluorophosphate	superoxide (O <sub>2</sub> <sup>•-</sup> ) stabilization
tetrabutyl ammonium triflate	Li <sub>2</sub> O <sub>2</sub> solubility
tetrathiafulvalene	redox mediator

complex should account for its stability and the ensuing electrochemical reversibility. Zhang et al. also reported the use of an ammonium salt with similar effects (Table 31), who rationalized from the angle of phase-transfer the capability of ammonium in ferrying O<sub>2</sub><sup>•-</sup> into the liquid phase.<sup>729</sup> The consensus shared by Laoire et al. and Zhang et al. was to remove O<sub>2</sub><sup>•-</sup> from the air cathode surface, so that its further reduction into harder-to-recharge products be circumvented.

Chen et al. reported an additive as redox mediator for Li/O<sub>2</sub> battery, which would help promote charge-transfer kinetics between the formed oxygen reduction products (such as Li<sub>2</sub>O<sub>2</sub>) and carbonaceous air cathode.<sup>730</sup> The conjugated structure of

tetrathiafulvalene (TTF) makes it a redox-active molecule with excellent reversibility at potentials higher than 2.95 V, where Li<sub>2</sub>O<sub>2</sub> oxidizes (Table 31). The presence of the TTF significantly improved the cell performance, as evidenced by the high rate capability as well as the decreased charge/discharge hysteresis, and its stability has been proved in a DMSO-based electrolyte over 100 cycles. The possibility of TTF interacting with metallic lithium anode has to be considered for longer-term applications.

**6.2.4. Li Salts.** The effect of lithium salts on Li/O<sub>2</sub> chemistry does not seem to be as obvious in LIB. Almost all lithium salts known to LIB researchers have been used, with slight preference for Li triflate, LiTFSI, and LiClO<sub>4</sub>, apparently for their insensitivity toward moisture. Regarding their chemical stability, Chalasani et al. reported that most commonly used lithium salts were stable against the nucleophilic attack of peroxide (Li<sub>2</sub>O<sub>2</sub>), with the exception of LiPF<sub>6</sub>, which rapidly broke down into LiF and oxyphosphate salt.<sup>693</sup>

Younesi et al. used LiB(CN)<sub>4</sub> (Table 12) as the main salt in ether-based electrolyte for Li/O<sub>2</sub> cell and described its rapid decomposition during the cell cycling.<sup>147</sup> Nasybulin et al. systematically evaluated a series of lithium salts and concluded that the decomposition of solvent outweighed that of lithium salts, although the surface analyses by XPS, XRD, and NMR did show significantly different discharge products when lithium salts varied.<sup>731</sup> Among the seven salts investigated, they found that most (LiTFSI, LiTf, LiPF<sub>6</sub>, LiClO<sub>4</sub>, and LiBr) favored the formation of Li<sub>2</sub>O<sub>2</sub>, while LiBF<sub>4</sub> and LiBOB dominated the cathode with their own decomposition products: the former leading to LiF and the latter to oxalates. Similar work performed by Veith et al. also revealed the effect of salt reduction products on the cycling performance of Li/O<sub>2</sub> chemistry.<sup>732</sup> Among the four salts studied, LiClO<sub>4</sub> seemed to be the least reactive. These authors suggested that the previous studies may have overlooked the possibility of salt anions being attacked by peroxide or oxygen, and emphasized that understanding the role of salt anions would more effectively help in designing and developing better electrolytes for Li/O<sub>2</sub> batteries.

**6.2.5. Potential Safety Concern of Li/O<sub>2</sub> Chemistry.** While most current efforts on Li/O<sub>2</sub> battery focused on how to improve the rechargeability of this promising chemistry by keeping the reduction of oxygen at metastable stages of superoxide (O<sub>2</sub><sup>•-</sup>) or peroxide (O<sub>2</sub><sup>2-</sup>) without forming the more stable but nonrechargeable oxide (O<sup>2-</sup>), it should be brought to attention that these incomplete reduction species of oxygen, or their reaction products with organic solvent molecules, pose certain potential risks. Ether compounds were known to form peroxides upon long-term storage in the presence of oxygen, and their explosive nature has been the major topic of safety training for Chemistry freshmen; esters or related carbonyl-containing compounds are not any safer either, with acetone as a typical representative, whose peroxide trimer has been used as one of the primary high explosives.

Usually the peroxide species are on the list of chemicals to avoid, but in Li/O<sub>2</sub> chemistry they are either the intended or the inevitable products if the electrochemistry proceeds as desired. Furthermore, during the complicated interactions between the reduced oxygen species and the electrolyte or electrode components, the possibility of forming compounds of similar or even higher instability cannot be excluded. The combination of these species with the most energetic anode material (metallic lithium) and inflammable nonaqueous

electrolytes makes the general safety of Li/O<sub>2</sub> chemistry a legitimate concern, as with any high energy density battery chemistry. The research on small lab devices has thus far found low risk associated with the chemistry, but when the performance of Li/O<sub>2</sub> or Li/air batteries reaches a certain maturity for practical deployment, their safety has to be more rigorously examined before substantial scale-up efforts are made.

### 6.3. Li/S Chemistry

The high abundance of sulfur in the Earth's crust makes it a low-cost cathode candidate of high specific capacity (1675 mAh/g), which promises a theoretical specific energy of 2500 Wh/kg (or 2800 Wh/L) assuming a complete reduction of sulfur to sulfide (S<sup>2-</sup>) with metallic lithium anode. A series of intermediates (S<sub>8</sub><sup>2-</sup>, S<sub>6</sub><sup>2-</sup>, S<sub>4</sub><sup>2-</sup>, S<sub>3</sub><sup>2-</sup>, and S<sub>2</sub><sup>2-</sup>) often form, corresponding to varying stages of incomplete reductions. Unlike their oxygen counterparts, these intermediates were not of particularly high reactivity toward solvent molecules, partially due to the better charge-delocalization in these polyatomic anions as well as their higher solubility in organic media. Even the final reduced form (S<sup>2-</sup>) could be rechargeable given sufficient electronic accessibility; therefore, the difficulties encountered in Li/O<sub>2</sub> chemistries, such as painstaking maintenance of electrochemical reactions at certain stages, no longer exist. However, these polysulfide anions were still nucleophiles toward carbonyl-containing compounds, and their high solubilities in nonaqueous electrolytes induced new concerns over the loss of active agents from the cathode, the parasitic reactions at lithium anode, as well as redox-shuttling between cathode and anode. Mainly because of these soluble polysulfide species, the theoretical specific capacity and the projected energy density of Li/S chemistry were almost never achieved experimentally; consequently, cycling behavior of a Li/S cell was typically characterized by a high initial capacity of >1000 mAh/g followed by gradual fading, which stabilized at a level <800 mAh/g.

Interest in rechargeable Li/S chemistry was rejuvenated in 2009 by Ji et al.,<sup>733</sup> following which an explosive growth of research activities ensued, especially after 2012. There have been a few reviews on the renaissance of this battery chemistry,<sup>4,734,735</sup> including a chapter in this issue by Manthiram et al. This section will only cover interphasial chemistries involved and studies on their mechanisms.

Ethers, both acyclic and cyclic, short chain or polymeric, or mixtures of them, were overwhelmingly preferred over carbonates as electrolyte solvents for Li/S batteries,<sup>736–743</sup> partially for their better solubility of polysulfide species in the electrolyte so that more complete utilization of the active materials could be realized, but more importantly for the reason that parasitic reactions occur between polysulfide species and carbonates. Gao et al. showed that the sulfur K-edge X-ray absorption spectra (XAS) for sulfur electrodes cycled in ether-based (DME, dioxane, and TEGDME) electrolytes differ significantly from those cycled in carbonate-based (EC and DEC) electrolyte (Figure 67A).<sup>744</sup> By likening to eq 34A proposed by Freunberger et al. for the Li/O<sub>2</sub> system,<sup>690</sup> they proposed a mechanism in which polysulfide anions perform a nucleophilic attack at ethereal carbons in EC and DEC molecules and result in esters or thioethers that contain polysulfur chain (eqs 37A and B).

Yim et al., on the other hand, believed that polysulfide anions should directly attack the electrophilic center on the carbonate

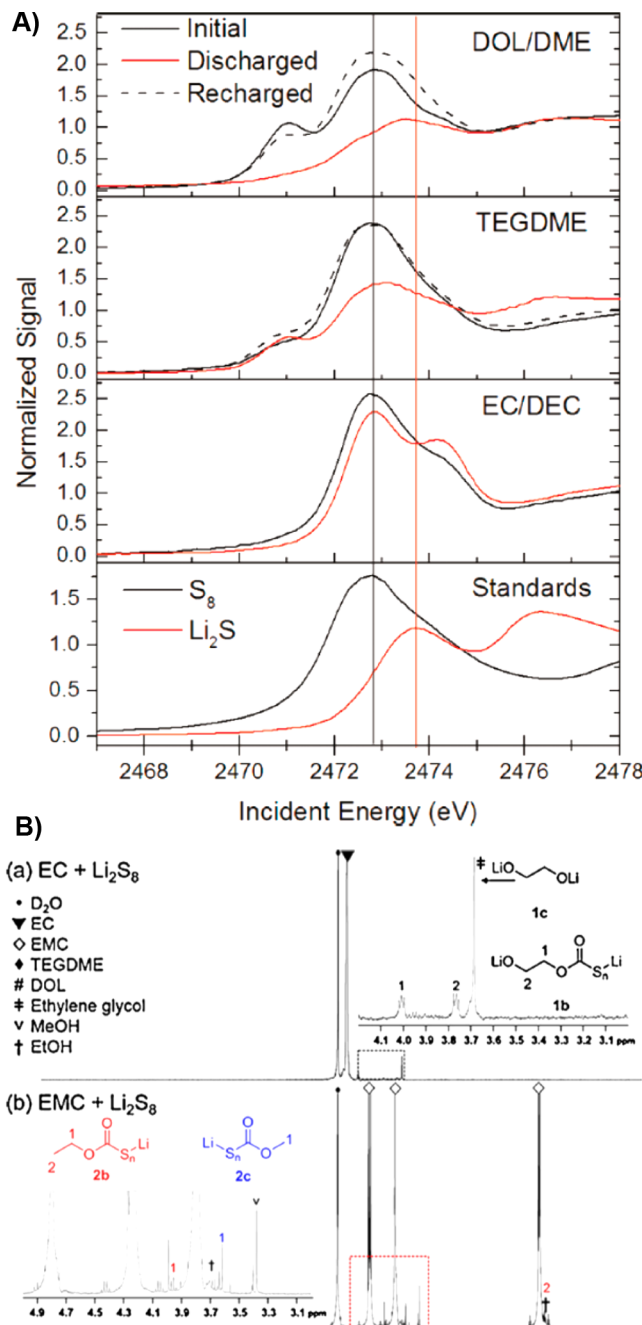
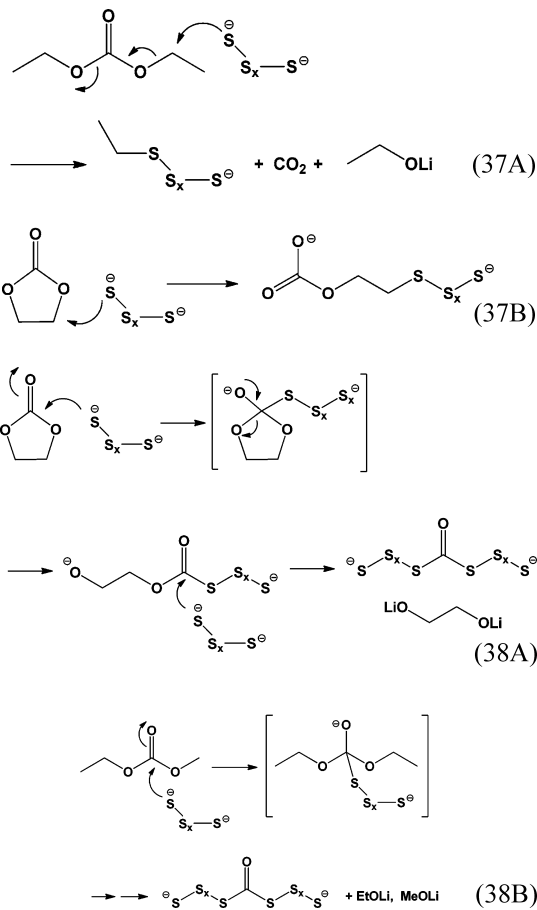


**Figure 67.** Electrolytes in Li/S batteries: (A) In situ sulfur K-edge XAS for 1.0 M LiClO<sub>4</sub>/DOL/DME, TEGDME, and EC/DEC along with S<sub>8</sub> and Li<sub>2</sub>S standards. Reprinted with permission from ref 744. Copyright 2011 American Chemical Society. (B) <sup>1</sup>H NMR of supernatant consisting of (a) EC with Li<sub>2</sub>S<sub>8</sub>, (b) EMC with Li<sub>2</sub>S<sub>8</sub>, and (c) TEGDME with Li<sub>2</sub>S<sub>8</sub>. Reprinted with permission from ref 745. Copyright 2013 Elsevier.

molecule, that is, the carbonyl rather than the ethereal carbon, leading to partially or completed substituted thiocarbonate species (eq 38A and B).<sup>745</sup>

The more structure-sensitive analytic means adopted by Yim et al., such as NMR and FTIR, made eqs 38A and B more convincing than eqs 37A and B, with the identification of a pair of triplets at 3.76 and 4.01 ppm (Figure 67B) and an absorption at 1620 cm<sup>-1</sup>, both of which corresponded to thiocarbonate intermediate as the ring-opening product of EC as a



consequence of nucleophilic attack by polysulfide anion as shown in eq 38A.

Carbonate-based electrolytes were occasionally used, but only limited to the cathode composite in which sulfur was either physically trapped within a carbon structure such as meso-/micropores and nanocavities, or covalently immobilized in polymeric composites.<sup>742,743,746–749</sup> The advantage of carbonate-based electrolytes not only lies in their higher anodic stability against oxidation than ethereal counterparts, but more importantly in the possibility that a LIB configuration could be adopted by using a graphitic anode, thus circumventing the pesky issue of protecting Li metal anode from dendrite formation. Of course, in such cases either a prelithiated sulfur cathode (i.e.,  $Li_2S$ ) or a prelithiated graphitic anode is a necessity.<sup>746</sup> More recently, Wang et al. leveraged earlier researches in nonflammable electrolytes,<sup>1</sup> and adopted a fluorinated alkyl phosphite as cosolvent with carbonates.<sup>750</sup> They found that not only the mixed electrolyte was rendered nonflammable, the presence of the phosphite also participated in the formation of a unique interphase on sulfurized carbon cathode during its first discharge. As a result, the diffusion coefficient of  $Li^+$  was increased by 10-fold, and the new interphase ensured stable cycling of the cell over 750 cycles at a high rate of 10 C.

Besides ethers and carbonates, various onium salts were also used, often in mixture with ethers either at the level of additives, as cosolvents, or as neat ionic liquid electrolyte.<sup>438,737,751,752</sup> There have been no detailed mechanism studies on how these salts affect the reduction/oxidation chemistries of sulfur/polysulfides, with the exception of Zhang, who observed that when tetraalkylammonium- or pyrrolidinium-based cosalts were used, both utilization and cycling

stability of Li/S cells were improved.<sup>752</sup> He believed that the interaction between these onium cations and polysulfide anions, both being soft acid or base according to Pearson HSAB theory, assisted in stabilizing these sulfur intermediates by forming complexes, which prevented them from being completely reduced to insoluble form  $S^{2-}$ . By this stabilization mechanism that is somehow similar to that observed for superoxide species in Li/O<sub>2</sub> chemistry,<sup>705,729</sup> electrochemical reversibility was improved.

Lin et al. reported phosphorus pentasulfide ( $P_2S_5$ ) as a functional additive at concentrations below 10% in ether-based electrolyte, which effectively improved the capacity utilization as well as cycling performance.<sup>753</sup> The presence of this sulfurized compound was believed to be dual: (1) forming a complex with the insoluble  $Li_2S$  or slightly soluble  $Li_2S_2$ , hence making them more readily accessible for the cathode utilization; (2) reacting with lithium surface and forming a SEI-like passivation layer that mainly consisted of  $Li_3PS_4$  and suppressed the shuttling of polysulfide species between anode and cathode surfaces.

#### 6.4. Protection of Lithium Anode

Contrary to LIB where  $Li^+$  is stored in a prelithiated-cathode lattice, most Li/O<sub>2</sub> and Li/S chemistries employed cathode active materials in nonlithiated form; hence the anode was the only lithium source available, and almost exclusively metallic lithium was the anode material of choice. This cell configuration would introduce a series of complications to practical manufacturing, because a cell in the charged state would become activated at the moment electrolyte was injected, which incurs higher safety concern and very likely cost hike. Yet more troublesome is the fundamental irreversibility of metallic lithium anode during prolonged cycling.<sup>1</sup> According to Monroe et al., for the growth of lithium dendritic crystals to be physically suppressed, a surface layer with 6 GPa or higher shear modulus must be present,<sup>397</sup> which obviously cannot be provided by any SEI formed in nonaqueous or polymeric electrolytes. This hypothesis was recently challenged by Khurana et al.,<sup>565</sup> who argued that high modulus might not be a requirement for dendrite-suppression. They showed with experiments that a cross-linked polymer electrolyte with  $1.0 \times 10^5$  Pa can sufficiently cycle a lithium anode for long-term without short-circuit. Nevertheless, most researchers still believe that an interphase or electrolyte of high mechanical strength is the key to suppress the growth of lithium dendrites.

Applying an artificial SEI on metallic lithium via coating, either with organic<sup>754</sup> or ceramic materials, is one feasible approach, among which LISCON-based technology has been quite successful with increasing applications in both Li/O<sub>2</sub> and Li/S chemistries,<sup>755–757</sup> although high cost and difficulty in scaling-up remain the major challenges to be overcome.

On the other hand, electrolyte cosolvent/cosalt or additives are still the preferred approaches of most researchers. For example, the presence of  $LiNO_3$  in ether-based electrolytes was found to effectively prevent the shuttling mechanism between  $Li_2S_6$  and metallic lithium, thus improving capacity utilization as well as Coulombic efficiencies.<sup>758</sup> This interphasial property of  $LiNO_3$  has been widely used in studies on Li/S system.<sup>738,740,741,759,760</sup> Xiong et al. systematically analyzed the interphase formed on metallic lithium in the presence of  $LiNO_3$ , and argued that its contribution equals in importance to that from polysulfide species, because, in the absence of the

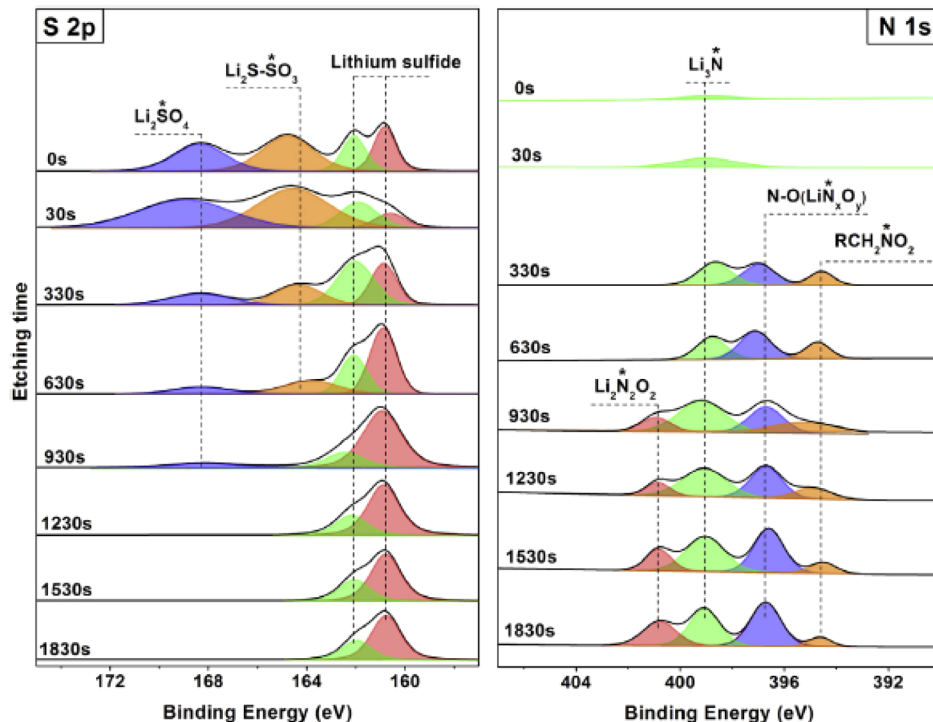


**Figure 68.** Electrolytes in Li/S batteries: SEI depth-profiles established with S 2p and N 1s XPS on metallic lithium formed in the presence of LiNO<sub>3</sub>. Reprinted with permission from ref 761. Copyright 2014 Elsevier.

latter, the growth of the interphase formed from LiNO<sub>3</sub> alone would not stabilize.<sup>761</sup> On the basis of XPS depth-profile established by Ar<sup>+</sup>-sputtering, they concluded that the SEI consists of two distinct sublayers, with the upper-layer being mainly oxidized products of polysulfide (Li<sub>2</sub>SO<sub>4</sub>, Li<sub>2</sub>S<sub>2</sub>O<sub>3</sub>) and the under-layer being more reduced form from both polysulfides (Li<sub>2</sub>S) and LiNO<sub>3</sub> (LiN<sub>x</sub>O<sub>y</sub>, Li<sub>2</sub>N<sub>2</sub>O<sub>2</sub>), as shown in Figure 68. While it sounds a little strange to detect “oxidized products” on the anode surface, the authors suggested that LiNO<sub>3</sub> in the electrolyte acted as an oxidizing agent to convert polysulfide anions into these oxidized forms. Upon closer examination, the S 2p signals near 168 eV seem more likely to be thiophosphate, the reaction product between PF<sub>6</sub><sup>-</sup> anion and polysulfide, rather than sulfate, which would be almost impossible to be produced by the oxidizing power of LiNO<sub>3</sub> and stably exist on a metallic lithium surface. Zhang, on the other hand, cautioned that, due to the strong oxidizing nature of LiNO<sub>3</sub>, the Li/S cells should not be overdischarged below 1.8 V if it is used as cosalt, because its irreversible reduction would occur on the cathode surface and worsen the already poor reversibility of Li<sub>2</sub>S.<sup>759</sup>

A similar protective effect against the polysulfide shuttle mechanism was achieved in carbonate-based electrolytes that contained FEC as additive/cosolvent while a polymeric film based on polyvinylidene difluoride was UV-cured.<sup>762</sup> In this case, the synergistic effect of fluorinated ingredients resulted in a robust SEI that was enriched with LiF along with Li<sub>x</sub>PF<sub>y</sub> and Li<sub>x</sub>POF<sub>y</sub>. Lithium protection was also achieved with P<sub>2</sub>S<sub>3</sub>,<sup>753</sup> which forms Li<sub>3</sub>PS<sub>4</sub>, a known superionic conductor that conducts Li<sup>+</sup> at high rate and retains a wide electrochemical stability window of 1.7–3.2 V.

Ryou et al. approached lithium protection from another angle.<sup>763,764</sup> Realizing that the interaction between separator and lithium surface could be an important factor that affects the distribution of Li<sup>+</sup>-flux across the lithium surface, they treated a polyolefin separator with a mussel-inspired polydopamine coating,

The resultant catecholic adhesion between the separator and lithium surface, which was much stronger than simple van de Waals interaction, not only ensured uniform Li<sup>+</sup>-flux but also effectively relieved the mechanical strain built up during the electrochemical deposition/stripping of metallic lithium. Excellent cycle life of lithium metal anodes was demonstrated in LiCoO<sub>2</sub>-based cathode half cells.

Directly addressing dendrite prevention, Ding et al. adopted a unique approach where Cs<sup>+</sup> or Rb<sup>+</sup> salts were used at an additive level.<sup>765</sup> Being in the same alkaline metal group with Li, these ions should have slightly higher reduction potentials and therefore would deposit on the electrode surface before Li<sup>+</sup> does. However, at small concentrations (<0.1 M), their “effective reduction potentials” were actually shifted negatively according to the Nernst equation (eq 39), resulting in slightly lower values than that of Li<sup>+</sup> (Table 32):

$$E_{\text{red}} = E_{\text{red}}^{\phi} - \frac{RT}{zF} \ln \frac{\alpha_{\text{red}}}{\alpha_{\text{ox}}} = E_{\text{red}}^{\phi} - \frac{0.05916 \text{ V}}{z} \log_{10} \frac{1}{\alpha_{\text{ox}}} \quad (39)$$

**Table 32. Effective Reduction Potentials (vs SHE) of Selected Cations at Various Concentrations**

cations	<i>E</i> <sup>°</sup> /V		effective reduction potential/V		
	1.0 M	0.001 M	0.01 M	0.05 M	0.1 M
Li <sup>+</sup>	-3.040				
Cs <sup>+</sup>	-3.026	-3.203	-3.144	-3.103	-3.085
Rb <sup>+</sup>	-2.980	-3.157	-3.098	-3.057	-3.039

where *R*, *T*,  $\alpha$ , *F*, and *z* are the universal gas constant, absolute temperature, chemical activity for related species, Faraday constant, and the valence number of involved species, respectively.

Thus, when Li<sup>+</sup> began deposition on the lithium surface, any budding dendrite would attract these additive cations due to the higher current density there than the flat surfaces. Yet these

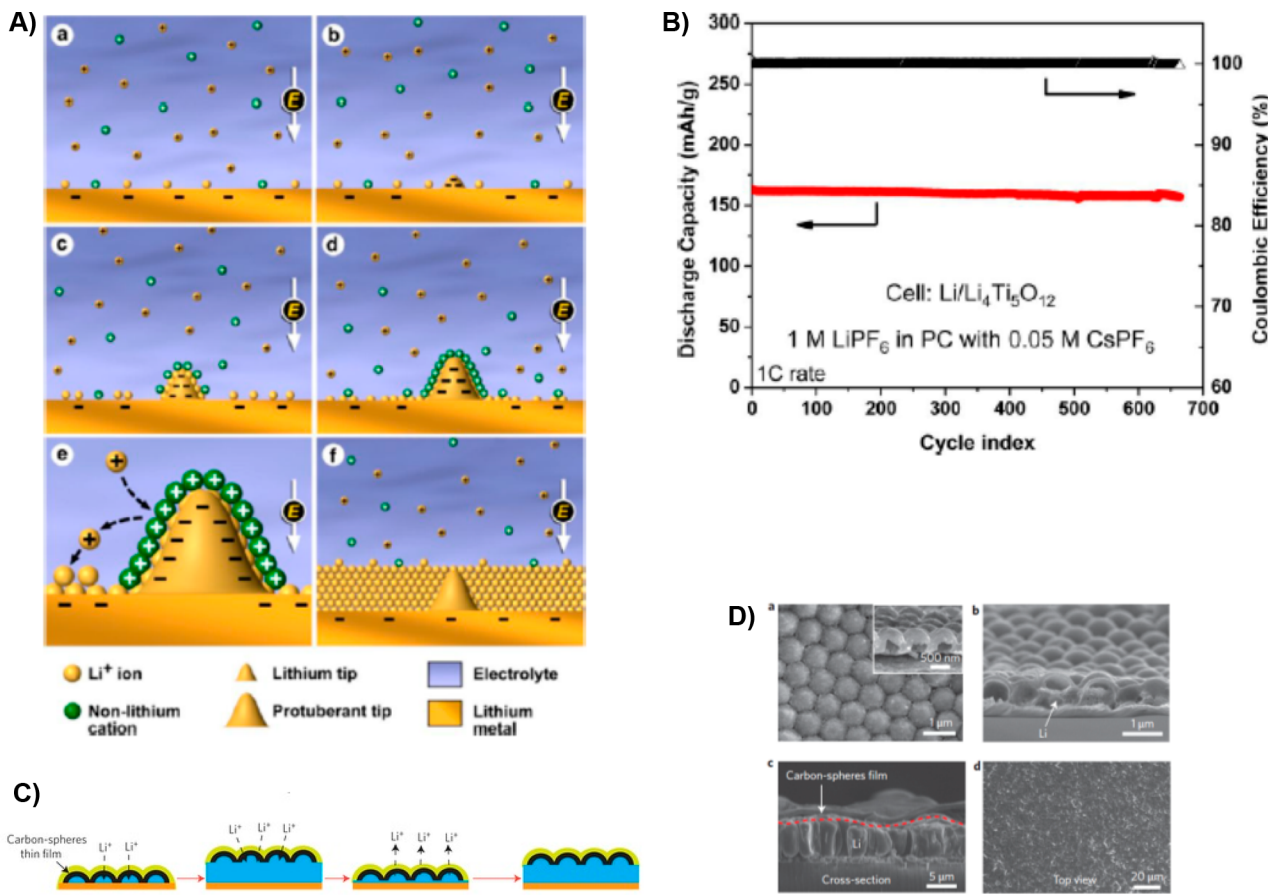


**Figure 69.** Protection of lithium: (A) Schematic illustration of “electrostatic shield” formed by  $\text{Cs}^+$  and  $\text{Rb}^+$  and the prevention of lithium dendrite formation. (B) Long-term cycling stability and Coulombic efficiency of  $\text{Li}/\text{Li}_4\text{Ti}_5\text{O}_{12}$  cell in 1.0 M  $\text{LiClO}_4/\text{PC}$  with 0.05 M  $\text{CsPF}_6$  additive. Reprinted with permission from ref 765. Copyright 2013 American Chemical Society. (C) Illustration of carbon nanosphere as interlayer between metallic lithium and electrolyte and the growth of SEI. (D) SEM images showing (a) top view of carbon nanosphere after SEI formation; (b) cross section of carbon nanosphere monolayer with lithium metal deposited underneath; (c) the monolayer of carbon nanosphere was lifted up by the deposited lithium layer; and (d) smooth surface of the modified lithium electrode. Reprinted with permission from ref 766. Copyright 2014 Macmillan Publishers Ltd.

cations would not reduce thanks to their lower “effective reduction potentials”; instead, the accumulation of these cations forms an “electrostatic shield” that repels incoming  $\text{Li}^+$ , which would be forced to adjacent regions and deposit. The net consequence was the overall “leveling” of the metallic lithium surface (Figure 69A). This mechanism was experimentally confirmed (Figure 69B). Not only was the dendrite formation suppressed in the presence of  $\text{Cs}^+$  salt at different concentrations, but the already-formed dendrite also gradually disappeared in the presence of the additive. However, it should be cautioned that such a safety margin created in reduction potentials by concentration (or activity) difference is rather fragile (Table 32), and accidental deviation from these quasi-equilibrium values, induced by high charging current or local polarization, would result in consumption of these additive cations and expiration of the protective mechanism.

Another innovative approach to address the dendrite formation on metallic lithium surface was reported by Zheng et al., who attempted to apply an artificial interlayer between lithium and electrolyte and ensure that interphase only grow on this interlayer instead of on lithium, so that the highly irreversible nature of lithium surface could be circumvented during the charge and discharge cycles.<sup>766</sup> Ideally, during the cycling where the volume of metallic lithium layer expands and

contracts, this interlayer would serve as a blanket that is both flexible and strong enough to accommodate the volume change (Figure 69C). By coating a monolayer of carbon nanosphere that is amorphous and hollow (Figure 69D), they seemed to have achieved the goal, and enabled reversible cycling of metallic lithium up to 150 cycles at rather high current of 1.0 mA/cm<sup>2</sup> and Coulombic efficiency of ~99%. It must be pointed out that the application of carbonaceous-coating on lithium has been proposed and performed by numerous efforts in the past with little success. What makes the work of Zheng et al. unique is their discovery that the carbon interlayer should not be too electronically conductive, otherwise lithium deposition would occur on top of the nanosphere instead of underneath it, hence defeating the purpose of the original design. Although the reversibility represented by a few hundred cycles remains remote from practical application in commercial devices, the innovative approaches of Zheng et al.<sup>766</sup> and Ding et al.<sup>765</sup> undoubtedly took a big step toward the solution of the most challenging problem that prevents the use of the ultimate anode material, that is, the “Holy Grail” of metallic lithium anode.

## 6.5. Dual-Intercalation Chemistry

A particularly interesting battery chemistry is based on the dual-intercalation concept that was originally proposed by Carlin et al., in which both cation and anion simultaneously intercalate

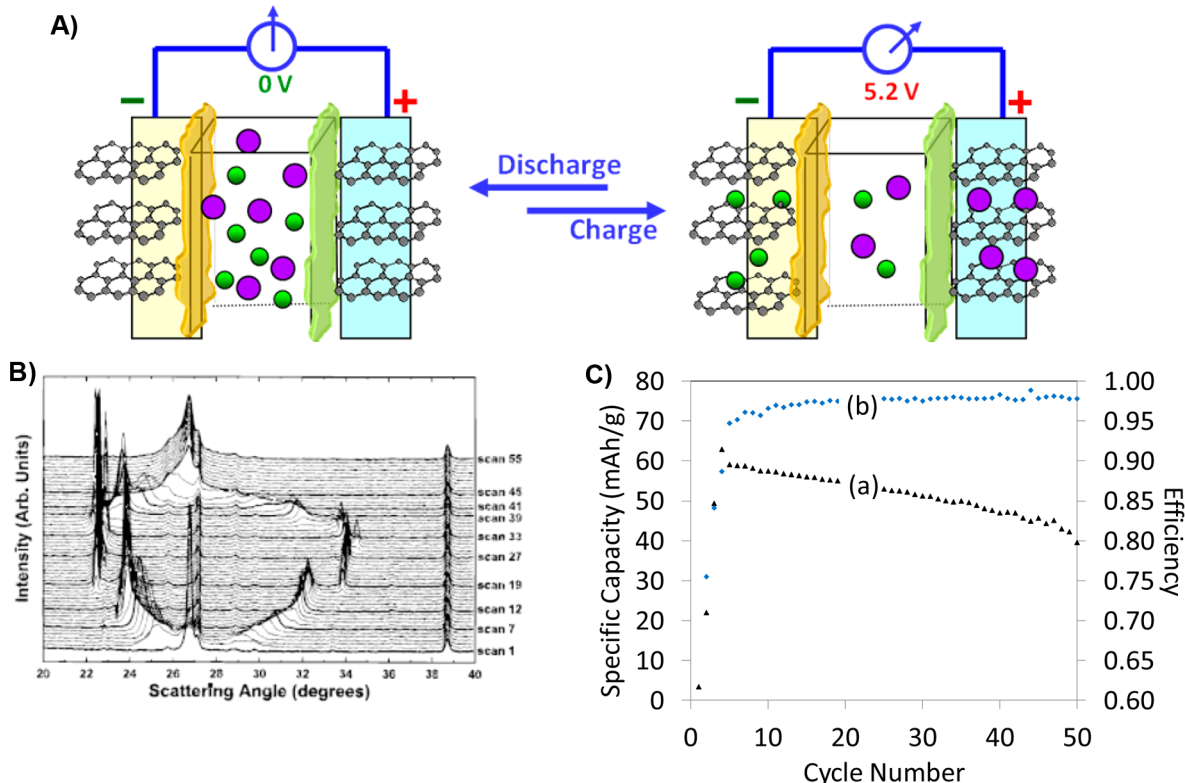


**Figure 70.** Dual-intercalation chemistry: (A) Schematic illustration of “dual graphite intercalation” cell. Reprinted with permission from ref 784. Copyright 2013 Royal Society of Chemistry. (B) In situ X-ray patterns for the anion-intercalation into the graphite structure in a cathode half cell. Reprinted with permission from ref 770. Copyright 2000 Electrochemical Society. (C) Cycling performance of a full graphite cell based on 1.2 M FEC/EMC (40:60) with 5 mM HFiP. Reprinted with permission from ref 784. Copyright 2013 Royal Society of Chemistry.

into graphitic structures upon charge and deintercalate upon discharge, as schematically illustrated in Figure 70.<sup>767</sup> Although Carlin demonstrated the concept with an ionic liquid electrolyte based on imidazolium cation and tetrachloroaluminate  $\text{AlCl}_4^-$  anion at  $\sim 3.5$  V cell voltage, the anions more familiar to LIB community, such as  $\text{BF}_4^-$ ,  $\text{PF}_6^-$ , and  $\text{ClO}_4^-$ , were observed much earlier to intercalate into graphitic structures at higher potentials ( $\sim 5.0$  V).<sup>674,768,769</sup> When the anion-intercalation at  $\sim 5.0$  V and  $\text{Li}^+$ -intercalation at graphitic anode at  $\sim 0.2$  V were coupled together, a possible 5 V battery chemistry could be created,<sup>675,770</sup> leading to a high voltage energy storage device that uses graphite as both electrodes. Assuming a stage 2 intercalation compound was formed,  $\sim 140$  mAh/g specific capacity is possible. Such a cell cannot compete with LIB in mobile or automotive applications; however, in stationary applications where cost and environmental concerns outweigh energy density, certain intrinsic advantages would be associated with such an all graphite battery. Unfortunately, for a long time no known available electrolyte could support such a cell chemistry with simultaneous formation of a protective interphase at the graphitic anode surface and electrochemical stability against oxidation at the graphitic cathode surface. This requirement imposes the most severe constraint on the electrolytes; consequently, in the related studies during the following decades, these graphite-anion intercalation compounds were either formed electrochemically with poor reversibility,<sup>771–776</sup> with  $\text{PF}_6^-$ , TFSI, or fluoroalkylborate as intercalants, or can only be formed via more powerful chemical routes using strong oxidants like elemental fluorine ( $\text{F}_2$ ) or  $\text{K}_2\text{MnF}_6$ , as in the case with methide, various fluoroalkyl sulfonates, and BOB as intercalants.<sup>777–779</sup> In those limited

examples of successful electrochemical preparations, exotic solvents such as nitromethanes or sulfones were often used to resist the oxidation at high potentials, but their stability still did suffice to support reversible cell chemistry upon long-term cyclings. Interestingly, Syzdek et al. noticed that the poor reversibility of  $\text{PF}_6^-$ -intercalation into carbon black within cathode of LIB occurred at  $\sim 4.0$  V, a potential much lower than the corresponding  $\text{PF}_6^-$ -intercalation into graphitic structure, and they believe this process was actually responsible for the structural degradation of LIB cathode.<sup>780</sup>

More recently, West et al. used a series of anion-receptors based on fluoroalkylborates or -boronates to form complex anions with fluoride ( $\text{F}^-$ ) and showed that anions of such sizes could still electrochemically intercalate into graphite at  $\sim 5.0$  V in PC, accompanied by an expansion in interlayer distance between graphene sheets to  $\sim 0.99$  nm.<sup>781</sup> Although the process was still demonstrated in a cathode half cell, decent reversibility was obtained in this case as compared to previous studies. Realizing that most of the electrolyte solvents cannot satisfy interphasial chemistry requirements at graphitic anodes and graphitic cathodes simultaneously, Placke et al. replaced the graphitic anode with another intercalation host,  $\text{Li}_4\text{Ti}_5\text{O}_{12}$ , which operates at 1.5 V and does not require SEI formation.<sup>782,783</sup> Employing an RTIL electrolyte with pyrrolidinium cation and TFSI anion, they achieved the “dual ion cell” concept consisting of graphite cathode and  $\text{Li}_4\text{Ti}_5\text{O}_{12}$  anode with excellent reversibility, as evidenced by 99% capacity retention over 500 cycles. Naturally, this compromised approach via circumventing graphitic anode came with an energy density penalty due to the higher potential of  $\text{Li}_4\text{Ti}_5\text{O}_{12}$  anode, which reduces the full cell voltage to 3–3.5 V.

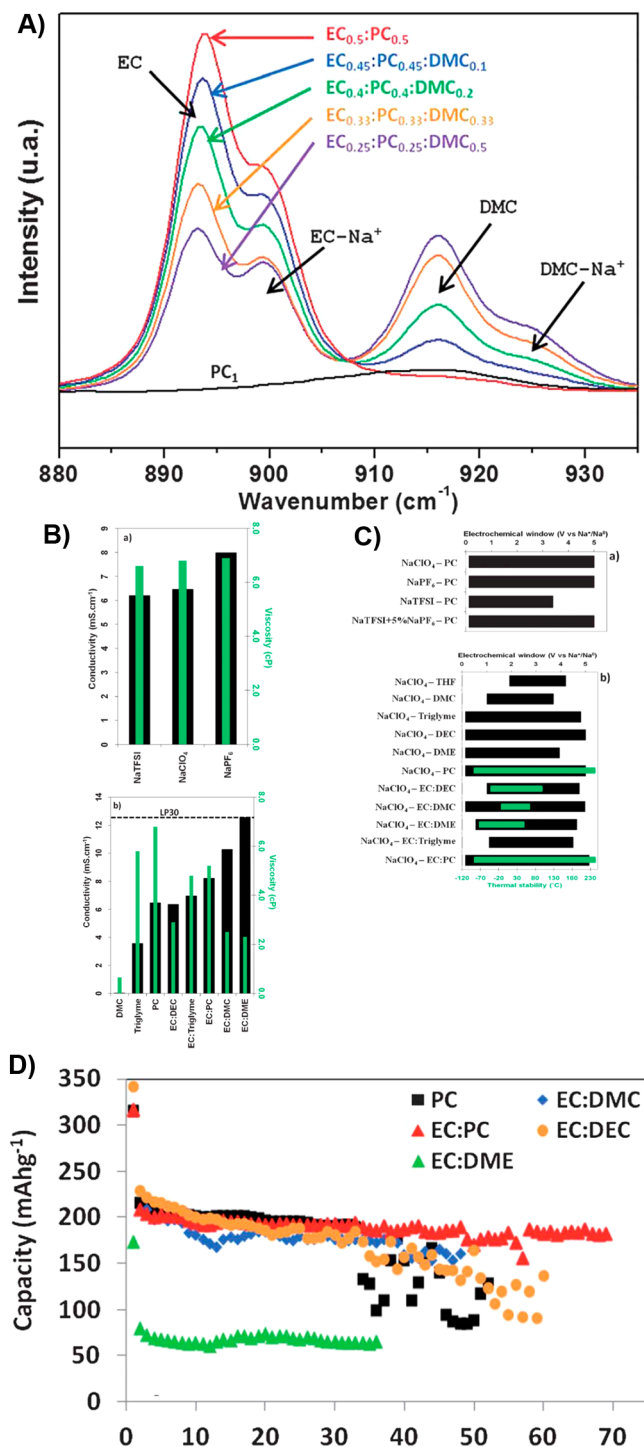


**Figure 71.** Electrolytes in Na-ion batteries: (A)  $\text{Na}^+$ -solvation sheath structure as revealed by Raman spectra. Note that EC was favored over acyclic carbonate as in the  $\text{Li}^+$ -solvation sheath. Reprinted with permission from ref 787. Copyright 2013 Royal Society of Chemistry. (B) Ion conductivity and (C) electrochemical stability window of (a) PC-based electrolytes with various sodium salts at 1.0 M and (b) electrolytes based on 1.0 M  $\text{NaClO}_4$  in various solvents as evaluated on Al electrodes; and (D) cycling performance of hard carbon anodes in the above Na electrolytes. Reprinted with permission from ref 786. Copyright 2012 Royal Society of Chemistry.

The first real “dual graphite cell” with  $\text{Li}^+$ , as illustrated in Figure 70A, was demonstrated by Read et al.,<sup>784</sup> which was made possible by high voltage electrolytes based on a

fluorinated solvent FEC and a fluorinated additive HFiP.<sup>10</sup> Figure 70C shows the cycling performance of a graphite full cell in 1.2 M FEC/EMC (40:60) with 5 mM HFiP. Given the fact that the corresponding cathode and anode half cells in the same electrolyte can cycle over 200 cycles with a Coulombic efficiency above >96%, it seemed that the major contributor to capacity fading came from the “cathode-anode dialog”, in which certain species generated by one electrode surface diffuse/migrate toward the other electrode and constitute a parasitic shuttle. Although capacity utilization and reversibility of this full cell still need significant improvement, the mere fact that such an all graphite configuration could work alludes to the possibility of a nascent rechargeable battery chemistry free of transition metal materials, with low cost and environmental impact.

## 6.6. Sodium Ion Chemistry

Given the success of LIB and the limited lithium reserve in the Earth’s crust,<sup>785</sup> sodium (Na) as the closest analogue of lithium in periodic table has been attracting intense interest as a potential replacement, in the hope that Na offers similar intercalation chemistries in electrode hosts at much lower cost. However, despite the chemical similarity between the two elements, electrochemical properties of Na differ significantly from that of Li. The advantage of a room-temperature rechargeable  $\text{Na}^+$ -chemistry lies in its low cost and environmental benefits instead of projected energy density, with the former supported by its high abundances in the Earth’s crust and seawater and relative convenience to recover, while the latter penalized by the bigger (by more than 30% in ionic radii than  $\text{Li}^+$ ) and heavier  $\text{Na}^+$  (by more than 3 times in mass than  $\text{Li}^+$ ) and its higher reduction potential ( $\sim 0.33$  V vs Li).<sup>673,786–789</sup> Consequently, one should not expect a simple transition of the knowledge accumulated on  $\text{Li}^+$ -electrolytes and their interphases to  $\text{Na}^+$ -counterparts, although the former still impose heavy influences on the development of the latter.

Earlier, Komaba et al. reported that  $\text{Na}^+$  was unable to intercalate into a graphitic host and form stoichiometric intercalation compounds as does  $\text{Li}^{+}$ <sup>213</sup> and hard carbon seemed to be the most promising anode material for  $\text{Na}^+$ . This choice of disordered carbonaceous materials relaxes the restriction on PC-rich electrolyte formulations, because the graphitic structure that is sensitive toward solvent cointercalation no longer constitutes the overwhelming morphology in these carbonaceous materials; however, SEI would still be expected to form considering the low potential ( $-2.7$  V vs SHE) at the hard carbon anode. On the other hand, most cathode intercalation hosts for  $\text{Na}^+$ -chemistry, based on variants of either transition metal oxides or phosphates, operate below 4.5 V, and hence the requirement for anodic stability was not particularly rigorous.

The nearly exhaustive evaluation on electrolyte solvents and solutes was carried out by Ponrouch et al., who characterized the  $\text{Na}^+$ -transport, viscosity, thermal stability, service temperature range, electrochemical stability window, as well as cycling performance of numerous mixtures of carbonate esters and ethers (Figure 71).<sup>786,787</sup> They found that, although the presence of ether such as DME benefited the ion conductivity, the electrochemical stability requirement overrules that of bulk transport property, and ethers were thus essentially disfavored because of its poor anodic stability on cathode surfaces. The optimized systems consist of mixtures of carbonates similar to the electrolytes used for LIB, but with much lower acyclic

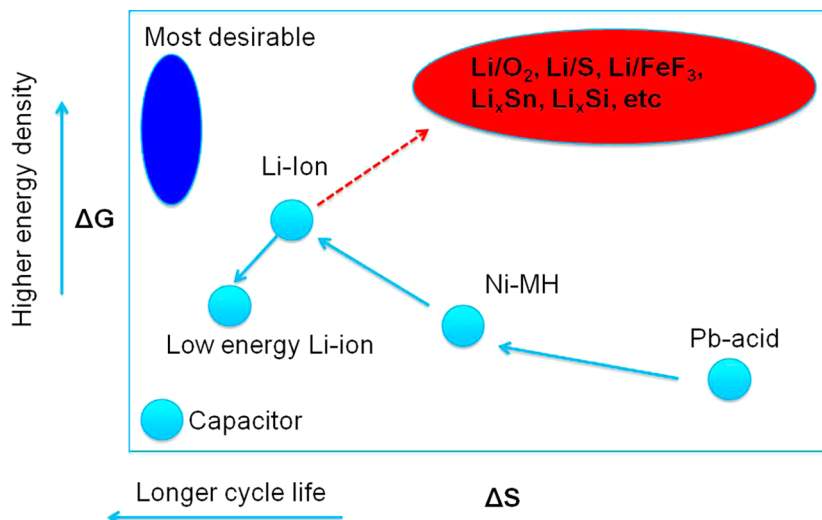


**Figure 72.** Evolution of battery technologies: the traditional compromise between energy density and reversibility, and the attempts to break it with new battery chemistries. Source: Ping Liu, U.S. Department of Energy ARPA-E.

carbonate ratios, mainly due to the poor solubilities of Na salts in those weakly polar solvents with low dielectric constant below 10. Either NaClO<sub>4</sub> or NaPF<sub>6</sub> has been used as electrolyte solutes in those carbonate binary or ternary mixtures, which have become the main stream electrolyte composition used for Na<sup>+</sup>-chemistry.<sup>790–793</sup>

Of particular interest is the finding that, like similar studies conducted on Li<sup>+</sup>-electrolytes, Na<sup>+</sup> also favors EC in its solvation sheath over acyclic carbonate (DMC), as evidenced by Raman spectra collected on a series of homologous electrolytes (Figure 71C), and this preferential solvation of Na<sup>+</sup> by EC was directly linked to the interphasial chemistry on hard carbon.<sup>794</sup> Komaba et al. conducted a more thorough investigation on the interphases formed on hard carbon anodes after Na<sup>+</sup> intercalation, and concluded on the basis of XPS and TOF-SIMS analyses that SEI thus formed was more inorganic in nature but, nevertheless, thinner (~30 nm), and more nonuniform as compared to its counterparts formed in Li<sup>+</sup>-electrolyte.<sup>789</sup> They also evaluated the effect of electrolyte additives on the performance of both hard carbon anode and metallic sodium electrode.<sup>793,795,796</sup> Among the additives studied, FEC was identified as the only one that worked efficiently, while VC, ES, and *trans*-difluoroethylene carbonate failed to perform despite their reputations in LIB applications.<sup>793</sup> However, Ponrouch et al. argued that the presence of FEC actually led to a more resistive SEI.<sup>797</sup>

Besides nonaqueous electrolytes based on carbonates, polymer gel and ionic liquid electrolytes were also evaluated.<sup>798,799</sup> Yet as for LIB, most of these systems remain remote from actual application than their nonaqueous liquid counterparts, because more issues were introduced than resolved, such as not sufficiently high ion conductivity, interfacial contacts with electrode surfaces, and electrochemical stabilities.

The safety of Na<sup>+</sup>-chemistry was investigated by Xia et al., who employed accelerated rate calorimetry (ARC) to evaluate the reactivity of fully sodiated or lithiated hard carbon (Na<sub>x</sub>C<sub>6</sub> or Li<sub>x</sub>C<sub>6</sub>) with various electrolyte solvents.<sup>794,800,801</sup> A rather intriguing “paradox” in terms of the salt chemical stability versus interphasial instability, which has been reported for LIB electrolytes,<sup>802</sup> was again identified in the comparison between

NaPF<sub>6</sub><sup>-</sup> and LiPF<sub>6</sub>-containing electrolytes, as the authors detected high reactivity of the former with Na<sub>x</sub>C<sub>6</sub>.<sup>794</sup> They attributed this discrepancy to the more stable chemical nature of NaPF<sub>6</sub>, which did not decompose easily and formed fluoride to passivate the Na<sub>x</sub>C<sub>6</sub> surface as LiPF<sub>6</sub> would do on the Li<sub>x</sub>C<sub>6</sub> surface. Surprisingly, NaTFSI that is even more stable than NaPF<sub>6</sub> did not follow the same paradoxical trend; instead, electrolyte based on NaTFSI showed less reactivity toward Na<sub>x</sub>C<sub>6</sub> than did NaPF<sub>6</sub>.<sup>801</sup> Between cyclic and acyclic carbonates, Na<sub>x</sub>C<sub>6</sub> was found to react more readily with the latter, and XRD analyses identified the formation of semi-carbonates, probably via similar reaction mechanisms that have been known for Li<sup>+</sup>-electrolytes.<sup>800</sup> The preferential solvation of Na<sup>+</sup> by EC also seemed to affect the reactivity between Na<sub>x</sub>C<sub>6</sub> and electrolyte, as the absence of sodium salt actually led to lower reactivity.<sup>794,800</sup> The authors believed that because EC would be preferentially “recruited” by Na<sup>+</sup> when sodium salt was present, leaving mostly acyclic carbonate molecules such as DMC or DEC in the bulk, the reaction between Na<sub>x</sub>C<sub>6</sub> and acyclic carbonate would be encouraged due to higher effective concentration of the latter.

### 6.7. Multivalent (Mg<sup>2+</sup>) Chemistry

Lithium was made the ultimate anode material by the fortuitous combination of three factors, which can never be reproduced by any other elements in the Periodic Table: (1) it is the metal with the lowest atomic number, hence possessing the largest theoretical specific capacity of 3860 mAh/g; (2) it is the most electropositive metal (−3.10 V vs SHE), hence generating the highest possible cell voltage against any given positive electrode; and (3) it is the lightest metal (0.54 g cm<sup>−3</sup>), hence rendering the highest possible gravimetric energy density if coupled with a cathode candidate.<sup>19</sup> These nearly irreplaceable advantages make lithium (or intercalation compounds and alloy of it) the promising anode material of choice even in many of the “beyond Li-ion” battery chemistries. The only element in the Periodic Table that could come close to lithium as an anode material of significance is magnesium (Mg), whose divalent chemical nature provides specific capacities (2206 mAh/g or 3833 mAh/cm<sup>3</sup>) close to or even higher than those of lithium (3884 mAh/g or 2046 mAh/cm<sup>3</sup>). Benefited by its low redox potential (−2.35 V vs SHE or

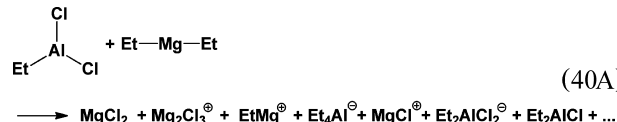
+0.65 V vs Li), a gravimetric energy density (500 Wh/kg) close to or a volumetric energy density (1600 Wh/L) potentially higher than that of lithium is possible.<sup>803</sup> An Mg-based battery chemistry with such merits becomes more appealing when cost effectiveness (\$/KWh) is considered, thanks to its high abundance in the Earth's crust. Yoo et al. recently summarized the history of the art comprehensively,<sup>804</sup> and a section (cf., Muldoon et al.) is also dedicated to Mg<sup>2+</sup>-intercalation chemistry in this thematical issue.

Aurbach and co-workers were the pioneers that conducted the trail-blazing research in this nascent battery chemistry.<sup>803–811</sup> They realized early on that, among the needs for new cathode and anode materials, the most severe challenge to a reversible Mg battery chemistry actually comes from the interphasial chemistry (or absence of it) on the metallic magnesium anode. Because of its divalent nature, Mg<sup>2+</sup> cannot migrate through a SEI consisting of magnesium salts as does Li<sup>+</sup> through an SEI of corresponding lithium salts. The underlying reason for this difficulty is certainly not the size issue (0.74 Å of Mg<sup>2+</sup> vs 0.68 Å of Li<sup>+</sup>) but the much stronger ionic attractions arising between Mg<sup>2+</sup> and its counter-anions or coordination cages formed by solvent molecules. Thus, any feasible electrolyte for the Mg-battery must remain thermodynamically stable with metallic magnesium, ensuring that no reductions occur between Mg and any electrolyte component. Moreover, any salt anions that might participate in the formation of interphases via electrochemical reduction should also be excluded, which cover perchlorates, triflates, and PF<sub>6</sub><sup>−</sup>. Application of these requirements essentially rules out any solvents based on ester, sulfone, or nitrile structures, leaving ethers as the only possible options, while organo-magnesium salts, well-known as Grignard reagents in organic synthesis, were selected as the electrolyte solute for their known stability against metallic magnesium surfaces.

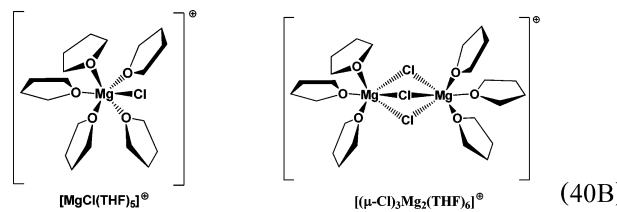
However, these organo-magnesium salts, usually in ethereal solvents, faced challenges on the cathode side, as the anions in these salts were essentially stabilized carbanions (C<sup>−</sup>), which are known to be unstable against oxidation. Their combination with ethereal solvents, also known to be anodically unstable, cannot possibly lead to an electrolyte with anodic stability limit beyond 2.0 V vs Mg. Moreover, the bonds between Mg<sup>2+</sup> and the carbanion are actually of a more covalent than ionic nature; thus the freedom of Mg<sup>2+</sup> was significantly restricted, as reflected in the sluggish kinetics of Mg<sup>2+</sup>-deposition and usually low ion conductivities of these Grignard-like electrolytes. The majority of the efforts since the first demonstration by Aurbach and co-workers concentrated on how to expand the anodic stability of such electrolytes beyond 3.0 V so that a viable Mg-battery chemistry could be supported, while maintaining their thermodynamic inertness toward a metallic magnesium surface.

Aurbach et al. proposed a strategy on the basis of the Lewis basicity neutralization, aiming at increasing the ionicity of Mg<sup>2+</sup> in those electrolytes by reacting organo-magnesium salts with Lewis acids based on Al, B, or P centers.<sup>805</sup> An exhaustive screening on organo-magnesium salts was thus conducted that covered a wide spectrum of variants in both alkyl- and halo-substituents on magnesium and aluminum, and identified chloride as the preferred halo-substituent with magnesium. In THF solutions, the coupling between Grignard reagents and AlCl<sub>3</sub> or other Lewis acids led to complete or partial transmetalation, with most chlorides transferred to Mg and alkyl-substituents to Al. Structural analysis of the solutions using

Raman, FTIR, multinuclei NMR, EQCM, as well as single-crystal X-ray diffraction revealed more complicated equilibria among the various species depending on both the ratio and the substituents, but it seemed that Mg and Al would always possess a coordination state of 6 and 4, respectively, and chloride often occupied the bridging positions that helped form dimeric inorganic magnesium species. Equation 40A illustrates, as an example, the electrolyte components formed by reacting EtAlCl<sub>2</sub> with Et<sub>2</sub>Mg in THF.



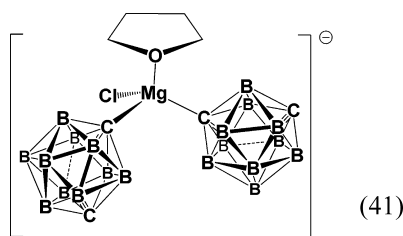
In those structures, solvent molecules actually often appeared as ligands of magnesium to satisfy its need of a coordination number of 6 (eq 40B).



The complexes such as MgCl<sup>+</sup> or Mg<sub>2</sub>Cl<sub>3</sub><sup>+</sup> (along with neutral solvent molecules therein) were most likely the conducting species, and electrolytes containing these complexes were characterized with excellent cathodic stabilities by allowing almost quantitative deposition/stripping of Mg without the formation of dendrites.<sup>807,810</sup> Surprisingly, aluminum deposition almost never occurred unless excess Al was used, despite its higher reduction potential (+0.70 V vs Mg). This stabilization of Al<sup>3+</sup> from reduction should obviously be attributed to the trans-metalation, during which most of the carbanions (alkyl-substituents) migrated to Al, thus tightly confining Al<sup>3+</sup> while freeing up Mg<sup>2+</sup> for conduction and electrochemical reactions. The anodic stability of the electrolytes, on the other hand, was found to be mainly determined by the choices of alkyl-substituents, and stability limits above 3.0 V have been described when phenyls or alkyls without β-hydrogen were used.<sup>811</sup>

The above general approach by Aurbach et al.<sup>803</sup> based on adjusting Lewis acidity has been followed by most researchers in search of new electrolyte compositions for this nascent battery chemistry.<sup>812–818</sup> Various modifications were made to the approach though, including the attempts by Kim et al., who replaced alkyl substituents on magnesium with N-based anion, hexamethyldisilazide, so that this non-nucleophilic substituent could remain stable against S-based cathode materials,<sup>814</sup> and the more recent efforts by Liu et al.<sup>819</sup> and Doe et al.,<sup>820</sup> respectively, who independently employed the direct reaction between MgCl<sub>2</sub> and Lewis acids AlCl<sub>3</sub> or AlPh<sub>3</sub> to circumvent the use of organo-magnesium compounds. It was believed that the dimeric complex (μ-Cl)<sub>3</sub>Mg<sub>2</sub>THF<sub>6</sub>, as shown in eq 40B, was formed as the main conducting species. Both works reported that the generated electrolyte solutions in either THF, DME, or tetraglyme support nearly 100% magnesium deposition/stripping while remaining anodically stable above 3.0 V.

Alternative efforts were also made to avoid the corrosive Lewis acid  $\text{AlCl}_3$  by pursuing inorganic anions of more benign nature as potential salts for Mg-electrolyte. Realizing that an effective way to keep a Mg surface free of SEI is to ensure that both salt anion and solvents are reduction-resistant at Mg-deposition potential, Mohtadi et al. explored magnesium salts based on borohydride anions, which have been used as popular reducing agents in organic/inorganic syntheses.<sup>821</sup> They showed that  $\text{Mg}(\text{BH}_4)_2$  in both THF and DME enabled reversible Mg-deposition/stripping with Coulombic efficiency close to 94%. However, the intrinsic reducing power of borohydrides makes it readily oxidizable; therefore, application of this class of Mg salt on high voltage (>3.0 V) Mg-cathode is questionable. Electrolyte formulated with  $\text{Mg}(\text{BH}_4)_2$  in the presence of  $\text{LiBH}_4$  as additive was shown to possess an oxidation stability limit of 2.3 V vs Mg in cyclic voltammetry, and supported the reversible operation of a Mg cell with Chevrel ( $\text{Mo}_6\text{S}_8$ ) as cathode (~1.7 V). Extending the above line of research, Carter et al. attempted to improve the anodic stability of Mg salts by modifying the borohydride anion structure with C–B bond.<sup>822</sup> Inspired by the knowledge in hydrogen storage materials, they synthesized a new class of magnesium salt based on carborane-cluster anion with closo-structure. The actual structure of the resultant complex salt in solid state was analyzed with X-ray single-crystal diffraction, which revealed a salt comprised of a chloride-bridged Mg dimeric cation (right, eq 40B) and a unique dicarboranyl Mg anion (eq 41). The authors believed that the same or similar



structures were maintained in solution state and responsible for the ion transport as well as electrochemical functions, judging from the fact that only subtle differences could be detected between the bulk electrolyte solution and the crystal with respect to the  $^{11}\text{B}$  NMR and FTIR spectra. In THF solution, this salt allowed for reversible Mg-deposition/stripping with Coulombic efficiency up to 98%, and showed an oxidation stability limit of ~3.2 V vs Mg on Pt electrode. A full Mg battery with Chevrel cathode was cycled in this electrolyte. As compared to  $\text{MgBH}_4$ , the carborane-cluster electrolyte not only showed higher capacity utilization (~90 vs 60 mAh/g), but also indicated faster kinetics as revealed by the distinctive two-phase intercalation process in the corresponding voltage profiles.

In most of the Mg electrolytes reported thus far, THF has been the dominant ethereal solvent used; however, considering its high volatility and inflammability, efforts were made to replace it with less volatile linear ethers such as DME or even tetraglyme.<sup>819,820</sup> Polymer gel systems based on PVdF<sup>805</sup> and ionic liquids based on imidazolium or pyrrolidinium<sup>823–825</sup> were also explored. Results varied, and controversies sometime arose, showing that further investigations were merited before successful deployment of an Mg battery becomes a reality.

## 7. CONCLUDING REMARKS

The decade between 2003–2014 witnessed exciting growth in energy storage research. As the essential component of any electrochemical device, electrolytes and the concomitant interphases are married together by the high reactivities of the electrode surfaces and the intrinsic instability of electrolyte components in batteries of high voltages (>3.0 V). With the maturing of  $\text{Li}^+$ -intercalation chemistry in graphitic structures, the fundamental understanding about its components, especially the interphasial chemistry and processes, has significantly deepened, which has been catalyzed by the application of various state-of-the-art characterization means. Meanwhile, the incessant development of cathode materials with increasing capacity, higher operating voltage, and distinct surface chemistries/morphologies and nanostructures continues to present new challenges to electrolytes and interphases. The emergence of the “beyond Li-ion” battery chemistries, some were genuinely new, and the others revisited from new angles and with new approaches, particularly raises the significance of electrolytes and interphases, because all of these chemistries pursue quantum-leaps in energy density ( $\Delta G$ ) at the expense of the structural integrity ( $\Delta S$ ) of electrodes during each energy storage/release cycle, as qualitatively described by Liu in Figure 72. In these scenarios, not only are the electrolytes and interphases inseparable, the electrodic reactions will also be closely interwoven with these two. Such dynamic structural transformation coupled with high operating potentials of the electrodes requires a robust electrolyte and interphase system to resist both electrochemical and mechanical stresses so that reasonable reversibility be ensured. In most cases, the formulation of new electrolytes and their ad hoc interphasial chemistries often dictate the fate of these new battery chemistries. In the upcoming decade, exciting breakthroughs in electrolytes and interphasial chemistry should be made in those fields.

## AUTHOR INFORMATION

### Corresponding Author

\*E-mail: conrad.k.xu.civ@mail.mil, kang\_xu@hotmail.com.

### Notes

The authors declare no competing financial interest.

### Biography



Having graduated with a B.S. (Southwest University, 1985), M.S. (Lanzhou Institute of Chemical Physics, Academy of Sciences, 1988), and Ph.D. (Arizona State University, 1996) in Chemistry, Kang Xu has been researching energy storage technologies for over 25 years. He

joined the U.S. Army Research Laboratory in 1997, and has been the PI/co-PI for various projects funded by US DOE ABR, BATT, and ARPA-E, the project leads for various DoD research projects, as well as the Contract Official Technical Representative for diversified research initiatives. His research interests cover both materials development and fundamental understanding of interphasial mechanisms for electrochemical energy storage devices, including lithium and beyond-lithium battery chemistries. He has been recognized multiple times, with four R&D Achievement Awards from the Department of the Army (1999, 2001, 2002, and 2011), the Publication Award (2005), the Army Science Conference Best Paper Award (2008), and the Science Award (2011). He has published over 130 papers in peer-reviewed journals (*h*-index 50), written 2 book chapters, coedited a book, and currently holds 20 issued U.S. patents (Google Scholar Profile: <http://scholar.google.com/citations?user=S6Eii30AAAAJ&hl=en&oi=ao>). The folder pile he leaned against in the picture contained part of the literature referenced in this review.

## ACKNOWLEDGMENTS

I want to thank my family for their patience and understanding with my extended hours at the office on this project. I am deeply grateful to the guest editor Prof. Whittingham for including me once again in this exciting thematic issue, and my supervisor Dr. Cynthia Lundgren for her strong support and encouragement. Gratitude also goes to my prestigious colleagues Drs./Profs. Daniel Abraham (Argonne National Laboratory), Khalil Amine (Argonne National Laboratory), Doron Aurbach (Bar Ilan University), Chunmei Ban (National Renewable Energy Laboratory), Yi Cui (Stanford University), Jeff Dahn (Dalhousie University), Tien Duong (U.S. Department of Energy, BATT), Joseph Dura (National Institute of Standards and Technology), Peter Faguy (U.S. Department of Energy, ABR), Stephen Harris (Lawrence Berkeley National Laboratory), Wesley Henderson (Pacific Northwest National Laboratory), Hong Li (Institute of Physics, Academia Sinica), Ping Liu (U.S. Department of Energy, ARPA-E), Wenjuan Liu (Microvast Power Systems), Brett Lucht (University of Rhode Island), Petr Novák (Paul Scherrer Institut), Jung-Ki Park (KAIST), Marshal Smart (Jet Propulsion Laboratory), Chunsheng Wang (University of Maryland), Martin Winter (Universität Münster), and Jie Xiao and Wu Xu (Pacific Northwest National Laboratory) for helpful suggestions, discussions, and sharing of unpublished data. My ARL colleagues, Drs. Josh Allen, Oleg Borodin, Arthur von Wald Cresce, Janet Ho, Jeff Read, Selena M. Russell, and Shengshui Zhang, provided valuable assistance from literature collection to discussions. Drs./Profs. Oleg Borodin (ARL), Arthur von Wald Cresce (ARL), Jeff Dahn (Dalhousie University), Joseph Dura (National Institute of Standards and Technology), Stephen Harris (Lawrence Berkeley National Laboratory), Selena M. Russell (ARL), Chunsheng Wang (University of Maryland), and Shengshui Zhang (ARL) critically proofread parts or the entirety of the manuscript. In particular, Dr. Selena M. Russell (ARL) meticulously constructed the EndNote library for flawless reference management and made extensive changes to the final draft, both scientific and editorial; and Dr. Oleg Borodin (ARL) offered tremendous help in digesting and organizing MD and DFT simulation work. Alice and Michael created the cover artwork. Finally, I want to thank Prof. C. Austen Angell (Arizona State University), who is not only my Ph.D. advisor, but also a lifelong mentor and friend. Happy 80th Birthday, Austen!

## REFERENCES

- (1) Xu, K. *Chem. Rev.* **2004**, *104*, 4303.
- (2) Ohzuku, T.; Brodd, R. J. *J. Power Sources* **2007**, *174*, 449.
- (3) Goodenough, J. B.; Kim, Y. *Chem. Mater.* **2009**, *22*, 587.
- (4) Manthiram, A.; Fu, Y.; Su, Y.-S. *Acc. Chem. Res.* **2012**, *46*, 1125.
- (5) GirishKumar, G.; McCloskey, B.; Luntz, A. C.; Swanson, S.; Wilcke, W. *J. Phys. Chem. Lett.* **2010**, *1*, 2193.
- (6) Poizot, P.; Laruelle, S.; Gruegeon, S.; Dupont, L.; Tarascon, J. M. *Nature* **2000**, *407*, 496.
- (7) Chung, S.-Y.; Bloking, J. T.; Chiang, Y.-M. *Nat. Mater.* **2002**, *1*, 123.
- (8) Kasavajjula, U.; Wang, C.; Appleby, A. J. *J. Power Sources* **2007**, *163*, 1003.
- (9) Chan, C. K.; Peng, H.; Liu, G.; McIlwrath, K.; Zhang, X. F.; Huggins, R. A.; Cui, Y. *Nat. Nanotechnol.* **2008**, *3*, 31.
- (10) Cresce, A. v. W.; Xu, K. *J. Electrochem. Soc.* **2011**, *158*, A337.
- (11) Zhang, Z.; Hu, L.; Wu, H.; Weng, W.; Koh, M.; Redfern, P. C.; Curtiss, L. A.; Amine, K. *Energy Environ. Sci.* **2013**, *6*, 1806.
- (12) Tarascon, J.-M.; Delacourt, C.; Prakash, A. S.; Morcrette, M.; Hegde, M. S.; Wurm, C.; Masquelier, C. *Dalton Trans.* **2004**, 2988.
- (13) Aurbach, D.; Talyosef, Y.; Markovsky, B.; Markevich, E.; Zinigrad, E.; Asraf, L.; Gnanaraj, J. S.; Kim, H.-J. *Electrochim. Acta* **2004**, *50*, 247.
- (14) Aricò, A. S.; Bruce, P.; Scrosati, B.; Tarascon, J.-M.; van Schalkwijk, W. *Nat. Mater.* **2005**, *4*, 366.
- (15) Aurbach, D. *J. Power Sources* **2005**, *146*, 71.
- (16) Johansson, P.; Jacobsson, P. *J. Power Sources* **2006**, *153*, 336.
- (17) Armand, M.; Tarascon, J. M. *Nature* **2008**, *451*, 652.
- (18) Winter, M. *Z. Phys. Chem.* **2009**, *223*, 1395.
- (19) Xu, K. In *Encyclopedia of Electrochemical Power Sources*; Garche, J., Dyer, C. K., Moseley, P. T., Ogumi, Z., Rand, D. A. J., Scrosati, B., Eds.; Elsevier: Amsterdam, 2009; Vol. 5, pp 51–70.
- (20) Zhang, S. S. *J. Power Sources* **2006**, *162*, 1379.
- (21) Huggins, R. A. *Advanced Batteries*; Springer: New York, 2009; pp 375–392.
- (22) Dunn, B.; Kamath, H.; Tarascon, J.-M. *Science* **2011**, *334*, 928.
- (23) Xu, K.; Cresce, A. v. W. *J. Mater. Chem.* **2011**, *21*, 9849.
- (24) Marom, R.; Amalraj, S. F.; Leifer, N.; Jacob, D.; Aurbach, D. *J. Mater. Chem.* **2011**, *21*, 9938.
- (25) *Lithium Batteries: Advanced Technologies and Applications*; Scrosati, B., Abraham, K. M., Schalkwijk, W. A. v., Hassoun, J., Eds.; Wiley: NJ, 2013.
- (26) Ding, M. S. *J. Electrochem. Soc.* **2004**, *151*, A40.
- (27) Ding, M. S.; Richard Jow, T. *J. Electrochem. Soc.* **2004**, *151*, A2007.
- (28) Aihara, Y.; Bando, T.; Nakagawa, H.; Yoshida, H.; Hayamizu, K.; Akiba, E.; Price, W. S. *J. Electrochem. Soc.* **2004**, *151*, A119.
- (29) Schweiger, H.-G.; Multerer, M.; Schweizer-Berberich, M.; Gores, H. *J. J. Electrochem. Soc.* **2005**, *152*, A577.
- (30) Ding, M. S.; Xu, K.; Zhang, S. S.; Amine, K.; Henriksen, G. L.; Jow, T. *R. J. Electrochem. Soc.* **2001**, *148*, A1196.
- (31) Niedzicki, L.; Kasprzyk, M.; Kuziak, K.; Żukowska, G. Z.; Armand, M.; Bukowska, M.; Marcinek, M.; Szczeciński, P.; Wieczorek, W. *J. Power Sources* **2009**, *192*, 612.
- (32) Zhao, J.; Wang, L.; He, X.; Wan, C.; Jiang, C. *J. Electrochem. Soc.* **2008**, *155*, A292.
- (33) Ghosh, A.; Wang, C.; Kofinas, P. *J. Electrochem. Soc.* **2010**, *157*, A846.
- (34) Zugmann, S.; Fleischmann, M.; Amereller, M.; Gschwind, R. M.; Wiemhöfer, H. D.; Gores, H. *J. Electrochim. Acta* **2011**, *56*, 3926.
- (35) Valøen, L. O.; Reimers, J. N. *J. Electrochim. Soc.* **2005**, *152*, A882.
- (36) Stewart, S.; Newman, J. *J. Electrochim. Soc.* **2008**, *155*, A458.
- (37) Bockris, J. O. M.; Reddy, A. K. N. *Modern Electrochemistry*, 2nd ed.; Plenum Press: New York, 2000.
- (38) Postupna, O. O.; Kolesnik, Y. V.; Kalugin, O. N.; Prezhdo, O. V. *J. Phys. Chem. B* **2011**, *115*, 14563.
- (39) Takeuchi, M.; Matubayasi, N.; Kameda, Y.; Minofar, B.; Ishiguro, S.-i.; Umebayashi, Y. *J. Phys. Chem. B* **2012**, *116*, 6476.

- (40) Deepa, M.; Agnihotry, S. A.; Gupta, D.; Chandra, R. *Electrochim. Acta* **2004**, *49*, 373.
- (41) Burba, C. M.; Frech, R. *J. Phys. Chem. B* **2005**, *109*, 15161.
- (42) Tsunekawa, H.; Narumi, A.; Sano, M.; Hiwara, A.; Fujita, M.; Yokoyama, H. *J. Phys. Chem. B* **2003**, *107*, 10962.
- (43) Matsubara, K.; Kaneuchi, R.; Maekita, N. *J. Chem. Soc., Faraday Trans.* **1998**, *94*, 3601.
- (44) Reddy, V. P.; Smart, M. C.; Chin, K. B.; Ratnakumar, B. V.; Surampudi, S.; Hu, J.; Yan, P.; Surya Prakash, G. K. *Electrochim. Solid-State Lett.* **2005**, *8*, A294.
- (45) Bogle, X.; Vazquez, R.; Greenbaum, S.; Cresce, A. v. W.; Xu, K. *J. Phys. Chem. Lett.* **2013**, *4*, 1664.
- (46) Zhuang, G. V.; Xu, K.; Yang, H.; Jow, T. R.; Ross, P. N. *J. Phys. Chem. B* **2005**, *109*, 17567.
- (47) Xu, K. *J. Electrochim. Soc.* **2007**, *154*, A162; Erratum: *J. Electrochim. Soc.* **2007**, *154*, S9.
- (48) Xu, K.; Lam, Y.; Zhang, S. S.; Jow, T. R.; Curtis, T. B. *J. Phys. Chem. C* **2007**, *111*, 7411.
- (49) Morita, M.; Asai, Y.; Yoshimoto, N.; Ishikawa, M. *J. Chem. Soc., Faraday Trans.* **1998**, *94*, 3451.
- (50) Borodin, O.; Smith, G. D. *J. Phys. Chem. B* **2009**, *113*, 1763.
- (51) Cresce, A. v. W.; Xu, K. *Electrochim. Solid-State Lett.* **2011**, *14*, A154.
- (52) Xu, K.; Cresce, A. v. W. *J. Mater. Res.* **2012**, *27*, 2327.
- (53) Yang, L.; Xiao, A.; Lucht, B. L. *J. Mol. Liq.* **2010**, *154*, 131.
- (54) Zavalij, P. Y.; Yang, S.; Whittingham, M. S. *Acta Crystallogr., Sect. B* **2004**, *60*, 716.
- (55) Henderson, W. A. *J. Phys. Chem. B* **2006**, *110*, 13177.
- (56) Seo, D. M.; Borodin, O.; Han, S.-D.; Ly, Q.; Boyle, P. D.; Henderson, W. A. *J. Electrochim. Soc.* **2012**, *159*, A553.
- (57) Seo, D. M.; Borodin, O.; Han, S.-D.; Boyle, P. D.; Henderson, W. A. *J. Electrochim. Soc.* **2012**, *159*, A1489.
- (58) Seo, D. M.; Borodin, O.; Balogh, D.; O'Connell, M.; Ly, Q.; Han, S.-D.; Passerini, S.; Henderson, W. A. *J. Electrochim. Soc.* **2013**, *160*, A1061.
- (59) Han, S.-D.; Allen, J. L.; Jónsson, E.; Johansson, P.; McOwen, D. W.; Boyle, P. D.; Henderson, W. A. *J. Phys. Chem. C* **2013**, *117*, 5521.
- (60) Vetter, J.; Novák, P. *J. Power Sources* **2003**, *119–121*, 338.
- (61) Vetter, J.; Buqa, H.; Holzapfel, M.; Novák, P. *J. Power Sources* **2005**, *146*, 355.
- (62) Chiba, K.; Ueda, T.; Yamaguchi, Y.; Oki, Y.; Saiki, F.; Naoi, K. *J. Electrochim. Soc.* **2011**, *158*, A1320.
- (63) Smart, M. C.; Ratnakumar, B. V.; Ryan-Mowrey, V. S.; Surampudi, S.; Prakash, G. K. S.; Hu, J.; Cheung, I. *J. Power Sources* **2003**, *119–121*, 359.
- (64) Achiha, T.; Nakajima, T.; Ohzawa, Y.; Koh, M.; Yamauchi, A.; Kagawa, M.; Aoyama, H. *J. Electrochim. Soc.* **2009**, *156*, A483.
- (65) Achiha, T.; Nakajima, T.; Ohzawa, Y.; Koh, M.; Yamauchi, A.; Kagawa, M.; Aoyama, H. *J. Electrochim. Soc.* **2010**, *157*, A707.
- (66) Xu, K. *J. Electrochim. Soc.* **2008**, *155*, A733.
- (67) Xu, K.; Deveney, B.; Nechev, K.; Lam, Y.; Jow, T. R. *J. Electrochim. Soc.* **2008**, *155*, A959.
- (68) Smart, M. C.; Ratnakumar, B. V.; Chin, K. B.; Whitcanack, L. D. *J. Electrochim. Soc.* **2010**, *157*, A1361.
- (69) Smart, M. C.; Lucht, B. L.; Dalavi, S.; Krause, F. C.; Ratnakumar, B. V. *J. Electrochim. Soc.* **2012**, *159*, A739.
- (70) Yaakov, D.; Gofer, Y.; Aurbach, D.; Halalay, I. C. *J. Electrochim. Soc.* **2010**, *157*, A1383.
- (71) Sato, K.; Zhao, L.; Okada, S.; Yamaki, J.-i. *J. Power Sources* **2011**, *196*, 5617.
- (72) Kaneko, F.; Masuda, Y.; Nakayama, M.; Wakihara, M. *Electrochim. Acta* **2007**, *53*, 549.
- (73) Lee, S.-Y.; Ueno, K.; Angell, C. A. *J. Phys. Chem. C* **2012**, *116*, 23915–23920.
- (74) Xue, L.; Ueno, K.; Lee, S.-Y.; Angell, C. A. *J. Power Sources* **2014**, *262*, 123.
- (75) Sun, X.-G.; Austen Angell, C. *Solid State Ionics* **2004**, *175*, 257.
- (76) Sun, X.-G.; Angell, C. A. *Electrochim. Commun.* **2005**, *7*, 261.
- (77) Sun, X.; Angell, C. A. *Electrochim. Commun.* **2009**, *11*, 1418.
- (78) Abouimrane, A.; Belharouak, I.; Amine, K. *Electrochim. Commun.* **2009**, *11*, 1073.
- (79) Xu, K.; Ding, S. P.; Jow, T. R. *J. Electrochim. Soc.* **1999**, *146*, 4172.
- (80) Chiba, K.; Ueda, T.; Yamaguchi, Y.; Oki, Y.; Shimodate, F.; Naoi, K. *J. Electrochim. Soc.* **2011**, *158*, A872.
- (81) Shao, N.; Sun, X.-G.; Dai, S.; Jiang, D.-e. *J. Phys. Chem. B* **2011**, *115*, 12120.
- (82) Li, S.; Zhao, Y.; Shi, X.; Li, B.; Xu, X.; Zhao, W.; Cui, X. *Electrochim. Acta* **2012**, *65*, 221.
- (83) Xing, L.; Vatamanu, J.; Borodin, O.; Smith, G. D.; Bedrov, D. J. *Phys. Chem. C* **2012**, *116*, 23871.
- (84) Sirenko, V. I.; Potapenko, A. V.; Prisiazhnyi, V. D. *J. Power Sources* **2008**, *175*, 581.
- (85) Yamada, Y.; Takazawa, Y.; Miyazaki, K.; Abe, T. *J. Phys. Chem. C* **2010**, *114*, 11680.
- (86) Wang, Q.; Zakeeruddin, S. M.; Exnar, I.; Grätzel, M. *J. Electrochim. Soc.* **2004**, *151*, A1598.
- (87) Wang, Q.; Pechy, P.; Zakeeruddin, S. M.; Exnar, I.; Grätzel, M. *J. Power Sources* **2005**, *146*, 813.
- (88) Gmitter, A. J.; Plitz, I.; Amatucci, G. G. *J. Electrochim. Soc.* **2012**, *159*, A370.
- (89) Abouimrane, A.; Davidson, I. J. *J. Electrochim. Soc.* **2007**, *154*, A1031.
- (90) Abu-Lebdeh, Y.; Davidson, I. J. *J. Electrochim. Soc.* **2009**, *156*, A60.
- (91) Abu-Lebdeh, Y.; Davidson, I. J. *Power Sources* **2009**, *189*, 576.
- (92) Duncan, H.; Salem, N.; Abu-Lebdeh, Y. *J. Electrochim. Soc.* **2013**, *160*, A838.
- (93) Nagahama, M.; Hasegawa, N.; Okada, S. *J. Electrochim. Soc.* **2010**, *157*, A748.
- (94) Dalavi, S.; Xu, M.; Ravdel, B.; Zhou, L.; Lucht, B. L. *J. Electrochim. Soc.* **2010**, *157*, A1113.
- (95) Xu, M.; Lu, D.; Garsuch, A.; Lucht, B. L. *J. Electrochim. Soc.* **2012**, *159*, A2130.
- (96) Jin, Z.; Wu, L.; Song, Z.; Yan, K.; Zhan, H.; Li, Z. *ECS Electrochim. Lett.* **2012**, *1*, A55.
- (97) Sazhin, S. V.; Harrup, M. K.; Gering, K. L. *J. Power Sources* **2011**, *196*, 3433.
- (98) Takeuchi, S.; Yano, S.; Fukutsuka, T.; Miyazaki, K.; Abe, T. *J. Electrochim. Soc.* **2012**, *159*, A2089.
- (99) Zhang, Z.; Sherlock, D.; West, R.; West, R.; Amine, K.; Lyons, L. *J. Macromolecules* **2003**, *36*, 9176.
- (100) Zhang, Z.; Lyons, L. J.; Amine, K.; West, R. *Macromolecules* **2005**, *38*, 5714.
- (101) Zhang, Z.; Lyons, L. J.; Jin, J. J.; Amine, K.; West, R. *Chem. Mater.* **2005**, *17*, 5646.
- (102) Amine, K.; Wang, Q.; Vissers, D. R.; Zhang, Z.; Rossi, N. A. A.; West, R. *Electrochim. Commun.* **2006**, *8*, 429.
- (103) Chen, Z.; Wang, H. H.; Vissers, D. R.; Zhang, Z.; West, R.; Lyons, L. J.; Amine, K. *J. Phys. Chem. C* **2008**, *112*, 2210.
- (104) Kusachi, Y.; Zhang, Z.; Dong, J.; Amine, K. *J. Phys. Chem. C* **2011**, *115*, 24013.
- (105) Guyomard, D.; Tarascon, J. M. *J. Electrochim. Soc.* **1993**, *140*, 3071.
- (106) Arai, J. *J. Electrochim. Soc.* **2003**, *150*, A219.
- (107) Naoi, K.; Iwama, E.; Ogihara, N.; Nakamura, Y.; Segawa, H.; Ino, Y. *J. Electrochim. Soc.* **2009**, *156*, A272.
- (108) Naoi, K.; Iwama, E.; Honda, Y.; Shimodate, F. *J. Electrochim. Soc.* **2010**, *157*, A190.
- (109) Xie, B.; Lee, H. S.; Li, H.; Yang, X. Q.; McBreen, J.; Chen, L. Q. *Electrochim. Commun.* **2008**, *10*, 1195.
- (110) Chen, Z.; Amine, K. *J. Electrochim. Soc.* **2006**, *153*, A1221.
- (111) Lee, Y. M.; Lee, Y.-G.; Kang, Y.-M.; Cho, K. Y. *Electrochim. Solid-State Lett.* **2010**, *13*, A55.
- (112) Chen, Z.; Amine, K. *J. Electrochim. Soc.* **2009**, *156*, A672.
- (113) Qin, Y.; Chen, Z.; Lee, H. S.; Yang, X. Q.; Amine, K. *J. Phys. Chem. C* **2010**, *114*, 15202.
- (114) Croce, F.; Curini, R.; Martinelli, A.; Persi, L.; Ronci, F.; Scrosati, B.; Caminiti, R. *J. Phys. Chem. B* **1999**, *103*, 10632.

- (115) Walls, H. J.; Zhou, J.; Yerian, J. A.; Fedkiw, P. S.; Khan, S. A.; Stowe, M. K.; Baker, G. L. *J. Power Sources* **2000**, *89*, 156.
- (116) Bhattacharyya, A. J.; Dollé, M.; Maier, J. *Electrochem. Solid-State Lett.* **2004**, *7*, A432.
- (117) Das, S. K.; Bhattacharyya, A. J. *J. Phys. Chem. B* **2010**, *114*, 6830.
- (118) Bhattacharyya, A. J. *J. Phys. Chem. Lett.* **2012**, *3*, 44.
- (119) Blazejczyk, A.; Wieczorek, W.; Kovarsky, R.; Golodnitsky, D.; Peled, E.; Scanlon, L. G.; Appetecchi, G. B.; Scrosati, B. *J. Electrochem. Soc.* **2004**, *151*, A1762.
- (120) Kalita, M.; Bukat, M.; Ciosek, M.; Siekierski, M.; Chung, S. H.; Rodríguez, T.; Greenbaum, S. G.; Kovarsky, R.; Golodnitsky, D.; Peled, E.; Zane, D.; Scrosati, B.; Wieczorek, W. *Electrochim. Acta* **2005**, *50*, 3942.
- (121) Ciosek, M.; Sannier, L.; Siekierski, M.; Golodnitsky, D.; Peled, E.; Scrosati, B.; Główkowski, S.; Wieczorek, W. *Electrochim. Acta* **2007**, *53*, 1409.
- (122) Golodnitsky, D.; Kovarsky, R.; Mazor, H.; Rosenberg, Y.; Lapides, I.; Peled, E.; Wieczorek, W.; Plewa, A.; Siekierski, M.; Kalita, M.; Settimi, L.; Scrosati, B.; Scanlon, L. G. *J. Electrochem. Soc.* **2007**, *154*, A547.
- (123) Scheers, J.; Kalita, M.; Johansson, P.; Zukowska, G. Z.; Wieczorek, W.; Jacobsson, P. *J. Electrochem. Soc.* **2009**, *156*, A305.
- (124) Johansson, P. *J. Phys. Chem. A* **2006**, *110*, 12077.
- (125) Markusson, H.; Johansson, P.; Jacobsson, P. *Electrochem. Solid-State Lett.* **2005**, *8*, A215.
- (126) Wielmann, U.; Bonrath, W.; Netscher, T.; Nöth, H.; Panitz, J.-C.; Wohlfahrt-Mehrens, M. *Chem.—Eur. J.* **2004**, *10*, 2451.
- (127) Nanbu, N.; Tsuchiya, K.; Sasaki, Y. *J. Power Sources* **2005**, *142*, 333.
- (128) Xiao, A.; Yang, L.; Lucht, B. L. *Electrochem. Solid-State Lett.* **2007**, *10*, A241.
- (129) Xu, M.; Xiao, A.; Li, W.; Lucht, B. L. *Electrochem. Solid-State Lett.* **2009**, *12*, A155.
- (130) Xu, M.; Xiao, A.; Li, W.; Lucht, B. L. *J. Electrochem. Soc.* **2010**, *157*, A115.
- (131) Xu, M.; Zhou, L.; Chalasani, D.; Dalavi, S.; Lucht, B. L. *J. Electrochem. Soc.* **2011**, *158*, A1202.
- (132) Qin, Y.; Chen, Z.; Liu, J.; Amine, K. *Electrochem. Solid-State Lett.* **2010**, *13*, A11.
- (133) Zhou, Z.-B.; Takeda, M.; Fujii, T.; Ue, M. *J. Electrochem. Soc.* **2005**, *152*, A351.
- (134) Appetecchi, G. B.; Zane, D.; Scrosati, B. *J. Electrochem. Soc.* **2004**, *151*, A1369.
- (135) Xu, W.; Shusterman, A. J.; Marzke, R.; Angell, C. A. *J. Electrochem. Soc.* **2004**, *151*, A632.
- (136) Nolan, B. G.; Strauss, S. H. *J. Electrochem. Soc.* **2003**, *150*, A1726.
- (137) Shaffer, A. R.; Deligonul, N.; Scherson, D. A.; Protasiewicz, J. D. *Inorg. Chem.* **2010**, *49*, 10756.
- (138) Zhang, S. S. *Electrochem. Commun.* **2006**, *8*, 1423.
- (139) Chen, Z.; Liu, J.; Amine, K. *Electrochem. Solid-State Lett.* **2007**, *10*, A45.
- (140) Abraham, D. P.; Furczon, M. M.; Kang, S. H.; Dees, D. W.; Jansen, A. N. *J. Power Sources* **2008**, *180*, 612.
- (141) Kang, S. H.; Abraham, D. P.; Xiao, A.; Lucht, B. L. *J. Power Sources* **2008**, *175*, 526.
- (142) Shkrob, I. A.; Zhu, Y.; Marin, T. W.; Abraham, D. P. *J. Phys. Chem. C* **2013**, *117*, 23750.
- (143) Williams, D.; Pleune, B.; Kouvetakis, J.; Williams, M. D.; Andersen, R. A. *J. Am. Chem. Soc.* **2000**, *122*, 7735.
- (144) Bernhardt, E.; Henkel, G.; Willner, H. Z. *Anorg. Allg. Chem.* **2000**, *626*, 560.
- (145) Scheers, J.; Johansson, P.; Jacobsson, P. *J. Electrochem. Soc.* **2008**, *155*, A628.
- (146) Scheers, J.; Pitawala, J.; Thebault, F.; Kim, J.-K.; Ahn, J.-H.; Matic, A.; Johansson, P.; Jacobsson, P. *Phys. Chem. Chem. Phys.* **2011**, *13*, 14953.
- (147) Younesi, R.; Hahlin, M.; Treskow, M.; Scheers, J.; Johansson, P.; Edström, K. *J. Phys. Chem. C* **2012**, *116*, 18597.
- (148) Scheers, J.; Lim, D.-H.; Kim, J.-K.; Paillard, E.; Henderson, W. A.; Johansson, P.; Ahn, J.-H.; Jacobsson, P. *J. Power Sources* **2014**, *251*, 451.
- (149) Arai, J.; Matsuo, A.; Fujisaki, T.; Ozawa, K. *J. Power Sources* **2009**, *193*, 851.
- (150) Hayamizu, K.; Matsuo, A.; Arai, J. *J. Electrochem. Soc.* **2009**, *156*, A744.
- (151) Ionica-Bousquet, C. M.; Muñoz-Rojas, D.; Casteel, W. J.; Pearlstein, R. M.; GirishKumar, G.; Pez, G. P.; Palacín, M. R. *J. Power Sources* **2010**, *195*, 1479.
- (152) Chen, Z.; Liu, J.; Jansen, A. N.; GirishKumar, G.; Casteel, B.; Amine, K. *Electrochem. Solid-State Lett.* **2010**, *13*, A39.
- (153) GirishKumar, G.; Bailey, W. H.; Peterson, B. K.; Casteel, W. J. *J. Electrochem. Soc.* **2011**, *158*, A146.
- (154) Chen, Z.; Ren, Y.; Jansen, A. N.; Lin, C.-k.; Weng, W.; Amine, K. *Nat. Commun.* **2013**, *4*, 1513.
- (155) Mandal, B.; Sooksimuang, T.; Griffin, B.; Padhi, A.; Filler, R. *Solid State Ionics* **2004**, *175*, 267.
- (156) Geiculescu, O. E.; Yang, J.; Zhou, S.; Shafer, G.; Xie, Y.; Albright, J.; Creager, S. E.; Pennington, W. T.; DesMarteau, D. D. *J. Electrochem. Soc.* **2004**, *151*, A1363.
- (157) Li, L.; Zhou, S.; Han, H.; Li, H.; Nie, J.; Armand, M.; Zhou, Z.; Huang, X. *J. Electrochem. Soc.* **2011**, *158*, A74.
- (158) Han, H.; Guo, J.; Zhang, D.; Feng, S.; Feng, W.; Nie, J.; Zhou, Z. *Electrochem. Commun.* **2011**, *13*, 265.
- (159) Zhou, S.; Han, H.; Nie, J.; Armand, M.; Zhou, Z.; Huang, X. *J. Electrochem. Soc.* **2012**, *159*, A1158.
- (160) Barbarich, T. J.; Driscoll, P. F. *Electrochem. Solid-State Lett.* **2003**, *6*, A113.
- (161) Johansson, P.; Béranger, S.; Armand, M.; Nilsson, H.; Jacobsson, P. *Solid State Ionics* **2003**, *156*, 129.
- (162) Armand, M.; Johansson, P. *J. Power Sources* **2008**, *178*, 821.
- (163) Tokuda, H.; Tabata, S.-i.; Susan, M. A. B. H.; Hayamizu, K.; Watanabe, M. *J. Phys. Chem. B* **2004**, *108*, 11995.
- (164) Tsujioka, S.; Nolan, B. G.; Takase, H.; Fauber, B. P.; Strauss, S. H. *J. Electrochem. Soc.* **2004**, *151*, A1418.
- (165) Kaskey, J. Dow Lithium-Ion Electrolyte Venture May Meet Half of Demand. *Bloomberg News* [Online] 2011, <http://www.bloomberg.com/news/2011-07-06/dow-lithium-ion-electrolyte-venture-may-meet-half-of-current-global-demand.html> (accessed July 6, 2011).
- (166) Vollmer, J. M.; Curtiss, L. A.; Vissers, D. R.; Amine, K. *J. Electrochem. Soc.* **2004**, *151*, A178.
- (167) Tasaki, K.; Kanda, K.; Kobayashi, T.; Nakamura, S.; Ue, M. *J. Electrochem. Soc.* **2006**, *153*, A2192.
- (168) Halls, M. D.; Tasaki, K. *J. Power Sources* **2010**, *195*, 1472.
- (169) Park, M. H.; Lee, Y. S.; Lee, H.; Han, Y.-K. *J. Power Sources* **2011**, *196*, 5109.
- (170) Xing, L.; Borodin, O.; Smith, G. D.; Li, W. *J. Phys. Chem. A* **2011**, *115*, 13896.
- (171) Leung, K. *J. Phys. Chem. C* **2012**, *117*, 1539.
- (172) Borodin, O.; Behl, W.; Jow, T. R. *J. Phys. Chem. C* **2013**, *117*, 8661.
- (173) El Ouattani, L.; Dedryvère, R.; Siret, C.; Biensan, P.; Reynaud, S.; Iratçabal, P.; Gonbeau, D. *J. Electrochem. Soc.* **2009**, *156*, A103.
- (174) Xiong, D.; Burns, J. C.; Smith, A. J.; Sinha, N.; Dahn, J. R. *J. Electrochem. Soc.* **2011**, *158*, A1431.
- (175) Burns, J. C.; Sinha, N. N.; Coyle, D. J.; Jain, G.; VanElzen, C. M.; Lamanna, W. M.; Xiao, A.; Scott, E.; Gardner, J. P.; Dahn, J. R. *J. Electrochem. Soc.* **2011**, *159*, A85.
- (176) Sinha, N. N.; Burns, J. C.; Dahn, J. R. *J. Electrochem. Soc.* **2013**, *160*, A709.
- (177) Lee, J.-T.; Lin, Y.-W.; Jan, Y.-S. *J. Power Sources* **2004**, *132*, 244.
- (178) Hu, Y.; Kong, W.; Wang, Z.; Huang, X.; Chen, L. *Solid State Ionics* **2005**, *176*, 53.
- (179) Abe, K.; Yoshitake, H.; Kitakura, T.; Hattori, T.; Wang, H.; Yoshio, M. *Electrochim. Acta* **2004**, *49*, 4613.

- (180) Abe, K.; Hattori, T.; Kawabe, K.; Ushigoe, Y.; Yoshitake, H. *J. Electrochem. Soc.* **2007**, *154*, A810.
- (181) Abe, K.; Miyoshi, K.; Hattori, T.; Ushigoe, Y.; Yoshitake, H. *J. Power Sources* **2008**, *184*, 449.
- (182) Lee, J.-T.; Wu, M.-S.; Wang, F.-M.; Lin, Y.-W.; Bai, M.-Y.; Chiang, P.-C. *J. J. Electrochem. Soc.* **2005**, *152*, A1837.
- (183) Liu, B.; Li, B.; Guan, S. *Electrochem. Solid-State Lett.* **2012**, *15*, A77.
- (184) Kinoshita, S.-c.; Kotato, M.; Sakata, Y.; Ue, M.; Watanabe, Y.; Morimoto, H.; Tobishima, S.-i. *J. Power Sources* **2008**, *183*, 755.
- (185) Komaba, S.; Kumagai, N.; Kataoka, Y. *Electrochim. Acta* **2002**, *47*, 1229.
- (186) Zhan, C.; Lu, J.; Jeremy Kropf, A.; Wu, T.; Jansen, A. N.; Sun, Y.-K.; Qiu, X.; Amine, K. *Nat. Commun.* **2013**, *4*.
- (187) Komaba, S.; Itabashi, T.; Ohtsuka, T.; Groult, H.; Kumagai, N.; Kaplan, B.; Yashiro, H. *J. Electrochem. Soc.* **2005**, *152*, A937.
- (188) Cho, I. H.; Kim, S.-S.; Shin, S. C.; Choi, N.-S. *Electrochem. Solid-State Lett.* **2010**, *13*, A168.
- (189) Ochida, M.; Doi, T.; Domi, Y.; Tsubouchi, S.; Nakagawa, H.; Yamanaka, T.; Abe, T.; Ogumi, Z. *J. Electrochem. Soc.* **2013**, *160*, A410.
- (190) Esbenshade, J. L.; Gewirth, A. A. *J. Electrochem. Soc.* **2014**, *161*, A513.
- (191) Ziv, B.; Levy, N.; Borgel, V.; Li, Z.; Levi, M. D.; Aurbach, D.; Pauric, A. D.; Goward, G. R.; Fuller, T. J.; Balogh, M. P.; Halalay, I. C. *J. Electrochem. Soc.* **2014**, *161*, A1213.
- (192) Chen, R.; Wu, F.; Li, L.; Guan, Y.; Qiu, X.; Chen, S.; Li, Y.; Wu, S. *J. Power Sources* **2007**, *172*, 395.
- (193) Sano, A.; Maruyama, S. *J. Power Sources* **2009**, *192*, 714.
- (194) Zuo, X.; Xu, M.; Li, W.; Su, D.; Liu, J. *Electrochem. Solid-State Lett.* **2006**, *9*, A196.
- (195) Xu, M. Q.; Li, W. S.; Zuo, X. X.; Liu, J. S.; Xu, X. *J. Power Sources* **2007**, *174*, 705.
- (196) Li, B.; Xu, M.; Li, T.; Li, W.; Hu, S. *Electrochim. Commun.* **2012**, *17*, 92.
- (197) Li, B.; Xu, M.; Li, B.; Liu, Y.; Yang, L.; Li, W.; Hu, S. *Electrochim. Acta* **2013**, *105*, 1.
- (198) Wang, B.; Qu, Q. T.; Xia, Q.; Wu, Y. P.; Li, X.; Gan, C. L.; van Ree, T. *Electrochim. Acta* **2008**, *54*, 816.
- (199) Burns, J. C.; Sinha, N. N.; Jain, G.; Ye, H.; VanElzen, C. M.; Lamanna, W. M.; Xiao, A.; Scott, E.; Choi, J.; Dahn, J. R. *J. Electrochem. Soc.* **2012**, *159*, A1105.
- (200) Burns, J. C.; Xia, X.; Dahn, J. R. *J. Electrochem. Soc.* **2013**, *160*, A383.
- (201) Zhang, S. *S. J. Power Sources* **2006**, *163*, 567.
- (202) Korepp, C.; Kern, W.; Lanzer, E. A.; Raimann, P. R.; Besenhard, J. O.; Yang, M. H.; Möller, K.-C.; Shieh, D.-T.; Winter, M. *J. Power Sources* **2007**, *174*, 387.
- (203) Korepp, C.; Kern, W.; Lanzer, E. A.; Raimann, P. R.; Besenhard, J. O.; Yang, M.; Möller, K.-C.; Shieh, D.-T.; Winter, M. *J. Power Sources* **2007**, *174*, 628.
- (204) Wu, F.; Xiang, J.; Li, L.; Chen, J.; Tan, G.; Chen, R. *J. Power Sources* **2012**, *202*, 322.
- (205) Wu, F.; Zhu, Q.; Li, L.; Chen, R.; Chen, S. *J. Mater. Chem. A* **2013**, *1*, 3659.
- (206) Xu, K.; Lee, U.; Zhang, S.; Allen, J. L.; Jow, T. R. *Electrochim. Solid-State Lett.* **2004**, *7*, A273.
- (207) Xu, K.; Zhang, S.; Jow, T. R. *Electrochim. Solid-State Lett.* **2005**, *8*, A365.
- (208) Yang, L.; Furczon, M. M.; Xiao, A.; Lucht, B. L.; Zhang, Z.; Abraham, D. P. *J. Power Sources* **2010**, *195*, 1698.
- (209) Aurbach, D.; Gnanaraj, J. S.; Geissler, W.; Schmidt, M. *J. Electrochem. Soc.* **2004**, *151*, A23.
- (210) Wu, M.-S.; Lin, J.-C.; Chiang, P.-C. *J. Electrochem. Solid-State Lett.* **2004**, *7*, A206.
- (211) Huang, Q.; Wang, T.; Yan, M.; Jiang, Z. *J. Electrochem. Soc.* **2006**, *153*, A2363.
- (212) Hao, X.; Liu, P.; Zhang, Z.; Lai, Y.; Wang, X.; Li, J.; Liu, Y. *Electrochim. Solid-State Lett.* **2010**, *13*, A118.
- (213) Komaba, S.; Itabashi, T.; Watanabe, M.; Groult, H.; Kumagai, N. *J. Electrochem. Soc.* **2007**, *154*, A322.
- (214) Sano, M.; Hattori, T.; Hibino, T.; Fujita, M. *Electrochim. Solid-State Lett.* **2007**, *10*, A270.
- (215) Chrétien, F.; Jones, J.; Damas, C.; Lemordant, D.; Willmann, P.; Anouti, M. *J. Power Sources* **2014**, *248*, 969.
- (216) Lee, H.-Y.; Lee, S.-M. *Electrochim. Commun.* **2004**, *6*, 465.
- (217) Liu, N.; Wu, H.; McDowell, M. T.; Yao, Y.; Wang, C.; Cui, Y. *Nano Lett.* **2012**, *12*, 3315.
- (218) Lee, Y. M.; Lee, J. Y.; Shim, H.-T.; Lee, J. K.; Park, J.-K. *J. Electrochem. Soc.* **2007**, *154*, A515.
- (219) Yen, Y.-C.; Chao, S.-C.; Wu, H.-C.; Wu, N.-L. *J. Electrochem. Soc.* **2009**, *156*, A95.
- (220) Profatilova, I. A.; Langer, T.; Badillo, J. P.; Schmitz, A.; Orthner, H.; Wiggers, H.; Passerini, S.; Winter, M. *J. Electrochem. Soc.* **2012**, *159*, A657.
- (221) Arreaga-Salas, D. E.; Sra, A. K.; Roodenko, K.; Chabal, Y. J.; Hinkle, C. L. *J. Phys. Chem. C* **2012**, *116*, 9072.
- (222) Schroder, K. W.; Celio, H.; Webb, L. J.; Stevenson, K. *J. Phys. Chem. C* **2012**, *116*, 19737.
- (223) Delpuech, N.; Dupré, N.; Mazouzi, D.; Gaubicher, J.; Moreau, P.; Bridel, J. S.; Guyomard, D.; Lestriez, B. *Electrochim. Commun.* **2013**, *33*, 72.
- (224) Elazari, R.; Salitra, G.; Gershinsky, G.; Garsuch, A.; Panchenko, A.; Aurbach, D. *J. Electrochem. Soc.* **2012**, *159*, A1440.
- (225) Etacheri, V.; Haik, O.; Goffer, Y.; Roberts, G. A.; Stefan, I. C.; Fasching, R.; Aurbach, D. *Langmuir* **2011**, *28*, 965.
- (226) Chen, L.; Wang, K.; Xie, X.; Xie, J. *Electrochim. Solid-State Lett.* **2006**, *9*, A512.
- (227) Dalavi, S.; Guduru, P.; Lucht, B. L. *J. Electrochem. Soc.* **2012**, *159*, A642.
- (228) Choi, N.-S.; Yew, K. H.; Kim, H.; Kim, S.-S.; Choi, W.-U. *J. Power Sources* **2007**, *172*, 404.
- (229) Li, M.-Q.; Qu, M.-Z.; He, X.-Y.; Yu, Z.-L. *J. Electrochem. Soc.* **2009**, *156*, A294.
- (230) Ryu, Y.-G.; Lee, S.; Mah, S.; Lee, D. J.; Kwon, K.; Hwang, S.; Doo, S. *J. Electrochim. Soc.* **2008**, *155*, A583.
- (231) Song, S.-W.; Baek, S.-W. *Electrochim. Solid-State Lett.* **2009**, *12*, A23.
- (232) Choi, N.-S.; Yew, K. H.; Lee, K. Y.; Sung, M.; Kim, H.; Kim, S.-S. *J. Power Sources* **2006**, *161*, 1254.
- (233) Nakai, H.; Kubota, T.; Kita, A.; Kawashima, A. *J. Electrochim. Soc.* **2011**, *158*, A798.
- (234) Fridman, K.; Sharabi, R.; Elazari, R.; Gershinsky, G.; Markevich, E.; Salitra, G.; Aurbach, D.; Garsuch, A.; Lampert, J. *Electrochim. Commun.* **2013**, *33*, 31.
- (235) Song, S.-W.; Reade, R. P.; Cairns, E. J.; Vaughney, J. T.; Thackeray, M. M.; Striebel, K. A. *J. Electrochim. Soc.* **2004**, *151*, A1012.
- (236) Wagner, M. R.; Raimann, P. R.; Trifonova, A.; Moeller, K.-C.; Besenhard, J. O.; Winter, M. *Electrochim. Solid-State Lett.* **2004**, *7*, A201.
- (237) Song, S.-W.; Baek, S.-W. *Electrochim. Acta* **2009**, *54*, 1312.
- (238) Baek, S.-W.; Hong, S.-J.; Kim, D.-W.; Song, S.-W. *J. Power Sources* **2009**, *189*, 660.
- (239) Zhu, Y.; Casselman, M. D.; Li, Y.; Wei, A.; Abraham, D. P. *J. Power Sources* **2014**, *246*, 184.
- (240) Hu, M.; Pang, X.; Zhou, Z. *J. Power Sources* **2013**, *237*, 229.
- (241) Xu, W.; Chen, X.; Ding, F.; Xiao, J.; Wang, D.; Pan, A.; Zheng, J.; Li, X. S.; Padmaperuma, A. B.; Zhang, J.-G. *J. Power Sources* **2012**, *213*, 304.
- (242) Täubert, C.; Fleischhammer, M.; Wohlfahrt-Mehrens, M.; Wietelmann, U.; Buhrmester, T. *J. Electrochim. Soc.* **2010**, *157*, A721.
- (243) Dalavi, S.; Xu, M.; Knight, B.; Lucht, B. L. *Electrochim. Solid-State Lett.* **2011**, *15*, A28.
- (244) Aravindan, V.; Cheah, Y. L.; Ling, W. C.; Madhavi, S. *J. Electrochim. Soc.* **2012**, *159*, A1435.
- (245) Zuo, X.; Fan, C.; Liu, J.; Xiao, X.; Wu, J.; Nan, J. *J. Electrochim. Soc.* **2013**, *160*, A1199.

- (246) Fu, M. H.; Huang, K. L.; Liu, S. Q.; Liu, J. S.; Li, Y. K. *J. Power Sources* **2010**, *195*, 862.
- (247) Yang, L.; Markmaitree, T.; Lucht, B. L. *J. Power Sources* **2011**, *196*, 2251.
- (248) Hu, M.; Wei, J.; Xing, L.; Zhou, Z. *J. Appl. Electrochem.* **2012**, *42*, 291.
- (249) Zhu, Y.; Li, Y.; Bettge, M.; Abraham, D. P. *J. Electrochem. Soc.* **2012**, *159*, A2109.
- (250) Horino, T.; Tamada, H.; Kishimoto, A.; Kaneko, J.; Iriyama, Y.; Tanaka, Y.; Fujinami, T. *J. Electrochem. Soc.* **2010**, *157*, A677.
- (251) Ping, P.; Xia, X.; Wang, Q. S.; Sun, J. H.; Dahn, J. R. *J. Electrochem. Soc.* **2013**, *160*, A426.
- (252) Sharabi, R.; Markevich, E.; Fridman, K.; Gershinsky, G.; Salitra, G.; Aurbach, D.; Semrau, G.; Schmidt, M. A.; Schall, N.; Bruenig, C. *Electrochem. Commun.* **2013**, *28*, 20.
- (253) Xiao, L.; Ai, X.; Cao, Y.; Yang, H. *Electrochim. Acta* **2004**, *49*, 4189.
- (254) Abe, K.; Takaya, T.; Yoshitake, H.; Ushigoe, Y.; Yoshio, M.; Wang, H. *Electrochim. Solid-State Lett.* **2004**, *7*, A462.
- (255) Abe, K.; Ushigoe, Y.; Yoshitake, H.; Yoshio, M. *J. Power Sources* **2006**, *153*, 328.
- (256) Lee, K.-S.; Sun, Y.-K.; Noh, J.; Song, K. S.; Kim, D.-W. *Electrochem. Commun.* **2009**, *11*, 1900.
- (257) Lee, Y.-S.; Lee, K.-S.; Sun, Y.-K.; Lee, Y. M.; Kim, D.-W. *J. Power Sources* **2011**, *196*, 6997.
- (258) Xing, L. Y.; Hu, M.; Tang, Q.; Wei, J. P.; Qin, X.; Zhou, Z. *Electrochim. Acta* **2012**, *59*, 172.
- (259) Hu, M.; Wei, J.; Xing, L.; Zhou, Z. *J. Power Sources* **2013**, *222*, 373.
- (260) Abouimrane, A.; Odom, S. A.; Tavassol, H.; Schulmerich, M. V.; Wu, H.; Bhargava, R.; Gewirth, A. A.; Moore, J. S.; Amine, K. J. *Electrochim. Soc.* **2013**, *160*, A268.
- (261) Yang, L.; Lucht, B. L. *Electrochim. Solid-State Lett.* **2009**, *12*, A229.
- (262) Tan, S.; Zhang, Z.; Li, Y.; Li, Y.; Zheng, J.; Zhou, Z.; Yang, Y. *J. Electrochim. Soc.* **2013**, *160*, A285.
- (263) Xu, M.; Liu, Y.; Li, B.; Li, W.; Li, X.; Hu, S. *Electrochim. Commun.* **2012**, *18*, 123.
- (264) Tang, M.; Newman, J. *J. Electrochim. Soc.* **2011**, *158*, A530.
- (265) Moshurchak, L. M.; Buhrmester, C.; Wang, R. L.; Dahn, J. R. *Electrochim. Acta* **2007**, *52*, 3779.
- (266) Buhrmester, C.; Chen, J.; Moshurchak, L.; Jiang, J.; Wang, R. L.; Dahn, J. R. *J. Electrochim. Soc.* **2005**, *152*, A2390.
- (267) Moshurchak, L. M.; Buhrmester, C.; Dahn, J. R. *J. Electrochim. Soc.* **2005**, *152*, A1279.
- (268) Chen, J.; Buhrmester, C.; Dahn, J. R. *Electrochim. Solid-State Lett.* **2005**, *8*, A59.
- (269) Dahn, J. R.; Jiang, J.; Moshurchak, L. M.; Fleischauer, M. D.; Buhrmester, C.; Krause, L. J. *J. Electrochim. Soc.* **2005**, *152*, A1283.
- (270) Buhrmester, C.; Moshurchak, L.; Wang, R. L.; Dahn, J. R. *J. Electrochim. Soc.* **2006**, *153*, A288.
- (271) Buhrmester, C.; Moshurchak, L. M.; Wang, R. L.; Dahn, J. R. *J. Electrochim. Soc.* **2006**, *153*, A1800.
- (272) Moshurchak, L. M.; Buhrmester, C.; Dahn, J. R. *J. Electrochim. Soc.* **2008**, *155*, A129.
- (273) Chen, Z.; Wang, Q.; Amine, K. *J. Electrochim. Soc.* **2006**, *153*, A2215.
- (274) Moshurchak, L. M.; Lamanna, W. M.; Bulinski, M.; Wang, R. L.; Garsuch, R. R.; Jiang, J.; Magnuson, D.; Triemert, M.; Dahn, J. R. *J. Electrochim. Soc.* **2009**, *156*, A309.
- (275) Han, Y.-K.; Jung, J.; Yu, S.; Lee, H. *J. Power Sources* **2009**, *187*, 581.
- (276) Chen, J.-H.; He, L.-M.; Wang, R. L. *J. Electrochim. Soc.* **2012**, *159*, A1636.
- (277) Lee, H.; Lee, J. H.; Ahn, S.; Kim, H.-J.; Cho, J.-J. *Electrochim. Solid-State Lett.* **2006**, *9*, A307.
- (278) Ma, Y.; Yin, G.; Zuo, P.; Tan, X.; Gao, Y.; Shi, P. *Electrochim. Solid-State Lett.* **2008**, *11*, A129.
- (279) Dippel, C.; Schmitz, R.; Müller, R.; Böttcher, T.; Kunze, M.; Lex-Balducci, A.; Röschenthal, G.-V.; Passerini, S.; Winter, M. *J. Electrochim. Soc.* **2012**, *159*, A1587.
- (280) Wang, D. Y.; Sinha, N. N.; Petibon, R.; Burns, J. C.; Dahn, J. R. *J. Power Sources* **2014**, *251*, 311.
- (281) Li, S. R.; Sinha, N. N.; Chen, C. H.; Xu, K.; Dahn, J. R. *J. Electrochim. Soc.* **2013**, *160*, A2014.
- (282) Groult, H.; Kaplan, B.; Komaba, S.; Kumagai, N.; Gupta, V.; Nakajima, T.; Simon, B. *J. Electrochim. Soc.* **2003**, *150*, G67.
- (283) Komaba, S.; Watanabe, M.; Groult, H.; Kumagai, N.; Okahara, K. *Electrochim. Solid-State Lett.* **2006**, *9*, A130.
- (284) Nobili, F.; Dsoke, S.; Mancini, M.; Tossici, R.; Marassi, R. *J. Power Sources* **2008**, *180*, 845.
- (285) Mancini, M.; Nobili, F.; Dsoke, S.; D'Amico, F.; Tossici, R.; Croce, F.; Marassi, R. *J. Power Sources* **2009**, *190*, 141.
- (286) Nobili, F.; Dsoke, S.; Mancini, M.; Marassi, R. *Fuel Cells* **2009**, *9*, 264.
- (287) Ui, K.; Kikuchi, S.; Mikami, F.; Kadoma, Y.; Kumagai, N. *J. Power Sources* **2007**, *173*, 518.
- (288) Komaba, S.; Ozeki, T.; Okushi, K. *J. Power Sources* **2009**, *189*, 197.
- (289) Lux, S. F.; Placke, T.; Engelhardt, C.; Nowak, S.; Bieker, P.; Wirth, K.-E.; Passerini, S.; Winter, M.; Meyer, H.-W. *J. Electrochim. Soc.* **2012**, *159*, A1849.
- (290) Wang, C.; Wu, H.; Chen, Z.; McDowell, M. T.; Cui, Y.; Bao, Z. *Nat. Chem.* **2013**, *5*, 1042.
- (291) Park, K. S.; Son, J. T.; Chung, H. T.; Kim, S. J.; Lee, C. H.; Kang, K. T.; Kim, H. G. *Solid State Commun.* **2004**, *129*, 311.
- (292) Choi, D.; Kumta, P. N. *J. Power Sources* **2007**, *163*, 1064.
- (293) Sisbandini, C.; Brandell, D.; Gustafsson, T.; Thomas, J. O. *Electrochim. Solid-State Lett.* **2009**, *12*, A99.
- (294) Liu, L.; Chen, L.; Huang, X.; Yang, X.-Q.; Yoon, W.-S.; Lee, H. S.; McBreen, J. *J. Electrochim. Soc.* **2004**, *151*, A1344.
- (295) Kim, J.-S.; Johnson, C. S.; Vaughey, J. T.; Hackney, S. A.; Walz, K. A.; Zeltner, W. A.; Anderson, M. A.; Thackeray, M. M. *J. Electrochim. Soc.* **2004**, *151*, A1755.
- (296) Ha, H.-W.; Jeong, K. H.; Yun, N. J.; Hong, M. Z.; Kim, K. *Electrochim. Acta* **2005**, *50*, 3764.
- (297) Verdier, S.; El Ouattani, L.; Dedryvère, R.; Bonhomme, F.; Biensan, P.; Gonbeau, D. *J. Electrochim. Soc.* **2007**, *154*, A1088.
- (298) Cho, J.; Kim, B.; Lee, J.-G.; Kim, Y.-W.; Park, B. *J. Electrochim. Soc.* **2005**, *152*, A32.
- (299) Bai, Y.; Liu, N.; Liu, J.; Wang, Z.; Chen, L. *Electrochim. Solid-State Lett.* **2006**, *9*, A552.
- (300) Kim, B.; Kim, C.; Kim, T.-G.; Ahn, D.; Park, B. *J. Electrochim. Soc.* **2006**, *153*, A1773.
- (301) Sun, Y.-K.; Han, J.-M.; Myung, S.-T.; Lee, S.-W.; Amine, K. *Electrochim. Commun.* **2006**, *8*, 821.
- (302) Sun, Y.-K.; Yoon, C. S.; Myung, S.-T.; Belharouak, I.; Amine, K. *J. Electrochim. Soc.* **2009**, *156*, A1005.
- (303) Amine, R.; Sun, H. H.; Sun, H. J.; Prakash, J. *Electrochim. Solid-State Lett.* **2010**, *13*, A101.
- (304) Sun, Y.-K.; Cho, S.-W.; Lee, S.-W.; Yoon, C. S.; Amine, K. *J. Electrochim. Soc.* **2007**, *154*, A168.
- (305) Zheng, J. M.; Zhang, Z. R.; Wu, X. B.; Dong, Z. X.; Zhu, Z.; Yang, Y. *J. Electrochim. Soc.* **2008**, *155*, A775.
- (306) Sun, Y.-K.; Myung, S.-T.; Park, B.-C.; Yashiro, H. *J. Electrochim. Soc.* **2008**, *155*, A705.
- (307) Park, Y.-S.; Choi, K.-H.; Park, H.-K.; Lee, S.-M. *J. Electrochim. Soc.* **2010**, *157*, A850.
- (308) Arrebolá, J.; Caballero, A.; Hernán, L.; Morales, J.; Rodríguez Castellón, E.; Ramos Barrado, J. R. *J. Electrochim. Soc.* **2007**, *154*, A178.
- (309) Liu, J.; Manthiram, A. *Chem. Mater.* **2009**, *21*, 1695.
- (310) Liu, J.; Manthiram, A. *J. Electrochim. Soc.* **2009**, *156*, A66.
- (311) Liu, J.; Manthiram, A. *J. Electrochim. Soc.* **2009**, *156*, A833.
- (312) Sclar, H.; Haik, O.; Menachem, T.; Grinblat, J.; Leifer, N.; Meitav, A.; Luski, S.; Aurbach, D. *J. Electrochim. Soc.* **2012**, *159*, A228.

- (313) Kim, M. C.; Kim, S. H.; Aravindan, V.; Kim, W. S.; Lee, S. Y.; Lee, Y. S. *J. Electrochem. Soc.* **2013**, *160*, A1003.
- (314) Kim, Y.; Dudney, N. J.; Chi, M.; Martha, S. K.; Nanda, J.; Veith, G. M.; Liang, C. *J. Electrochem. Soc.* **2013**, *160*, A3113.
- (315) Snyder, M. Q.; Trebukhova, S. A.; Ravdel, B.; Wheeler, M. C.; DiCarlo, J.; Tripp, C. P.; DeSisto, W. J. *J. Power Sources* **2007**, *165*, 379.
- (316) Jung, Y. S.; Cavanagh, A. S.; Dillon, A. C.; Groner, M. D.; George, S. M.; Lee, S.-H. *J. Electrochem. Soc.* **2010**, *157*, A75.
- (317) Cheng, H.-M.; Wang, F.-M.; Chu, J. P.; Santhanam, R.; Rick, J.; Lo, S.-C. *J. Phys. Chem. C* **2012**, *116*, 7629.
- (318) Woo, J. H.; Trevey, J. E.; Cavanagh, A. S.; Choi, Y. S.; Kim, S. C.; George, S. M.; Oh, K. H.; Lee, S.-H. *J. Electrochem. Soc.* **2012**, *159*, A1120.
- (319) Jung, Y. S.; Cavanagh, A. S.; Yan, Y.; George, S. M.; Manthiram, A. *J. Electrochem. Soc.* **2011**, *158*, A1298.
- (320) Jung, Y. S.; Cavanagh, A. S.; Riley, L. A.; Kang, S.-H.; Dillon, A. C.; Groner, M. D.; George, S. M.; Lee, S.-H. *Adv. Mater.* **2010**, *22*, 2172.
- (321) Bettge, M.; Li, Y.; Sankaran, B.; Rago, N. D.; Spila, T.; Haasch, R. T.; Petrov, I.; Abraham, D. P. *J. Power Sources* **2013**, *233*, 346.
- (322) Angell, C. A.; Ansari, Y.; Zhao, Z. *Faraday Discuss.* **2012**, *154*, 9.
- (323) Peng, C.; Yang, L.; Zhang, Z.; Tachibana, K.; Yang, Y. *J. Power Sources* **2007**, *173*, 510.
- (324) Mun, J.; Yim, T.; Choi, C. Y.; Ryu, J. H.; Kim, Y. G.; Oh, S. M. *Electrochem. Solid-State Lett.* **2010**, *13*, A109.
- (325) MacFarlane, D. R.; Meakin, P.; Sun, J.; Amini, N.; Forsyth, M. *J. Phys. Chem. B* **1999**, *103*, 4164.
- (326) MacFarlane, D. R.; Huang, J.; Forsyth, M. *Nature* **1999**, *402*, 792.
- (327) Shin, J.-H.; Henderson, W. A.; Passerini, S. *Electrochem. Commun.* **2003**, *5*, 1016.
- (328) Shin, J.-H.; Henderson, W. A.; Passerini, S. *Electrochem. Solid-State Lett.* **2005**, *8*, A125.
- (329) Armand, M.; Endres, F.; MacFarlane, D. R.; Ohno, H.; Scrosati, B. *Nat. Mater.* **2009**, *8*, 621.
- (330) Umebayashi, Y.; Mitsugi, T.; Fukuda, S.; Fujimori, T.; Fujii, K.; Kanzaki, R.; Takeuchi, M.; Ishiguro, S.-I. *J. Phys. Chem. B* **2007**, *111*, 13028.
- (331) Saito, Y.; Umecky, T.; Niwa, J.; Sakai, T.; Maeda, S. *J. Phys. Chem. B* **2007**, *111*, 11794.
- (332) Sagane, F.; Abe, T.; Ogumi, Z. *J. Electrochem. Soc.* **2012**, *159*, A1766.
- (333) Lee, S.-Y.; Yong, H. H.; Lee, Y. J.; Kim, S. K.; Ahn, S. *J. Phys. Chem. B* **2005**, *109*, 13663.
- (334) Ong, S. P.; Andreussi, O.; Wu, Y.; Marzari, N.; Ceder, G. *Chem. Mater.* **2011**, *23*, 2979.
- (335) Huang, J. Y.; Zhong, L.; Wang, C. M.; Sullivan, J. P.; Xu, W.; Zhang, L. Q.; Mao, S. X.; Hudak, N. S.; Liu, X. H.; Subramanian, A.; Fan, H.; Qi, L.; Kushima, A.; Li, J. *Science* **2010**, *330*, 1515.
- (336) Garcia, B.; Lavallée, S.; Perron, G.; Michot, C.; Armand, M. *Electrochim. Acta* **2004**, *49*, 4583.
- (337) Borgel, V.; Markevich, E.; Aurbach, D.; Semrau, G.; Schmidt, M. *J. Power Sources* **2009**, *189*, 331.
- (338) Seki, S.; Kobayashi, Y.; Miyashiro, H.; Ohno, Y.; Usami, A.; Mita, Y.; Kihira, N.; Watanabe, M.; Terada, N. *J. Phys. Chem. B* **2006**, *110*, 10228.
- (339) Seki, S.; Ohno, Y.; Kobayashi, Y.; Miyashiro, H.; Usami, A.; Mita, Y.; Tokuda, H.; Watanabe, M.; Hayamizu, K.; Tsuzuki, S.; Hattori, M.; Terada, N. *J. Electrochem. Soc.* **2007**, *154*, A173.
- (340) Seki, S.; Ohno, Y.; Mita, Y.; Serizawa, N.; Takei, K.; Miyashiro, H. *ECS Electrochem. Lett.* **2012**, *1*, A77.
- (341) Best, A. S.; Bhatt, A. I.; Hollenkamp, A. F. *J. Electrochem. Soc.* **2010**, *157*, A903.
- (342) Kurig, H.; Vestli, M.; Tönurist, K.; Jänes, A.; Lust, E. *J. Electrochem. Soc.* **2012**, *159*, A944.
- (343) Seki, S.; Serizawa, N.; Hayamizu, K.; Tsuzuki, S.; Umebayashi, Y.; Takei, K.; Miyashiro, H. *J. Electrochem. Soc.* **2012**, *159*, A967.
- (344) Seki, S.; Mita, Y.; Tokuda, H.; Ohno, Y.; Kobayashi, Y.; Usami, A.; Watanabe, M.; Terada, N.; Miyashiro, H. *Electrochem. Solid-State Lett.* **2007**, *10*, A237.
- (345) Srour, H.; Rouault, H.; Santini, C. *J. Electrochem. Soc.* **2013**, *160*, A66.
- (346) Lu, Y.; Das, S. K.; Moganty, S. S.; Archer, L. A. *Adv. Mater.* **2012**, *24*, 4430.
- (347) Unemoto, A.; Ogawa, H.; Ito, S.; Honma, I. *J. Electrochem. Soc.* **2013**, *160*, A138.
- (348) Henderson, W. A.; Passerini, S. *Chem. Mater.* **2004**, *16*, 2881.
- (349) Castriona, M.; Caruso, T.; Agostino, R. G.; Cazzanelli, E.; Henderson, W. A.; Passerini, S. *J. Phys. Chem. A* **2004**, *109*, 92.
- (350) Huang, J.; Hollenkamp, A. F. *J. Phys. Chem. C* **2010**, *114*, 21840.
- (351) Borodin, O.; Smith, G. D.; Henderson, W. *J. Phys. Chem. B* **2006**, *110*, 16879.
- (352) Bhatt, A. I.; Kao, P.; Best, A. S.; Hollenkamp, A. F. *J. Electrochem. Soc.* **2013**, *160*, A1171.
- (353) Howlett, P. C.; Brack, N.; Hollenkamp, A. F.; Forsyth, M.; MacFarlane, D. R. *J. Electrochem. Soc.* **2006**, *153*, A595.
- (354) Howlett, P. C.; MacFarlane, D. R.; Hollenkamp, A. F. *Electrochem. Solid-State Lett.* **2004**, *7*, A97.
- (355) Fericola, A.; Croce, F.; Scrosati, B.; Watanabe, T.; Ohno, H. *J. Power Sources* **2007**, *174*, 342.
- (356) Mun, J.; Kim, S.; Yim, T.; Ryu, J. H.; Kim, Y. G.; Oh, S. M. *J. Electrochem. Soc.* **2010**, *157*, A136.
- (357) Mun, J.; Yim, T.; Park, K.; Ryu, J. H.; Kim, Y. G.; Oh, S. M. *J. Electrochem. Soc.* **2011**, *158*, A453.
- (358) Zhou, Q.; Henderson, W. A.; Appetecchi, G. B.; Montanino, M.; Passerini, S. *J. Phys. Chem. B* **2008**, *112*, 13577.
- (359) Paillard, E.; Zhou, Q.; Henderson, W. A.; Appetecchi, G. B.; Montanino, M.; Passerini, S. *J. Electrochem. Soc.* **2009**, *156*, A891.
- (360) Matsumoto, H.; Sakaue, H.; Tatsumi, K.; Kikuta, M.; Ishiko, E.; Kono, M. *J. Power Sources* **2006**, *160*, 1308.
- (361) Seki, S.; Kobayashi, Y.; Miyashiro, H.; Ohno, Y.; Mita, Y.; Terada, N.; Charest, P.; Guerfi, A.; Zaghib, K. *J. Phys. Chem. C* **2008**, *112*, 16708.
- (362) Markevich, E.; Baranchugov, V.; Salitra, G.; Aurbach, D.; Schmidt, M. A. *J. Electrochem. Soc.* **2008**, *155*, A132.
- (363) Fericola, A.; Weise, F. C.; Greenbaum, S. G.; Kagimoto, J.; Scrosati, B.; Soleto, A. *J. Electrochem. Soc.* **2009**, *156*, A514.
- (364) Salem, N.; Nicodemou, L.; Abu-Lebdeh, Y.; Davidson, I. J. *J. Electrochem. Soc.* **2011**, *159*, A172.
- (365) Lane, G. H.; Best, A. S.; MacFarlane, D. R.; Hollenkamp, A. F.; Forsyth, M. *J. Electrochem. Soc.* **2010**, *157*, A876.
- (366) Sato, T.; Maruo, T.; Marukane, S.; Takagi, K. *J. Power Sources* **2004**, *138*, 253.
- (367) Seki, S.; Kobayashi, Y.; Miyashiro, H.; Ohno, Y.; Mita, Y.; Usami, A.; Terada, N.; Watanabe, M. *Electrochem. Solid-State Lett.* **2005**, *8*, A577.
- (368) Kobayashi, Y.; Mita, Y.; Seki, S.; Ohno, Y.; Miyashiro, H.; Terada, N. *J. Electrochem. Soc.* **2007**, *154*, A677.
- (369) Seki, S.; Ohno, Y.; Miyashiro, H.; Kobayashi, Y.; Usami, A.; Mita, Y.; Terada, N.; Hayamizu, K.; Tsuzuki, S.; Watanabe, M. *J. Electrochem. Soc.* **2008**, *155*, A421.
- (370) Egashira, M.; Okada, S.; Yamaki, J.-i.; Dri, D. A.; Bonadies, F.; Scrosati, B. *J. Power Sources* **2004**, *138*, 240.
- (371) Egashira, M.; Nakagawa, M.; Watanabe, I.; Okada, S.; Yamaki, J.-i. *J. Power Sources* **2005**, *146*, 685.
- (372) Doyle, K. P.; Lang, C. M.; Kim, K.; Kohl, P. A. *J. Electrochem. Soc.* **2006**, *153*, A1353.
- (373) Tsunashima, K.; Sugiya, M. *Electrochem. Solid-State Lett.* **2008**, *11*, A17.
- (374) Vega, J. A.; Zhou, J.; Kohl, P. A. *J. Electrochem. Soc.* **2009**, *156*, A253.
- (375) Tsunashima, K.; Sugiya, M. *Electrochem. Commun.* **2007**, *9*, 2353.
- (376) Tsunashima, K.; Yonekawa, F.; Kikuchi, M.; Sugiya, M. *J. Electrochem. Soc.* **2010**, *157*, A1274.

- (377) Tsunashima, K.; Yonekawa, F.; Sugiya, M. *Electrochim. Solid-State Lett.* **2009**, *12*, A54.
- (378) Serizawa, N.; Seki, S.; Tsuzuki, S.; Hayamizu, K.; Umebayashi, Y.; Takei, K.; Miyashiro, H. *J. Electrochem. Soc.* **2011**, *158*, A1023.
- (379) Wang, Y.; Zaghib, K.; Guerfi, A.; Bazito, F. F. C.; Torresi, R. M.; Dahn, J. R. *Electrochim. Acta* **2007**, *52*, 6346.
- (380) Fenton, D. E.; Parker, J. M.; Wright, P. V. *Polymer* **1973**, *14*, 589.
- (381) Tominaga, Y.; Shimomura, T.; Nakamura, M. *Polymer* **2010**, *51*, 4295.
- (382) Nakamura, M.; Tominaga, Y. *Electrochim. Acta* **2011**, *57*, 36.
- (383) Tominaga, Y.; Nanthana, V.; Tohyama, D. *Polym. J.* **2012**, *44*, 1155.
- (384) Tominaga, Y.; Yamazaki, K. *Chem. Commun.* **2014**, *50*, 4448.
- (385) Kato, Y.; Yokoyama, S.; Yabe, T.; Ikuta, H.; Uchimoto, Y.; Wakihara, M. *Electrochim. Acta* **2004**, *50*, 281.
- (386) Tabata, S.-i.; Hirakimoto, T.; Tokuda, H.; Susan, M. A. B. H.; Watanabe, M. *J. Phys. Chem. B* **2004**, *108*, 19518.
- (387) Ciosek, M.; Marcinek, M.; Źukowska, G.; Wieczorek, W. *Electrochim. Acta* **2009**, *54*, 4487.
- (388) Shin, J.-H.; Henderson, W. A.; Passerini, S. *J. Electrochem. Soc.* **2005**, *152*, A978.
- (389) Fisher, A. S.; Khalid, M. B.; Widstrom, M.; Kofinas, P. *J. Electrochem. Soc.* **2012**, *159*, A592.
- (390) Fisher, A. S.; Khalid, M. B.; Kofinas, P. *J. Electrochem. Soc.* **2012**, *159*, A2124.
- (391) Wang, C.; Sakai, T.; Watanabe, O.; Hirahara, K.; Nakanishi, T. *J. Electrochem. Soc.* **2003**, *150*, A1166.
- (392) Niitani, T.; Shimada, M.; Kawamura, K.; Dokko, K.; Rho, Y.-H.; Kanamura, K. *Electrochim. Solid-State Lett.* **2005**, *8*, A385.
- (393) Niitani, T.; Amaike, M.; Nakano, H.; Dokko, K.; Kanamura, K. *J. Electrochim. Soc.* **2009**, *156*, A577.
- (394) Panday, A.; Mullin, S.; Gomez, E. D.; Wanakule, N.; Chen, V. L.; Hexemer, A.; Pople, J.; Balsara, N. P. *Macromolecules* **2009**, *42*, 4632.
- (395) Hallinan, D. T., Jr.; Mullin, S. A.; Stone, G. M.; Balsara, N. P. *J. Electrochim. Soc.* **2013**, *160*, A464.
- (396) Stone, G. M.; Mullin, S. A.; Teran, A. A.; Hallinan, D. T., Jr.; Minor, A. M.; Hexemer, A.; Balsara, N. P. *J. Electrochim. Soc.* **2012**, *159*, A222.
- (397) Monroe, C.; Newman, J. *J. Electrochim. Soc.* **2005**, *152*, A396.
- (398) Jiang, G.; Maeda, S.; Yang, H.; Wang, C.; Saito, Y.; Tanase, S.; Sakai, T. *J. Electrochim. Soc.* **2004**, *151*, A1886.
- (399) Trapa, P. E.; Won, Y.-Y.; Mui, S. C.; Olivetti, E. A.; Huang, B.; Sadoway, D. R.; Mayes, A. M.; Dallek, S. *J. Electrochim. Soc.* **2005**, *152*, A1.
- (400) Nunes, S. C.; de Zea Bermudez, V.; Ostrovskii, D.; Silva, M. M.; Barros, S.; Smith, M. J.; Carlos, L. D.; Rocha, J.; Morales, E. *J. Electrochim. Soc.* **2005**, *152*, A429.
- (401) Walkowiak, M.; Schroeder, G.; Gierczyk, B.; Waszak, D.; Osińska, M. *Electrochim. Commun.* **2007**, *9*, 558.
- (402) Gadjourova, Z.; Andreev, Y. G.; Tunstall, D. P.; Bruce, P. G. *Nature* **2001**, *412*, 520.
- (403) Stoeva, Z.; Martin-Litas, I.; Staunton, E.; Andreev, Y. G.; Bruce, P. G. *J. Am. Chem. Soc.* **2003**, *125*, 4619.
- (404) Christie, A. M.; Lilley, S. J.; Staunton, E.; Andreev, Y. G.; Bruce, P. G. *Nature* **2005**, *433*, 50.
- (405) Capiglia, C.; Imanishi, N.; Takeda, Y.; Henderson, W. A.; Passerini, S. *J. Electrochim. Soc.* **2003**, *150*, A525.
- (406) Golodnitsky, D.; Livshits, E.; Kovarsky, R.; Peled, E.; Chung, S. H.; Suarez, S.; Greenbaum, S. G. *Electrochim. Solid-State Lett.* **2004**, *7*, A412.
- (407) Ratner, M. A.; Shriver, D. F. *Chem. Rev.* **1988**, *88*, 109.
- (408) Snyder, J. F.; Ratner, M. A.; Shriver, D. F. *J. Electrochim. Soc.* **2003**, *150*, A1090.
- (409) Trapa, P. E.; Acar, M. H.; Sadoway, D. R.; Mayes, A. M. *J. Electrochim. Soc.* **2005**, *152*, A2281.
- (410) Ghosh, A.; Kofinas, P. *J. Electrochim. Soc.* **2008**, *155*, A428.
- (411) Aoki, T.; Konno, A.; Fujinami, T. *J. Electrochim. Soc.* **2004**, *151*, A887.
- (412) Zhu, Y. S.; Gao, X. W.; Wang, X. J.; Hou, Y. Y.; Liu, L. L.; Wu, Y. P. *Electrochim. Commun.* **2012**, *22*, 29.
- (413) Maitra, P.; Wunder, S. L. *Electrochim. Solid-State Lett.* **2004**, *7*, A88.
- (414) Zhang, H.; Kulkarni, S.; Wunder, S. L. *J. Electrochim. Soc.* **2006**, *153*, A239.
- (415) Wang, C.; Zhang, X.-W.; Appleby, A. J. *J. Electrochim. Soc.* **2005**, *152*, A205.
- (416) Stephan, A. M.; Kumar, T. P.; Kulandainathan, M. A.; Lakshmi, N. A. *J. Phys. Chem. B* **2009**, *113*, 1963.
- (417) Aoki, T.; Konno, A.; Fujinami, T. *J. Power Sources* **2005**, *146*, 412.
- (418) Aoki, T.; Fujinami, T. *J. Electrochim. Soc.* **2005**, *152*, A2352.
- (419) Smart, M. C.; Ratnakumar, B. V.; Behar, A.; Whitcanack, L. D.; Yu, J. S.; Alamgir, M. *J. Power Sources* **2007**, *165*, 535.
- (420) Nyman, A.; Behm, M.; Lindbergh, G. *J. Electrochim. Soc.* **2011**, *158*, A628.
- (421) Nyman, A.; Behm, M.; Lindbergh, G. *J. Electrochim. Soc.* **2011**, *158*, A636.
- (422) Song, M.-K.; Kim, Y.-T.; Cho, J.-Y.; Cho, B. W.; Popov, B. N.; Rhee, H.-W. *J. Power Sources* **2004**, *125*, 10.
- (423) Passerini, S.; Lisi, M.; Momma, T.; Ito, H.; Shimizu, T.; Osaka, T. *J. Electrochim. Soc.* **2004**, *151*, A578.
- (424) Choi, S. W.; Jo, S. M.; Lee, W. S.; Kim, Y. R. *Adv. Mater.* **2003**, *15*, 2027.
- (425) Choi, S. W.; Kim, J. R.; Jo, S. M.; Lee, W. S.; Kim, Y.-R. *J. Electrochim. Soc.* **2005**, *152*, A989.
- (426) Lee, J.-T.; Wu, M.-S.; Wang, F.-M.; Liao, H.-W.; Li, C.-C.; Chang, S.-M.; Yang, C.-R. *Electrochim. Solid-State Lett.* **2007**, *10*, A97.
- (427) El-Enany, G.; Lacey, M. J.; Johns, P. A.; Owen, J. R. *Electrochim. Commun.* **2009**, *11*, 2320.
- (428) Hwang, S. S.; Cho, C. G.; Kim, H. *Electrochim. Commun.* **2010**, *12*, 916.
- (429) Zhu, Y. S.; Wang, X. J.; Hou, Y. Y.; Gao, X. W.; Liu, L. L.; Wu, Y. P.; Shimizu, M. *Electrochim. Acta* **2013**, *87*, 113.
- (430) Kottegoda, I. R. M.; Bakenov, Z.; Ikuta, H.; Wakihara, M. *J. Electrochim. Soc.* **2005**, *152*, A1533.
- (431) Morita, M.; Niida, Y.; Yoshimoto, N.; Adachi, K. *J. Power Sources* **2005**, *146*, 427.
- (432) Angell, C. A.; Liu, C.; Sanchez, E. *Nature* **1993**, *362*, 137.
- (433) Jeong, S.-K.; Inaba, M.; Iriyama, Y.; Abe, T.; Ogumi, Z. *Electrochim. Solid-State Lett.* **2003**, *6*, A13.
- (434) Matsumoto, K.; Inoue, K.; Nakahara, K.; Yuge, R.; Noguchi, T.; Utsugi, K. *J. Power Sources* **2013**, *231*, 234.
- (435) McOwen, D. W.; Seo, D. M.; Borodin, O.; Vatamanu, J.; Boyle, P. D.; Henderson, W. A. *Energy Environ. Sci.* **2014**, *7*, 416.
- (436) Pappfenbus, T. M.; Henderson, W. A.; Owens, B. B.; Mann, K. R.; Smyrl, W. H. *J. Electrochim. Soc.* **2004**, *151*, A209.
- (437) Pappfenbus, T. M.; Mann, K. R.; Smyrl, W. H. *Electrochim. Solid-State Lett.* **2004**, *7*, A254.
- (438) Shin, J. H.; Cairns, E. J. *J. Electrochim. Soc.* **2008**, *155*, A368.
- (439) Tamura, T.; Hachida, T.; Yoshida, K.; Tachikawa, N.; Dokko, K.; Watanabe, M. *J. Power Sources* **2010**, *195*, 6095.
- (440) Tamura, T.; Yoshida, K.; Hachida, T.; Tsuchiya, M.; Nakamura, M.; Kazue, Y.; Tachikawa, N.; Dokko, K.; Watanabe, M. *Chem. Lett.* **2010**, *39*, 753.
- (441) Yoshida, K.; Nakamura, M.; Kazue, Y.; Tachikawa, N.; Suzuki, S.; Seki, S.; Dokko, K.; Watanabe, M. *J. Am. Chem. Soc.* **2011**, *133*, 13121.
- (442) Yoshida, K.; Tsuchiya, M.; Tachikawa, N.; Dokko, K.; Watanabe, M. *J. Phys. Chem. C* **2011**, *115*, 18384.
- (443) Seki, S.; Takei, K.; Miyashiro, H.; Watanabe, M. *J. Electrochim. Soc.* **2011**, *158*, A769.
- (444) Ueno, K.; Yoshida, K.; Tsuchiya, M.; Tachikawa, N.; Dokko, K.; Watanabe, M. *J. Phys. Chem. B* **2012**, *116*, 11323.
- (445) Lee, D.-J.; Hassoun, J.; Panero, S.; Sun, Y.-K.; Scrosati, B. *Electrochim. Commun.* **2012**, *14*, 43.

- (446) Suo, L.; Hu, Y.-S.; Li, H.; Armand, M.; Chen, L. *Nat. Commun.* **2013**, *4*, 1481.
- (447) Florjańczyk, Z.; Zygaldo-Monikowska, E.; Wieczorek, W.; Ryszawy, A.; Tomaszevska, A.; Fredman, K.; Golodnitsky, D.; Peled, E.; Scrosati, B. *J. Phys. Chem. B* **2004**, *108*, 14907.
- (448) Shin, J.-H.; Henderson, W. A.; Tizzani, C.; Passerini, S.; Jeong, S.-S.; Kim, K.-W. *J. Electrochem. Soc.* **2006**, *153*, A1649.
- (449) Zhu, C.; Cheng, H.; Yang, Y. *J. Electrochem. Soc.* **2008**, *155*, A569.
- (450) Ye, H.; Huang, J.; Xu, J. J.; Khalfan, A.; Greenbaum, S. G. *J. Electrochem. Soc.* **2007**, *154*, A1048.
- (451) Hu, Y.; Wang, Z.; Li, H.; Huang, X.; Chen, L. *J. Electrochem. Soc.* **2004**, *151*, A1424.
- (452) Chen, R.; Wu, F.; Liang, H.; Li, L.; Xu, B. *J. Electrochem. Soc.* **2005**, *152*, A1979.
- (453) Hu, Y.; Li, H.; Huang, X.; Chen, L. *Electrochem. Commun.* **2004**, *6*, 28.
- (454) Chen, R.; Wu, F.; Li, X. B.; Qiu, X.; Chen, S. *J. Phys. Chem. C* **2007**, *111*, 5184.
- (455) Boisset, A.; Menne, S.; Jacquemin, J.; Balducci, A.; Anouti, M. *Phys. Chem. Chem. Phys.* **2013**, *15*, 20054.
- (456) Yamada, Y.; Furukawa, K.; Sodeyama, K.; Kikuchi, K.; Yaegashi, M.; Tateyama, Y.; Yamada, A. *J. Am. Chem. Soc.* **2014**, *136*, 5039.
- (457) Takeno, K.; Ichimura, M.; Takano, K.; Yamaki, J. *J. Power Sources* **2005**, *142*, 298.
- (458) Broussely, M.; Biensan, P.; Bonhomme, F.; Blanchard, P.; Herreyre, S.; Nechev, K.; Staniewicz, R. *J. Power Sources* **2005**, *146*, 90.
- (459) Vetter, J.; Novák, P.; Wagner, M. R.; Veit, C.; Möller, K. C.; Besenhard, J. O.; Winter, M.; Wohlfahrt-Mehrens, M.; Vogler, C.; Hammouche, A. *J. Power Sources* **2005**, *147*, 269.
- (460) Balakrishnan, P. G.; Ramesh, R.; Prem Kumar, T. *J. Power Sources* **2006**, *155*, 401.
- (461) Safari, M.; Morcrette, M.; Teyssot, A.; Delacourt, C. *J. Electrochem. Soc.* **2009**, *156*, A145.
- (462) Castro, L.; Dedryvère, R.; Ledeuil, J.-B.; Bréger, J.; Tessier, C.; Gonbeau, D. *J. Electrochem. Soc.* **2012**, *159*, A357.
- (463) Huang, C.; Zhuang, S.; Tu, F. *J. Electrochem. Soc.* **2013**, *160*, A376.
- (464) Pinson, M. B.; Bazant, M. Z. *J. Electrochem. Soc.* **2013**, *160*, A243.
- (465) Lu, D.; Xu, M.; Zhou, L.; Garsuch, A.; Lucht, B. L. *J. Electrochem. Soc.* **2013**, *160*, A3138.
- (466) Smith, A. J.; Burns, J. C.; Trussler, S.; Dahn, J. R. *J. Electrochem. Soc.* **2010**, *157*, A196.
- (467) Smith, A. J.; Burns, J. C.; Dahn, J. R. *Electrochem. Solid-State Lett.* **2010**, *13*, A177.
- (468) Burns, J. C.; Jain, G.; Smith, A. J.; Eberman, K. W.; Scott, E.; Gardner, J. P.; Dahn, J. R. *J. Electrochem. Soc.* **2011**, *158*, A255.
- (469) Smith, A. J.; Burns, J. C.; Zhao, X.; Xiong, D.; Dahn, J. R. *J. Electrochem. Soc.* **2011**, *158*, A447.
- (470) Kawamura, T.; Okada, S.; Yamaki, J.-i. *J. Power Sources* **2006**, *156*, 547.
- (471) Sasaki, T.; Abe, T.; Iriyama, Y.; Inaba, M.; Ogumi, Z. *J. Power Sources* **2005**, *150*, 208.
- (472) Sasaki, T.; Jeong, S.-K.; Abe, T.; Iriyama, Y.; Inaba, M.; Ogumi, Z. *J. Electrochem. Soc.* **2005**, *152*, A1963.
- (473) Zhou, L.; Li, W.; Xu, M.; Lucht, B. L. *Electrochem. Solid-State Lett.* **2011**, *14*, A161.
- (474) Xu, K. *J. Electrochem. Soc.* **2009**, *156*, A751.
- (475) Tasaki, K.; Goldberg, A.; Lian, J.-J.; Walker, M.; Timmons, A.; Harris, S. J. *J. Electrochem. Soc.* **2009**, *156*, A1019.
- (476) Yoshida, T.; Takahashi, M.; Morikawa, S.; Ihara, C.; Katsukawa, H.; Shiratsuchi, T.; Yamaki, J.-i. *J. Electrochem. Soc.* **2006**, *153*, A576.
- (477) Shigematsu, Y.; Kinoshita, S.-i.; Ue, M. *J. Electrochem. Soc.* **2006**, *153*, A2166.
- (478) Lu, Z.; Yang, L.; Guo, Y. *J. Power Sources* **2006**, *156*, 555.
- (479) Yang, H.; Bang, H.; Amine, K.; Prakash, J. *J. Electrochem. Soc.* **2005**, *152*, A73.
- (480) Watanabe, I.; Yamaki, J.-i. *J. Power Sources* **2006**, *153*, 402.
- (481) Wang, Q.; Sun, J.; Yao, X.; Chen, C. *J. Electrochem. Soc.* **2006**, *153*, A329.
- (482) Jiang, J.; Dahn, J. R. *J. Electrochem. Soc.* **2006**, *153*, A310.
- (483) Zhou, M.; Zhao, L.; Okada, S.; Yamaki, J.-i. *J. Electrochem. Soc.* **2011**, *159*, A44.
- (484) Argue, S.; Davidson, I. J.; Ammundsen, B.; Paulsen, J. *J. Power Sources* **2003**, *119–121*, 664.
- (485) Jiang, J.; Eberman, K. W.; Krause, L. J.; Dahn, J. R. *J. Electrochem. Soc.* **2005**, *152*, A566.
- (486) Wang, Q.; Sun, J.; Chen, C. *J. Electrochem. Soc.* **2007**, *154*, A263.
- (487) Plett, G. L. *ECS Electrochem. Lett.* **2013**, *2*, A63.
- (488) Burns, J. C.; Kassam, A.; Sinha, N. N.; Downie, L. E.; Solnickova, L.; Way, B. M.; Dahn, J. R. *J. Electrochem. Soc.* **2013**, *160*, A1451.
- (489) Campion, C. L.; Li, W.; Euler, W. B.; Lucht, B. L.; Ravdel, B.; DiCarlo, J. F.; Gitzendanner, R.; Abraham, K. M. *Electrochem. Solid-State Lett.* **2004**, *7*, A194.
- (490) Li, W.; Campion, C.; Lucht, B. L.; Ravdel, B.; DiCarlo, J.; Abraham, K. M. *J. Electrochem. Soc.* **2005**, *152*, A1361.
- (491) Larush-Asraf, L.; Biton, M.; Teller, H.; Zinograd, E.; Aurbach, D. *J. Power Sources* **2007**, *174*, 400.
- (492) Sasaki, T.; Abe, T.; Iriyama, Y.; Inaba, M.; Ogumi, Z. *J. Electrochem. Soc.* **2005**, *152*, A2046.
- (493) Hyung, Y. E.; Vissers, D. R.; Amine, K. *J. Power Sources* **2003**, *119–121*, 383.
- (494) Nam, T.-H.; Shim, E.-G.; Kim, J.-G.; Kim, H.-S.; Moon, S.-I. *J. Electrochem. Soc.* **2007**, *154*, A957.
- (495) Wang, Q.; Sun, J.; Yao, X.; Chen, C. *Electrochem. Solid-State Lett.* **2005**, *8*, A467.
- (496) Shim, E.-G.; Nam, T.-H.; Kim, J.-G.; Kim, H.-S.; Moon, S.-I. *J. Power Sources* **2008**, *175*, 533.
- (497) Wang, X.; Yamada, C.; Naito, H.; Segami, G.; Kibe, K. *J. Electrochem. Soc.* **2006**, *153*, A135.
- (498) Izquierdo-Gonzales, S.; Li, W.; Lucht, B. L. *J. Power Sources* **2004**, *135*, 291.
- (499) Mandal, B. K.; Padhi, A. K.; Shi, Z.; Chakraborty, S.; Filler, R. *J. Power Sources* **2006**, *161*, 1341.
- (500) Bakenov, Z.; Nakayama, M.; Wakihara, M. *Electrochem. Solid-State Lett.* **2007**, *10*, A208.
- (501) Zhang, H. P.; Xia, Q.; Wang, B.; Yang, L. C.; Wu, Y. P.; Sun, D. L.; Gan, C. L.; Luo, H. J.; Bebeda, A. W.; Ree, T. v. *Electrochem. Commun.* **2009**, *11*, 526.
- (502) Shigematsu, Y.; Ue, M.; Yamaki, J.-i. *J. Electrochem. Soc.* **2009**, *156*, A176.
- (503) Chen, Z.; Qin, Y.; Liu, J.; Amine, K. *Electrochem. Solid-State Lett.* **2009**, *12*, A69.
- (504) Smart, M. C.; Lucht, B. L.; Ratnakumar, B. V. *J. Electrochem. Soc.* **2008**, *155*, A557.
- (505) Li, W.; Xiao, A.; Lucht, B. L.; Smart, M. C.; Ratnakumar, B. V. *J. Electrochem. Soc.* **2008**, *155*, A648.
- (506) Ihara, M.; Hang, B. T.; Sato, K.; Egashira, M.; Okada, S.; Yamaki, J.-i. *J. Electrochem. Soc.* **2003**, *150*, A1476.
- (507) Jiang, J.; Fortier, H.; Reimers, J. N.; Dahn, J. R. *J. Electrochem. Soc.* **2004**, *151*, A609.
- (508) Jiang, J.; Dahn, J. R. *Electrochem. Commun.* **2004**, *6*, 39.
- (509) Li, W.; Lucht, B. L. *J. Power Sources* **2007**, *168*, 258.
- (510) Chang, C.-C.; Chen, T.-K.; Her, L.-J.; Fey, G. T.-K. *J. Electrochem. Soc.* **2009**, *156*, A828.
- (511) Ping, P.; Wang, Q.; Sun, J.; Xiang, H.; Chen, C. *J. Electrochem. Soc.* **2010**, *157*, A1170.
- (512) Sinha, N. N.; Burns, J. C.; Sanderson, R. J.; Dahn, J. R. *J. Electrochem. Soc.* **2011**, *158*, A1400.
- (513) Veith, G. M.; Dudney, N. J. *J. Electrochem. Soc.* **2011**, *158*, A658.

- (514) Markovsky, B.; Amalraj, F.; Gottlieb, H. E.; Gofer, Y.; Martha, S. K.; Aurbach, D. *J. Electrochem. Soc.* **2010**, *157*, A423.
- (515) Krämer, E.; Schedlbauer, T.; Hoffmann, B.; Terborg, L.; Nowak, S.; Gores, H. J.; Passerini, S.; Winter, M. *J. Electrochem. Soc.* **2013**, *160*, A356.
- (516) Kawamura, T.; Tanaka, T.; Egashira, M.; Watanabe, I.; Okada, S.; Yamaki, J.-i. *Electrochim. Solid-State Lett.* **2005**, *8*, A459.
- (517) Murmann, P.; Schmitz, R.; Nowak, S.; Gores, H.; Ignatiev, N.; Sartori, P.; Passerini, S.; Winter, M.; Schmitz, R. W. *J. Electrochem. Soc.* **2013**, *160*, A535.
- (518) Abouimrane, A.; Ding, J.; Davidson, I. *J. Power Sources* **2009**, *189*, 693.
- (519) Conte, L.; Gambaretto, G.; Caporiccio, G.; Alessandrini, F.; Passerini, S. *J. Fluorine Chem.* **2004**, *125*, 243.
- (520) Han, H.-B.; Zhou, S.-S.; Zhang, D.-J.; Feng, S.-W.; Li, L.-F.; Liu, K.; Feng, W.-F.; Nie, J.; Li, H.; Huang, X.-J.; Armand, M.; Zhou, Z.-B. *J. Power Sources* **2011**, *196*, 3623.
- (521) Li, J.; Xie, K.; Lai, Y.; Zhang, Z. a.; Li, F.; Hao, X.; Chen, X.; Liu, Y. *J. Power Sources* **2010**, *195*, 5344.
- (522) Verma, P.; Maire, P.; Novák, P. *Electrochim. Acta* **2010**, *55*, 6332.
- (523) *Lithium-Ion Batteries: Solid-Electrolyte Interphase*; Balbuena, P. B., Wang, Y., Eds.; Imperial College Press: London, 2004.
- (524) Christensen, J.; Newman, J. *J. Electrochem. Soc.* **2004**, *151*, A1977.
- (525) Tasaki, K. *J. Phys. Chem. B* **2005**, *109*, 2920.
- (526) Tang, M.; Newman, J. *J. Electrochem. Soc.* **2012**, *159*, A1922.
- (527) Tang, M.; Miyazaki, K.; Abe, T.; Newman, J. *J. Electrochem. Soc.* **2012**, *159*, A634.
- (528) Tang, M.; Newman, J. *J. Electrochem. Soc.* **2012**, *159*, A281.
- (529) Downie, L. E.; Nelson, K. J.; Petitbon, R.; Chevrier, V. L.; Dahn, J. R. *ECS Electrochem. Lett.* **2013**, *2*, A106.
- (530) Xu, K.; Zhuang, G. V.; Allen, J. L.; Lee, U.; Zhang, S. S.; Ross, P. N.; Jow, T. R. *J. Phys. Chem. B* **2006**, *110*, 7708.
- (531) Dedryvère, R.; Gireaud, L.; Gruegeon, S.; Laruelle, S.; Tarascon, J. M.; Gonbeau, D. *J. Phys. Chem. B* **2005**, *109*, 15868.
- (532) Gireaud, L.; Gruegeon, S.; Laruelle, S.; Pilard, S.; Tarascon, J. M. *J. Electrochem. Soc.* **2005**, *152*, A850.
- (533) Zhuang, G. V.; Yang, H.; Ross, P. N.; Xu, K.; Jow, T. R. *Electrochim. Solid-State Lett.* **2006**, *9*, A64.
- (534) Borodin, O.; Zhuang, G. V.; Ross, P. N.; Xu, K. *J. Phys. Chem. C* **2013**, *117*, 7433.
- (535) Tsubouchi, S.; Domi, Y.; Doi, T.; Ochida, M.; Nakagawa, H.; Yamanaka, T.; Abe, T.; Ogumi, Z. *J. Electrochem. Soc.* **2012**, *159*, A1786.
- (536) Nie, M.; Chalasani, D.; Abraham, D. P.; Chen, Y.; Bose, A.; Lucht, B. L. *J. Phys. Chem. C* **2013**, *117*, 1257.
- (537) Nie, M.; Abraham, D. P.; Chen, Y.; Bose, A.; Lucht, B. L. *J. Phys. Chem. C* **2013**, *117*, 13403.
- (538) Shu, J. *Electrochim. Solid-State Lett.* **2008**, *11*, A238.
- (539) Dedryvère, R.; Leroy, S.; Martinez, H.; Blanchard, F.; Lemordant, D.; Gonbeau, D. *J. Phys. Chem. B* **2006**, *110*, 12986.
- (540) Marom, R.; Haik, O.; Aurbach, D.; Halalay, I. C. *J. Electrochem. Soc.* **2010**, *157*, A972.
- (541) Augustsson, A.; Herstedt, M.; Guo, J. H.; Edstrom, K.; Zhuang, G. V.; Ross, J. P. N.; Rubensson, J. E.; Nordgren, J. *Phys. Chem. Chem. Phys.* **2004**, *6*, 4185.
- (542) Zhao, L.; Watanabe, I.; Doi, T.; Okada, S.; Yamaki, J.-i. *J. Power Sources* **2006**, *161*, 1275.
- (543) Spahr, M. E.; Palladino, T.; Wilhelm, H.; Würsig, A.; Goers, D.; Buqa, H.; Holzapfel, M.; Novák, P. *J. Electrochem. Soc.* **2004**, *151*, A1383.
- (544) Wuersig, A.; Scheifele, W.; Novák, P. *J. Electrochem. Soc.* **2007**, *154*, A449.
- (545) Novák, P.; Goers, D.; Hardwick, L.; Holzapfel, M.; Scheifele, W.; Ufheil, J.; Würsig, A. *J. Power Sources* **2005**, *146*, 15.
- (546) La Mantia, F.; Novák, P. *Electrochim. Solid-State Lett.* **2008**, *11*, A84.
- (547) Mogi, R.; Inaba, M.; Iriyama, Y.; Abe, T.; Ogumi, Z. *J. Power Sources* **2003**, *119*–*121*, 597.
- (548) Kong, W.; Li, H.; Huang, X.; Chen, L. *J. Power Sources* **2005**, *142*, 285.
- (549) Onuki, M.; Kinoshita, S.; Sakata, Y.; Yanagidate, M.; Otake, Y.; Ue, M.; Deguchi, M. *J. Electrochem. Soc.* **2008**, *155*, A794.
- (550) Xiao, A.; Yang, L.; Lucht, B. L.; Kang, S.-H.; Abraham, D. P. *J. Electrochem. Soc.* **2009**, *156*, A318.
- (551) Shkrob, I. A.; Zhu, Y.; Marin, T. W.; Abraham, D. *J. Phys. Chem. C* **2013**, *117*, 19255.
- (552) Ota, H.; Sakata, Y.; Inoue, A.; Yamaguchi, S. *J. Electrochem. Soc.* **2004**, *151*, A1659.
- (553) Tavassol, H.; Butthiker, J. W.; Ferguson, G. A.; Curtiss, L. A.; Gewirth, A. A. *J. Electrochem. Soc.* **2012**, *159*, A730.
- (554) Tavassol, H.; Chan, M. K. Y.; Catarello, M. G.; Greeley, J.; Cahill, D. G.; Gewirth, A. A. *J. Electrochem. Soc.* **2013**, *160*, A888.
- (555) Shkrob, I. A.; Zhu, Y.; Marin, T. W.; Abraham, D. *J. Phys. Chem. C* **2013**, *117*, 19270.
- (556) Leifer, N.; Smart, M. C.; Prakash, G. K. S.; Gonzalez, L.; Sanchez, L.; Smith, K. A.; Bhalla, P.; Grey, C. P.; Greenbaum, S. G. *J. Electrochem. Soc.* **2011**, *158*, A471.
- (557) Schmitz, R.; Ansgar Müller, R.; Wilhelm Schmitz, R.; Schreiner, C.; Kunze, M.; Lex-Balducci, A.; Passerini, S.; Winter, M. *J. Power Sources* **2013**, *233*, 110.
- (558) Zhuang, G. V.; Ross, P. N., Jr. *Electrochim. Solid-State Lett.* **2003**, *6*, A136.
- (559) Edström, K.; Herstedt, M.; Abraham, D. P. *J. Power Sources* **2006**, *153*, 380.
- (560) Malmgren, S.; Rensmo, H.; Gustafsson, T.; Gorgoi, M.; Edström, K. *ECS Trans.* **2010**, *25*, 201.
- (561) Bryngelsson, H.; Stjerndahl, M.; Gustafsson, T.; Edström, K. *J. Power Sources* **2007**, *174*, 970.
- (562) Leung, K. *Chem. Phys. Lett.* **2013**, *568*–*569*, 1.
- (563) Harilal, S. S.; Allain, J. P.; Hassanein, A.; Hendricks, M. R.; Nieto-Perez, M. *Appl. Surf. Sci.* **2009**, *255*, 8539.
- (564) Vatamanu, J.; Borodin, O.; Smith, G. D. *J. Phys. Chem. C* **2012**, *116*, 1114.
- (565) Borodin, O. In *Electrolytes for Lithium and Lithium-Ion Batteries*; Jow, T. R., Xu, K., Borodin, O., Ue, M., Eds.; Modern Aspects of Electrochemistry Series Vol. 58; Springer: New York, 2014; Vol. 58, p 371.
- (566) Tasaki, K.; Harris, S. *J. J. Phys. Chem. C* **2010**, *114*, 8076.
- (567) Lu, P.; Harris, S. *J. Electrochem. Commun.* **2011**, *13*, 1035.
- (568) Shi, S.; Lu, P.; Liu, Z.; Qi, Y.; Hector, L. G.; Li, H.; Harris, S. *J. Am. Chem. Soc.* **2012**, *134*, 15476.
- (569) Shi, S.; Qi, Y.; Li, H.; Hector, L. G. *J. Phys. Chem. C* **2013**, *117*, 8579.
- (570) Borodin, O.; Smith, G. D.; Fan, P. *J. Phys. Chem. B* **2006**, *110*, 22773.
- (571) Lu, P.; Li, C.; Schneider, E. W.; Harris, S. *J. J. Phys. Chem. C* **2014**, *118*, 896.
- (572) Abe, T.; Fukuda, H.; Iriyama, Y.; Ogumi, Z. *J. Electrochem. Soc.* **2004**, *151*, A1120.
- (573) Abe, T.; Ohtsuka, M.; Sagane, F.; Iriyama, Y.; Ogumi, Z. *J. Electrochem. Soc.* **2004**, *151*, A1950.
- (574) Abe, T.; Sagane, F.; Ohtsuka, M.; Iriyama, Y.; Ogumi, Z. *J. Electrochem. Soc.* **2005**, *152*, A2151.
- (575) Yamada, Y.; Sagane, F.; Iriyama, Y.; Abe, T.; Ogumi, Z. *J. Phys. Chem. C* **2009**, *113*, 14528.
- (576) Yamada, Y.; Iriyama, Y.; Abe, T.; Ogumi, Z. *Langmuir* **2009**, *25*, 12766.
- (577) Xu, K.; Cresce, A. v. W.; Lee, U. *Langmuir* **2010**, *26*, 11538.
- (578) Hahn, M.; Buqa, H.; Ruch, P. W.; Goers, D.; Spahr, M. E.; Ufheil, J.; Novák, P.; Kötz, R. *Electrochim. Solid-State Lett.* **2008**, *11*, A151.
- (579) Buqa, H.; Würsig, A.; Vetter, J.; Spahr, M. E.; Krumeich, F.; Novák, P. *J. Power Sources* **2006**, *153*, 385.
- (580) Märkle, W.; Lu, C.-Y.; Novák, P. *J. Electrochem. Soc.* **2011**, *158*, A1478.

- (581) Naoi, K.; Oghara, N.; Igarashi, Y.; Kamakura, A.; Kusachi, Y.; Utsugi, K. *J. Electrochem. Soc.* **2005**, *152*, A1047.
- (582) Wagner, M. R.; Albering, J. H.; Moeller, K. C.; Besenhard, J. O.; Winter, M. *Electrochem. Commun.* **2005**, *7*, 947.
- (583) Jeong, S.-K.; Inaba, M.; Iriyama, Y.; Abe, T.; Ogumi, Z. *J. Power Sources* **2008**, *175*, 540.
- (584) Yamada, Y.; Koyama, Y.; Abe, T.; Ogumi, Z. *J. Phys. Chem. C* **2009**, *113*, 8948.
- (585) Jeong, S.-K.; Song, H.-Y.; Kim, S. I.; Abe, T.; Jeon, W. S.; Yin, R.-Z.; Kim, Y. S. *Electrochem. Commun.* **2013**, *31*, 24.
- (586) Cresce, A. v. W.; Borodin, O.; Xu, K. *J. Phys. Chem. C* **2012**, *116*, 26111.
- (587) Ganesh, P.; Jiang, D.-e.; Kent, P. R. C. *J. Phys. Chem. B* **2011**, *115*, 3085.
- (588) Bhatt, M.; Cho, M.; Cho, K. *J. Phys. Chem. Lett.* **2012**, *16*, 435.
- (589) Nie, M.; Abraham, D. P.; Seo, D. M.; Chen, Y.; Bose, A.; Lucht, B. L. *J. Phys. Chem. C* **2013**, *117*, 25381.
- (590) Zhang, H.-L.; Sun, C.-H.; Li, F.; Liu, C.; Tan, J.; Cheng, H.-M. *J. Phys. Chem. C* **2007**, *111*, 4740.
- (591) Whittingham, M. S. *Chem. Rev.* **2004**, *104*, 4271.
- (592) Gnanaraj, J. S.; Thompson, R. W.; Iaconatti, S. N.; DiCarlo, J. F.; Abraham, K. M. *Electrochem. Solid-State Lett.* **2005**, *8*, A128.
- (593) Gnanaraj, J. S.; Thompson, R. W.; DiCarlo, J. F.; Abraham, K. M. *J. Electrochem. Soc.* **2007**, *154*, A185.
- (594) Zhuang, G. V.; Yang, H.; Blizanac, B.; Ross, P. N. *Electrochem. Solid-State Lett.* **2005**, *8*, A441.
- (595) Takenaka, N.; Suzuki, Y.; Sakai, H.; Nagaoka, M. *J. Phys. Chem. C* **2014**, *118*, 10874.
- (596) Zhao, H.; Park, S.-J.; Shi, F.; Fu, Y.; Battaglia, V.; Ross, P. N.; Liu, G. *J. Electrochem. Soc.* **2014**, *161*, A194.
- (597) Würsig, A.; Buqa, H.; Holzapfel, M.; Krumeich, F.; Novák, P. *Electrochem. Solid-State Lett.* **2005**, *8*, A34.
- (598) He, P.; Zhang, X.; Wang, Y.-G.; Cheng, L.; Xia, Y.-Y. *J. Electrochem. Soc.* **2008**, *155*, A144.
- (599) Dupré, N.; Martin, J.-F.; Oliveri, J.; Soudan, P.; Guyomard, D.; Yamada, A.; Kanno, R. *J. Electrochem. Soc.* **2009**, *156*, C180.
- (600) Wang, Z.; Huang, X.; Chen, L. *J. Electrochem. Soc.* **2003**, *150*, A199.
- (601) Wang, Z.; Sun, Y.; Chen, L.; Huang, X. *J. Electrochem. Soc.* **2004**, *151*, A914.
- (602) Wang, Z.; Huang, X.; Chen, L. *J. Electrochem. Soc.* **2004**, *151*, A1641.
- (603) Ménétrier, M.; Vaysse, C.; Croguennec, L.; Delmas, C.; Jordy, C.; Bonhomme, F.; Biensan, P. *Electrochem. Solid-State Lett.* **2004**, *7*, A140.
- (604) Lei, J.; Li, L.; Kostecki, R.; Muller, R.; McLarnon, F. *J. Electrochem. Soc.* **2005**, *152*, A774.
- (605) Liu, N.; Li, H.; Wang, Z.; Huang, X.; Chen, L. *Electrochem. Solid-State Lett.* **2006**, *9*, A328.
- (606) Hirayama, M.; Sonoyama, N.; Ito, M.; Minoura, M.; Mori, D.; Yamada, A.; Tamura, K.; Mizuki, J. i.; Kanno, R. *J. Electrochem. Soc.* **2007**, *154*, A1065.
- (607) Goonetilleke, P. C.; Zheng, J. P.; Roy, D. *J. Electrochem. Soc.* **2009**, *156*, A709.
- (608) Aurbach, D.; Markovsky, B.; Salitra, G.; Markevich, E.; Talyossef, Y.; Koltypin, M.; Nazar, L.; Ellis, B.; Kovacheva, D. *J. Power Sources* **2007**, *165*, 491.
- (609) Liu, H.; Tong, Y.; Kuwata, N.; Osawa, M.; Kawamura, J.; Ye, S. *J. Phys. Chem. C* **2009**, *113*, 20531.
- (610) Yu, L.; Liu, H.; Wang, Y.; Kuwata, N.; Osawa, M.; Kawamura, J.; Ye, S. *Angew. Chem., Int. Ed.* **2013**, *52*, 5753.
- (611) Xing, L.; Li, W.; Wang, C.; Gu, F.; Xu, M.; Tan, C.; Yi, J. *J. Phys. Chem. B* **2009**, *113*, 16596.
- (612) Murakami, M.; Yamashige, H.; Arai, H.; Uchimoto, Y.; Ogumi, Z. *Electrochem. Solid-State Lett.* **2011**, *14*, A134.
- (613) Yang, L.; Ravdel, B.; Lucht, B. L. *Electrochem. Solid-State Lett.* **2010**, *13*, A95.
- (614) Vogdanis, L.; Heitz, W. *Makromol. Chem., Rapid Commun.* **1986**, *7*, 543.
- (615) Markovsky, B.; Talyossef, Y.; Salitra, G.; Aurbach, D.; Kim, H.-J.; Choi, S. *Electrochem. Commun.* **2004**, *6*, 821.
- (616) Demeaux, J.; Caillon-Caravanier, M.; Galiano, H.; Lemordant, D.; Claude-Montigny, B. *J. Electrochem. Soc.* **2012**, *159*, A1880.
- (617) Dedryvère, R.; Foix, D.; Franger, S.; Patoux, S.; Daniel, L.; Gonbeau, D. *J. Phys. Chem. C* **2010**, *114*, 10999.
- (618) Duncan, H.; Abu-Lebdeh, Y.; Davidson, I. *J. J. Electrochem. Soc.* **2010**, *157*, A528.
- (619) Duncan, H.; Duguay, D.; Abu-Lebdeh, Y.; Davidson, I. *J. J. Electrochem. Soc.* **2011**, *158*, A537.
- (620) Carroll, K. J.; Yang, M.-C.; Veith, G. M.; Dudney, N. J.; Meng, Y. S. *Electrochem. Solid-State Lett.* **2012**, *15*, A72.
- (621) Markevich, E.; Sharabi, R.; Gottlieb, H.; Borgel, V.; Fridman, K.; Salitra, G.; Aurbach, D.; Semrau, G.; Schmidt, M. A.; Schall, N.; Bruenig, C. *Electrochem. Commun.* **2012**, *15*, 22.
- (622) Allen, J. L.; Jow, T. R.; Wolfenstine, J. *J. Power Sources* **2011**, *196*, 8656.
- (623) Hu, L.; Zhang, Z.; Amine, K. *Electrochem. Commun.* **2013**, *35*, 76.
- (624) Delacourt, C.; Kwong, A.; Liu, X.; Qiao, R.; Yang, W. L.; Lu, P.; Harris, S. J.; Srinivasan, V. *J. Electrochem. Soc.* **2013**, *160*, A1099.
- (625) MahootcheianAsl, N.; Kim, J.-H.; Pieczonka, N. P. W.; Liu, Z.; Kim, Y. *Electrochem. Commun.* **2013**, *32*, 1.
- (626) Li, S. R.; Chen, C. H.; Xia, X.; Dahn, J. R. *J. Electrochem. Soc.* **2013**, *160*, A1524.
- (627) Norberg, N. S.; Lux, S. F.; Kostecki, R. *Electrochem. Commun.* **2013**, *34*, 29.
- (628) Krueger, S.; Kloepsch, R.; Li, J.; Nowak, S.; Passerini, S.; Winter, M. *J. Electrochem. Soc.* **2013**, *160*, A542.
- (629) Duduta, M.; Ho, B.; Wood, V. C.; Limthongkul, P.; Brunini, V. E.; Carter, W. C.; Chiang, Y.-M. *Adv. Energy Mater.* **2011**, *1*, 511.
- (630) Niehoff, P.; Passerini, S.; Winter, M. *Langmuir* **2013**, *29*, 5806.
- (631) Cabana, J. In *Electrolytes for Lithium and Lithium-Ion Batteries*; Jow, T. R., Xu, K., Borodin, O., Ue, M., Eds.; Modern Aspects of Electrochemistry Series Vol. 58; Springer: New York, 2014; p 323.
- (632) Blanc, F.; Leskes, M.; Grey, C. P. *Acc. Chem. Res.* **2013**, *46*, 1952.
- (633) Kwon, K.; Kong, F.; McLarnon, F.; Evans, J. W. *J. Electrochem. Soc.* **2003**, *150*, A229.
- (634) Lucas, I. T.; Syzdek, J.; Kostecki, R. *Electrochem. Commun.* **2011**, *13*, 1271.
- (635) Lux, S. F.; Lucas, I. T.; Pollak, E.; Passerini, S.; Winter, M.; Kostecki, R. *Electrochem. Commun.* **2012**, *14*, 47.
- (636) McArthur, M. A.; Trussler, S.; Dahn, J. R. *J. Electrochem. Soc.* **2012**, *159*, A198.
- (637) Mukherjee, P.; Lagutchev, A.; Dlott, D. D. *J. Electrochem. Soc.* **2012**, *159*, A244.
- (638) Lee, S.-H.; You, H.-G.; Han, K.-S.; Kim, J.; Jung, I.-H.; Song, J.-H. *J. Power Sources* **2014**, *247*, 307.
- (639) Wang, F.; Graetz, J.; Moreno, M. S.; Ma, C.; Wu, L. J.; Volkov, V.; Zhu, Y. M. *ACS Nano* **2011**, *5*, 1190.
- (640) Jo, M.; Hong, Y.-S.; Choo, J.; Cho, J. *J. Electrochem. Soc.* **2009**, *156*, A430.
- (641) Ohzuku, T.; Tomura, H.; Sawai, K. *J. Electrochem. Soc.* **1997**, *144*, 3496.
- (642) Rhodes, K.; Dudney, N.; Lara-Curcio, E.; Daniel, C. *J. Electrochem. Soc.* **2010**, *157*, A1354.
- (643) Komagata, S.; Kuwata, N.; Baskaran, R.; Kawamura, J.; Sato, K.; Mizusaki, J. *ECS Trans.* **2010**, *25*, 163.
- (644) Kircheva, N.; Genies, S.; Brun-Buisson, D.; Thivel, P.-X. *J. Electrochem. Soc.* **2011**, *159*, A18.
- (645) Wang, H.; Downing, R. G.; Dura, J. A.; Hussey, D. S. In *Polymers for Energy Storage and Delivery: Polyelectrolytes for Batteries and Fuel Cells*; Page, K. A., Soles, C. L., Runt, J., Eds.; ACS Symposium Series Vol. 1096; American Chemical Society: Washington, DC, 2012; p 91.
- (646) Bridges, C. A.; Sun, X.-G.; Zhao, J.; Paranthaman, M. P.; Dai, S. *J. Phys. Chem. C* **2012**, *116*, 7701.

- (647) Owejan, J. E.; Owejan, J. P.; DeCaluwe, S. C.; Dura, J. A. *Chem. Mater.* **2012**, *24*, 2133.
- (648) Baddour-Hadjean, R.; Pereira-Ramos, J.-P. *Chem. Rev.* **2009**, *110*, 1278.
- (649) Kostecki, R.; Norin, L.; Song, X.; McLarnon, F. *J. Electrochem. Soc.* **2004**, *151*, A522.
- (650) Kwon, K.; Evans, J. W. *Electrochim. Acta* **2004**, *49*, 867.
- (651) Li, J.-T.; Chen, S.-R.; Fan, X.-Y.; Huang, L.; Sun, S.-G. *Langmuir* **2007**, *23*, 13174.
- (652) Serizawa, N.; Seki, S.; Takei, K.; Miyashiro, H.; Yoshida, K.; Ueno, K.; Tachikawa, N.; Dokko, K.; Katayama, Y.; Watanabe, M.; Miura, T. *J. Electrochem. Soc.* **2013**, *160*, A1529.
- (653) Edström, K.; Herranen, M. *J. Electrochem. Soc.* **2000**, *147*, 3628.
- (654) Aurbach, D.; Teller, H.; Koltypin, M.; Levi, E. *J. Power Sources* **2003**, *119–121*, 2.
- (655) Beaulieu, L. Y.; Beattie, S. D.; Hatchard, T. D.; Dahn, J. R. *J. Electrochem. Soc.* **2003**, *150*, A419.
- (656) Inaba, M.; Ogumi, Z. In *Lithium-ion Batteries: Solid-electrolyte Interphase*; Balbuena, P. B., Wang, Y., Eds.; Imperial College Press: London, 2004; p 198.
- (657) Inaba, M.; Jeong, S.-K.; Ogumi, Z. *ECS Interface* **2011**, *20*, 55.
- (658) Domi, Y.; Ochida, M.; Tsubouchi, S.; Nakagawa, H.; Yamanaka, T.; Doi, T.; Abe, T.; Ogumi, Z. *J. Phys. Chem. C* **2011**, *115*, 25484.
- (659) Inaba, M.; Siroma, Z.; Kawatake, Y.; Funabiki, A.; Ogumi, Z. *J. Power Sources* **1997**, *68*, 221.
- (660) Jeong, S.-K.; Inaba, M.; Iriyama, Y.; Abe, T.; Ogumi, Z. *J. Power Sources* **2003**, *119–121*, 555.
- (661) Inaba, M.; Tomiyasu, H.; Tasaka, A.; Jeong, S.-K.; Ogumi, Z. *Langmuir* **2004**, *20*, 1348.
- (662) Ochida, M.; Domi, Y.; Doi, T.; Tsubouchi, S.; Nakagawa, H.; Yamanaka, T.; Abe, T.; Ogumi, Z. *J. Electrochem. Soc.* **2012**, *159*, A961.
- (663) Zhang, J.; Wang, R.; Yang, X.; Lu, W.; Wu, X.; Wang, X.; Li, H.; Chen, L. *Nano Lett.* **2012**, *12*, 2153.
- (664) Balke, N.; Jesse, S.; Morozovska, A. N.; Eliseev, E.; Chung, D. W.; Kim, Y.; Adamczyk, L.; Garcia, R. E.; Dudney, N.; Kalinin, S. V. *Nat. Nanotechnol.* **2010**, *5*, 749.
- (665) Domi, Y.; Ochida, M.; Tsubouchi, S.; Nakagawa, H.; Yamanaka, T.; Doi, T.; Abe, T.; Ogumi, Z. *J. Electrochem. Soc.* **2012**, *159*, A1292.
- (666) Domi, Y.; Doi, T.; Yamanaka, T.; Abe, T.; Ogumi, Z. *J. Electrochem. Soc.* **2013**, *160*, A678.
- (667) Tsubouchi, S.; Domi, Y.; Doi, T.; Ochida, M.; Nakagawa, H.; Yamanaka, T.; Abe, T.; Ogumi, Z. *J. Electrochem. Soc.* **2013**, *160*, A575.
- (668) Lucas, I. T.; Pollak, E.; Kostecki, R. *Electrochem. Commun.* **2009**, *11*, 2157.
- (669) Cresce, A. v.; Russell, S. M.; Baker, D. R.; Gaskell, K. J.; Xu, K. *Nano Lett.* **2014**, *14*, 1405.
- (670) Inaba, M.; Uno, T.; Tasaka, A. *J. Power Sources* **2005**, *146*, 473.
- (671) Tokranov, A.; Sheldon, B. W.; Li, C.; Minne, S.; Xiao, X. *ACS Appl. Mater. Interfaces* **2014**, *6*, 6672.
- (672) Cabana, J.; Monconduit, L.; Larcher, D.; Palacín, M. R. *Adv. Mater.* **2010**, *22*, E170.
- (673) Chevrier, V. L.; Ceder, G. *J. Electrochem. Soc.* **2011**, *158*, A1011.
- (674) Brenner, A. *J. Electrochem. Soc.* **1971**, *118*, 461.
- (675) Dahn, J. R.; Seel, J. A. *J. Electrochem. Soc.* **2000**, *147*, 899.
- (676) Hu, J.; Li, H.; Huang, X.; Chen, L. *Solid State Ionics* **2006**, *177*, 2791.
- (677) Balaya, P.; Li, H.; Kienle, L.; Maier, J. *Adv. Funct. Mater.* **2003**, *13*, 621.
- (678) Dupont, L.; Laruelle, S.; Gruegon, S.; Dickinson, C.; Zhou, W.; Tarascon, J. M. *J. Power Sources* **2008**, *175*, 502.
- (679) Gmitter, A. J.; Badway, F.; Rangan, S.; Bartynski, R. A.; Halajko, A.; Pereira, N.; Amatucci, G. G. *J. Mater. Chem.* **2010**, *20*, 4149.
- (680) Oh, D.; Dang, X.; Yi, H.; Allen, M. A.; Xu, K.; Lee, Y. J.; Belcher, A. M. *Small* **2012**, *8*, 1006.
- (681) Laruelle, S.; Pilard, S.; Guenot, P.; Gruegon, S.; Tarascon, J.-M. *J. Electrochem. Soc.* **2004**, *151*, A1202.
- (682) Abraham, K. M.; Jiang, Z. *J. Electrochem. Soc.* **1996**, *143*, 1.
- (683) Read, J. *J. Electrochem. Soc.* **2002**, *149*, A1190.
- (684) Ogasawara, T.; Débart, A.; Holzapfel, M.; Novák, P.; Bruce, P. G. *J. Am. Chem. Soc.* **2006**, *128*, 1390.
- (685) Lu, L.; Li, L.; Park, J.-B.; Sun, Y.-K.; Wu, F.; Amine, K. *Chem. Rev.* **2014**.
- (686) Abraham, K. M.; Jiang, Z.; Carroll, B. *Chem. Mater.* **1997**, *9*, 1978.
- (687) Xu, W.; Xiao, J.; Wang, D.; Zhang, J.; Zhang, J.-G. *J. Electrochem. Soc.* **2010**, *157*, A219.
- (688) Read, J. *J. Electrochem. Soc.* **2006**, *153*, A96.
- (689) Kuboki, T.; Okuyama, T.; Ohsaki, T.; Takami, N. *J. Power Sources* **2005**, *146*, 766.
- (690) Freunberger, S. A.; Chen, Y.; Peng, Z.; Griffin, J. M.; Hardwick, L. J.; Bardé, F.; Novák, P.; Bruce, P. G. *J. Am. Chem. Soc.* **2011**, *133*, 8040.
- (691) McCloskey, B. D.; Bethune, D. S.; Shelby, R. M.; Girishkumar, G.; Luntz, A. C. *J. Phys. Chem. Lett.* **2011**, *2*, 1161.
- (692) Xu, W.; Xu, K.; Viswanathan, V. V.; Towne, S. A.; Hardy, J. S.; Xiao, J.; Nie, Z.; Hu, D.; Wang, D.; Zhang, J.-G. *J. Power Sources* **2011**, *196*, 9631.
- (693) Bryantsev, V. S.; Blanco, M. *J. Phys. Chem. Lett.* **2011**, *2*, 379.
- (694) Takechi, K.; Higashi, S.; Mizuno, F.; Nishikoori, H.; Iba, H.; Shiga, T. *ECS Electrochem. Lett.* **2012**, *1*, A27.
- (695) Chalasani, D.; Lucht, B. L. *ECS Electrochem. Lett.* **2012**, *1*, A38.
- (696) Freunberger, S. A.; Chen, Y.; Drewett, N. E.; Hardwick, L. J.; Bardé, F.; Bruce, P. G. *Angew. Chem., Int. Ed.* **2011**, *50*, 8609.
- (697) Laoire, C. Ó.; Mukerjee, S.; Plichta, E. J.; Hendrickson, M. A.; Abraham, K. M. *J. Electrochem. Soc.* **2011**, *158*, A302.
- (698) Lim, H.-D.; Park, K.-Y.; Gwon, H.; Hong, J.; Kim, H.; Kang, K. *Chem. Commun.* **2012**, *48*, 8374.
- (699) Xu, W.; Hu, J.; Engelhard, M. H.; Towne, S. A.; Hardy, J. S.; Xiao, J.; Feng, J.; Hu, M. Y.; Zhang, J.; Ding, F.; Gross, M. E.; Zhang, J.-G. *J. Power Sources* **2012**, *215*, 240.
- (700) Jung, H.-G.; Hassoun, J.; Park, J.-B.; Sun, Y.-K.; Scrosati, B. *Nat. Chem.* **2012**, *4*, 579.
- (701) Ryan, K. R.; Trahey, L.; Ingram, B. J.; Burrell, A. K. *J. Phys. Chem. C* **2012**, *116*, 19724.
- (702) Sharon, D.; Etacheri, V.; Garsuch, A.; Afri, M.; Frimer, A. A.; Aurbach, D. *J. Phys. Chem. Lett.* **2012**, *4*, 127.
- (703) Barile, C. J.; Gewirth, A. A. *J. Electrochem. Soc.* **2013**, *160*, A549.
- (704) McCloskey, B. D.; Bethune, D. S.; Shelby, R. M.; Mori, T.; Scheffler, R.; Speidel, A.; Sherwood, M.; Luntz, A. C. *J. Phys. Chem. Lett.* **2012**, *3*, 3043.
- (705) Laoire, C. O.; Mukerjee, S.; Abraham, K. M.; Plichta, E. J.; Hendrickson, M. A. *J. Phys. Chem. C* **2010**, *114*, 9178.
- (706) Peng, Z.; Freunberger, S. A.; Chen, Y.; Bruce, P. G. *Science* **2012**, *337*, 563.
- (707) Xu, D.; Wang, Z.-I.; Xu, J.-j.; Zhang, L.-l.; Zhang, X.-b. *Chem. Commun.* **2012**, *48*, 6948.
- (708) Trahan, M. J.; Mukerjee, S.; Plichta, E. J.; Hendrickson, M. A.; Abraham, K. M. *J. Electrochem. Soc.* **2013**, *160*, A259.
- (709) De Giorgio, F.; Soavi, F.; Mastragostino, M. *Electrochem. Commun.* **2011**, *13*, 1090.
- (710) Hayyan, M.; Mjalli, F. S.; Hashim, M. A.; AlNashef, I. M.; Al-Zahrani, S. M.; Chooi, K. L. *J. Electroanal. Chem.* **2012**, *664*, 26.
- (711) Kim, B. G.; Lee, J.-N.; Lee, D. J.; Park, J.-K.; Choi, J. W. *ChemSusChem* **2013**, *6*, 443.
- (712) Bryantsev, V. S.; Giordani, V.; Walker, W.; Blanco, M.; Zecevic, S.; Sasaki, K.; Uddin, J.; Addison, D.; Chase, G. V. *J. Phys. Chem. A* **2011**, *115*, 12399.
- (713) Bryantsev, V. S.; Uddin, J.; Giordani, V.; Walker, W.; Addison, D.; Chase, G. V. *J. Electrochem. Soc.* **2013**, *160*, A160.
- (714) Walker, W.; Giordani, V.; Uddin, J.; Bryantsev, V. S.; Chase, G. V.; Addison, D. *J. Am. Chem. Soc.* **2013**, *135*, 2076.

- (715) Bryantsev, V. S.; Giordani, V.; Walker, W.; Uddin, J.; Lee, I.; van Duin, A. C. T.; Chase, G. V.; Addison, D. *J. Phys. Chem. C* **2013**, *117*, 11977.
- (716) Chen, Y.; Freunberger, S. A.; Peng, Z.; Bardé, F.; Bruce, P. G. *J. Am. Chem. Soc.* **2012**, *134*, 7952.
- (717) Peng, Z.; Freunberger, S. A.; Hardwick, L. J.; Chen, Y.; Giordani, V.; Bardé, F.; Novák, P.; Graham, D.; Tarascon, J.-M.; Bruce, P. G. *Angew. Chem., Int. Ed.* **2011**, *50*, 6351.
- (718) Wang, H.; Liao, X.-Z.; Li, L.; Chen, H.; Jiang, Q.-Z.; He, Y.-S.; Ma, Z.-F. *J. Electrochem. Soc.* **2012**, *159*, A1874.
- (719) Zheng, D.; Yang, X.-Q.; Qu, D. *Chem.—Asian J.* **2011**, *6*, 3306–3311.
- (720) Mohamed, S. N.; Johari, N. A.; Ali, A. M. M.; Harun, M. K.; Yahya, M. Z. A. *J. Power Sources* **2008**, *183*, 351.
- (721) Zhang, D.; Li, R.; Huang, T.; Yu, A. *J. Power Sources* **2010**, *195*, 1202.
- (722) Kumar, B.; Kumar, J.; Leese, R.; Fellner, J. P.; Rodrigues, S. J.; Abraham, K. M. *J. Electrochem. Soc.* **2010**, *157*, A50.
- (723) Hassoun, J.; Croce, F.; Armand, M.; Scrosati, B. *Angew. Chem., Int. Ed.* **2011**, *50*, 2999.
- (724) Li, F.; Kitaura, H.; Zhou, H. *Energy Environ. Sci.* **2013**, *6*, 2302.
- (725) Xu, W.; Xiao, J.; Wang, D.; Zhang, J.; Zhang, J.-G. *Electrochim. Solid-State Lett.* **2010**, *13*, A48.
- (726) Zheng, D.; Lee, H.-S.; Yang, X.-Q.; Qu, D. *Electrochim. Commun.* **2013**, *28*, 17.
- (727) Zhang, S. S.; Xu, K.; Read, J. *J. Power Sources* **2011**, *196*, 3906.
- (728) Wang, Y.; Zheng, D.; Yang, X.-Q.; Qu, D. *Energy Environ. Sci.* **2011**, *4*, 3697.
- (729) Zhang, S. S.; Foster, D.; Read, J. *Electrochim. Acta* **2011**, *56*, 1283.
- (730) Chen, Y.; Freunberger, S. A.; Peng, Z.; Fontaine, O.; Bruce, P. G. *Nat. Chem.* **2013**, *5*, 489.
- (731) Nasybulin, E.; Xu, W.; Engelhard, M. H.; Nie, Z.; Burton, S. D.; Cosimbescu, L.; Gross, M. E.; Zhang, J.-G. *J. Phys. Chem. C* **2013**, *117*, 2635.
- (732) Veith, G. M.; Nanda, J.; Delmau, L. H.; Dudney, N. *J. J. Phys. Chem. Lett.* **2012**, *3*, 1242.
- (733) Ji, X.; Lee, K. T.; Nazar, L. F. *Nat. Mater.* **2009**, *8*, 500.
- (734) Yang, Y.; Zheng, G.; Cui, Y. *Chem. Soc. Rev.* **2013**, *42*, 3018.
- (735) Zhang, S. S. *J. Power Sources* **2013**, *231*, 153.
- (736) Ryu, H.-S.; Ahn, H.-J.; Kim, K.-W.; Ahn, J.-H.; Cho, K.-K.; Nam, T.-H.; Kim, J.-U.; Cho, G.-B. *J. Power Sources* **2006**, *163*, 201.
- (737) Wang, J.; Chew, S. Y.; Zhao, Z. W.; Ashraf, S.; Wexler, D.; Chen, J.; Ng, S. H.; Chou, S. L.; Liu, H. K. *Carbon* **2008**, *46*, 229.
- (738) Diao, Y.; Xie, K.; Xiong, S.; Hong, X. *J. Electrochim. Soc.* **2012**, *159*, A421.
- (739) Barchasz, C.; Leprêtre, J.-C.; Patoux, S.; Alloin, F. *J. Electrochim. Soc.* **2013**, *160*, A430.
- (740) Wang, W.; Li, G.-c.; Wang, Q.; Li, G.-r.; Ye, S.-h.; Gao, X.-p. *J. Electrochim. Soc.* **2013**, *160*, A805.
- (741) Hagen, M.; Feisthammel, G.; Fanz, P.; Grossmann, H. T.; Dörfler, S.; Tübke, J.; Hoffmann, M. J.; Börner, D.; Joos, M.; Althues, H.; Kaskel, S. *J. Electrochim. Soc.* **2013**, *160*, A996.
- (742) Jeddi, K.; Zhao, Y.; Zhang, Y.; Konarov, A.; Chen, P. *J. Electrochim. Soc.* **2013**, *160*, A1052.
- (743) Jache, B.; Mogwitz, B.; Klein, F.; Adelhelm, P. *J. Power Sources* **2014**, *247*, 703.
- (744) Gao, J.; Lowe, M. A.; Kiya, Y.; Abruña, H. D. *J. Phys. Chem. C* **2011**, *115*, 25132.
- (745) Yim, T.; Park, M.-S.; Yu, J.-S.; Kim, K. J.; Im, K. Y.; Kim, J.-H.; Jeong, G.; Jo, Y. N.; Woo, S.-G.; Kang, K. S.; Lee, I.; Kim, Y.-J. *Electrochim. Acta* **2013**, *107*, 454.
- (746) He, X.; Ren, J.; Wang, L.; Pu, W.; Wan, C.; Jiang, C. *Ionics* **2009**, *15*, 477.
- (747) Takeuchi, T.; Kageyama, H.; Nakanishi, K.; Inada, Y.; Katayama, M.; Ohta, T.; Senoh, H.; Sakaebe, H.; Sakai, T.; Tatsumi, K.; Kobayashi, H. *J. Electrochim. Soc.* **2011**, *159*, A75.
- (748) Zhang, Y.; Zhao, Y.; Bakenov, Z.; Babaa, M.-R.; Konarov, A.; Ding, C.; Chen, P. *J. Electrochim. Soc.* **2013**, *160*, A1194.
- (749) Fanous, J.; Wegner, M.; Spera, M. B. M.; Buchmeiser, M. R. *J. Electrochim. Soc.* **2013**, *160*, A1169.
- (750) Wang, J.; Lin, F.; Jia, H.; Yang, J.; Monroe, C. W.; NuLi, Y. *Angew. Chem.* **2014**, *53*, 10099.
- (751) Yuan, L. X.; Feng, J. K.; Ai, X. P.; Cao, Y. L.; Chen, S. L.; Yang, H. X. *Electrochim. Commun.* **2006**, *8*, 610.
- (752) Zhang, S. S. *Electrochim. Acta* **2013**, *97*, 226.
- (753) Lin, Z.; Liu, Z.; Fu, W.; Dudney, N. J.; Liang, C. *Adv. Funct. Mater.* **2013**, *23*, 1064.
- (754) Kang, I. S.; Lee, Y.-S.; Kim, D.-W. *J. Electrochim. Soc.* **2014**, *161*, A53.
- (755) Chung, K.-i.; Kim, W.-S.; Choi, Y.-K. *J. Electroanal. Chem.* **2004**, *566*, 263.
- (756) Zhang, T.; Imanishi, N.; Shimonishi, Y.; Hirano, A.; Takeda, Y.; Yamamoto, O.; Sammes, N. *Chem. Commun.* **2010**, *46*, 1661.
- (757) Puech, L.; Cantau, C.; Vinatier, P.; Toussaint, G.; Stevens, P. J. *Power Sources* **2012**, *214*, 330.
- (758) Aurbach, D.; Pollak, E.; Elazari, R.; Salitra, G.; Kelley, C. S.; Affinito, J. *J. Electrochim. Soc.* **2009**, *156*, A694.
- (759) Zhang, S. S. *J. Electrochim. Soc.* **2012**, *159*, 920.
- (760) Zhang, S. S.; Read, J. *A. J. Power Sources* **2012**, *200*, 77.
- (761) Xiong, S.; Xie, K.; Diao, Y.; Hong, X. *J. Power Sources* **2014**, *246*, 840.
- (762) Song, J.-H.; Yeon, J.-T.; Jang, J.-Y.; Han, J.-G.; Lee, S.-M.; Choi, N.-S. *J. Electrochim. Soc.* **2013**, *160*, A873.
- (763) Ryou, M.-H.; Lee, D. J.; Lee, J.-N.; Lee, Y. M.; Park, J.-K.; Choi, J. W. *Adv. Energy Mater.* **2012**, *2*, 645.
- (764) Ryou, M.-H.; Lee, Y. M.; Park, J.-K.; Choi, J. W. *Adv. Mater.* **2011**, *23*, 3066.
- (765) Ding, F.; Xu, W.; Graff, G. L.; Zhang, J.; Sushko, M. L.; Chen, X.; Shao, Y.; Engelhard, M. H.; Nie, Z.; Xiao, J.; Liu, X.; Sushko, P. V.; Liu, J.; Zhang, J.-G. *J. Am. Chem. Soc.* **2013**, *135*, 4450.
- (766) Zheng, G.; Lee, S. W.; Liang, Z.; Lee, H.-W.; Yan, K.; Yao, H.; Wang, H.; Li, W.; Chu, S.; Cui, Y. *Nat. Nano* **2014**, *9*, 618.
- (767) Carlin, R. T.; De Long, H. C.; Fuller, J.; Trulove, P. C. *J. Electrochim. Soc.* **1994**, *141*, L73.
- (768) Deshpande, S. L.; Bennion, D. N. *J. Electrochim. Soc.* **1978**, *125*, 687.
- (769) Matsuda, Y.; Morita, M.; Katsuma, H. *J. Electrochim. Soc.* **1984**, *131*, 104.
- (770) Seel, J. A.; Dahn, J. R. *J. Electrochim. Soc.* **2000**, *147*, 892.
- (771) Yan, W.; Lerner, M. M. *J. Electrochim. Soc.* **2001**, *148*, D83.
- (772) Yan, W.; Lerner, M. M. *J. Electrochim. Soc.* **2003**, *150*, D169.
- (773) Yan, W.; Lerner, M. M. *J. Electrochim. Soc.* **2004**, *151*, J15.
- (774) Ishihara, T.; Koga, M.; Matsumoto, H.; Yoshio, M. *Electrochim. Solid-State Lett.* **2007**, *10*, A74.
- (775) Ishihara, T.; Yokoyama, Y.; Kozono, F.; Hayashi, H. *J. Power Sources* **2011**, *196*, 6956.
- (776) Zhang, X.; Sukpirom, N.; Lerner, M. M. *Mater. Res. Bull.* **1999**, *34*, 363.
- (777) Yan, W.; Lerner, M. M. *Carbon* **2004**, *42*, 2981.
- (778) Katinonkul, W.; Lerner, M. M. *J. Phys. Chem. Lett.* **2007**, *68*, 394.
- (779) Yan, W.; Kabalnova, L.; Sukpirom, N.; Zhang, S.; Lerner, M. M. *Fluorine Chem.* **2004**, *125*, 1703.
- (780) Syzdek, J.; Marcinek, M.; Kostecki, R. *J. Power Sources* **2014**, *245*, 739.
- (781) West, W. C.; Whitacre, J. F.; Leifer, N.; Greenbaum, S.; Smart, M.; Bugga, R.; Blanco, M.; Narayanan, S. R. *J. Electrochim. Soc.* **2007**, *154*, A929.
- (782) Placke, T.; Fromm, O.; Lux, S. F.; Bieker, P.; Rothermel, S.; Meyer, H.-W.; Passerini, S.; Winter, M. *J. Electrochim. Soc.* **2012**, *159*, A1755.
- (783) Placke, T.; Rothermel, S.; Fromm, O.; Meister, P.; Lux, S. F.; Huesker, J.; Meyer, H.-W.; Winter, M. *J. Electrochim. Soc.* **2013**, *160*, A1979.
- (784) Read, J. A.; Cresce, A. v. W.; Ervin, M. H.; Xu, K. *Energy Environ. Sci.* **2014**, *7*, 617.
- (785) Tarascon, J.-M. *Philos. Trans. R. Soc., A* **2010**, *368*, 3227.

- (786) Ponrouch, A.; Marchante, E.; County, M.; Tarascon, J.-M.; Palacin, M. R. *Energy Environ. Sci.* **2012**, *5*, 8572.
- (787) Ponrouch, A.; Dedryvere, R.; Monti, D.; Demet, A. E.; Ateba Mba, J. M.; Croguennec, L.; Masquelier, C.; Johansson, P.; Palacin, M. R. *Energy Environ. Sci.* **2013**, *6*, 2361.
- (788) Zhu, Y.; Han, X.; Xu, Y.; Liu, Y.; Zheng, S.; Xu, K.; Hu, L.; Wang, C. *ACS Nano* **2013**, *7*, 6378.
- (789) Komaba, S.; Murata, W.; Ishikawa, T.; Yabuuchi, N.; Ozeki, T.; Nakayama, T.; Ogata, A.; Gotoh, K.; Fujiwara, K. *Adv. Funct. Mater.* **2011**, *21*, 3859.
- (790) Thorne, J. S.; Dunlap, R. A.; Obrovac, M. N. *J. Electrochem. Soc.* **2013**, *160*, A361.
- (791) Kataoka, R.; Mukai, T.; Yoshizawa, A.; Sakai, T. *J. Electrochem. Soc.* **2013**, *160*, A933.
- (792) Zhu, H.; Jia, Z.; Chen, Y.; Weadock, N.; Wan, J.; Vaaland, O.; Han, X.; Li, T.; Hu, L. *Nano Lett.* **2013**, *13*, 3093.
- (793) Komaba, S.; Ishikawa, T.; Yabuuchi, N.; Murata, W.; Ito, A.; Ohsawa, Y. *ACS Appl. Mater. Interfaces* **2011**, *3*, 4165.
- (794) Xia, X.; Obrovac, M. N.; Dahn, J. R. *Electrochem. Solid-State Lett.* **2011**, *14*, A130.
- (795) Komaba, S.; Matsuura, Y.; Ishikawa, T.; Yabuuchi, N.; Murata, W.; Kuze, S. *Electrochem. Commun.* **2012**, *21*, 65.
- (796) Yabuuchi, N.; Kajiyama, M.; Iwatate, J.; Nishikawa, H.; Hitomi, S.; Okuyama, R.; Usui, R.; Yamada, Y.; Komaba, S. *Nat. Mater.* **2012**, *11*, 512.
- (797) Ponrouch, A.; Goñi, A. R.; Palacín, M. R. *Electrochem. Commun.* **2013**, *27*, 85.
- (798) Palomares, V.; Serras, P.; Villaluenga, I.; Hueso, K. B.; Carretero-Gonzalez, J.; Rojo, T. *Energy Environ. Sci.* **2012**, *5*, 5884.
- (799) Yamamoto, T.; Nohira, T.; Hagiwara, R.; Fukunaga, A.; Sakai, S.; Nitta, K.; Inazawa, S. *J. Power Sources* **2012**, *217*, 479.
- (800) Xia, X.; Dahn, J. R. *J. Electrochem. Soc.* **2012**, *159*, A515.
- (801) Xia, X.; Lamanna, W. M.; Dahn, J. R. *J. Electrochem. Soc.* **2013**, *160*, A607.
- (802) MacNeil, D. D.; Dahn, J. R. *J. Electrochem. Soc.* **2003**, *150*, A21.
- (803) Aurbach, D.; Lu, Z.; Schechter, A.; Gofer, Y.; Gizbar, H.; Turgeman, R.; Cohen, Y.; Moshkovich, M.; Levi, E. *Nature* **2000**, *407*, 724.
- (804) Yoo, H. D.; Shterenberg, I.; Gofer, Y.; Gershinsky, G.; Pour, N.; Aurbach, D. *Energy Environ. Sci.* **2013**, *6*, 2265.
- (805) Aurbach, D.; Weissman, I.; Gofer, Y.; Levi, E. *Chem. Rec.* **2003**, *3*, 61.
- (806) Chusid, O.; Gofer, Y.; Gizbar, H.; Vestfrid, Y.; Levi, E.; Aurbach, D.; Riech, I. *Adv. Mater.* **2003**, *15*, 627.
- (807) Gizbar, H.; Vestfrid, Y.; Chusid, O.; Gofer, Y.; Gottlieb, H. E.; Marks, V.; Aurbach, D. *Organometallics* **2004**, *23*, 3826.
- (808) Levi, M. D.; Lancry, E.; Gizbar, H.; Lu, Z.; Levi, E.; Gofer, Y.; Aurbach, D. *J. Electrochem. Soc.* **2004**, *151*, A1044.
- (809) Gofer, Y.; Chusid, O.; Gizbar, H.; Viestfrid, Y.; Gottlieb, H. E.; Marks, V.; Aurbach, D. *Electrochem. Solid-State Lett.* **2006**, *9*, A257.
- (810) Vestfrid, Y.; Chusid, O.; Goffer, Y.; Aped, P.; Aurbach, D. *Organometallics* **2007**, *26*, 3.
- (811) Mizrahi, O.; Amir, N.; Pollak, E.; Chusid, O.; Marks, V.; Gottlieb, H.; Larush, L.; Zinigrad, E.; Aurbach, D. *J. Electrochem. Soc.* **2008**, *155*, A103.
- (812) Nakayama, Y.; Kudo, Y.; Oki, H.; Yamamoto, K.; Kitajima, Y.; Noda, K. *J. Electrochem. Soc.* **2008**, *155*, A754.
- (813) Matsui, M. *J. Power Sources* **2011**, *196*, 7048.
- (814) Kim, H. S.; Arthur, T. S.; Allred, G. D.; Zajicek, J.; Newman, J. G.; Rodnyansky, A. E.; Oliver, A. G.; Boggess, W. C.; Muldoon, J. *Nat. Commun.* **2011**, *2*, 427.
- (815) Arthur, T. S.; Glans, P.-A.; Matsui, M.; Zhang, R.; Ma, B.; Guo, J. *Electrochem. Commun.* **2012**, *24*, 43.
- (816) Guo, Y.-s.; Zhang, F.; Yang, J.; Wang, F.-f.; NuLi, Y.; Hirano, S.-i. *Energy Environ. Sci.* **2012**, *5*, 9100.
- (817) Muldoon, J.; Bucur, C. B.; Oliver, A. G.; Sugimoto, T.; Matsui, M.; Kim, H. S.; Allred, G. D.; Zajicek, J.; Kotani, Y. *Energy Environ. Sci.* **2012**, *5*, 5941.
- (818) Lv, D.; Xu, T.; Saha, P.; Datta, M. K.; Gordin, M. L.; Manivannan, A.; Kumta, P. N.; Wang, D. *J. Electrochem. Soc.* **2013**, *160*, A351.
- (819) Liu, T.; Shao, Y.; Li, G.; Gu, M.; Hu, J.; Xu, S.; Nie, Z.; Chen, X.; Wang, C.; Liu, J. *J. Mater. Chem. A* **2014**, *2*, 3430.
- (820) Doe, R. E.; Han, R.; Hwang, J.; Gmitter, A. J.; Shterenberg, I.; Yoo, H. D.; Pour, N.; Aurbach, D. *Chem. Commun.* **2014**, *50*, 243.
- (821) Mohtadi, R.; Matsui, M.; Arthur, T. S.; Hwang, S.-J. *Angew. Chem., Int. Ed.* **2012**, *51*, 9701.
- (822) Carter, T. J.; Mohtadi, R.; Arthur, T. S.; Mizuno, F.; Zhang, R.; Shirai, S.; Kampf, J. W. *Angew. Chem., Int. Ed.* **2014**, *53*, 3173.
- (823) NuLi, Y.; Yang, J.; Wu, R. *Electrochem. Commun.* **2005**, *7*, 1105.
- (824) Amir, N.; Vestfrid, Y.; Chusid, O.; Gofer, Y.; Aurbach, D. *J. Power Sources* **2007**, *174*, 1234.
- (825) Cheek, G. T.; O'Grady, W. E.; El Abedin, S. Z.; Moustafa, E. M.; Endres, F. *J. Electrochem. Soc.* **2008**, *155*, D91.